Impacts of Cascadia Subduction Zone M9 Earthquakes on Bridges in Washington State

Kan-Jen Liu

A thesis
submitted in partial fulfillment of the
requirements for the degree of

MASTER OF SCIENCE IN CIVIL AND ENVIRONMENTAL ENGINEERING

University of Washington

2022

Committee:
Marc O. Eberhard, Chair
Jeffrey W. Berman, Co-Chair
Brett Maurer
Nasser Marafi

Program Authorized to Offer Degree:
Civil and Environmental Engineering

University of Washington

Abstract

Impacts of Cascadia Subduction Zone M9 Earthquakes on Bridges in Washington State

Kan-Jen Liu

Chair of the Supervisory Committee:
Marc O. Eberhard and Jeffrey W. Berman
Civil and Environmental Engineering

The Cascadia Subduction Zone (CSZ) poses a major seismic hazard to the western portions of Washington State, Oregon State and Northern California. To plan for community resilience, it is important to understand the impacts of a large magnitude CSZ earthquake on highway bridges. Previous researchers have developed 30 sets of potential M9 ground motions at numerous locations throughout Washington State for several site classes. These motions have been combined with single-degree-of-freedom (SDOF) models to investigate bridge performance. These models are computationally efficient, however, SDOF models have limitations in predicting bridge seismic response. In particular, such models neglect the effects of bridge abutments.

Typical characteristics of bridges in Washington State were identified by studying a database compiled by the Washington State Department of Transportation (WSDOT) engineers and University of Washington researchers. Based on this study, a three-dimensional, multi-degree-of-freedom (MDOF) bridge model was developed to represent typical highway bridges in Washington State. The reference bridge had three spans, a continuous superstructure, and an L-type (Seat) abutment with bearing pads and transverse shear keys. Using that model, a series of

parametric studies were conducted to evaluate the effects of bridge location, site class, abutment characteristics and properties of the columns at the intermediate supports.

The simulated deformation responses of the bridges in the longitudinal direction were consistently smaller than those in the transverse direction due to the high resistance provided by the abutment and backfill soil. In the transverse direction, the largest displacement responses were calculated for the coastal cities and for site class D1. The responses tended to decrease as the distance from the coast increased. The transverse displacements increased significantly when the shear keys were removed for all locations and site classes. For bridges without shear keys, increases in column heights resulted in higher response in cities underlaid by sedimentary basins. These findings provide engineers from WSDOT an opportunity to develop cost and time-efficient prioritization bridge retrofit plans in the future.

Table of Contents

Figures

Tables

Acknowledgements

This thesis is the final product of my research work and graduate journey in the past two years as an international student in the US. Without the help, support, and guidance of many wonderful people, the completion of this thesis would not be possible. I would like to begin by thanking my advisors Marc Eberhard and Jeffrey Berman, who have always been there to provide advice and encouragement. Even though I am a second language speaker, both Marc and Jeff trusted in my ability to accomplish challenging tasks and gave me the opportunity to work on this amazing project. Their guidance all the way was the key to my success and has helped me become a better and more confident researcher.

An equally important person in this work has been Nasser Marafi. I have always been amazed by Nasser's knowledge both as an engineer and as a scholar. Nasser taught me a tremendous amount in the analyzing and programming side of the project. Most importantly, I must thank him for spending time, even as a busy professional who lives 8 hours away in London, participating in our regular meetings. We are extremely fortunate to have such a brilliant researcher to contribute to our team.

I also want to mention my friends and housemates who helped me to get through this difficult COVID world. In particular, I want to thank my friend Sunny, who has always been there for me whenever I need someone to talk to. In those darkest and scariest moments, it was you who showed me the optimistic side of things and taught me to believe in myself. Your emotional support has become a big part of what I have accomplished. And of course, all the great adventures and memories we created in these past few months have already become the best experience of my graduate life.

The most important people to my success are my family who is more than 6000 miles away on the other side of the world. I would not have been able to make it to this point without your unconditional love and support. To Mom and Dad, thank you for giving me the freedom to explore different possibilities overseas without any concerns, both emotionally and financially. To my sister, who is as well a current graduate student now finishing up an advanced degree, I hope I have been an example that hard work can lead to success and that you can fulfill your own dream with high confidence. “謝謝你們一路以來的鼓勵跟支持!”

Lastly, there are so many other people I have met along the way who provided me help and company in this sometimes-lonely journey studying abroad. I want to thank everyone who is part of this success and I look forward to the next chapter of my life.

Chapter 1: Introduction

1.1 Background

The Cascadia Subduction Zone (CSZ) runs over 1,000 kilometers from Northern Vancouver Island to Cape Mendocino, California (Figure 1.1). It is the dividing line between the Juan de Fuca and the North American tectonic plates. The subduction zone has the potential to generate large "megathrust" earthquakes with magnitude over 9.0. Geological evidence indicates at least 7 such events occurred in the last 3500 years, and the last event happened in 1700. Such events have the potential to cause tremendous damage to the western portions of Washington State, Oregon State and Northern California. (PNSN 2021)

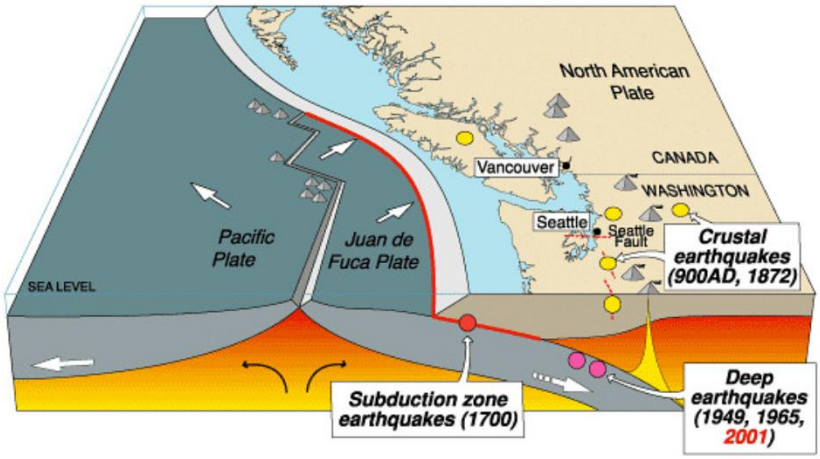

Source	Affected area	Max. Size	Recurrence
Subduction Zone	W.WA, OR, CA	M 9	500-600 yr
Deep Juan de Fuca plate	W.WA, OR,	M 7+	30-50 yr
Crustal faults	WA, OR, CA	M 7+	Hundreds of yr?

Figure 1.1: Cascadia subduction zone (CSZ) (USGS 2017)

Coastal communities in Washington State are close to the CSZ source, so it is expected that these locations will experience intense ground motions with large spectral accelerations. The post-earthquake functionality of the transportation system for these communities is critical because this system will be needed to recover from the effects of an earthquake, and possibly, an ensuing tsunami.

The major cities in the Puget Sound region, including Seattle, are further from the sources of M9 earthquakes, but these cities lie on top of deep sedimentary basins. The presence of such basins is a concern because deep basins are known to affect ground motions as a result of impedance contrast at the boundary of the basin, focusing (and de-focusing) due to the irregular geometry of the basin, and surface-wave conversion at the edge of basins (Figure 1.2).

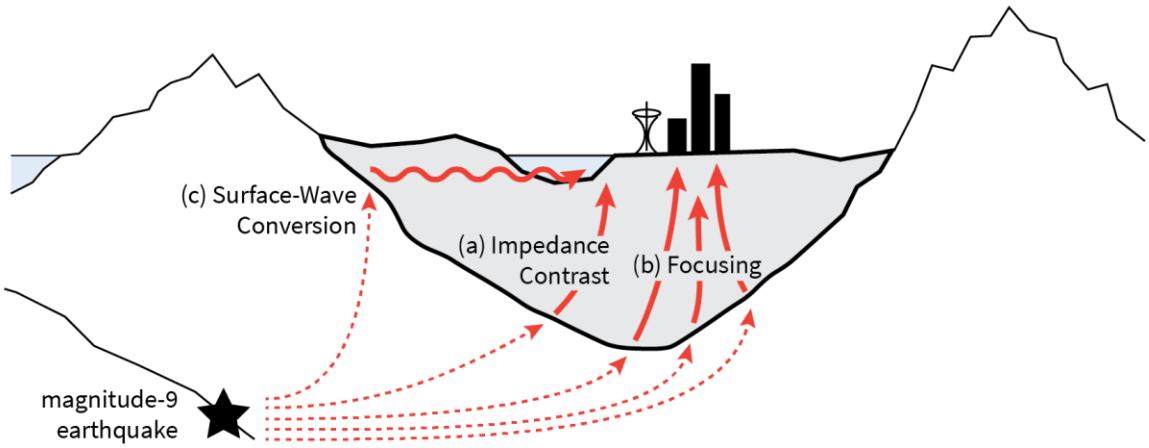

Figure 1.2: Cities located above a sedimentary basin (Marafi 2018)

Basins tend to amplify the longer period content of the motion (above 1 sec) and can have damaging spectral shapes (Marafi et al. 2017). The resulting, basin modified CSZ ground motions pose a considerable risk to these highly populated areas, particularly to structures with periods of

1 second and above (Marafi et al. 2017, 2020). Nevertheless, the current US seismic hazard design maps for bridges do not consider the effect of basin amplification (Marafi, 2017).

1.2 Research Objectives

Communities rely on their transportation infrastructure after an earthquake for the delivery of relief supplies, for evacuation following an earthquake and tsunami (along the coasts) and for economic recovery. Consequently, the performance of bridges in a CSZ event is an essential feature of the resilience of these communities. Considering 6 representative cities in Western Washington States, this study aims to investigate the impacts of these earthquakes on typical bridges for a variety of site classes, source distances, presence of basin, and key bridge features.

Previous researchers developed suites of ground motions resulting from an M9 CSZ earthquake for the western portions of Washington and Oregon (Frankel et al. 2018, Wirth et al. 2018). De Zamacona (2019) evaluated the effects of these motions for 10 cities in Washington State using single-degree-of-freedom (SDOF) models of bridges, assuming that the lateral strength of the system was 50% above the minimum strength required by the AASHTO bridge design provisions (AASHTO, 2017). Kortum et al. (2022) also idealized bridges as nonlinear, SDOF oscillators, but they also considered how various site classes might affect motions, and they estimated the strength of the oscillators based on the actual properties of bridges on major highways within the Puget Sound region.

The previous research, which is summarized in Chapter 2, had some limitations.

- The SDOF oscillators neglected the resistance provided by the end abutments, including the effects of bearings, end walls and shear keys
- The SDOF oscillators used simple relationships to represent the cyclic deterioration of

reinforced concrete columns

- The SDOF models did not consider the 3D behavior of the bridges (e.g., skew, curve) and effects of simultaneous application of both horizontal components of ground motion
- Shear failure of columns was not considered
- Foundation failure, including the possibility of liquefaction, was not considered

This study aims to resolve some of these limitations by using a three-dimensional, multi-degree-of-freedom (MDOF) finite-element bridge model that captures more detailed behaviors of critical bridge components. This model is thus able to better characterize the risk to Washington State bridges in the event of an M9 earthquake. The characteristics modeled for the various bridge components were developed through the study of a bridge database compiled by the Washington Statement Department of Transportation (WSDOT) and university researchers. Furthermore, this study reviews 94 bridge plans to extract data for the modeling of the abutment structures, which was not previously available from the WSDOT database.

The main research goals of this study were to:

- Identify key characteristics (including trends) of bridges that are typical in Washington State
- Evaluate the effects of geographic location and soil class on the expected performance of a bridge with typical characteristics
- Investigate the effects of variations in the key bridge characteristics on the expected performance of typical bridges

1.3 Research Approach

The research described in this report builds directly on the results of recent research. Chapter 2 summarizes the development of the M9 baseline motions (Frankel et al. 2018), the effects of sedimentary basins (Marafi et al. 2019), and effects of local site conditions on ground motions (de Zamacona 2019). This chapter also reviews previous investigations of the effects of such ground motions on idealized SDOF bridge structures (de Zamacona 2019, Kortum et al. 2022).

Based on a newly assembled database, the distribution of key properties was established for bridges along major highways in the Puget Sound area (Chapter 3). These typical properties were used to define a typical reference bridge. The bridges were modeled using OpenSeesPy (Zhu et al. 2018) by combining finite-element methodologies used in previous research (Ranf 2007, Ramanathan et al. 2012, and Mangalathu et al. 2017). Chapter 4 reviews these methodologies and illustrates the development of the idealized reference bridge model in OpenSeesPy. This model is used as a baseline for the parametric study in later chapters.

The performance of the reference bridge model was interrogated in detail to confirm that it performed as expected. Chapter 5 presents the results of a series of analyses of the bridge model, including pushover analyses, cyclic analyses, and bi-directional, dynamic analyses. This chapter also compares the dynamic response of the MDOF model and the SDOF model from prior research (Kortum et al. 2022).

The reference bridge model was used to perform a comprehensive parametric study to evaluate the impacts on bridge performance of bridge location, site class, abutment properties and column properties. Chapter 6 describes the effect of geographic location and site class on the bridge response while Chapter 7 and Chapter 8 discusses the effect of variation of the abutment and column properties on the bridge performance, respectively.

Lastly, Chapter 9 summarizes the results of this research, provides suggestions for engineers at WSDOT, identifies its limitations, and proposes new directions for future research.

Chapter 2: Previous Research on Bridge Performance during CSZ M9 Earthquakes

This chapter provides an overview of the development of M9 ground motions as well as of previous studies that investigated the impacts of these simulated ground motions on bridges in Washington State. The previous work includes:

- The development of a methodology to simulate ground motions for a set of 30 M9 earthquake scenarios (Frankel et. al. 2018, and Wirth et. al. 2018) (Section 2.1)
- The selection of 10 cities to represent a variety of distance-to-source and basin combinations (Section 2.2)
- The evaluation of the effects of site-source distance and basins on the resulting ground motions (Section 2.3)
- The generation of soil-adjusted ground motions that consider the effects of local site conditions. (Section 2.4)
- Simulation of bridges with single-degree-of-freedom (SDOF) models (de Zamacona 2019, Kortum et al. 2022) to simulate impacts on bridges in Washington State under M9 ground motions (Section 2.5)

2.1 Modeling of Cascadia Subduction Zone M9 Earthquakes

Synthetic seismograms for magnitude 9 in the Cascadia Subduction Zone earthquakes were generated by researchers from the United States Geological Survey (USGS) and the University of Washington (UW). To develop these ground motion simulations, synthetic seismograms derived from 3D finite difference simulations were combined with finite-source, stochastic synthetics (Frankel et al. 2018). The synthetic seismograms were designed to capture a wide range of possible M9 events by including a variety of rupture features (Frankel et al. 2018). The motion's hypocenter, rupture velocity, and the number and location of sub events were all factors in the rupture simulation (Wirth et al. 2018). The ground motions were generated using a two-component model: first, massive slip motions with long durations, and second, large stress-drop magnitude 8 subevents (Frankel et al. 2018). The final simulated M9 motions were created by superimposing these two components on top of each other.

The baseline ground motion pairs were computed for 30 rupture scenarios (30 realizations) for 169 locations within the Cascadia Subduction Zone Model, corresponding to a soil profile having a V_{s30} of 1968 ft./s (600 m/s). These ground motions can be accessed through the online data repository, DesignSafe (https://www.designsafe-ci.org/) supported by the National Science Foundation, under the citation Frankel et al. (2018).

2.2 Selection of Representative Locations

In order to understand the impact of M9 ground motions in various locations over Washington State, de Zamacona 2019 and Kortum et al. 2022 selected 10 cities such that they had various site-to-source distances and sedimentary basin conditions. The locations of these cities are

shown in Figure 2.1, and their coordinates are listed in Table 2.1. Table 2.1 also provides the locations for each of the 10 cities along with the corresponding station ID and its coordinates for the seismic model (Section 2.1).

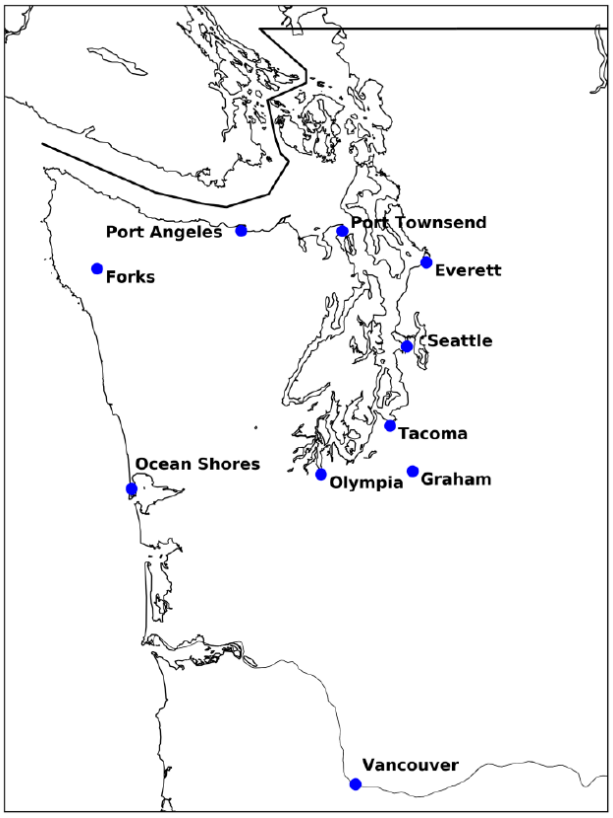

Figure 2.1: Locations of 10 representative cities (de Zamacona 2019)

The depth from the surface to a soil layer with shear-wave velocity of 2500 m/s (8200 ft/s), $Z_{2.5}$, has been defined as an indicator of the presence or absence of sedimentary basin. Locations with thick sedimentary deposits within the basin usually have lower shear wave velocities, so these locations tend to have higher values of $Z_{2.5}$ (Marafi et al. 2019). The cities were categorized into four groups based on distance to the faults and the values of $Z_{2.5}$. Cities with a $Z_{2.5}$ lower than 2.0 km were categorized as having no basin. Cities with $Z_{2.5}$ between 2.0 and 3.0 km were classified

as having a shallow basin, and cities with $Z_{2.5}$ greater than 3.0 km were classified as having a deep basin. The 10 cities were grouped as follows:

- Coastal cities (closer to the fault) outside of the basin (Forks and Ocean Shores),
- Inland cities (further from the fault) outside of basin (Olympia, Vancouver, and Graham),
- Inland cities on a shallow/medium-depth basin (Port Townsend, Port Angeles, and Tacoma), and
- Inland cities on a deep basin (Seattle and Everett).

Table 2.1: Ten representative cities in Western Washington State (de Zamacona 2019)

City Locations			**Closest Station Locations**			**Basin Depth (km)**	**Classification**
City Name	Latitude	Longitude	Station ID	Latitude	Longitude		
Forks	47.9504	-124.386	Z0FORK	47.9456	-124.566	0.76	Coastal Outside of Basin
Ocean Shores	46.9737	-124.156	Z0XOCS	46.9778	-124.154	0.98	Coastal Outside of Basin
Port Angeles	48.1181	-123.431	Z0XANG	48.1191	-123.431	2.29	Inland Shallow Basin
Olympia	47.0379	-122.901	Z00CPW	46.9717	-123.138	1.96	Inland Outside of Basin
Port Townsend	48.117	-122.76	Z0XTWN	48.1146	-122.756	2.84	Inland Shallow Basin
Vancouver	45.6272	-122.673	Z0HUBA	45.6287	-122.653	1.76	Inland Outside of Basin
Tacoma	47.2529	-122.444	Z0TBPA	47.2559	-122.368	2.86	Inland Shallow Basin
Seattle	47.6062	-122.332	Z0XWLK	47.612	-122.338	6.70	Inland Deep Basin
Graham	47.0529	-122.294	Z00GHW	47.0395	-122.274	0.20	Inland Outside

City Locations			Closest Station Locations			Basin Depth (km)	Classification
City Name	Latitude	Longitude	Station ID	Latitude	Longitude		
							of Basin
Everett	47.979	-122.202	Z0EVCC	48.0056	-122.204	3.42	Inland Deep Basin

2.3 Baseline Ground Motions

Figure 2.2 shows the response spectra of the baseline M9 ground motions for the cities listed in Table 2.1. The spectral accelerations shown in each figure correspond to the geometric mean (of the 30 realizations) of both the North-South and East-West components at a given period.

The coastal locations have large spectral accelerations for low periods, but the spectral accelerations rapidly decrease with increasing periods for periods above 0.3 to 0.5s. None of the coastal locations are located on sedimentary basins. The inland locations that are located outside of basins have similar spectral shapes, but the spectral accelerations are much lower.

The amplification of the ground motion by the sedimentary basins at longer periods (>1.0 sec) can be seen in Figure 2.2. In these locations, the spectral acceleration increases once the period reaches 1.0 sec, demonstrating amplification at the longer periods.

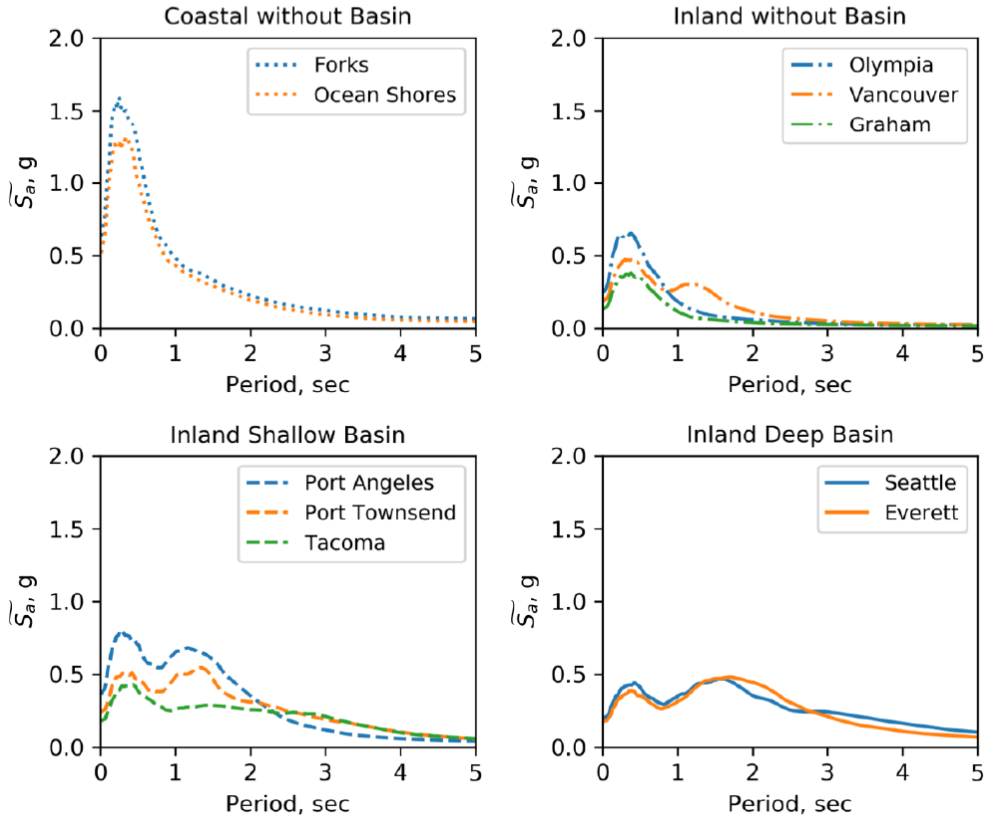

Figure 2.2: Response spectra from baseline simulated M9 ground motions for the city categories (de Zamacona 2019)

2.4 Soil-Adjusted Ground Motions

Since the M9 baseline ground motions described above were developed for a site with a soil profile having a V_{s30} value of 1968 ft/s (= 600 m/s, corresponding to site class C in NEHRP site classes), this section describes the modifications made to the baseline ground motions in order to consider the effect under various soil types within Washington State.

Figure 2.3 shows the map of King County, WA, and the various soil classes found there. Large portions of major highways in Washington State lie in areas that are categorized as site class C, D, E, and F profiles. As a result, alex grant from the United States of Geological Survey (USGS)

generated soil-adjusted M9 ground motions that capture the effects of various soil site classes (de Zamacona 2019).

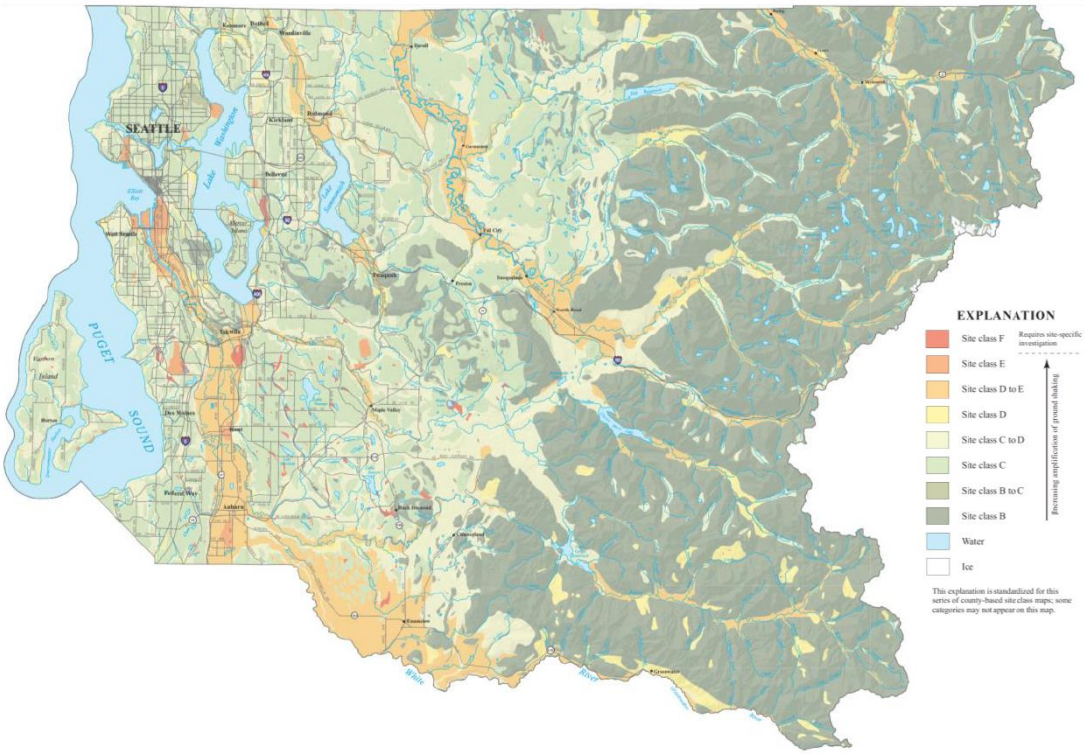

Figure 2.3: Site class map of King County, Washington (Palmer et al. 2007)

The solid-adjusted M9 ground motions were generated using equivalent site response analysis and used the soil profiles provided by Pacific Northwest shear-wave velocity profiles by Adhi et al. (2017). The soil profiles shallower than 32.8 feet and deeper than 3281 feet were removed due to insufficient data. Figure 2.4 shows the number of soil profiles within each site class before and after the reduction.

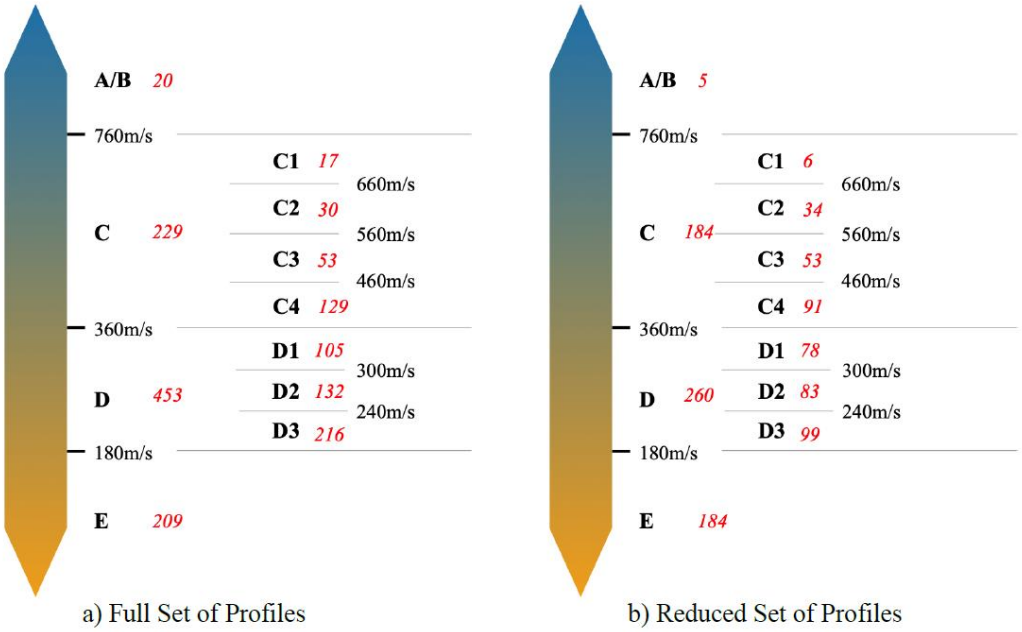

Figure 2.4: Data available from Ahdi et al. for PNW velocity profiles (de Zamacona 2019)

Figure 2.5 illustrates the median spectral accelerations of the geometric mean of the two horizontal components for the 30 baseline and the soil-adjusted M9 grounds of each selected soil subclass (C2, C4, D1, D3). In each soil subclass in Figure 2.5, 30 soil profiles were randomly selected from the reduced set in Figure 2.4. For all the 10 cities, site class C2 has the closest value to the baseline spectral accelerations, which is expected as site class C2 has the V_{s30} that are closer to that used to develop baseline M9 ground motions. At longer periods, the effect of soil site class starts to become apparent. The softest site class that was considered, D3, has the highest spectral acceleration at periods greater than 1.0 sec, followed by site class D1, C4, and C2. This phenomenon is due to the amplification of softer soils at longer periods. Notably, the site class D3 ground motions deamplify the strong short period content of the ground motions for the coastal locations.

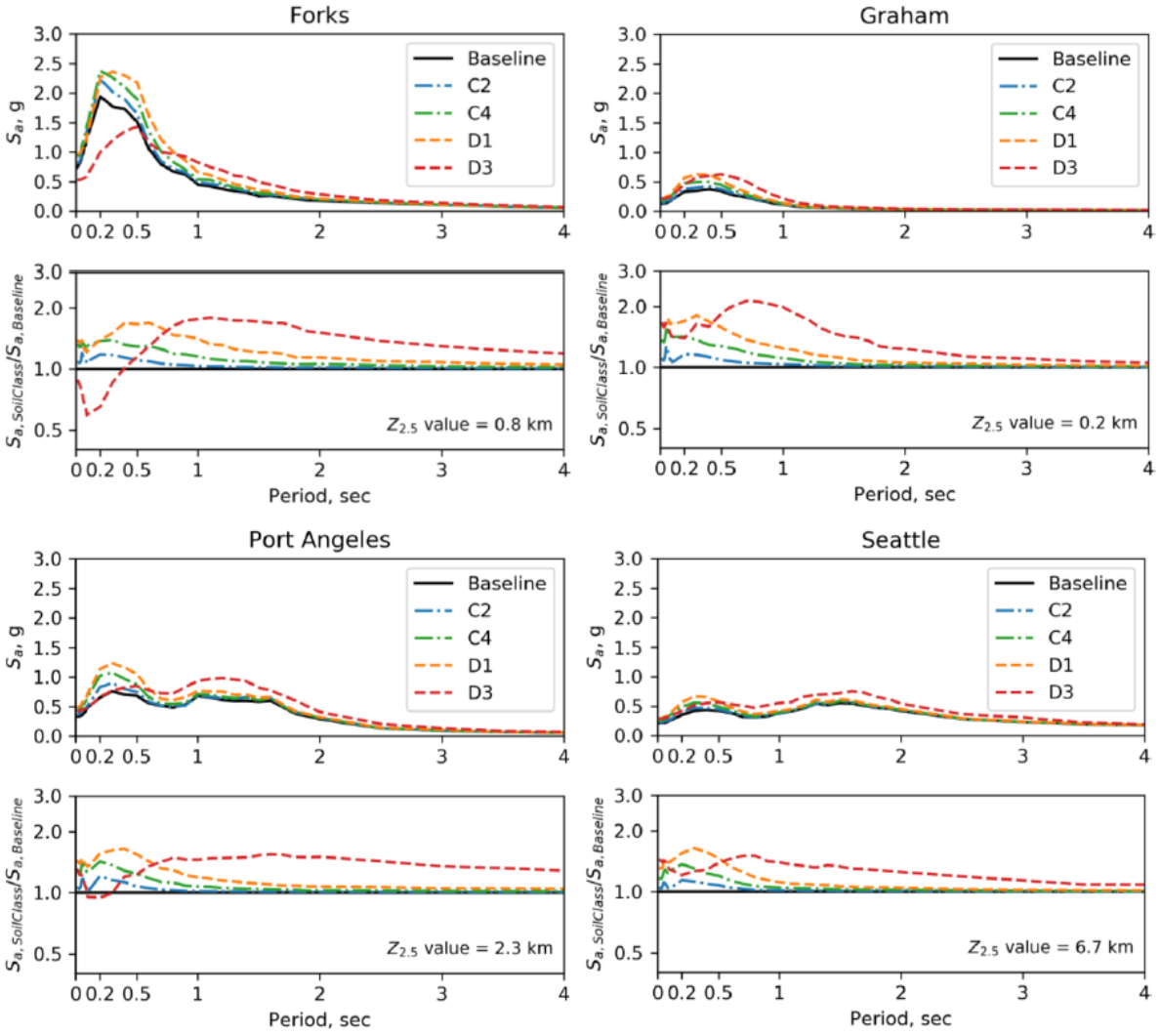

Figure 2.5: Median spectral accelerations for site adjusted M9 ground motions and median spectral acceleration normalized by the baseline ground motion spectra (de Zamacona 2019)

From the site classes listed in Figure 2.4, site class C2, C4, D1, and D3 were selected for the parametric studies in Chapter 6 to investigate the effect of different site conditions on M9 ground motions. These 4 site classes were chosen because their V_{s30} ranges are commonly found within Washington State. Furthermore, for computational expediency, 10 soil profiles were randomly selected from the reduced set in Figure 2.4 for each site class to use in the analyses. As

discussed later (Section 6.2), each of the 10 soil profiles in each of the four site classes were used with the 30 M9 earthquake realizations to create the ground motion sets used for analysis here.

2.5 Effects of M9 Ground Motions on SDOF Idealized Bridge Models

In order to understand the impact of the M9 earthquakes on bridges in Western Washington State, de Zamacona (2019) and Kortum et al. (2022) developed single-degree-of-freedom models in OpenSees. The strengths of de Zamacona's (2019) oscillators were set to be 50% higher than the 2019 WSDOT code-minimum values for bridges. Her results showed that structures with short-period were severely damaged in cities along the fault, whereas those with longer-period were severely damaged in cities located on sedimentary basins.

Kortum et al. (2022) further improved the single-degree-of-freedom oscillator by including more detailed model parameters and covered a wider range of oscillator periods, locations, and soil types to better understand the impact of M9 earthquakes on bridges. The model was simplified to a spring with a given stiffness and considered the deterioration of columns by including the Modified Ibarra-Medina Krawinkler (IMK) Deterioration Model with Peak-Oriented Hysteretic Response material in OpenSees.

The study results showed spectral acceleration amplification effects can be observed in cities that lie on top of sedimentary basins at higher periods (> 1 sec) and that the strong shaking along the coast was potentially damaging to bridges. He also found that most bridges in the database had exceeded the strength required by the design code and performed better than expected.

The following sections describe detailed modeling methodologies of the SDOF model from Kortum et al. (2022).

2.5.1 Development of SDOF Bridge Models

The identification of key properties of the idealized SDOF model was based on the lifeline bridge database compiled by WSDOT engineers with statistical studies completed by UW, and Washington State University researchers. Kortum et al. (2022) utilized the compiled database and conducted regression analysis to approximate the relationship between bridge strength and bridge period for the lifeline bridges. The stiffnesses were calculated based on the recommendations of Elwood and Eberhard (2009), the masses were estimated from detailed calculations for typical bridges, and the strengths were estimated by moment-curvature analysis with the column properties provided by the database. Figure 2.6 shows the relationship between normalized lateral strengths (with respect to bridge weight) and periods of the old (pre-1976) and new (1976-2018) bridges.

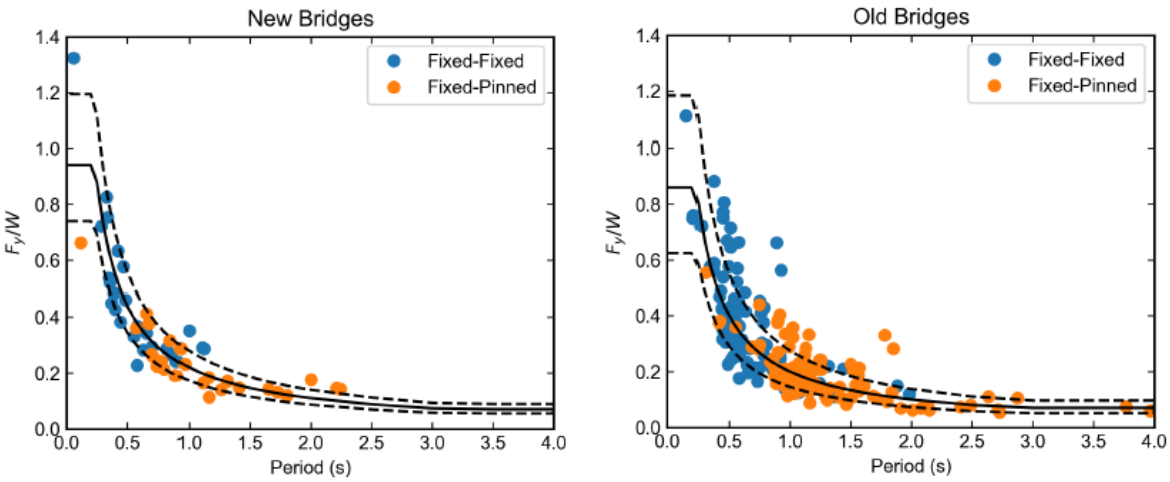

Figure 2.6: Normalized base shear strength for new and old bridges (Kortum 2021)

The SDOF model used the Modified Ibarra-Medina-Krawinkler (IMK) Deterioration Model with Peak-Oriented Hysteretic Response material in OpenSees to consider the deterioration of bridge columns. The IMK model required several input parameters to define the backbone curve (Figure 2.7).

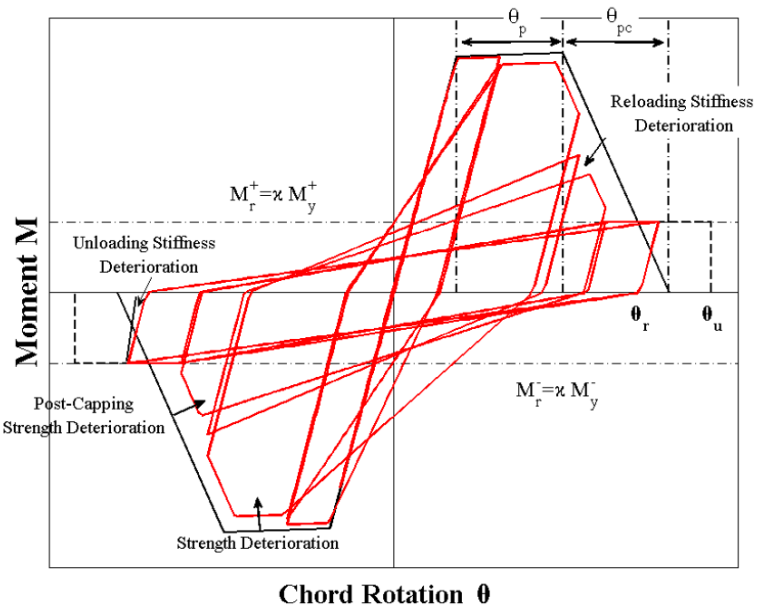

Figure 2.7: IMK model behavior (Lignos and Krawinkler 2012)

In order to model the behavior of the bridge columns, the response of the IMK model was calibrated to match the cyclic force-displacement response of selected reinforced concrete circular columns from UW-PEER Structural Performance Database (UW-PEER 2020). In particular, two of the input parameters, λ and θ_p, od the IMK model were used for the calibration against the transverse reinforcement ratio. A series of calibration results for the cyclic loading tests are shown in Figure 2.8.

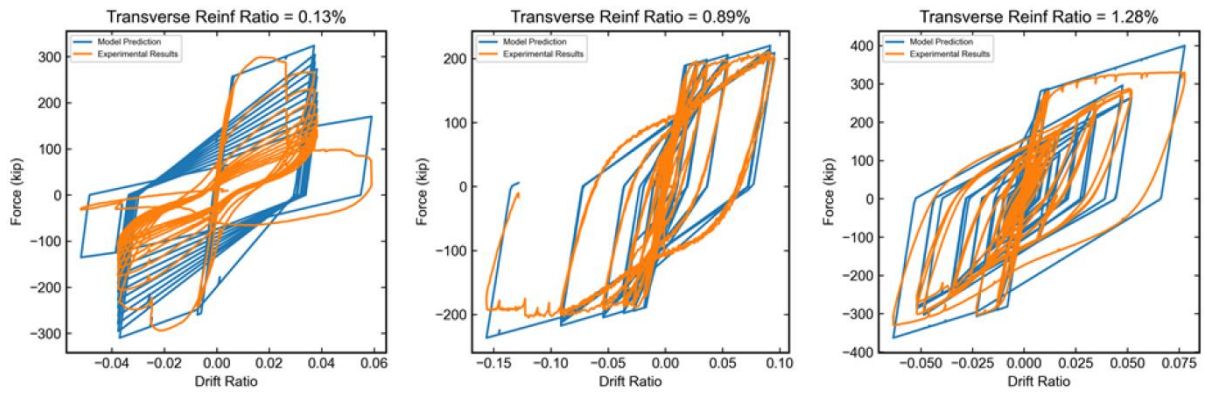

Figure 2.8: Fully calibrated IMK results for a lightly reinforced column (left), moderately reinforced column (center), and heavily reinforced column (right) (Kortum 2021)

2.5.2 Effects of M9 Ground Motions on SDOF Idealized IMK Bridge Model

Ground motions for 10 cities (Table 2.1), 30 scenarios, 4 site classes, and 30 soil profiles for each site class were considered to study the effects of M9 earthquakes on highway bridges in Washington. The study found that the response of the model varied between different cities and site classes.

Figure 2.9 shows the median ductility demands of older bridges for different site classes in various cities. The bridges tend to have higher response in coastal cities that are closer to the fault line at lower periods (< 0.5 sec). For various site classes, the response of the model has greater ductility demands at sites that have softer soil (site class D3) at higher periods (around or greater than 1.0 sec).

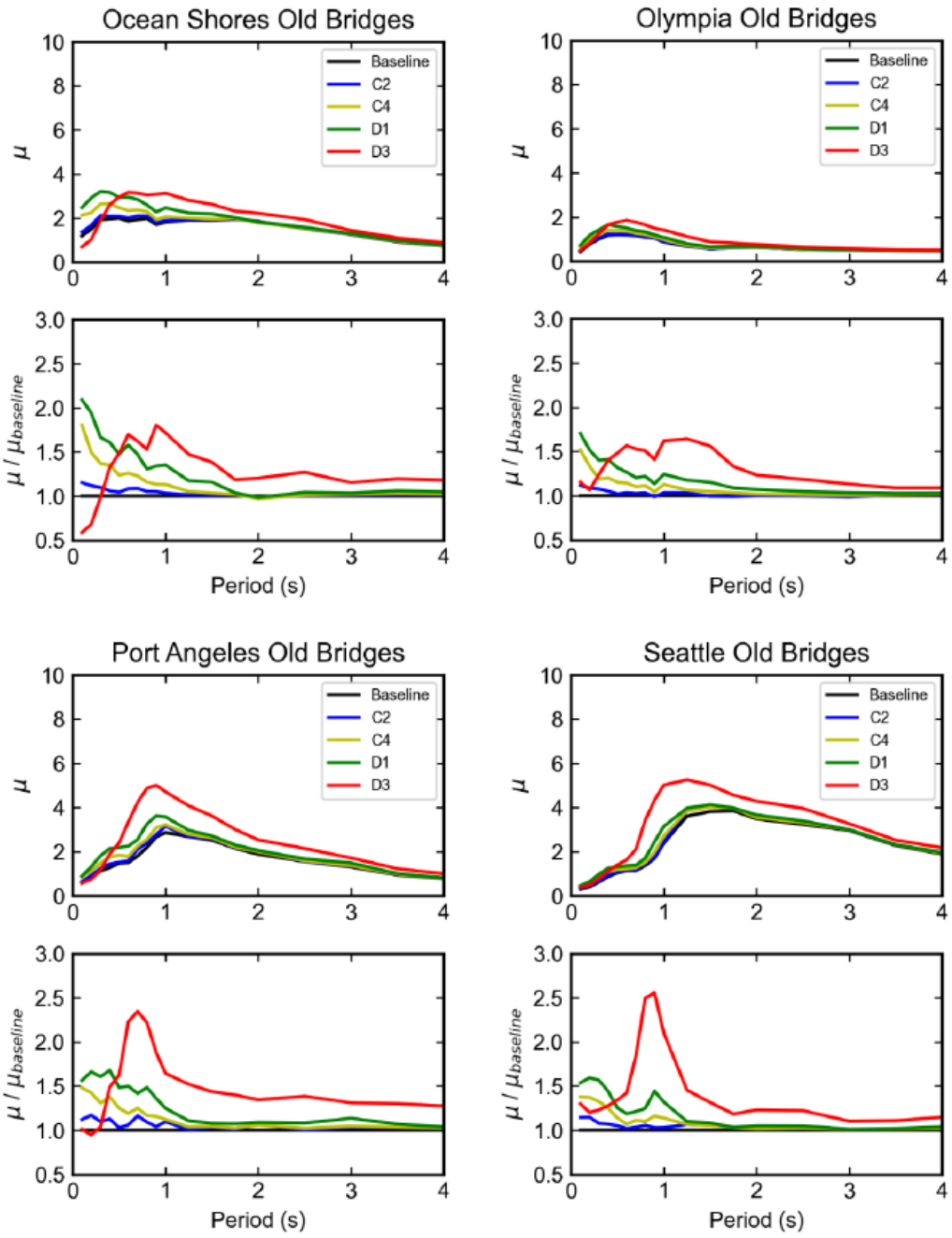

Figure 2.9: Median displacement ductility demands and median displacement ductility demands normalized by baseline values for various soil types (Kortum 2021)

Although the SDOF model from Kortum et al. (2022) intended to reflect the bridge behavior by studying the bridge inventory from WSDOT and including the deterioration model,

the results come with important caveats leaving opportunities for further works. In particular, the models did not consider the existence of the abutments and the shear or flexure-shear failure of bridge columns. Thus, a multi-degree-of-freedom model that includes more detailed modeling components could predict the response of bridges more accurately.

Chapter 3: Properties of Typical WSDOT Bridges

This chapter provides statistics of key properties of bridges that are documented within a database compiled by the Washington State Department of Transportation (WSDOT) engineers and University of Washington researchers. The database provides properties of 609 structures along major highways in the Puget Sound region, including 582 highway bridges. These bridges were located along I-90 between Seattle and Snoqualmie Pass, I-5 between Tacoma and Everett, I-405, as well as portions of State Route 512 and State Route 167 (Figure 3.1).

Figure 3.1: Locations of bridges documented in WSDOT database (Kortum 2021)

WSDOT engineers extracted the structural properties for these bridges from the bridge plans. The information compiled by WSDOT was later supplemented with additional properties collected by the researchers from the University of Washington. This database will be referred to in this report as the "WSDOT Bridge Database".

- Section 3.1 provides properties of the highway bridges within the WSDOT Bridge Database.
- Of the 582 highway bridges, 74 (12.7%) had only one span, and 508 (87.3%) had multiple spans. The vast majority (416 bridges, 81.9%) of these multiple-span bridges were supported by columns. Section 3.2 discusses the properties of the 416 multi-span bridges with columns.
- The original WSDOT database did not include information about the bridge abutments, so the research team identified the abutment properties for 94 bridges with multiple spans by reviewing the bridge plans provided by WSDOT. These abutment properties are discussed in Section 3.3.
- The properties of these bridges were used to identify typical characteristics of bridges within the WSDOT database. A set of typical bridge properties (Section 3.4) was then selected based on this data and used to develop a model of a typical bridge (Chapter 4).

3.1 Properties of Bridges within WSDOT Database

The WSDOT Bridge Database documents key properties for 582 highway bridges, 4 culverts, 10 tunnels, 2 detention vaults, and 1 pedestrian bridge. This thesis discusses only the properties of the highway bridges. Among other properties, the database documents the year of

construction, superstructure type, column dimensions, column transverse and longitudinal reinforcement, and number of spans of each bridge.

3.1.1 Year of Construction

The year of construction of the highway bridges in the WSDOT Bridge Database ranges from 1930 to 2018. As shown in Figure 3.2, nearly 70% of the bridges (398, 68.4%) were built between 1960 and 1975. Only 37 (6.4%) of these bridges were built before 1960, 83 (14.3%) were built between 1976 and 2000, and 64 (11%) bridges were built after 2000.

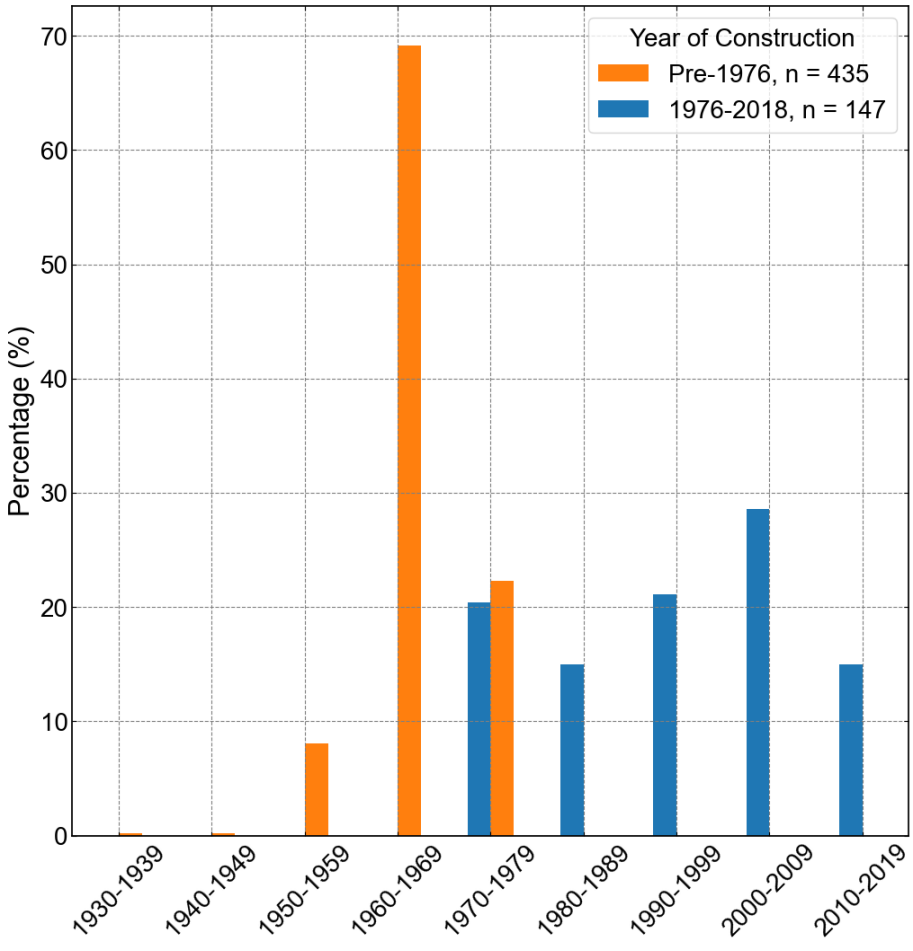

Figure 3.2: Year of construction

Earthquake design practice in Washington State changed significantly around 1976 following the 1971 San Fernando earthquake. For the purpose of illustrating the differences in properties between bridges that were built before and after the design practice changed, the statistics presented in this chapter are usually provided for two categories: pre-1976 (435 bridges, 74.7%) and 1976-2018 (147 bridges, 25.2%). Table 3.1 provides overall statistics for the bridge inventory for these two year-of-construction categories.

Table 3.1: Key properties of WSDOT bridge database

	Total	**pre-1976**	**1976-2018**
Number of Highway Bridges	582	435	147
Number of Single-Span Bridges	74	34	40
Number of Bridges with Multiple Spans	508	401	107
Number of Bridges Supported by Columns	416	318	98
Number of Bridges Supported by Circular Columns	318	274	44

3.1.2 Superstructure Type

The database provided information for 582 bridges, but 18 of those had two superstructure types, so for the purpose of compiling superstructure statistics, each superstructure was counted independently, resulting in 600 (582+18) incidences of superstructure type.

As shown in Fig. 3.3, nearly 90% (538, 89.7%) of the superstructures were constructed of concrete, with the most common types being prestressed concrete girders (294, 49.0%), concrete boxes (154, 25.7%), concrete slabs (86, 14.3%), and concrete tee beams (21, 3.5%). An additional 39 (6.5%) bridges had steel superstructures, including 35 that were steel girders. The percentage of prestressed concrete girder bridges, concrete slab bridges, and concrete Tee-beam bridges did not differ greatly between the pre-1976 and 1976-2018 age ranges. However, compared with superstructures in the older age range, bridges built more recently had approximately half the percentage of concrete box superstructures and approximately three times the percentage of steel superstructures.

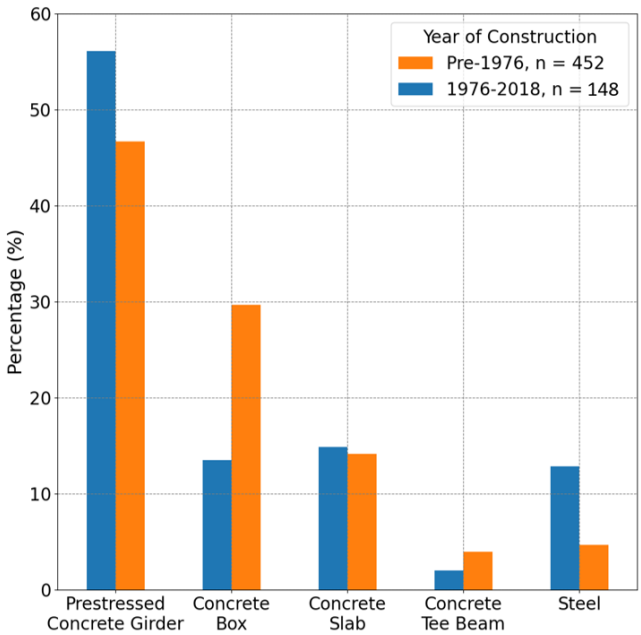

Figure 3.3: Superstructure types

3.1.3 Substructure Type at Intermediate Supports

The substructure at the intermediate supports was not documented clearly for one of the 582 bridges, so the substructure statistics are reported for 581 bridges. A total of 74 bridges had a single span and therefore did not have any intermediate supports. Out of 508 bridges with multiple spans, 416 (71.6%) of the intermediate supports contained at least one column, with 102 (17.6%) bridges supported by single-column bents and 314 (54.0%) supported by multiple-column bents. A smaller number of other bridges are supported by pier walls (44, 7.6%) or piles (42, 7.2%), or have unknown support types (6, 1.0%). The statistics did not vary greatly between the two age ranges.

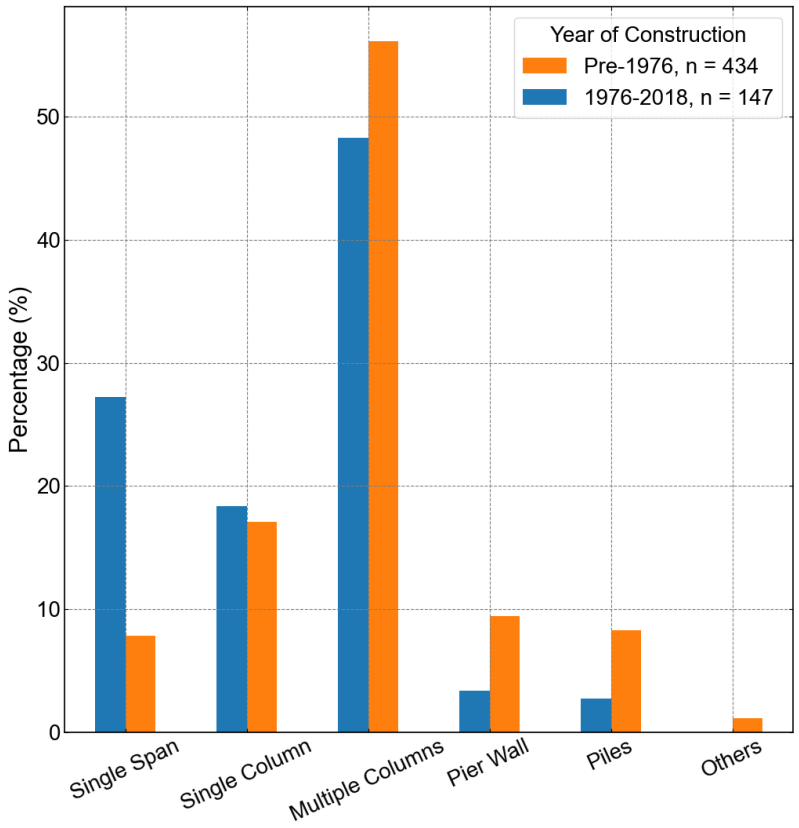

Figure 3.4: Substructure types

3.1.4 Span Continuity

Span continuity refers to the end conditions of the spans within the superstructure. A continuous superstructure can resist negative moments at the end of each span, whereas in simply supported structures, the end moment is equal to zero and there is usually a joint at each intermediate support. The presence of a joint also limits the forces that are transmitted along the length of the superstructure to the abutments. The span continuity was documented for 504 of the 508 multi-span bridges, and one bridge had a portion that was continuous and a portion that was simply supported, so statistics were computed for 505 incidences of span continuity.

As can be seen in Figure 3.5, most multi-span bridges (80.2%, 405 out of 505) have continuous spans. The percentage of multi-span bridges with continuous spans was higher for modern bridges (97.2%, 103 bridges) than older bridges (75.7%, 302 bridges).

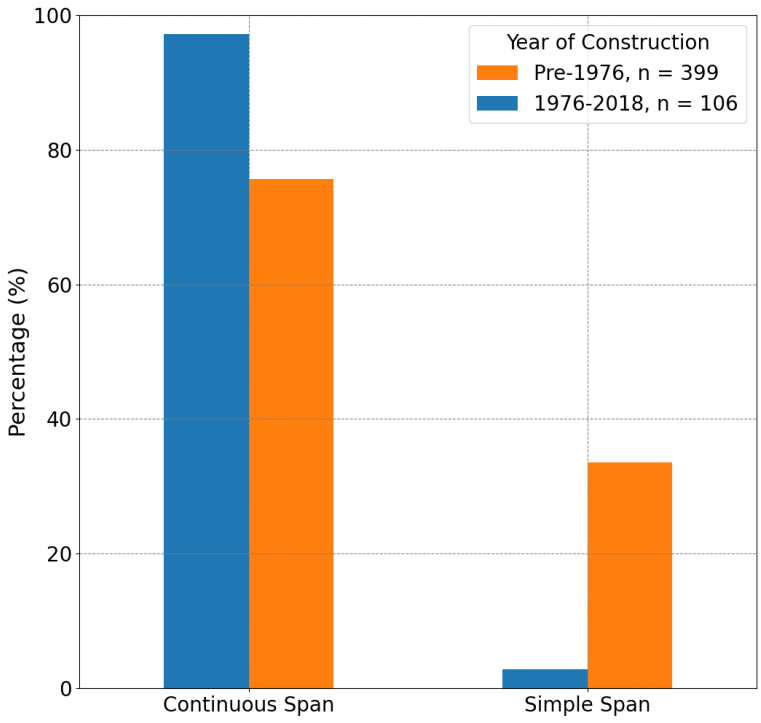

Figure 3.5: Span continuity for multiple-span bridges

3.2 Properties of Bridges with Columns

If bridges in which the deck does not unseat, most earthquake damage has been observed in the columns. The 416 bridges with columns are discussed in this section. Out of the 416 bridges with columns, 318 (76.4%) of them were built before 1976, whereas 98 (23.6%) of them were built from 1976-2018 (Figure 3.6).

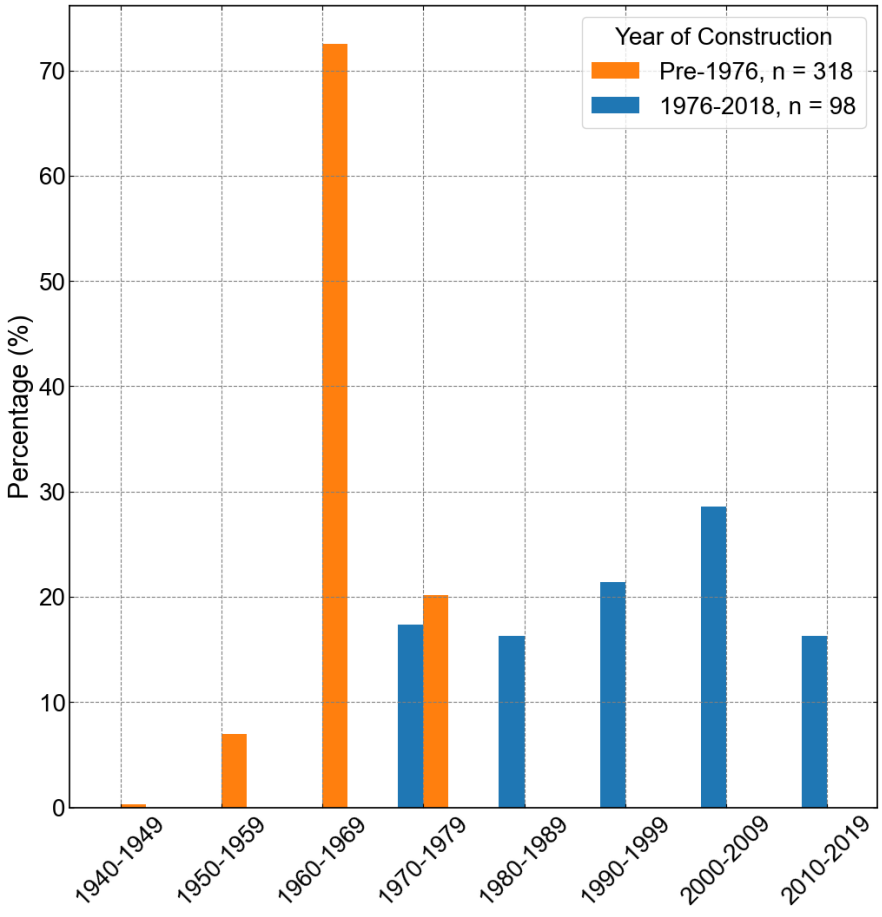

Figure 3.6: Years of construction (bridges with columns)

3.2.1 Number of Spans

The number of spans for bridges with columns at intermediate supports are shown in Figure 3.7. Although the bridges have a wide variety of span numbers, ranging from 2 to 48, most of them fall between 2 to 4 for bridges in both eras. Out of these 416 bridges, 316 (76%) have span numbers within this range. The main difference between the age categories was that the percentage of bridges built with two spans was larger for the 1976-2018 age range than the earlier age range. This difference might be attributable to the increased spans that are possible for newer bridges built of stronger materials.

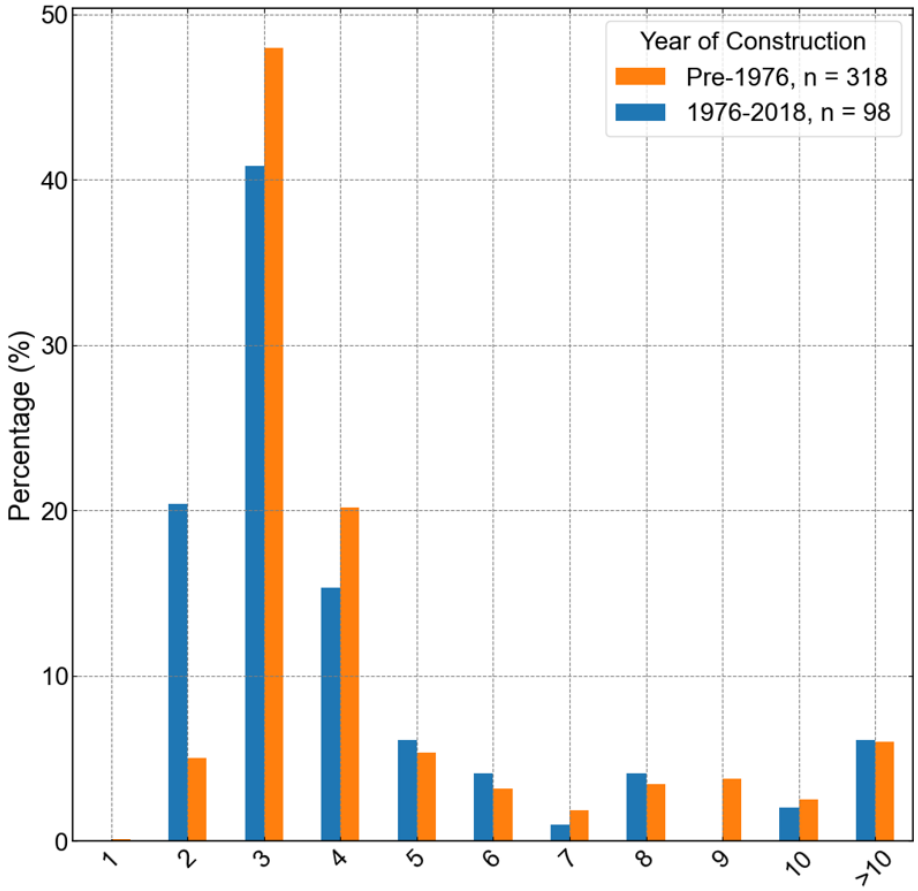

Figure 3.7: Number of spans

3.2.2 Foundation Type at Intermediate Piers

Foundation types are usually related to the bearing capacity of the soils and to the space available to construct the foundations. In most cases, spread footings are used at sites with stronger/stiffer soils, whereas shafts and piles tend to be used in structures located on softer soils. Additionally, some bridges have a combination of foundation types, which is commonly found in bridges whose decks were expanded later.

As shown in Figure 3.8, for both newer and older bridges, spread footings are the most common foundation types (43% for older and 37% for newer bridges).

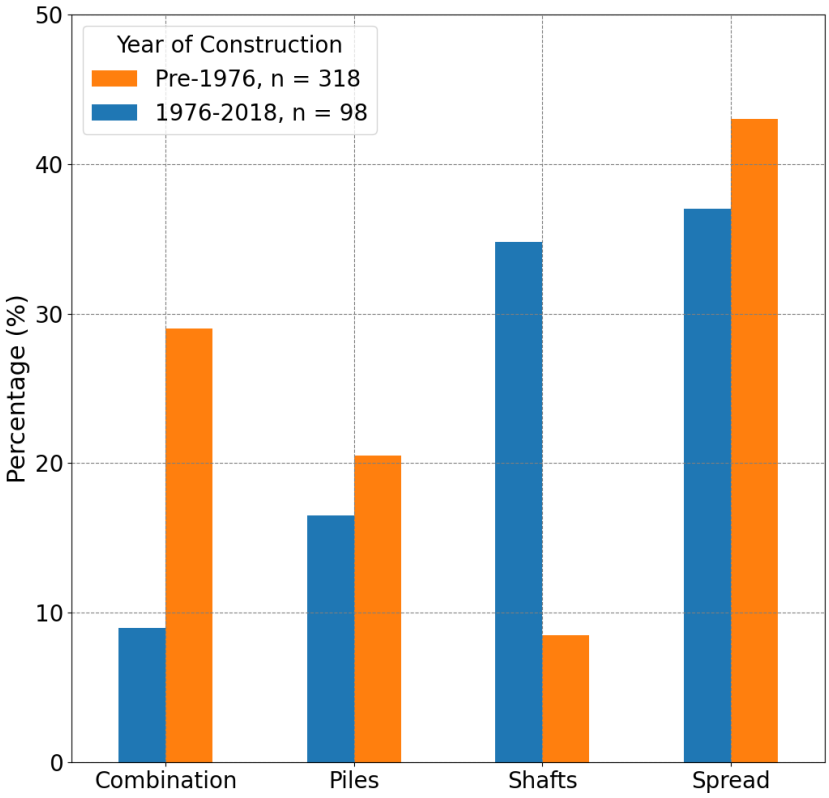

Figure 3.8: Intermediate bent foundation types

3.2.3 Column Shape

The cross-section shapes of the columns were divided into three groups: circular, rectangular, and others (e.g., octagonal or oval) (Fig. 3.9). Circular column cross-sections were most common (348, 76%), particularly for bridges built before 1976 (274 bridges, 86.2%). The percentage of circular columns was lower for more recently constructed bridges (44 bridges, 44.9%). For newer bridges, circular and rectangular columns have about the same percentage (~40%).

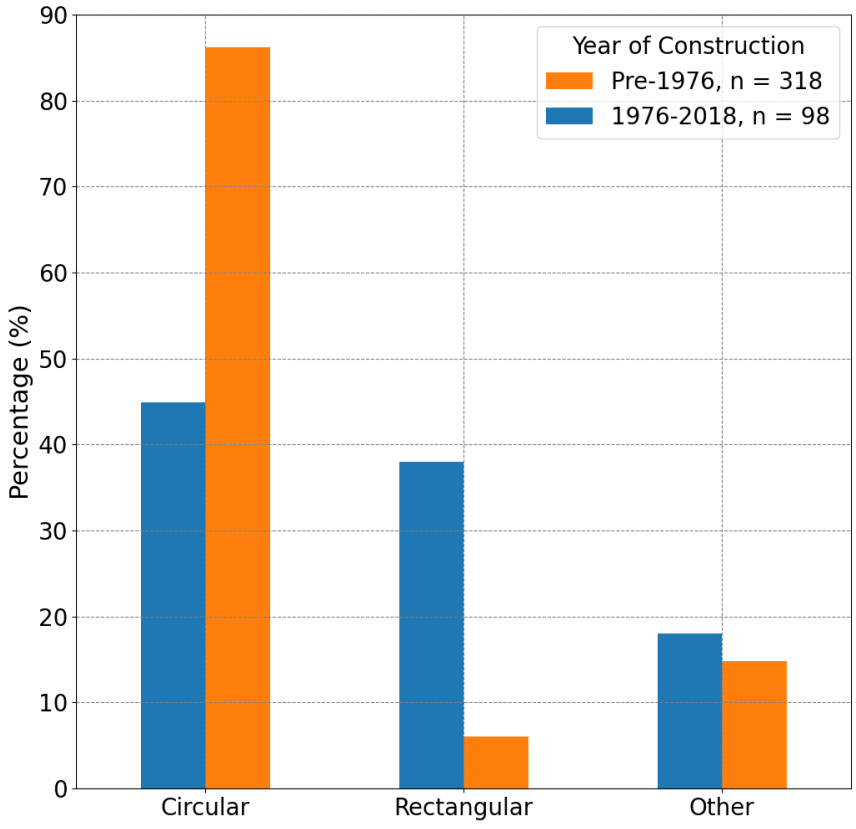

Figure 3.9: Column cross-section shapes

3.2.4 Diameters of Circular Columns

For bridges that have intermediate supports consisting of circular columns and with available diameter data (n=318), almost all of them have cross section diameters ranging from 30 to 60 inches for older columns (306, 93%) and newer columns (77, 88%). Furthermore, approximately half of the columns had a diameter between 31 (space) and 40 inches.

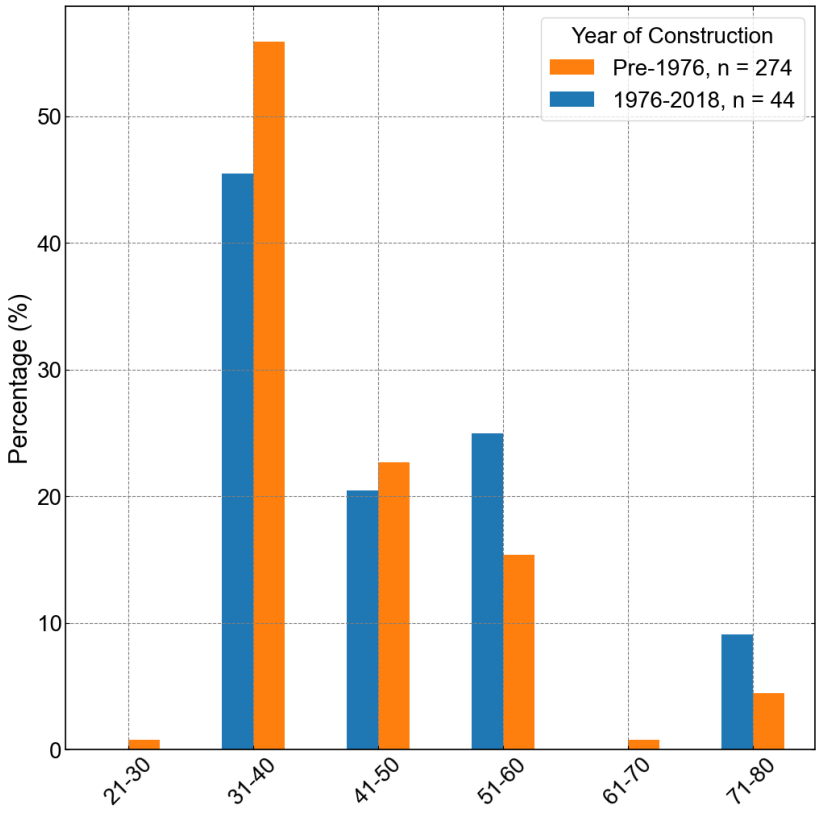

Figure 3.10: Distribution of diameters for bridges with circular columns

3.2.5 Number of Columns at Intermediate Piers

The distribution of the number of columns at each pier are shown in Figure 3.11. When this number is equal to 1, the bridge is categorized as a single-column bridge, and it is categorized as a multiple-column bridge when this number is greater or equal to 2. As shown in Figure 3.11, regardless of the age of the bridges, the number of columns supporting the intermediate bent mostly lies within 1~5, with nearly 83.2% (254) of the older bridges in this range and almost all (85) of the newer bridges.

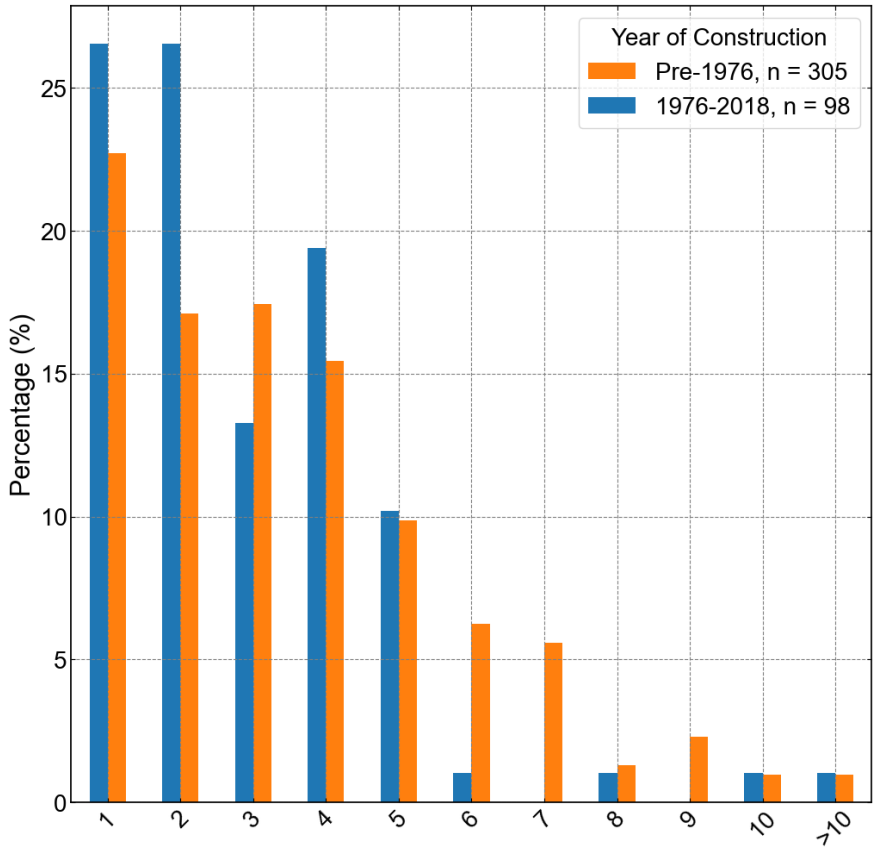

Figure 3.11: Number of columns at each pier

3.2.6 Effective Column Height

The WSDOT Bridge Database provided column heights for the shortest and tallest column on each bridge. The column heights vary within each bridge, in order to capture the overall column behavior with an idealized bridge that has columns with the same length, Kortum et al. (2022) proposed the calculation of effective column height. A bridge with all of its columns having the effective column height provides approximately the same stiffness compared to the bridge with its original varying heights.

Effective column height information is summarized in Figure 3.12, with most of them ranging between 11~30 feet for bridges in both eras. Furthermore, effective column heights between 21~25 feet are particularly common (89, 27.9% for older bridges and 29, 30.5% for newer bridges).

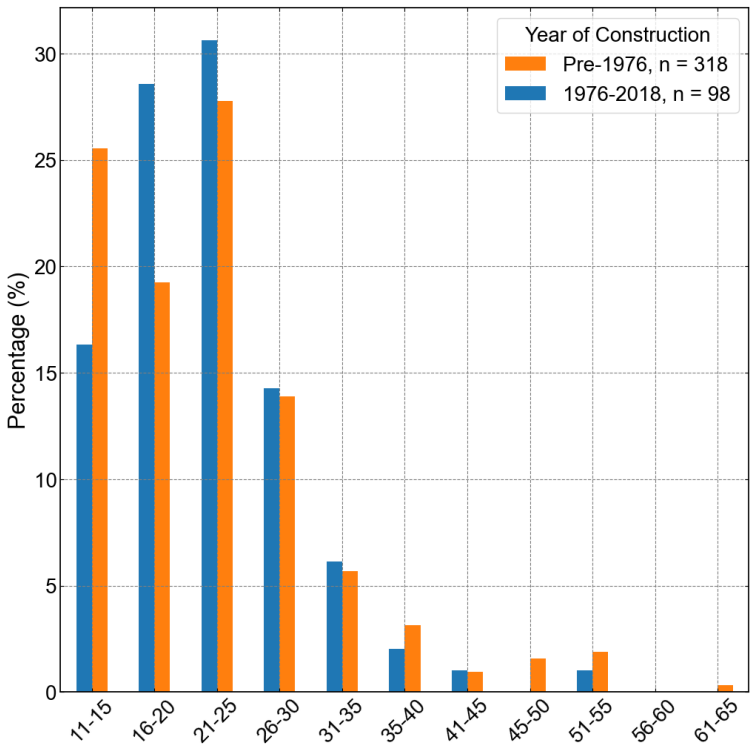

Figure 3.12: Effective column heights

3.2.7 Longitudinal Reinforcement Ratio

The longitudinal reinforcement ratio strongly affects the flexural strength of bridge columns. The longitudinal reinforcement ratio is calculated as the total area of longitudinal reinforcement, normalized by the gross-section area of the column. Although the reinforcement ratio varies greatly, the majority (70%) of bridge column reinforcement ratios for both new and old bridges fall between 1% and 2.5%. Furthermore, the longitudinal reinforcement ratio does not appear to differ considerably between old and new bridge columns (Figure 3.13).

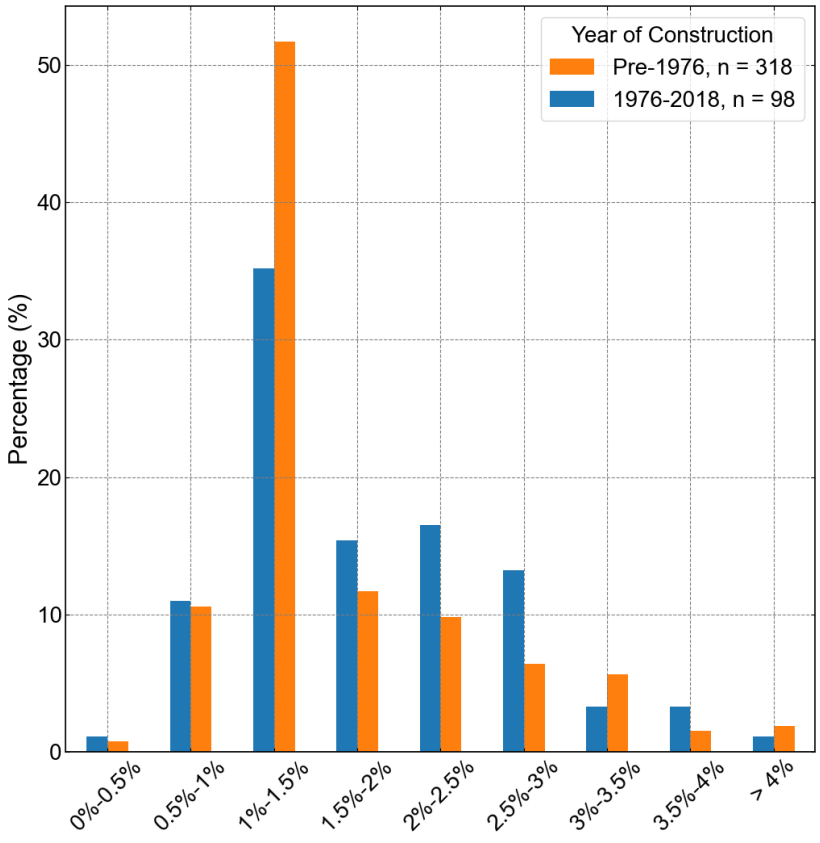

Figure 3.13: Longitudinal reinforcement ratio of shortest columns

3.2.8 Transverse Reinforcement Ratio

Transverse reinforcement enhances the ductility of reinforced concrete columns by providing confinement to the concrete within the spiral and by providing lateral support to the longitudinal flexurement. As the column height information, WSDOT provided reinforcement ratios for the shortest and tallest columns of bridges.

The transverse reinforcement ratio is computed as the ratio of the volume of transverse bars to the volume of the confined concrete core, with the confined core extending to the centerline of the transverse reinforcement. Compared to longitudinal reinforcement ratio, the difference of transverse reinforcement ratio between older and newer bridges is far more significant. Most older bridge columns (~85%) have a reinforcement ratio between 0~0.5% while for newer bridge columns, nearly 50% of them have a ratio greater than 1.0%. This phenomenon reflects the change of design code that happened in the mid-1970s.

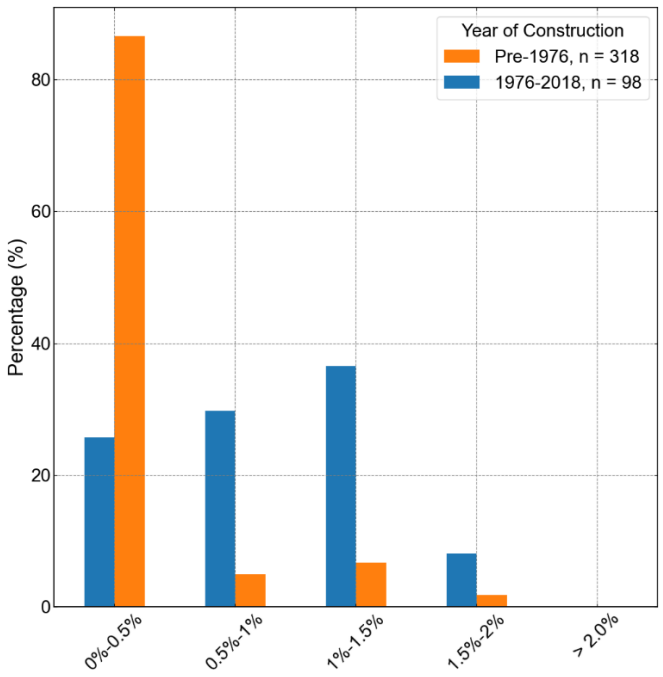

Figure 3.14: Transverse reinforcement ratio of tallest columns

3.2.9 Column Retrofit

The determination of whether a bridge had experienced a column retrofit (Figure 3.15) is based on the information of column jacket existence provided by WSDOT. Bridges with column jackets are classified as retrofit, whereas those without are classified as non-retrofit. The reported data shows more than half of the bridges (~64%) built before 1976 are non-retrofitted, and as expected, almost none of the newer bridges (1%) had been retrofitted.

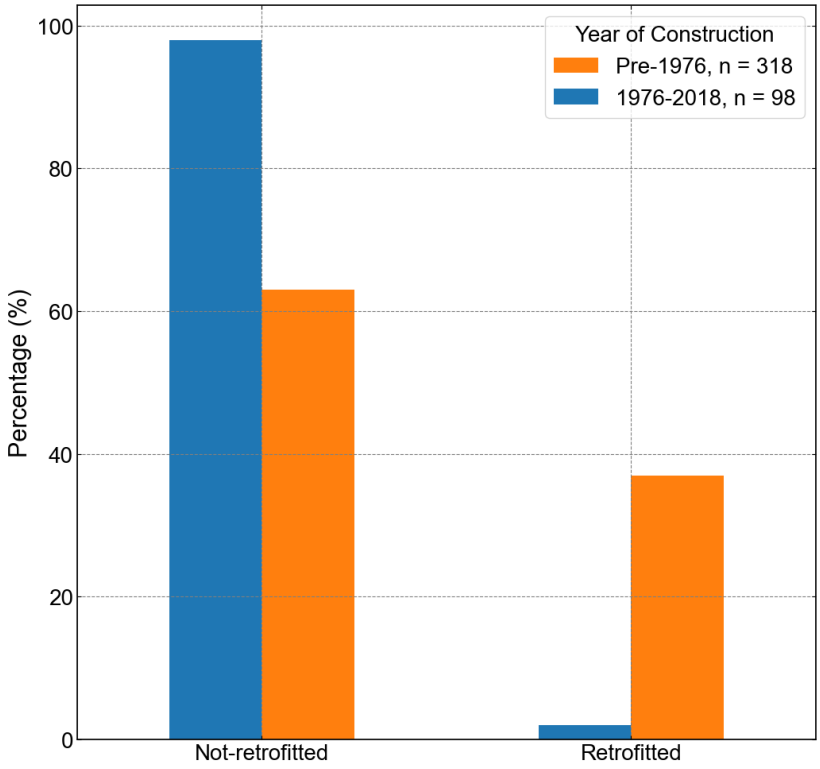

Figure 3.15: Percentage of retrofitted column-supported bridges

3.3 Abutment Properties

Key features of the abutments were identified from the construction documents for 94 out of the 416 bridges with columns in the bridge inventory. The list of selected bridges could be found in Appendix A. For these bridges, the researchers compiled information about the abutment type, abutment foundation type, and shear key existence. Out of these 94 bridges, 75 (79.8%) were built before 1976 and 19 (20.2%) were built between 1976 and 2018. In this report, this subset of 94 bridges will be referred to as the "Abutment Database." The bridges were selected such that the distribution of year-of-construction and intermediate pier type would be similar for the 94 selected bridges and the bridges supported on columns. Figure 3.16 and Figure 3.17 show that these two bridge populations had roughly similar years of construction and intermediate support foundation type distribution.

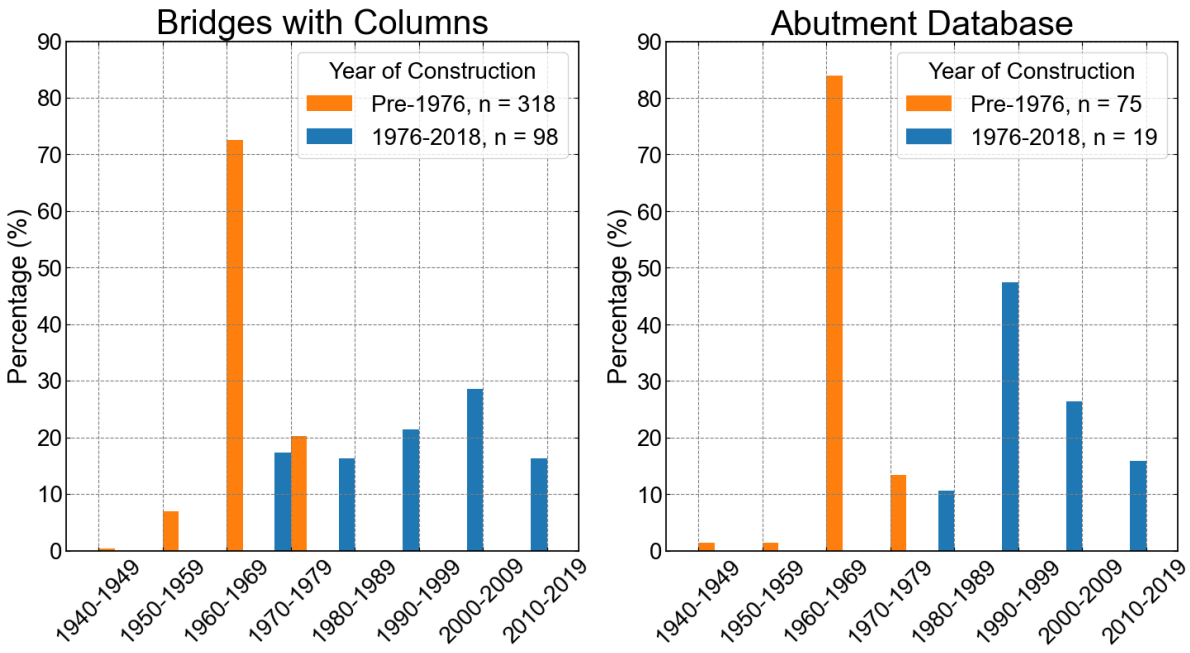

Figure 3.16: Years of construction for Bridges with Columns (left) and Abutment Database (right)

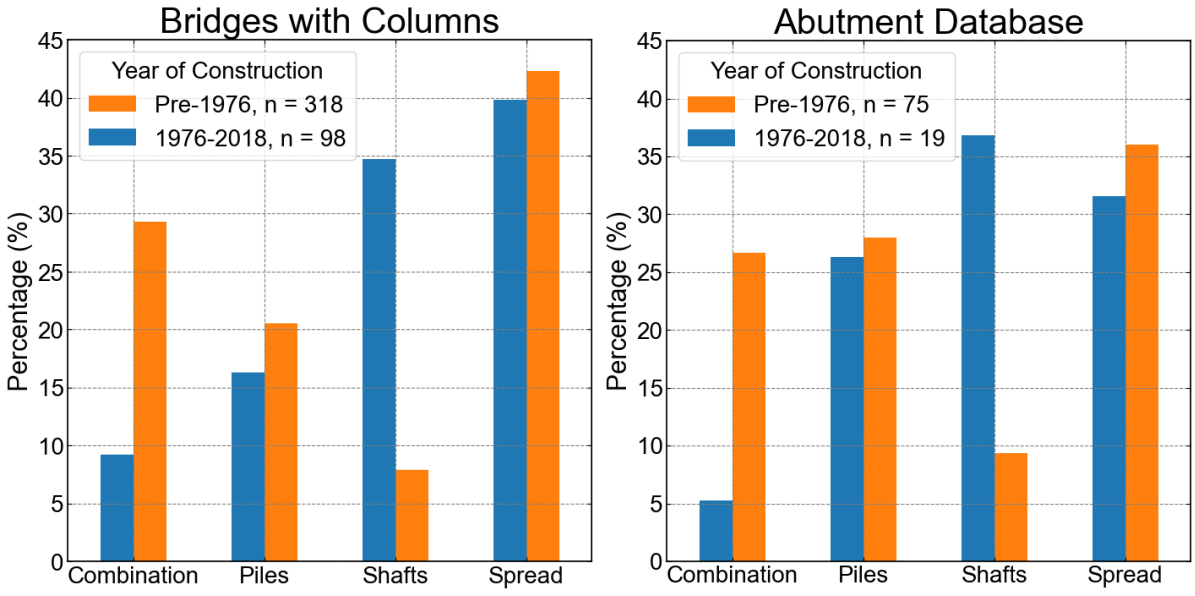

Figure 3.17: Intermediate foundation types for Bridges with Columns (left) and Abutment Database (right)

3.3.1 Abutment Type

Abutment type is one of the most important features that determines the resistance provided by the abutment. Detailed information about the various abutment types can be found in the bridge modeling chapter (Section 4.4). L-type abutments were the most common type of abutment in general, and their percentages were similar for both the older (41/75 bridges, 54.6%) and newer bridges (9/19 bridges, 47.3%). Semi-integral abutments were second most commonly used, but they were more frequent in newer bridges. Semi-integral abutments were used in 16% (12) of the older bridges and 47.3% (9 bridges) of newer bridges (same percentage as for L-type abutments).

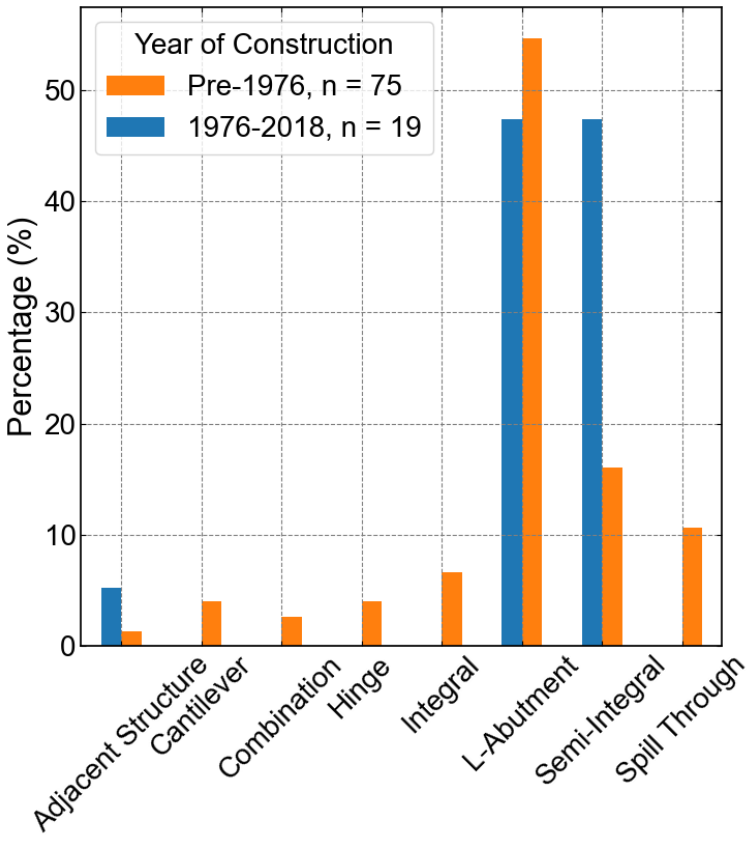

Figure 3.18: Abutment types

3.3.2 Abutment Foundation Type

The abutment foundation plays an important role in providing lateral-load resistance for an abutment. Figure 3.19 shows that, for both older and newer bridges, spread footings and piles are the most common abutment foundation types, followed by shafts and combinations of spread and piles. The main difference between the two populations is that new bridges tend to have piles less frequently and shafts more frequently than older bridges.

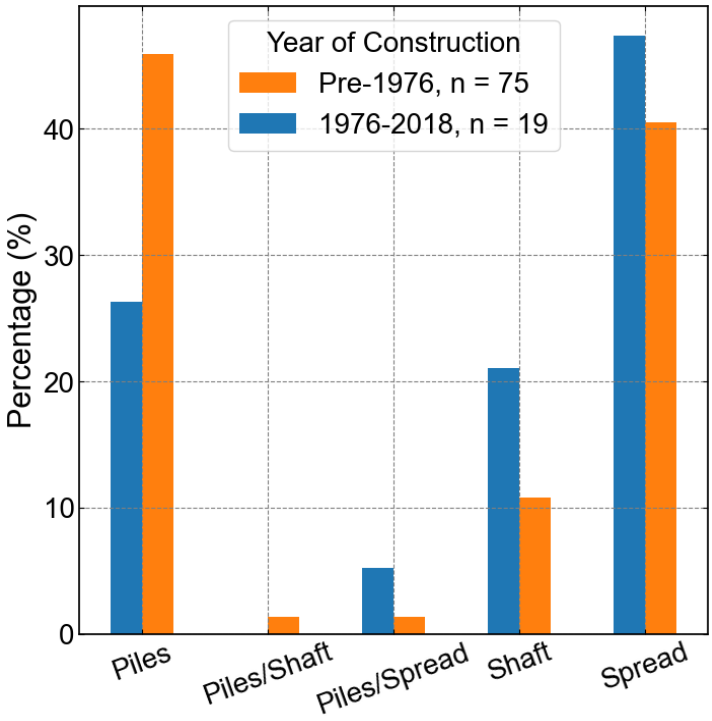

Figure 3.19: Foundation types

3.3.3 Presence of Shear Key

Shear keys provide a significant amount of resistance in the transverse direction preventing restraint to relative displacement between the superstructure deck and the abutments. As a result, the existence of shear keys is expected to strongly affect the performance of bridges during earthquakes.

The shear-key configurations for three bridges constructed before 1976 were unclear in the drawings, so these bridges were excluded from the statistical calculations. Almost all the bridges had shear keys, including 90.3% (65/72 bridges) of the older bridges and 100% (19 bridges) of newer bridges. As shown in Figure 3.20, the bridges with box girders tended to have external shear keys, whereas the bridges with prestressed girders or beams tended to have internal shear keys.

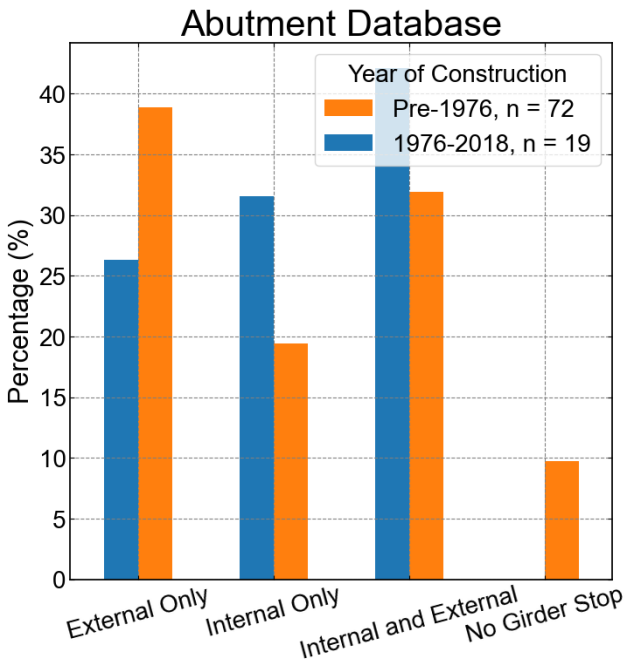

(a) Abutment Database bridges

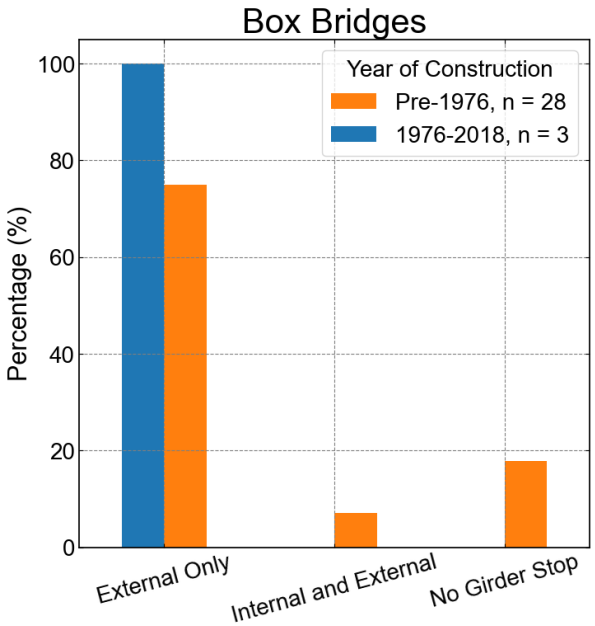

(b) Abutment Database bridges with box girders

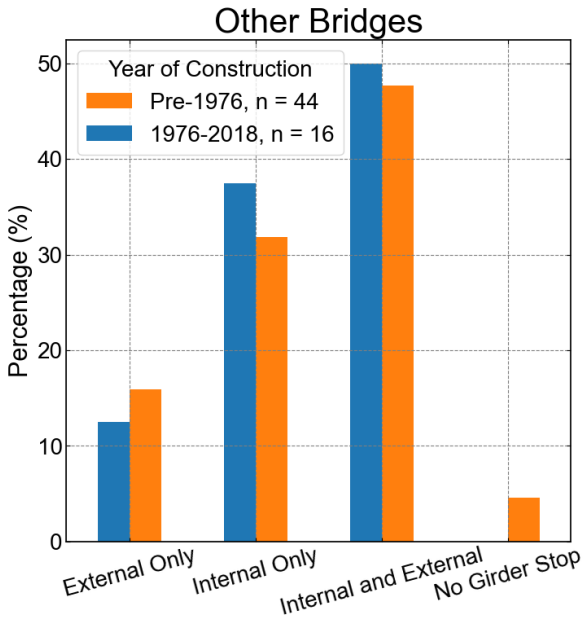

(c) Abutment Database bridges with other types of girders

Figure 3.20: Presence of shear key for (a) Abutment Database bridges, (b) Abutment Database bridges with box girders, and (c) Abutment Database bridges with other types of girders

3.4 Representative Bridge

Based on the statistics of the bridge properties presented in previous sections, Table 3.2 provides a summary of the desired characteristics to represent bridges constructed before 1976 and from 1976-2018. The table also provides references to the report section where that property was characterized.

One bridge (405/23E-N) built in 1997 approximately matches the identified features and was selected as a reference bridge. This selected bridge is built upon for the reference bridge that was used for the model development and the parametric study in subsequent chapters. The key features of the reference bridge features are also listed in Table 3.2. Additionally, as mentioned in section 3.2.8, since transverse reinforcement ratio reflects the code change around 1976, it is not surprising that the transverse reinforcement ratio appears to be the only major parameter listed below that is different between older and newer bridges. As a result, the transverse reinforcement ratio sufficiently reflects the age of the bridges.

Table 3.2: Properties of target and selected bridges

	Pre-1976 (target)	**1976-2018 (target)**	**Chapter Section**	**Identified Bridge 405/23E-N**	**Reference Bridge**
Column cross-section	Circular	Circular, Rectangular	3.2.3	Circular	Circular
Column diameter (in.)	30~40	30~60	3.2.4	36	36
Effective column height (ft)	10~25	10~25	3.2.6	21.3	21.3
Tallest column long reinf ratio (%)	1.0~1.5	1.0~1.5	3.2.8	1.3	1.3

	Pre-1976 (target)	1976-2018 (target)	Chapter Section	Identified Bridge 405/23E-N	Reference Bridge
Shortest column long reinf ratio (%)	1.0~1.5	1.0~1.5	3.2.7	1.3	1.3
Tallest column trans reinf ratio (%)	0.0~0.5	1.0~1.5	3.2.8	0.7	0.5
Shortest column trans reinf ratio (%)	0.0~0.5	1.0~1.5	3.2.7	0.7	0.5
Span numbers	3, 4	2, 3	3.2.1	3	3
Span continuity	Continuous	Continuous	3.1.4	Continuous	Continuous
Superstructure type	Prestressed -girder	Prestressed -girder	3.1.2	Prestressed -girder	Prestressed -girder
Intermediate pier type	Multiple columns	Multiple columns	3.1.3	Multiple columns	Multiple columns
Intermediate pier column numbers	1~5	1~5	3.2.5	3	3
Retrofit	Not-retrofitted	Not-retrofitted	3.2.9	Not-retrofitted	Not-retrofitted
Intermediate foundation type	Spread	Spread	3.2.2	Spread	Spread
Abutment type	L, semi-integral	L, semi-integral	3.3.1	Semi-integral	L
Abutment foundation type	Spread, Piles	Spread, Piles	3.3.2	Spread	Piles
Shear key existence	Yes	Yes	3.3.3	Yes	Yes

The overall geometry of the reference bridge follows the bridge plan of the identified bridge 405/23E-N. The original bridge plans of bridge 405/23E-N can be found in Appendix B. Table 3.3 lists the important dimensions for the bridge superstructure, substructure, and abutment of the reference bridge.

Table 3.3: Dimensions of the reference bridge

Superstructure Dimensions			
Span 1 length	L_{span1}	61	ft
Span 2 length	L_{span2}	110	ft
Span 3 length	L_{span3}	61	ft
Deck width	W_{deck}	37.4	ft
Deck depth	D_{deck}	5.75	ft
Deck length	L_{deck}	232	ft
Substructure Dimensions			
Cross-beam width	W_{beam}	5.33	ft
Cross-beam depth	D_{beam}	4	ft
Cross-beam length	L_{beam}	39.3	ft
Column spacing	S_{col}	16.2	ft
Column height	H_{col}	21.3	ft
Column diameter	d_{col}	36	in.
Column clear cover	d_{cover}	2	in.
Concrete core diameter	d_{core}	31.5	in.
Number of rebars	$\#_{rebar}$	13	
Column rebar diameter	d_{rebar}	1.128	in.
Column rebar area	A_{rebar}	1	in2
Spiral confined reinforcement diameter	d_{spiral}	0.5	in.

Spiral confined reinforcement diameter rebar area	A_{spiral}	0.196	in2
Spiral confined reinforcement spacing	$D_{spacing}$	3.5	in.
Abutment Dimensions			
Abutment width	W_{abut}	37.4	ft
Abutment back wall height	H_{abut}	7.5	ft

Chapter 4: Model Development

This chapter presents the numerical modeling strategies adopted here for an idealized reference reinforced concrete WSDOT highway bridge, which is denoted here as the reference bridge. The chapter presents both the system numerical model and provides details on modeling of key components. The reference bridge model is the baseline for parametric study in Chapter 6. The reference bridge configuration was discussed in Chapter 3 and was the result of interrogating the database of WSDOT bridges. The numerical modeling strategies were extended from and built upon the work of Ranf (2007), Ramanathan et al. (2012) and Mangalathu et al. (2017).

As shown in Figure 4.1, a typical highway reinforced concrete bridge has two primary components classified as the superstructure and substructure. The superstructure consists of deck slab, traffic barriers, and girders, while the substructure includes intermediate bent supports (cross-beams, columns, and foundation), abutments, shear keys, and bearings, depending on the type of the bridge abutment. The implementation of numerical models for these key components and their assembly into a complete bridge model is the focus of this chapter. The three-dimensional numerical model of the reference bridge was developed in OpenSeesPy (Zhu et al. 2018), a Python-compiled version of the finite element modeling package OpenSees, to simulate the dynamic response of the 3-span, 2-bent structure.

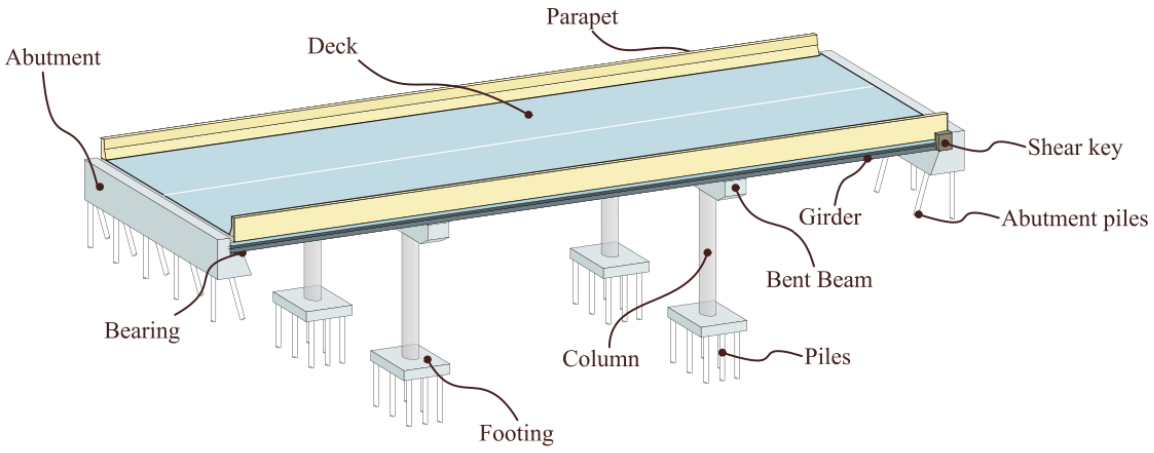

Figure 4.1: Typical highway concrete bridge components (Mangalathu 2017)

Section 4.1 provides an overview of the developed OpenSeesPy bridge model. Sections 4.2 to 4.4 present the various components of the model and their modeling strategies. In Section 4.5, summary tables for the values of required modeling parameters are provided.

4.1 Bridge Model Overview

Figure 4.2 shows a schematic of the overall bridge model. The bridge superstructure was modeled as a spine of multiple connected elastic beam-column elements in OpenSeesPy since the bridge deck was expected to remain elastic during earthquake excitations. Where the deck was connected to substructures (intermediate bents and abutments) a series of stiff elastic beam-column elements were used to extend from the centerline spine of the deck out to the full deck width. At the columns, rigid links were used to connect the extension of the deck to the top of columns. Rotational and translational springs were attached to the base of columns to capture the behavior of the intermediate bent foundations. Zero length fiber sections were assigned to both ends of the columns to simulate the anchorage flexibility due to bond slip.

Three different types of abutments, including integral, semi-integral, and L (seat) abutments, were considered in this study. Zero length elements capturing backfill soil and bi-directional forces (abutment piles/spread footings and friction surface) were connected in parallel and linked to the ends of deck elements for the integral abutment case. For semi-integral and L (seat) abutments, a zero length element was connected in series with the backfill element to reflect pounding between backfill soil and deck. Additionally, zero length elements for the shear keys and bearing pads were also placed in parallel with the pounding elements. Detailed modeling strategies for abutment are introduced in Section 4.4.

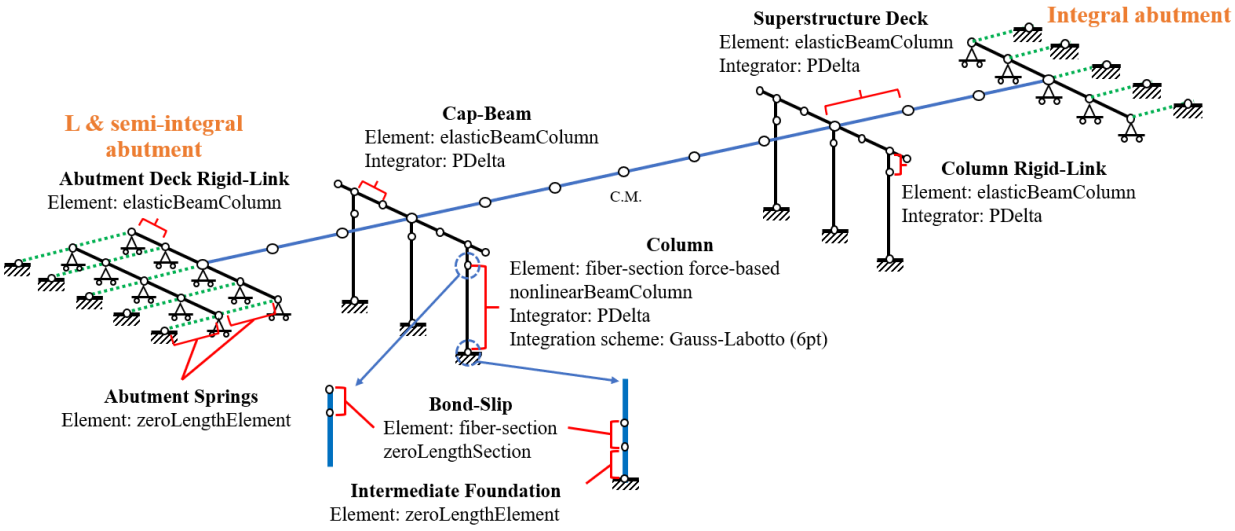

Figure 4.2: Numerical modeling of various bridge components

4.2 Superstructure

The superstructure was modeled with multiple connected elastic beam-column elements and remains elastic during the earthquake loading. The mass of the superstructure was uniformly assigned to the longitudinal deck nodes according to the tributary area of the deck and the length of the traffic barrier. Rigid and massless elastic beam-column elements were used for the transverse deck elements. The elastic modulus, E_c, and shear modulus, G_c, for the deck elements were computed using Equations. 4-1 and 4-2, and a concrete strength, f_c, equal to 6 ksi and the concrete material poisson's ratio, ν_c, equal to 0.2. The resulting E_c and G_c were 4415.2 psi and 1839.7 ksi, respectively.

$$E_c = 57000\sqrt{f_c}\ (psi) \qquad \text{(Equation. 4-1)}$$

$$G_c = \frac{E_c}{2*(1+\nu_c)}\ (ksi) \qquad \text{(Equation. 4-2)}$$

4.3 Intermediate Bent Supports

As illustrated in Figure 4.3, the intermediate bents included cross-beams, columns, and foundations. The intermediate bents were modeled using a combination of nonlinear beam-column elements and rigid links that captures the transfer of moments and forces between bent members. The rotational and translational springs were placed at the base of columns for foundations. Detailed properties for each component are described in the sections that follow.

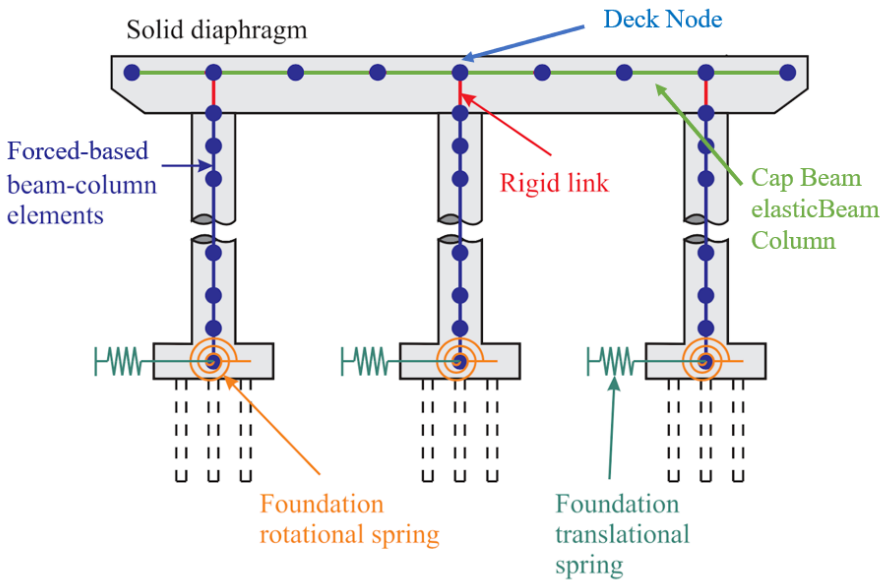

Figure 4.3: Finite element discretization of bents (Ramanathan et al. 2012)

4.3.1 Cross-Beams

Elastic beam-column elements with large elastic modulus and shear modulus (E_c and G_c in Section 4.2 times 100) were used to model cross-beams and are connected to the top of columns with rigid links. The resulting elastic modulus, E_{c-beam}, and shear modulus, G_{c-beam}, for cross-beams are 4415200 ksi and 1839700 ksi, making these elements essentially rigid.

4.3.2 Columns

As shown in Figure 4.4, the model for the circular columns were composed of four different parts. The inelastic flexural response was modeled using distributed plasticity forced-based beam column elements (nonlinearBeamColumn), which captured the local strain response at the column-anchorage interfaces and required cross-sections to be defined at each of the integration points. The elastic shear and torsional behaviors were aggregated to the cross-sections using the Section Aggregator command in OpenSeesPy. Furthermore, the anchorage rotation was simulated with a zero length element at both ends of the column. Each column component is discussed in the following sections.

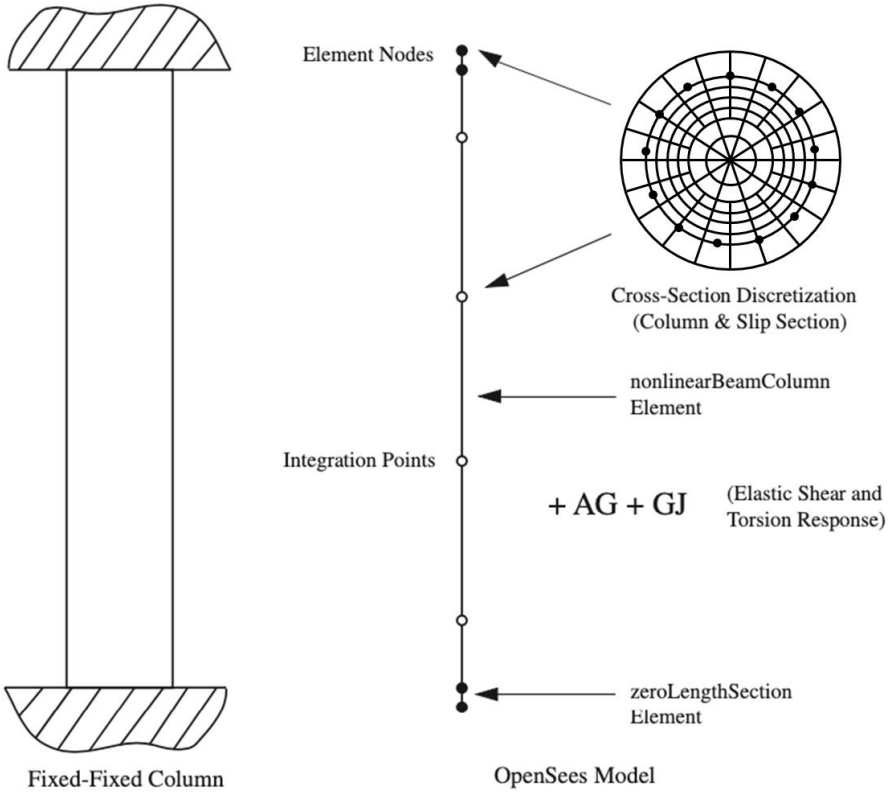

Figure 4.4: Components of numerical column model (Ranf 2007)

4.3.2.1 Column Nonlinear Material Models

One of the advantages of the fiber-section defined nonlinear beam-column element is its ability to assign unique material properties over the cross section. The Mander and Priestley (1988) model was used to define the monolithic stress-strain curve of the confined and unconfined concrete. The unconfined maximum concrete stress, f_c, was assumed to be 1.5 times the specified concrete strength, f'_c, and the corresponding unconfined strain was given as ϵ_c. For the reference bridge f_c is 6 ksi and ϵ_c is 0.002. By providing the f_c and ϵ_c, the confined concrete strength, f_{cc}, and its corresponding strain, ϵ_{cc}, can be calculated by the following equations:

$$f_{cc} = f_c * [-1.254 + (2.254\sqrt{1 + \frac{7.94 f_{lp}}{f_c}}) - 2\frac{f_{lp}}{f_c}] \quad \text{(Equation. 4-3)}$$

$$\epsilon_{cc} = \epsilon_c \left(5\frac{f_{cc}}{f_c} - 4\right) \quad \text{(Equation. 4-4)}$$

The resulting values for f_{cc} and ϵ_{cc} were 7.11 ksi and 0.00385.

where f_{lp} is the effective lateral confining pressure, and can be given as:

$$f_{lp} = k_e * \frac{\rho_{hoop} * f_y}{2} \quad \text{(Equation. 4-5)}$$

where ρ_{hoop} is the transverse reinforcement ratio, f_y is the yield strength of the transverse reinforcement, and k_e is the effective confinement coefficient. The effective confinement coefficient, k_e, is given as the ratio of effective confined concrete area and the area of concrete core. The transverse reinforcement ratio, ρ_{hoop}, is provided as a user input for the bridge model to reflect columns designed pre- and post-1976 (0.5% for old and 1.5% for new columns).

The ultimate confined concrete stress and strain can be calculated as:

$$\epsilon_{cu} = \epsilon_u + \frac{1.4\rho_{hoop} * f_y * \epsilon_{su}}{f_{cc}} \quad \text{(Equation. 4-6)}$$

$$f_{cu} = \frac{f_{cc} * x_{conf} * r_{conf}}{r_{conf} - 1 + x_{conf}^{r_{conf}}} \quad \text{(Equation. 4-7)}$$

where ϵ_{su} is the ultimate strain of reinforcement equal to 0.12 and ϵ_u is the unconfined concrete ultimate strain equal to 0.004. And r_{conf} and x_{conf} can be given as:

$$r_{conf} = \frac{E_c}{E_c - E_{secant}} \quad \text{(Equation. 4-8)}$$

$$E_{secant} = \frac{f_{cc}}{\epsilon_{cc}} \quad \text{(Equation. 4-9)}$$

$$x_{conf} = \frac{\epsilon_{cu}}{\epsilon_{cc}} \quad \text{(Equation. 4-10)}$$

where E_{secant} denotes the concrete secant elastic modulus. The resulting values for f_{cu} and ϵ_{cu} are 4855.6 psi and 0.0122, respectively.

Additionally, a linear model up to an assumed strength is used for the tension behavior of both confined and unconfined concrete. The maximum tension stress and strain, f_t and ϵ_t, are the same for both confined and unconfined concrete model and are calculated as:

$$f_t = 0.1 f_{cc} \quad \text{(Equation. 4-11)}$$

$$\epsilon_t = \frac{f_t}{E_c} \quad \text{(Equation. 4-12)}$$

The resulting values for f_t and ϵ_t are 0.711 ksi and 0.000136, respectively.

The residual stresses are assumed to be 0.2 and 0.01 of f_t for confined and unconfined concrete, resulting in 0.142 ksi (f_{r-c}) and 0.00711 ksi (f_{r-uc}), respectively.

For both longitudinal and transverse reinforcement, the ultimate tensile strength, f_y (equal to 69.6 ksi), is assumed to be 1.16 of the specified steel strength to capture overstrength

(Bournonville et al. 2004). The steel elastic modulus, E_s, is 29000 ksi and the strain hardening ratio, b_{col}, of the reinforcement is assumed to be 1.5%.

Concrete04 and Steel02 material models in OpenSeesPy are used to represent the behavior of concrete and reinforcement over the column fiber-sections and the stress-strain curves are given in Figure 4.5 and Figure 4.6.

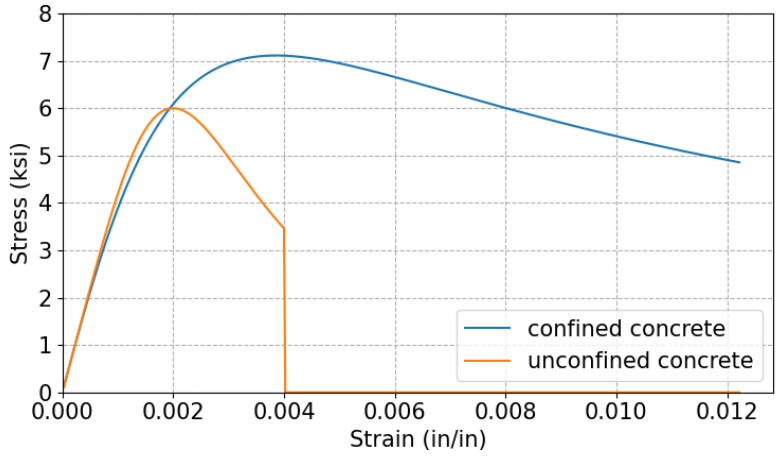

Figure 4.5: Concrete04 material model for column fiber section

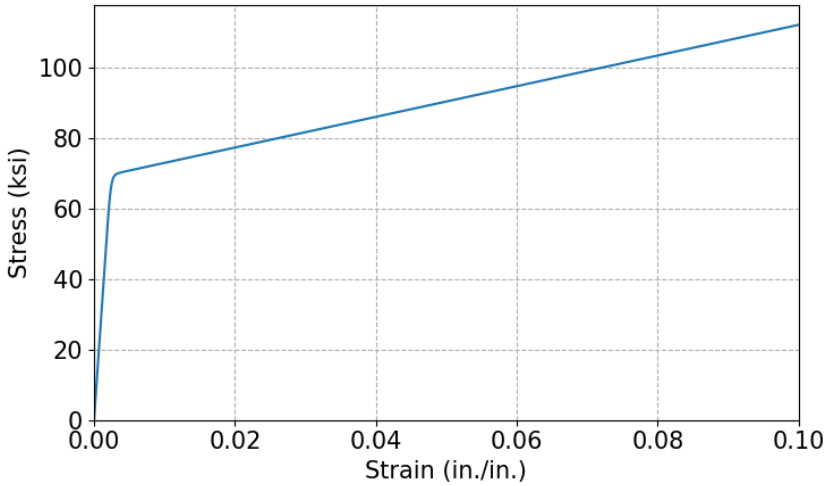

Figure 4.6: Steel02 material model for column fiber section

4.3.2.2 Column Elastic Shear and Torsional Response

The elastic shear and torsional properties are calculated based on the shear modulus of concrete and the gross area of the column, assuming the Poisson's ratio, ν_c, of the cross-section to be 0.2. The shear modulus, G_c, is 1839.7 and the torsional constant J is 164896 in^4. The elastic properties are then aggregated to the inelastic flexural response to capture the overall behavior of the column elements. The "Aggregator" command is used to integrate the elastic and inelastic properties in OpenSeesPy.

4.3.2.3 Cross Section Discretization

The number of fibers defined for the cross section of the columns is a balance between the efficiency and accuracy of the analysis. Berry (2006) conducted a convergence study with different discretization schemes and compared analysis results to column test results from the UW-PEER column database (Berry et al. 2004). The study found that the discretization schemes shown in Figure 4.7 adequately captured the moment-curvature relationship while maintaining computational efficiency. This modeling strategy is adopted for the fiber-sections of the column and the anchorage slip in this study.

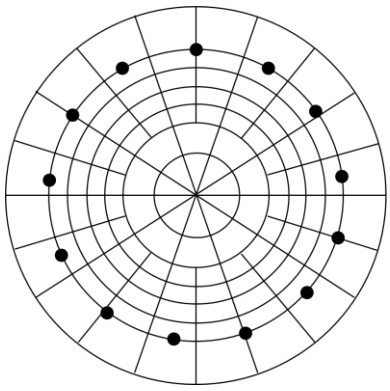

Section	Disc. Dir.	Disc. #
cover	tangential	20
	radial	1
inner core	tangential	10
	radial	2
outer core	tangential	20
	radial	5

Figure 4.7: Bond-slip and column fiber-section with discretization as recommended by Berry et al. (2004)

4.3.2.4 Anchorage Slip

The anchorage slip models are included to capture slip of the longitudinal reinforcing steel at both ends of columns. The zeroLength section is used in OpenSeesPy with the cross-section discretization scheme as described in Section 4.3.2.3.

The steel stress-displacement for a bar is based on a bond slip model (Lehman and Moehle 2000) and later modified by Ranf (2006). As shown in Figure 4.8, the shear-stress relationship with bar anchorage can be ideally described in three segments as:

$$\tau(\sigma)\begin{cases}\tau_e \frac{\sigma}{\sigma_d} = a\frac{\sigma}{\sigma_d}\sqrt{f_c'} & \sigma < \sigma_d \\ \tau_e = \lambda_e\sqrt{f_c'} & \sigma_d \le \sigma \le \sigma_y \\ \tau_i = \lambda_i\sqrt{f_c'} & \sigma_y \le \sigma\end{cases} \qquad \text{(Equation. 4-13)}$$

where τ is the bar shear, σ is the bar stress, λ_e and λ_i are the elastic and inelastic bond-stress coefficients, respectively.

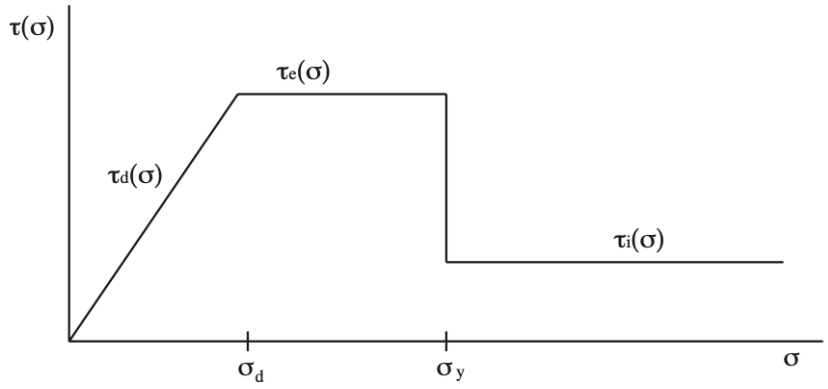

Figure 4.8: Bond slip shear-stress relationship (Berry-Eberhard, 2008)

The change in strain (change in stress) along the reinforcement can then be calculated as:

$$\frac{dF}{dx} = \frac{\pi d_b^2 d\sigma}{4}\frac{d\sigma}{dx} = \tau(\sigma)\pi d_b \qquad \text{(Equation. 4-14)}$$

$$\frac{d\sigma}{dx} = \frac{4\tau(\sigma)}{d_b} \qquad \text{(Equation. 4-15)}$$

By integrating the strain along the anchorage zone, the stress-displacement envelope of the rebar can be calculated. The final relationship along with a simplified bi-linear model, which is used in the bridge model here and implemented with the Steel02 material model in OpenSeesPy, is illustrated in Figure 4.9. The resulting reinforcement elastic modulus, E_{s-slip}, and the yield strength, f_{y-slip}, were calculated as 2085.12 ksi/in and 60 ksi. The bond slip rebar strain hardening ratio, b_{slip}, was 1.08 %.

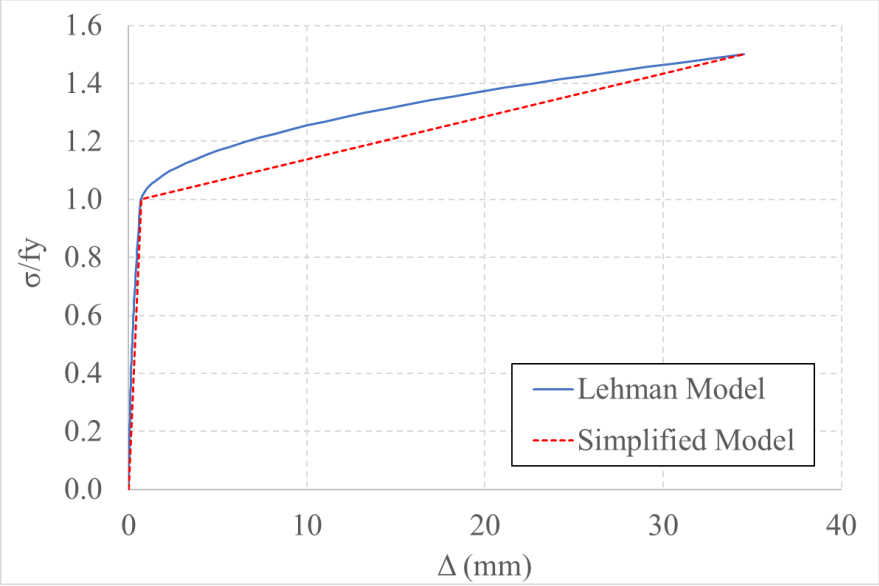

Figure 4.9: Comparison of the stress-displacement curve for modeling bond slip as proposed by Lehman and Moehle (2000) and the simplified bi-linear response

For the concrete material model used at the bond slip section, due to the sufficient confinement provided by the steel and the surrounding concrete around the anchorage zone, the concrete is assumed to not degrade after the maximum stress. This behavior can be accomplished by multiplying the ultimate concrete strain by an effective concrete depth. Berry (2006) used eight test columns from the UW-PEER column database (Berry et al. 2004) and calibrated the effective concrete depth, e_{depth}. The result suggested e_{depth} to have a value of approximately 29% of the column diameter, which is adopted in the concrete model of this study. The concrete strain at peak strength, ϵ_{c-slip} , and the ultimate concrete strain, ϵ_{u-slip} were 0.04 and 127.

The Concrete01 model is used in OpenSeesPy for this study to model the concrete at bond slip sections. The stress-displacement relationship is illustrated in Figure 4.10.

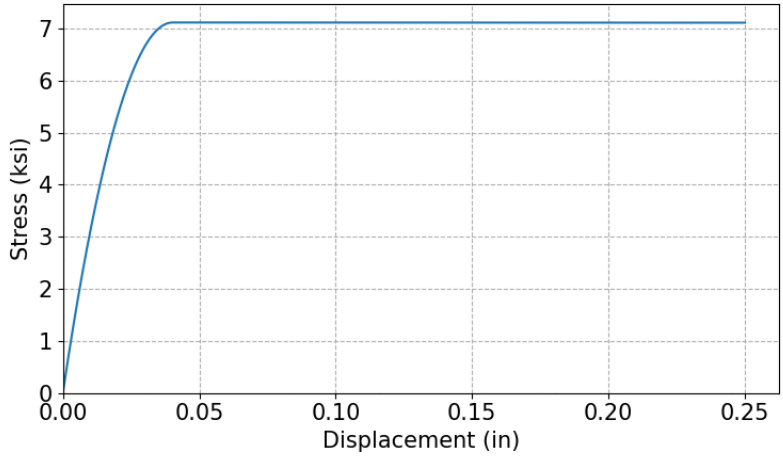

Figure 4.10: Concrete01 stress-displacement relationship for bond-slip section

4.3.3 Intermediate Foundations

As presented in Figure 4.11, the intermediate foundations are idealized as elastic rotational and translational springs modeled as zero length elements at the base of columns. Ramanathan (2012) studied the numerical values of the spring stiffnesses according to the configurations of various bridge structures. In this study, the numbers for Multiple-span continuous concrete I-girder (MSCC-IG) bridges from that previous work are used for the reference bridge model and can be found in Section 4.4. The rotational spring stiffness, K_r, and translational spring stiffness, K_t, were taken to be 7*1e06 (kip-in/rad) and 1300 (kip/in), respectively (Ramanathan 2012).

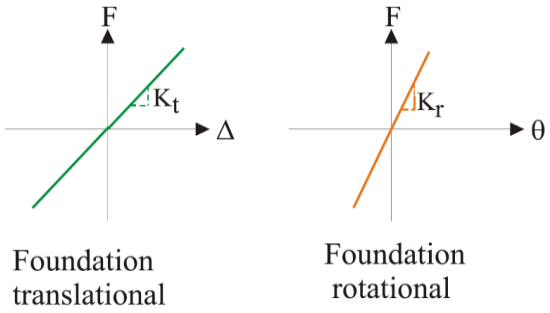

Figure 4.11: Rotational and translational spring for foundations (Mangalathu 2017)

4.4 Abutments

The abutments that are most commonly observed in the bridge inventory can be classified into three categories: integral, semi-integral, and L abutments. Integral abutments are cast monolithically with the superstructure and provide restriction for the movement of deck in both the transverse and longitudinal directions. The stiffness and resistance of integral abutments are high and are only limited by the backfill soil and the abutment foundations. While semi-integral abutments are not cast together with the superstructure, they have the same behavior in the longitudinal direction compared to integral abutments as the deck goes beyond the abutment backwall and engages directly with the backfill soil. In the transverse direction, semi-integral and L abutments provide bearing supports to the superstructure whose motion is restrained by shear keys at both ends of the bridge. Both semi-integral and L abutments are typically supported by but they may also be found on spread footings. The longitudinal motion of the superstructures in the case of L abutments is restrained by bearing pads, the abutment backwall and the backfill soil. To capture the abutment behaviors described above, two different spring systems consisting of various types of zero length elements are used as shown in Figure 4.12. Although semi-integral and L abutments use the same type of spring systems, the stiffness of the bearing springs differ in the longitudinal direction, with the former modeled as rigid and the latter as flexible.

The following sections introduce the numerical models used for the spring elements that appear in Figure 4.12 and are used to simulate various bearing, abutment and soil behaviors.

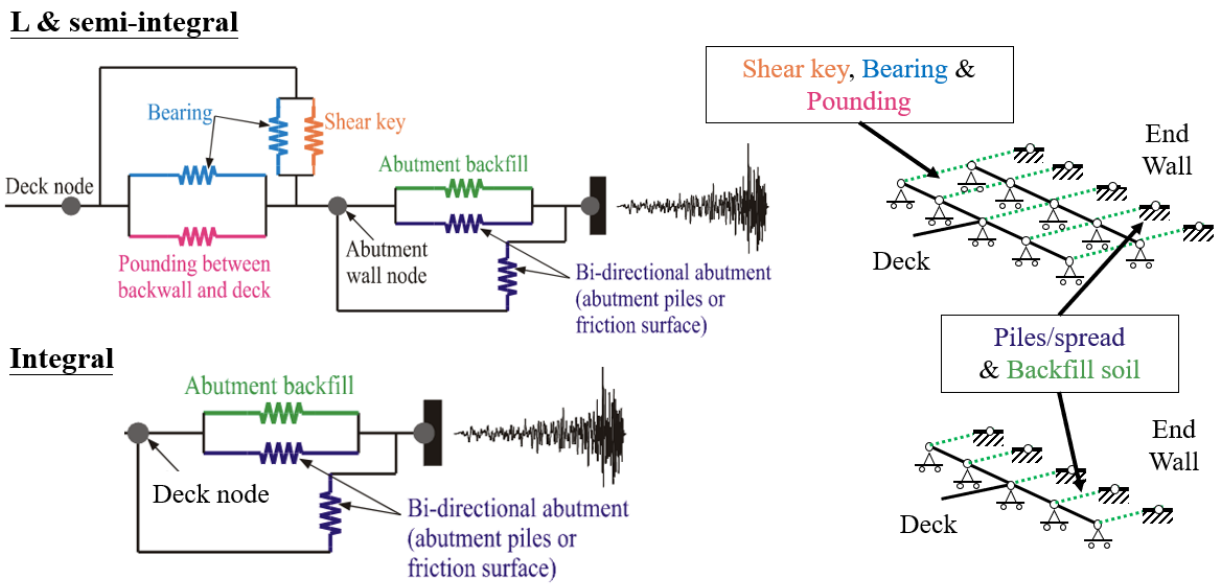

Figure 4.12: Zero length spring system for L and semi-integral abutment (upper) types, and for integral abutments (lower)

4.4.1 Backfill Soil

The passive response of the abutment backwall is captured by a hyperbolic soil model established by Shamsabadi and Yan (2008). The model is based on experiments conducted at University of California Los Angeles, using a test specimen with a 4.5ft high abutment backwall. The closed form force-displacement response can be described as:

$$F(\Delta) = \frac{8\Delta}{1+3\Delta} H^{1.5} \qquad Granular\ backfills$$

$$= \frac{8\Delta}{1+1.3\Delta} H \qquad Cohesive\ backfills \qquad \text{(Equation. 4-16)}$$

where F is the interaction force in (kip/in) per width of backwall, Δ is the displacement given in inches, and H is the back wall height in feet. Note that the equation for cohesive soil is used for this study as it is conservative in terms of calculated strength and stiffness.

The maximum displacements for granular and cohesive soils are $0.05H$ and $0.1H$ respectively (Shamsabadi and Yan 2008). Using these maximum displacements and the 7.5 ft backwall height for the reference bridge in Equation 4.16, the ultimate force, F_{ult}, is calculated to be equal to 2735 (kip) for cohesive soils. Furthermore, the stiffness at specific displacements can be calculated by differentiating Equation 4.16 with respect to delta, given as Equation 4.17 for the case of cohesive soil.

$$K(\Delta) = F'(\Delta) = \frac{8H^{1.5}(1+6\Delta)}{(1+3\Delta)^2} \qquad \text{(Equation. 4-17)}$$

The HyperbolicGapMaterial in OpenSeesPy, shown in Figure 4.13, is adopted for modeling the backfill soil and its behavior is given as:

$$F(\Delta) = \frac{\Delta}{\frac{1}{K_{max}} + R_f \frac{\Delta}{F_{ult}}} \qquad \text{(Equation. 4-18)}$$

where R_f is failure ratio given as 0.7 (Mangalathu, 2017), and K_{max} , the initial stiffness, is calculated to be 15503 (kip/in) from Equation 4.17 by substituting Δ equal to 0. The gap distance in the HyberbolicGapMaterial is assumed to be a small value as the backfill soil is likely to be compacted against the back wall and is neglected. However, once the material is compressed, a gap is created and increases with repeated cycling.

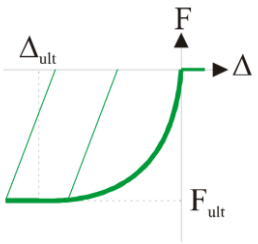

Figure 4.13: HyperbolicGapMaterial model for abutment backfill (Mangalathu 2017)

4.4.2 Abutment Foundations

Two types of abutment foundations were considered in this study. The modeling for abutment foundations included 6 soil types: soft clay, medium clay, stiff clay, soft sand, medium sand, stiff sand (the reference bridge was set to sit on medium sand and medium clay soil was considered for the parametric study in Chapter 6). The soil types influenced the input parameters for the abutment foundation material models and reflected the effect of different soil types.

4.4.2.1 Abutment Spread Footing

The abutment spread footings were assumed to have elastic-plastic behavior and the yield force is obtained by the multiplication of normal force and the friction coefficient, μ_{spread}. The friction coefficients were assumed to have different values for different types of soils and are listed in Table 4.1 where the bold value is that used for the reference bridge.

Table 4.1: μ_{spread} for different soil types (with bold value used for the reference bridge)

	Soft clay	**Medium clay**	**Stiff clay**	**Soft sand**	**Medium sand**	**Stiff sand**
μ_{spread}	0.3	0.4	0.5	0.31	**0.47**	0.79

The normal force is assumed to be half of the self-weight of the span that sits on the bearing pads and the yield displacement, $\Delta_{y-spread}$, is set to be 0.75 (in) (Mangalathu, 2017). The stiffness, E_{spread}, is then calculated to be 37.1 (kip/in). ElasticPP model shown in Figure 4.14 is used to simulate spread footings.

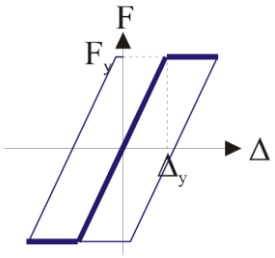

Figure 4.14: Piles spread footing material model (Mangalathu 2017)

4.4.2.2 Abutment Piles

Modeling of the abutment piles followed lateral pile force-deflection curves developed by Evans and Duncan (1982). Evans and Duncan proposed charts describing the relationship between pile lateral load and lateral deflection for different soil types. The soil types were described in terms of the axial strain at which 50 percent of the soil strength is mobilized, denoted as ϵ_{50}. The characteristic shear load of a pile, V_c, is defined as:

$$V_c = \lambda B^2 E R_I \left(\frac{\sigma_p}{E R_I}\right)^m {\epsilon_{50}}^n \quad \text{(Equation. 4-19)}$$

$R_I = 1.0$ for circular cross sections (considered in this study)

For plastic clay and sand:

$$\lambda = 1.00 \quad \text{(Equation. 4-20)}$$

For brittle clay:

$$\lambda = (0.14)^n \quad \text{(Equation. 4-21)}$$

For clay:

$$\sigma_p = 4.2 S_u \quad \text{(Equation. 4-22)}$$

For sand:

$$\sigma_p = 2 C_{p\phi} \gamma B tan^2(45 + \phi'/2) \quad \text{(Equation. 4-23)}$$

Where:

λ = A dimensionless parameter dependent on the soil's stress-strain behavior

B = Diameter of foundation pile

E = Modulus of elasticity of foundation piles (assume to be equal to Ec for this study)

I = Moment of inertia of foundation piles ($= \pi B^4/64$ for circular piles)

R_I = Moment of inertia ratio ($= \frac{I}{\pi B^4/64}$, 1.0 for circular piles)

σ_p = Representative passive pressure of soil

ϵ_{50} = Axial strain at which 50 percent of the soil strength is mobilized (Table 4.2)

m, n = Exponents terms (Table 4.2)

S_u = Undrained shear strength of soil (Table 4.2)

ϕ' = Effective friction angle of soil (deg) (Table 4.2)

$C_{p\phi}$ = Passive pressure factor = $\phi'/10$

γ = Unit weight of soil (assumed to be 110 (lb/ft^3) in this study)

Table 4.2: Soil parameters for clay and sand soil types (with bold values indicated those used for the reference bridge) (Evan and Duncan 1982)

Soil type	ϵ_{50}	**m**	**n**	ϕ' **(deg)**	S_u **(kPa)**
Soft clay	0.02	0.683	-0.22	-	25
Medium clay	0.01	0.683	-0.22	-	50
Stiff clay	0.005	0.683	-0.22	-	75
Soft sand	0.002	0.57	-0.22	25	-
Medium sand	**0.002**	**0.57**	**-0.22**	**50**	**-**
Stiff sand	0.002	0.57	-0.22	75	-

Figure 4.15 and Figure 4.16 show the lateral force versus deflection curves for soil types from Evans and Duncan for clay and sand, respectively.

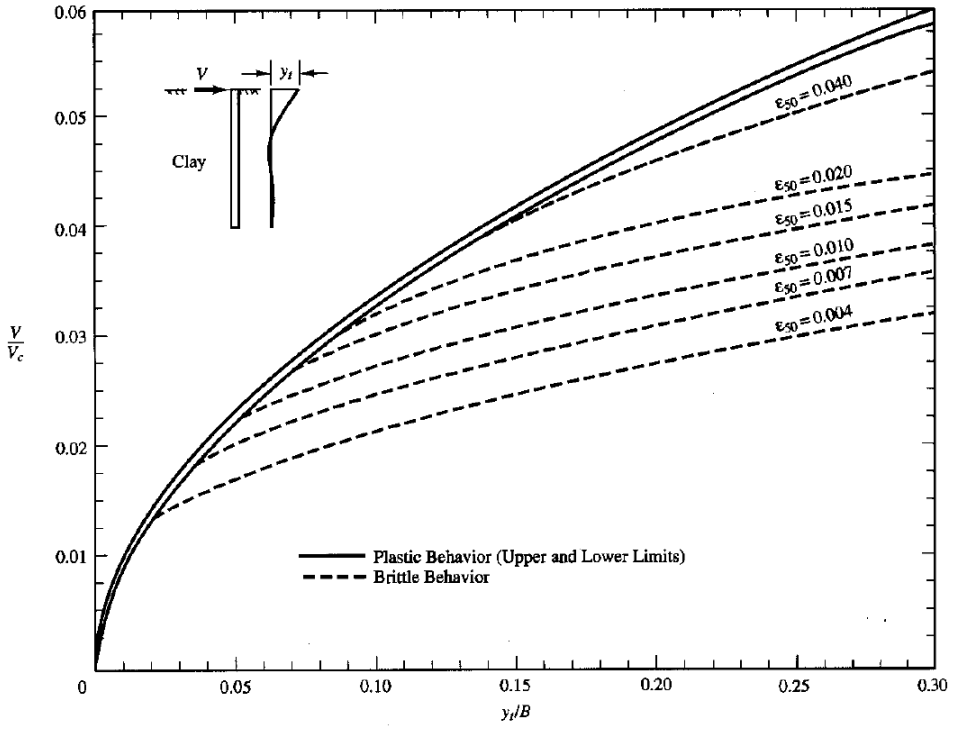

Figure 4.15: Piles lateral load and deflection relationship for clay (Evan and Duncan 1982)

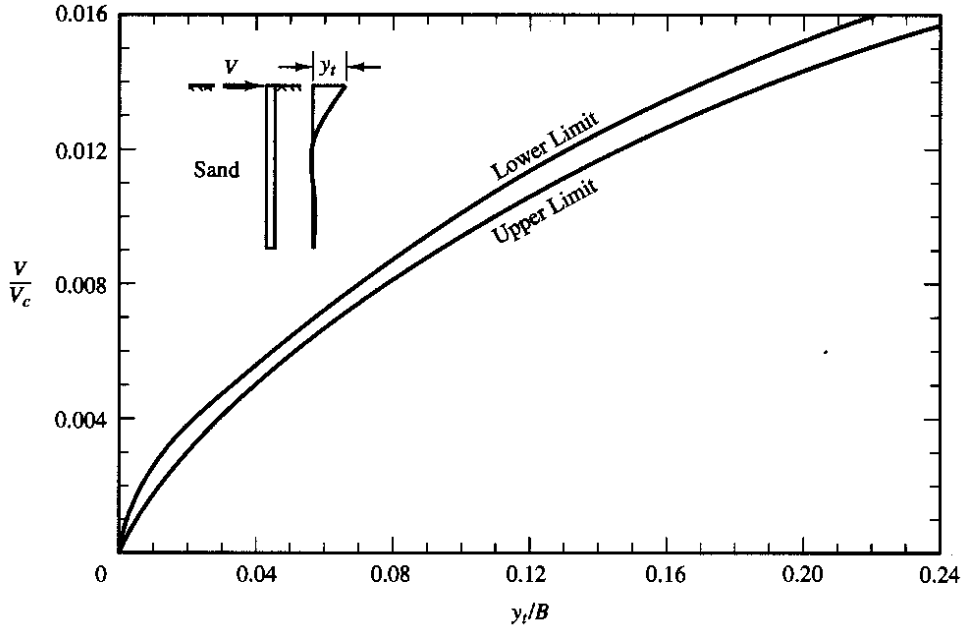

Figure 4.16: Piles lateral load and deflection relationship for sand (Evan and Duncan 1982)

The total lateral load of abutment piles, $V_{c_{total}}$, was calculated by:

$$V_{c_{total}} = V_c * (\#piles) \quad \text{(Equation. 4-24)}$$

where $\#piles$ is the equivalent number of 13-inch diameter piles at the abutments and was derived from the deck width. The 13-inch pile diameter is often the standard among bridges.

The equivalent number of 13-inch piles at the abutments, $\#piles$, was calculated as:

$$\#piles = \#piles_{actual} * d_{actual} \,/\, 13 \quad \text{(Equation. 4-25)}$$

where $\#piles_{actual}$ is the actual number of piles and d_{actual} is the actual pile diameter.

For the selected bridges from Abutment Database (Chapter 3) that had sufficient information for abutment piles, Figure 4.17 shows the relationship between $\#piles$ and bridge deck width.

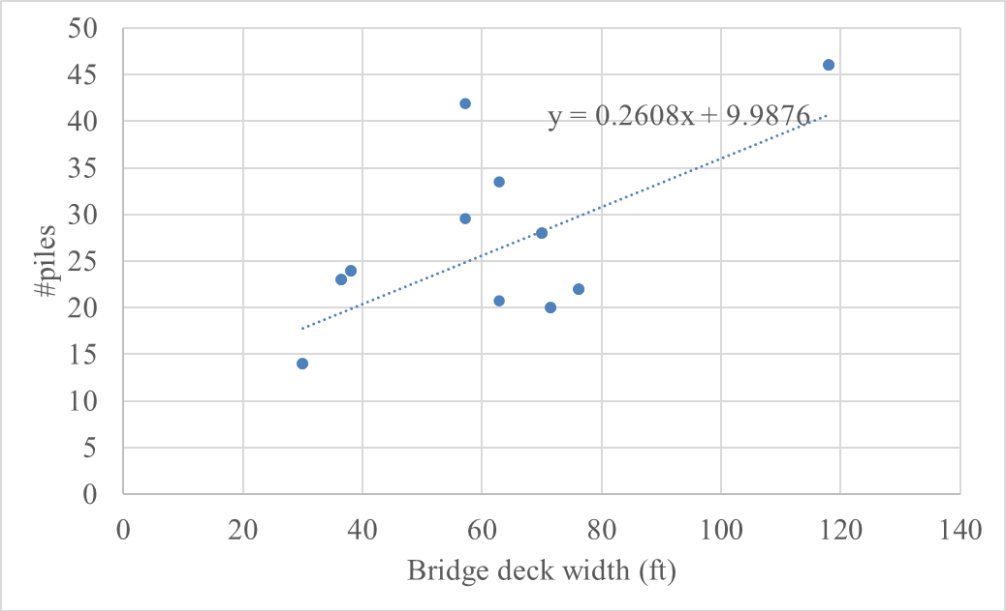

Figure 4.17: Equivalent 13-inch diameter pile numbers versus bridge deck width

In this study, the curves in Figures 4.15 and 4.16 were idealized as bi-linear curves followed by a constant relationship between pile lateral load and the deflection and were modeled with

Hysteretic material model in OpenSeesPy. Figure 4.18 illustrates the hysteretic model for the abutment piles and the first and second yield points, (Δ_{1-pile}, F_{1-pile}) and (Δ_{2-pile}, F_{2-pile}), for different soil types are listed in Table 4.3. The pinching parameters in the hysteretic material model, $pinchX_{pile}$ and $pinchY_{pile}$, are set to be 0.75 and 0.5, respectively (Mangalathu 2017).

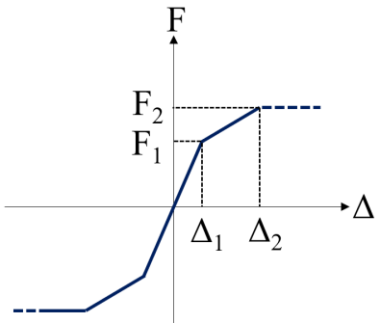

Figure 4.18: Abutment pile hysteretic model (Mangalathu 2017)

Table 4.3: Abutment pile hysteretic model force and displacement input values (with the bold values indicated for the reference bridge)

Soil types	$\boldsymbol{\Delta_1}$ **(in)**	$\boldsymbol{\Delta_2}$ **(in)**	$\boldsymbol{F_1}$ **(kip)**	$\boldsymbol{F_2}$ **(kip)**
Soft clay	1.13	3.9	30	45
Medium clay	0.65	3.9	42	71
Stiff clay	0.34	3.9	42	97
Soft sand	1.17	2.99	31	56
Medium sand	**1.17**	**2.99**	**88**	**157**
Stiff sand	1.17	2.99	356	633

4.4.3 Shear Keys

Shear keys provide important constraints for the superstructure in the transverse direction at semi-integral and L abutments during earthquakes.

Megally (2002) studied the capacity of a series of interior and exterior shear keys at the University of California San Diego. An example of the experimental results is shown in Figure 4.19 in terms of shear force versus displacement. As seen in Figure 4.19, the shear key reaches its capacity at a displacement that is equal to the gap between the deck and the shear key, and starts deteriorating until a maximum displacement of 4.0 inches is reached when it loses all resistance.

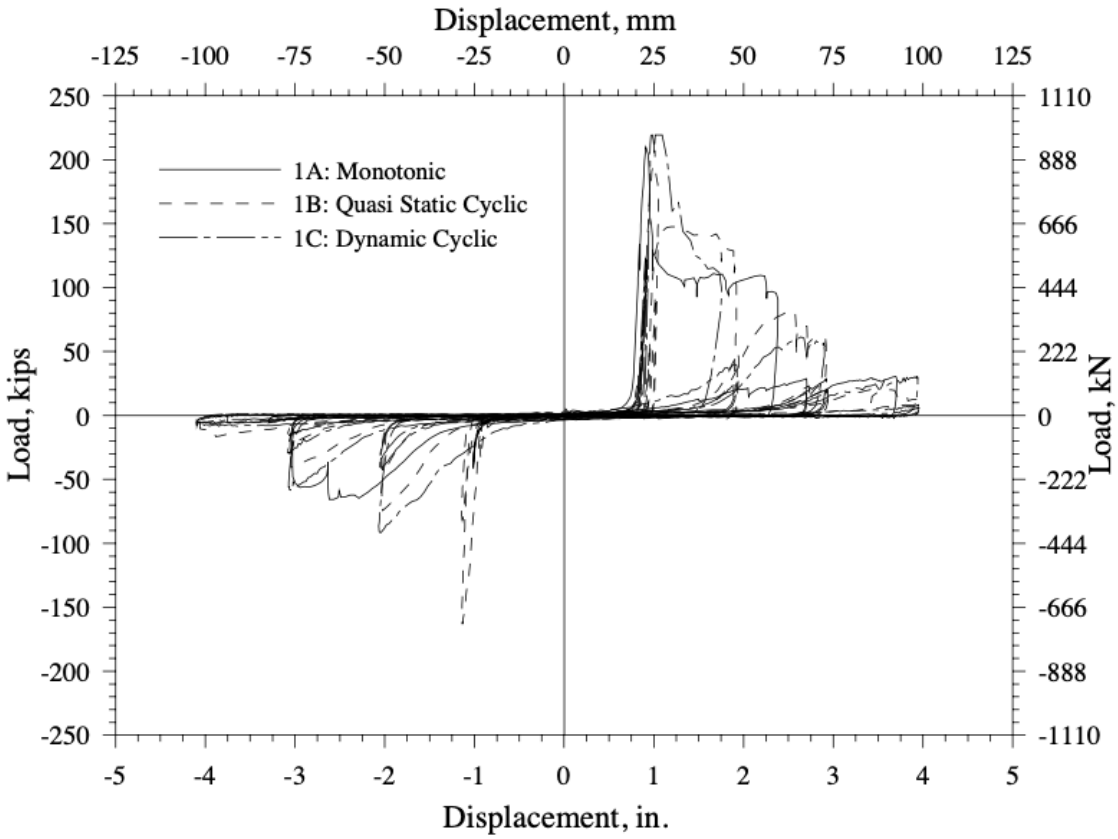

Figure 4.19: Shear key experimental results from Megally (2002)

Figure 4.20 shows an example schematic of a typical interior shear key, where b is width, d is depth, and h is height. The interior shear key capacity can be calculated for different failure mechanisms based on its aspect ratio, α (which is equal to h/d).

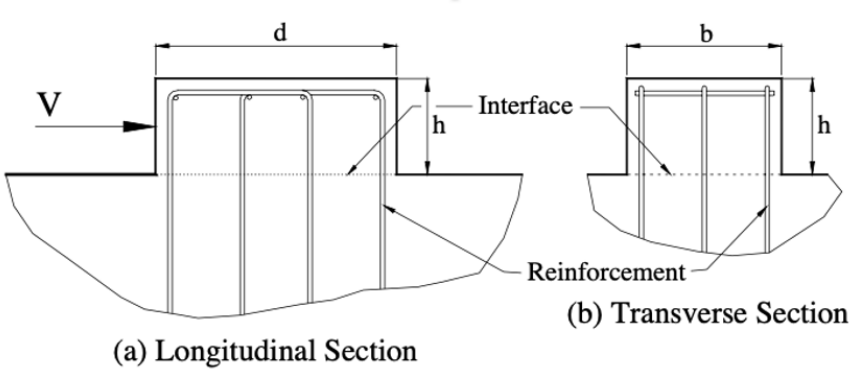

Figure 4.20: Shear key material model (Megally 2002)

Table 4.4 lists the different capacity calculations with their corresponding failure modes where $f'c$ is the concrete strength in psi.

Table 4.4: Shear key capacity based on failure modes

Aspect Ratio (α)	**Failure Mechanism**	**Shear Stress (V_N) (psi)**
$\alpha < 0.5$	Shear Friction	$11.3\sqrt{f'c}$
$0.5 < \alpha < 1.0$	Bracket and corbel	$800\ f'c$
$1.0 < \alpha$	Flexural (cantilever beam)	$0.2\ f'c$

In this study, only interior shear keys at the abutments are considered, with their capacities integrated and assigned to two shear key models at opposite ends of the abutments. Interior shear keys were found in the survey of WSDOT bridges to be most common. With this simplification,

four shear key spring elements are included for the entire bridge model. The derived shear key capacity, F_{shear}, is 2240.25 (kip) for a shear key model in the reference bridge.

The Hysteretic material model in OpenSeesPy is used to simulate the force-displacement curve and deterioration after maximum strength of the shear keys. The initial gap, Δ_{init}, is assumed to be 0.5 inches and the maximum displacement, Δ_{max}, is assumed to be Δ_{init} + 3.5 inches (Megally et. al 2002). The pinching parameters in the hysteretic material model, $pinchX_{shear}$ and $pinchY_{shear}$, are set to be 1.0 and 0.0, respectively, to produce the pinched behavior observed in Figure 4.19. Figure 4.21 shows the material model of the shear key.

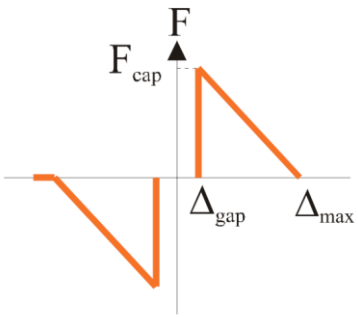

Figure 4.21: Shear key material model (Mangalathu 2017)

4.4.4 Bearings

Since the reference bridge contains elastomeric bearings, elastomeric bearing pads are considered for the study. The bearing pads are assumed to have elastic-plastic behavior (Mangalathu 2017), where the elastic portion represents the deformation of the bearing pads and the portion after yielding represents the slip between the girder and the end plate of the bearings. The yield force, $F_{y-bearing}$, is obtained by the multiplication of normal force, N_b, subjected to bearing pads and the friction coefficient, μ_b. N_b was equal to 59.6 (kip) to and μ_b was set to be 0.3 (Mangalathu 2017). The stiffness for the bearing pad, K_{pad}, followed the suggestion by Mangalathu (2017) and was set to be 14.51 (kip/in). The Steel02 material model in OpenSeesPy is used to simulate bearing pads and is shown in Figure 4.22 with a hardening ratio, $b_{bearing}$, assumed to be 1%.

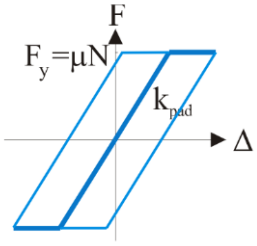

Figure 4.22: Elasto-Plastic bearing model (Mangalathu 2017)

4.4.5 Pounding

Pounding elements are used to reflect the impact between the bridge decks and the abutments during seismic events. The ImpactMaterial model is used to model pounding at these locations in OpenSeesPy. The material model is based on work proposed by Muthukumar and DesRoches (2006) that accounts for hysteretic energy loss caused by the impact (Figure 4.23). Following the assumptions from Mangalathu (2017), the maximum displacement, Δ_m, is 1.0 inches and the yield deformation, $\Delta_{y-pounding}$, is $0.10\Delta_m$. The stiffnesses, k_1 and k_2 are assumed to be 1022.3 (kip/in) and 351.755 (kip/in) per ft width of backwall, respectively (Mangalathu 2017).

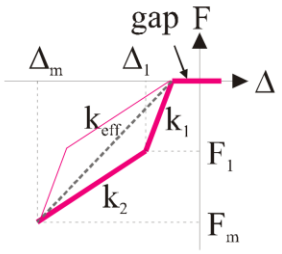

Figure 4.23: ImpactMaterial for pounding elements (Mangalathu 2017)

4.5 Parameter Summary Tables for the Reference Bridge

This section provides summary tables for the important input parameters for the material models described in the earlier sections of this chapter. Table 4.5 provides parameters of bridge deck, column, cross-beam, and bond-slip while Table 4.6 provides the parameters for the various components of bridge abutment.

Table 4.5: Parameters for bridge deck, column, cross-beam, and bond-slip

Bridge Deck, Column, and Cross-Beam			
concrete elastic modulus	E_c	4415.2	ksi
concrete shear modulus	G_c	1839.7	ksi
concrete poisson's ratio	ν_c	0.2	
concrete strength	f_c	6	ksi
cross-beam concrete elastic modulus	E_{c-beam} $(=E_c * 1000)$	441520	ksi
cross-beam concrete shear modulus	G_{c-beam} $(=G_c * 1000)$	183970	ksi
specified concrete strength	f'_c	4	ksi
unconfined concrete strain at peak strength	ϵ_c	0.002	
unconfined concrete ultimate strain	ϵ_u	0.004	
confined concrete strength	f_{cc}	7.11	ksi
confined concrete strain at peak strength	ϵ_{cc}	0.00385	
confined concrete ultimate stress	ϵ_{cu}	0.0122	
confined concrete ultimate strain	f_{cu}	4855.6	ksi
concrete maximum tension stress	f_t	0.711	ksi

concrete maximum tension strain	ϵ_t	0.000136	
confined concrete residual stress	f_{r-c}	0.142	ksi
unconfined concrete residual stress	f_{r-uc}	0.00711	ksi
transverse reinforcement ratio	ρ_{hoop}	0.5	%
reinforcement ultimate strain	ϵ_{su}	0.12	
column reinforcement yield strength	f_y	69.6	ksi
reinforcement elastic modulus	E_s	29000	ksi
column reinforcement strain hardening ratio	b_{col}	1.5	%
column torsional constant	J	164896	in4
Bond Slip			
bond-slip reinforcement strain hardening ratio	b_{slip}	1.08	%
bond-slip reinforcement yield strength	f_{y-slip}	60	ksi
bond slip reinforcement elastic modulus	E_{s-slip}	2085.12	kip/in
effective concrete depth	e_{depth}	10.44	in
bond slip concrete ultimate strain	ϵ_{u-slip} $(= \epsilon_{u-slip} * e_{depth})$	12.7	
bond slip concrete strain at peak strength	ϵ_{c-slip}	0.04	
Intermediate Foundation Springs			
Intermediate foundation rotational spring stiffness	K_r	7000000	kip-in/rad
Intermediate foundation translational spring stiffness	K_t	1300	kip/in

Table 4.6: Parameters for abutment spring material models

Backfill Soil			
backfill soil initial stiffness	K_{max}	15503	kip/in
backfill soil ultimate force	F_{ult}	-2375	kips
backfill soil failure ratio	R_f	0.7	
backfill gap distance	Δ_{abut}	1.00E-05	in
Abutment Spread Footing			
spread footing yield displacement	$\Delta_{y-spread}$	0.75	in
spread footing initial stiffness	E_{spread}	37.1	kip/in
Abutment Pile			
abutment piles first yield displacement	Δ_{1-pile}	1.17	in
abutment piles first yield force	F_{1-pile}	88	kip
abutment piles second yield displacement	Δ_{2-pile}	2.99	in
abutment piles second yield force	F_{2-pile}	157	kip
pinchX	$pinchX_{pile}$	0.75	
pinchY	$pinchY_{pile}$	0.5	
Shear Key			
shear key capacity	F_{shear}	2240.25	kips
shear key initial gap	Δ_{init}	0.5	in
shear key maximum displacement	Δ_{max}	4	in
pinchX	$pinchX_{shear}$	1	
pinchY	$pinchY_{shear}$	0	
Bearing Pad			
bearing yield force	$F_{y-bearing}$	17.88	kips
bearing friction coefficient	μ_b	0.3	

bearing initial stiffness	K_{pad}	14.51	kip/in
Bearing strain hardening ratio	$b_{bearing}$	1	%
Pounding			
pounding yield deformation	$\Delta_{y-pounding}$	0.1	in
pounding maximum displacement	Δ_m	1	in
pounding first stiffness	k_1	1022.3	kip/in/ft
pounding second stiffness	k_2	351.755	kip/in/ft

Chapter 5: Response of the Reference Bridge Model

The MDOF model of the reference bridge developed in Chapter 4 consists of detailed numerical modeling strategies for the columns and abutments. In order to understand the static and dynamic behavior of the reference bridge model before variations in key parameters are studied in later chapters, this chapter presents an array of simplified analyses. The analyses were used to verify the behaviors of different components of the reference MDOF bridge model and to compare with the idealized SDOF bridge model (Kortum et al. 2022) from the previous study (Section 2.4).

Section 5.1 presents the pushover analyses that were used to ensure the model components are behaving as expected. Section 5.2 similarly shows the response of the reference bridge mode for quasi-static cyclic loading. In Section 5.3, the response of the bridge along with its various detailed abutment components are shown under bi-directional earthquake excitation. Finally, in Section 5.4, the dynamic analysis response of the reference model and the idealized SDOF model were compared for selected ground motions.

5.1 Pushover Analysis

The purpose of this section is to show that under static pushover loading the key components of the model developed in Chapter 4 are behaving as expected. As shown in Figure 5.1, the abutment model developed in Chapter 4 consists of various spring elements. For bridges with semi-integral and L abutments, shear keys, bearing pads, poundings, spread footings/piles,

and backfill soil were included in the model while for integral abutments, only the spread footings/piles, and backfill soil were included.

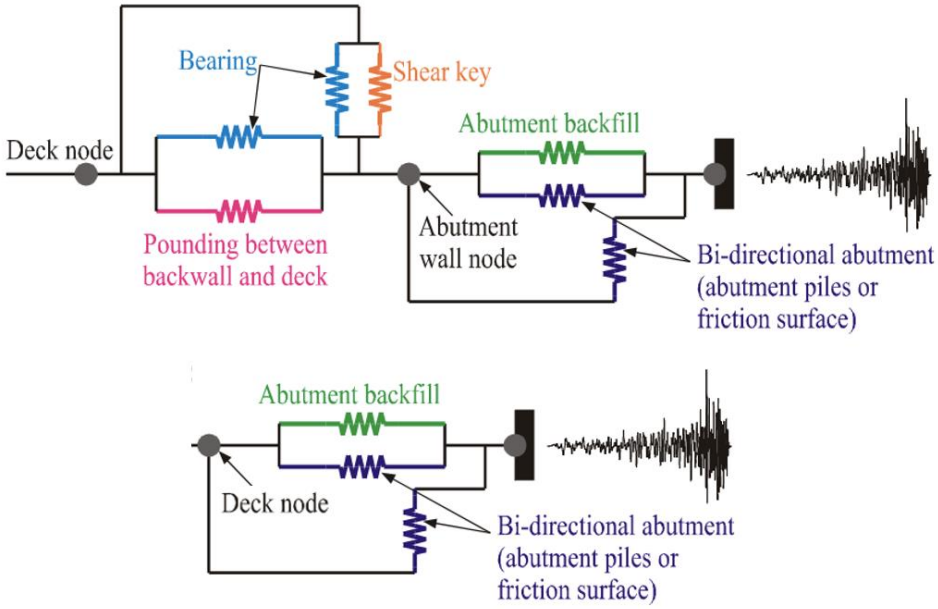

Figure 5.1: Zero length spring system for semi-integral and L abutment (upper) types, and for integral abutments (lower)

To verify the behavior of the bridge model, pushover analysis was done with different end support types and variations of the stiffness of each spring element. Only the L abutment model was included for the pushover analysis since it includes all the spring elements above while the semi-integral and integral abutment models did not. Section 5.1.1 lists the different bridge model cases that were considered, and Section 5.1.2 discusses the pushover analysis results.

5.1.1 Configurations of Abutment Spring Systems

Table 5.1 shows 4 different cases of the abutment model for the reference bridge that were used for the pushover analysis in both horizontal directions (transverse and longitudinal) to validate the modeling approach. As shown, the pushover analyses were done assuming each spring in the abutment model has 3 possible stiffness conditions in the horizontal directions, namely:

- soft: the element was assumed to have negligible stiffness
- stiff: the element was assumed to have large stiffness and behave like a rigid element
- actual: the element had the actual material model properties

The results of the pushover analyses for each case are presented and discussed in Section 5.1.2.

Table 5.1: Abutment model cases for modeling approach validation

Case number	**Abutment type**	**Shear keys stiffness**	**Bearing stiffness**	**Pounding stiffness**	**Piles/Spread footings stiffness**	**Backfill Soil stiffness**
1	L abutment	soft	soft	soft	stiff	stiff
2	L abutment	soft	actual	soft	stiff	stiff
3	L abutment	actual	actual	actual	stiff	stiff
4	L abutment	actual	actual	actual	actual	actual

5.1.2 Response of Pushover Analysis

The pushover analyses in the transverse and longitudinal directions were conducted for each case in Table 5.1 to a displacement at the center of mass of the bridge to be 15 inches.

Results for Case 1 are shown in Figure 5.2, where the forces in each abutment element are compared with the sum of the shear forces in all the columns and the total base shear. In case 1, the forces for all the abutment springs were zero since the bearings, shear keys, and pounding elements had no resistance due to their negligible stiffnesses. The piles or spread footing springs and backfill springs also had no force since they were connected in series to the bearing, shear keys, and pounding elements. As a result, the lateral load for the bridge was resisted only by the columns, causing the black (entire bridge) and red (sum of all columns forces) lines to lie on top of each other. Furthermore, the pushover curves are almost identical in two horizontal directions. The slight difference between the pushover response in the longitudinal and transverse directions results from the overturning resistance provided by the bent in the transverse direction that come from the column axial force couple.

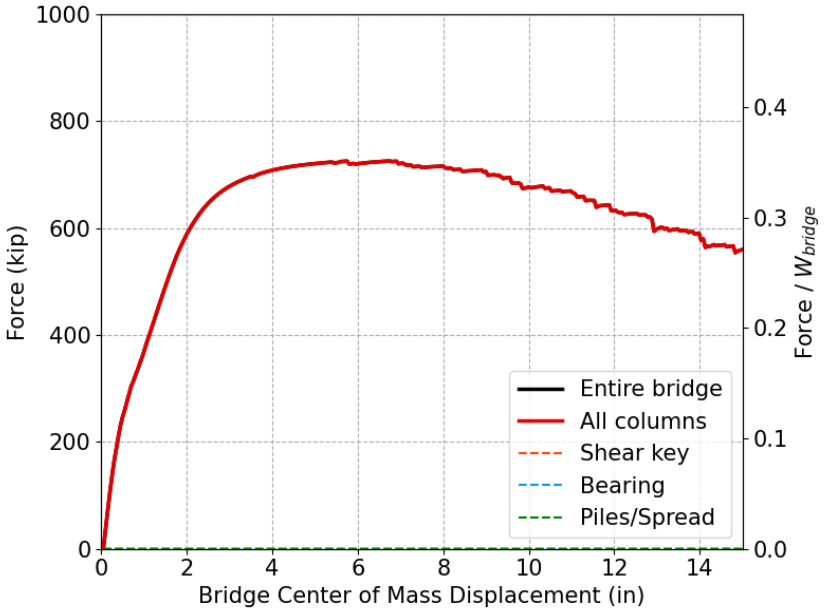

(a) Transverse direction

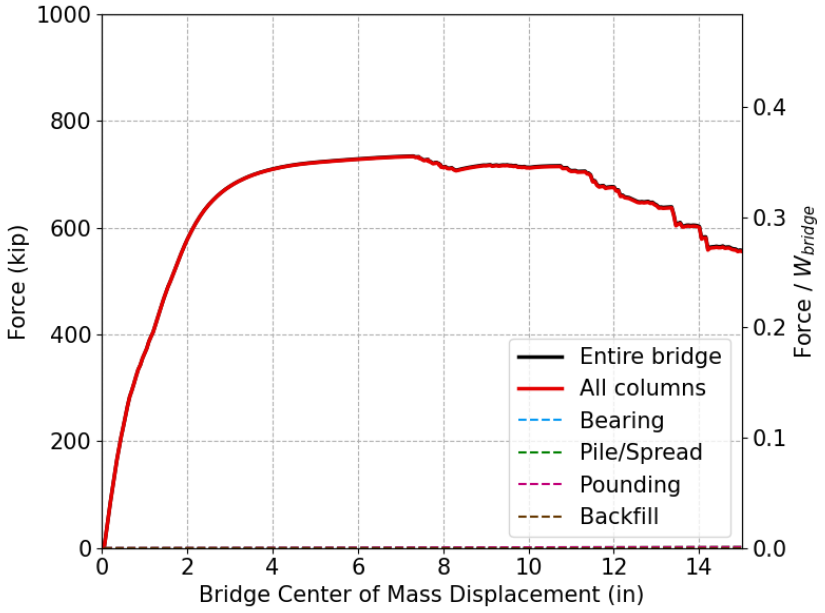

(b) Longitudinal direction

Figure 5.2: Case 1 pushover curves in the (a) transverse and (b) longitudinal directions

The bearings in Case 2 had the actual stiffness as computed in Chapter 4. The pushover results for Case 2 are in Figure 5.3. In the transverse direction, the bearing pads resisted their maximum force and that force was transmitted to the transverse piles/spread springs, resulting in the overlapping light blue (bearing) and green (piles/spread) lines. The difference between total pushover force and the sum of the load in the columns was the force resisted by the bearings. In the longitudinal direction, the bearing pads also resisted loads that were then transmitted to the piles/spread springs. Although both piles/spread springs and backfill elements were set to "stiff", the stiffness for the piles/spread springs was considerably larger, resulting in the bearing force being largely transferred to the piles/spread elements. Pounding and shear key elements resisted no force because their resistance was zero. Again, the response in both lateral directions are similar.

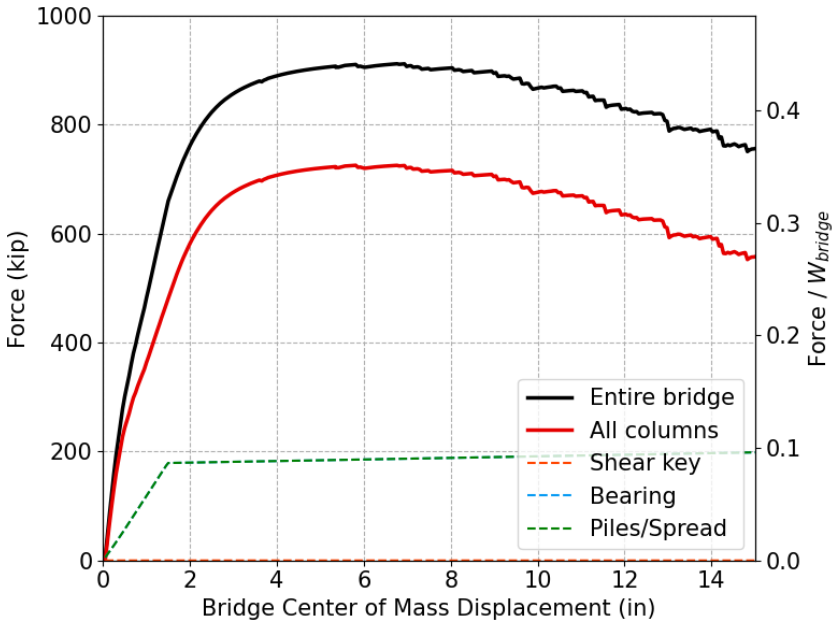

(a) Transverse direction

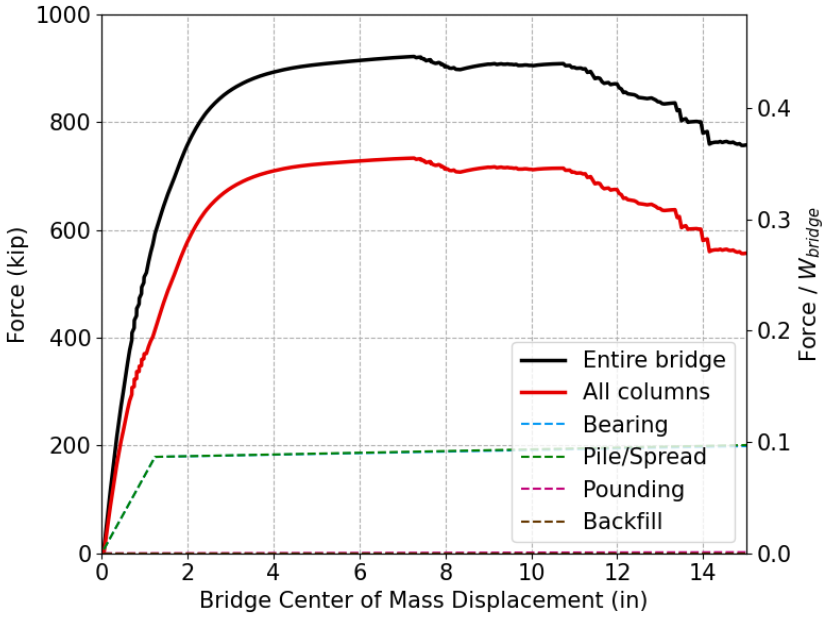

(b) Longitudinal direction

Figure 5.3: Case 2 pushover curves in the (a) transverse and (b) longitudinal directions

Figure 5.4 shows the pushover response for Case 3, which had shear key, bearing, and pounding elements with their actual stiffnesses while piles/spread springs and backfill stiffnesses were set to be stiff. In the transverse direction, when displacement was less than the shear key gap (around 0.5 inches), the bearings and piles/spread springs had the same forces due to their series connection. The forces in the shear key elements started increasing when the shear key gap was closed and eventually peaked at around 5500 kips followed by its failure consistent with the prescribed behavior discussed in Chapter 4. The remaining resistance was then only from the bearing, piles/spread elements, and the columns. In the longitudinal direction, when displacement was less than the pounding gap (approximately 0.95 inches), the bearings and piles/spread elements had the same forces due to their series connection. The forces in the pounding elements started increasing after the pounding gap was closed. Furthermore, the sum of force of bearing and pounding elements are equal to the sum of forces in the piles/spread elements and the backfill elements.

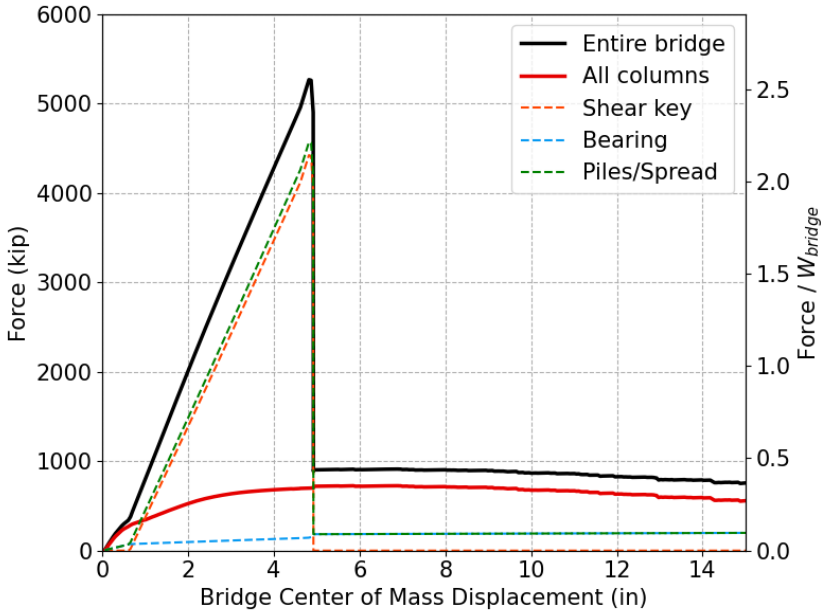

(a) Transverse direction

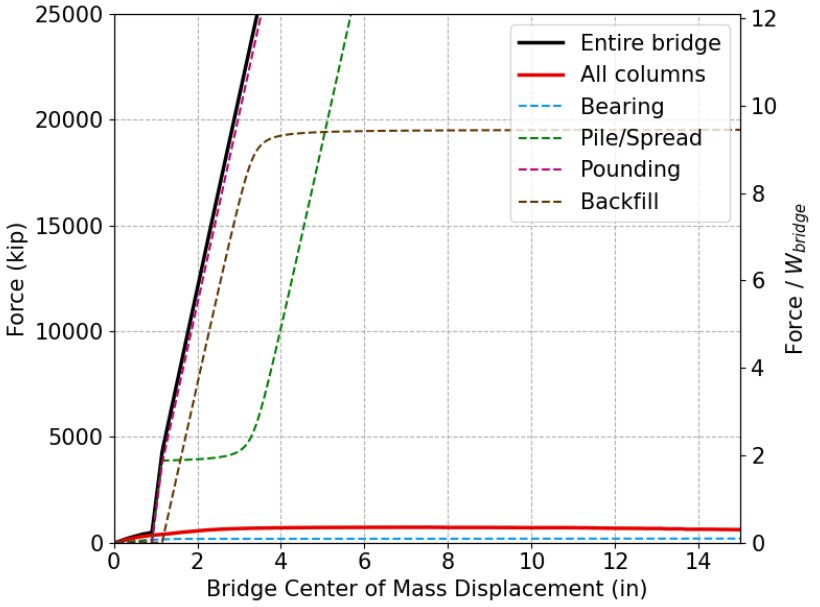

(b) Longitudinal direction

Figure 5.4: Case 3 pushover curves in the (a) transverse and (b) longitudinal directions

Figure 5.5 presents the pushover results for the bridge model with all of the abutment elements having the actual stiffnesses as developed in Chapter 4. In the transverse direction, the lateral force began to increase rapidly after the shear key gap was closed. Then, the lateral force was limited by the piles/spread elements until their maximum capacity of the piles/spread elements (approximately around 2300 kips) was reached. In the longitudinal direction, the lateral force began increasing after the pounding gap was closed. Then, the lateral force was capped at the maximum capacity of backfill elements (around 20000 kips) and the pushover curve matches the hyperbolic curve prescribed for the backfill elements.

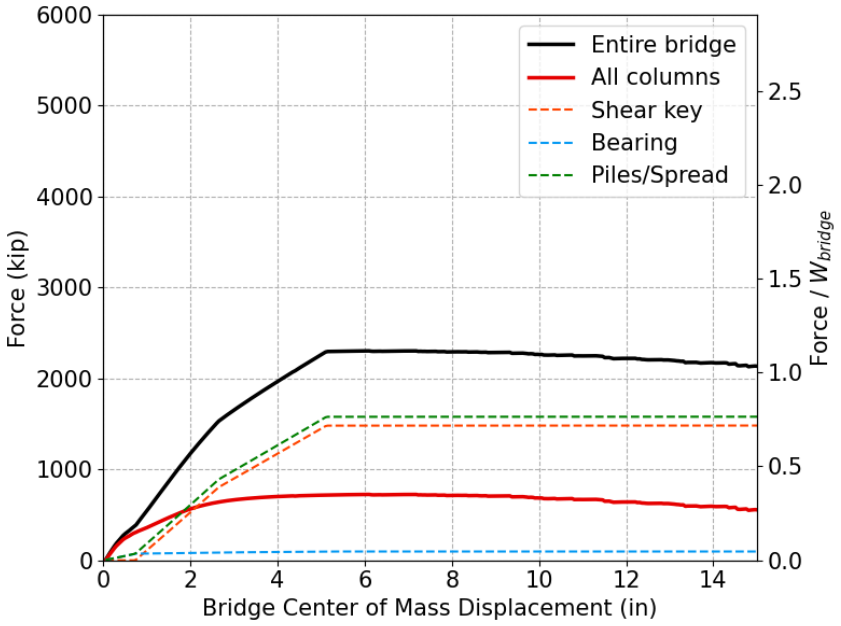

(a) Transverse direction

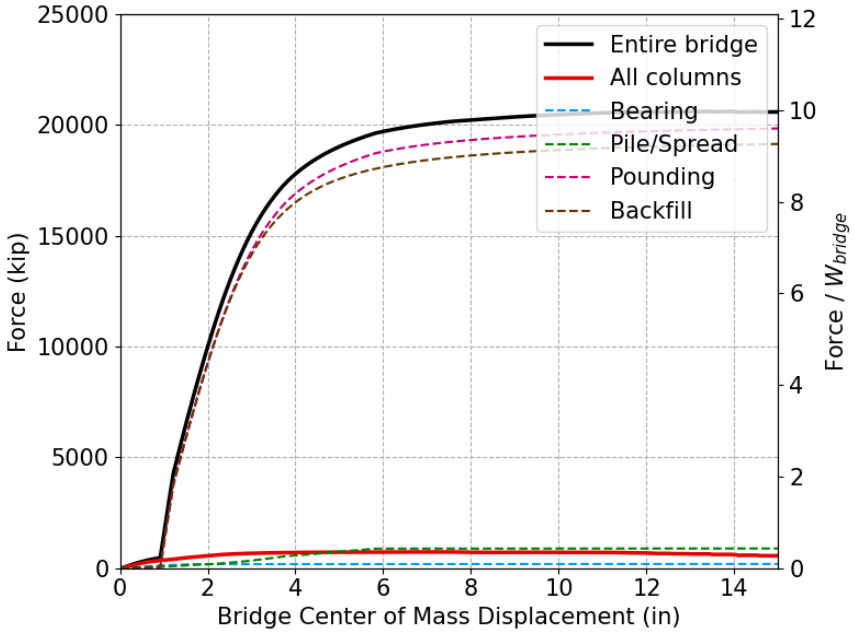

(b) Longitudinal direction

Figure 5.5: Case 4 pushover curves in the (a) transverse and (b) longitudinal directions

5.2 Quasi-Static Cyclic Analysis of the Reference Bridge Columns

Quasi-static cyclic displacement loading is often used to observe the deterioration of structures both in the laboratory and in numerical analysis. To show the deterioration behavior of the columns in the reference bridge model, quasi-static cyclic loading was applied in the transverse direction to the bridge model corresponding to Case 1 in Table 5.1. Cycles were applied at increasing amplitude drift ratios that ranged from 0.2% (0.5 inches) ~ 5.0% (13.0 inches).

As shown in Figure 5.6, the columns yield at a bridge lateral force of about 625 kips and a center of mass displacement of 2.5 inches. This is followed by a secondary slope resulting from strain-hardening in the reinforcing steel. Stiffness deterioration and pinching is evident in the cyclic response and the overall response is consistent with the expectations for the column models developed in Chapter 4.

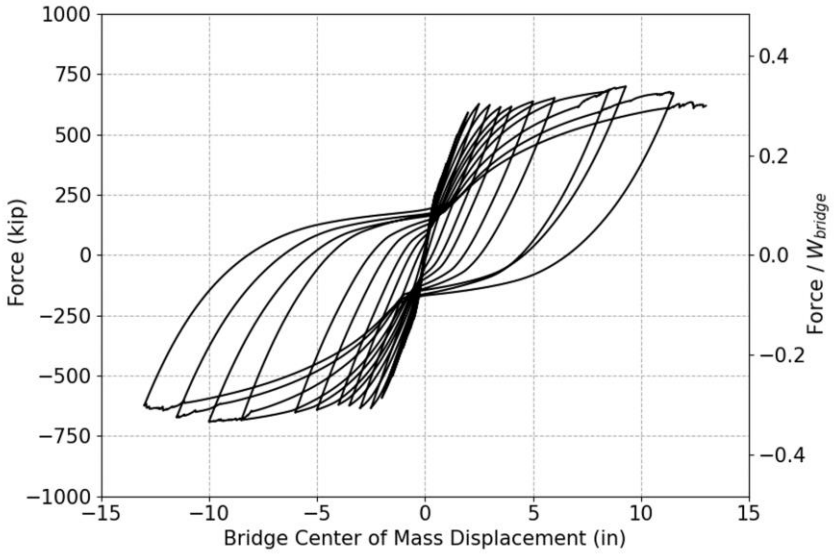

Figure 5.6: Cyclic lateral force versus bridge center of mass displacement for Case 1 showing the cyclic behavior and deterioration for the bridge columns in transverse direction

5.3 Bi-directional Dynamic Analysis

This section presents detailed results for a bi-directional dynamic analysis for the reference bridge (corresponding to Case 4 in Table 5.1). The baseline M9 ground motion selected for this demonstration analysis was realization csz002 for the Ocean Shores site and Figure 5.7 shows the original ground motion time history in unit g. Both horizontal components of the ground motions were applied, with the x-direction component applied to the transverse direction and the y-direction component applied to the longitudinal direction of the bridge model.

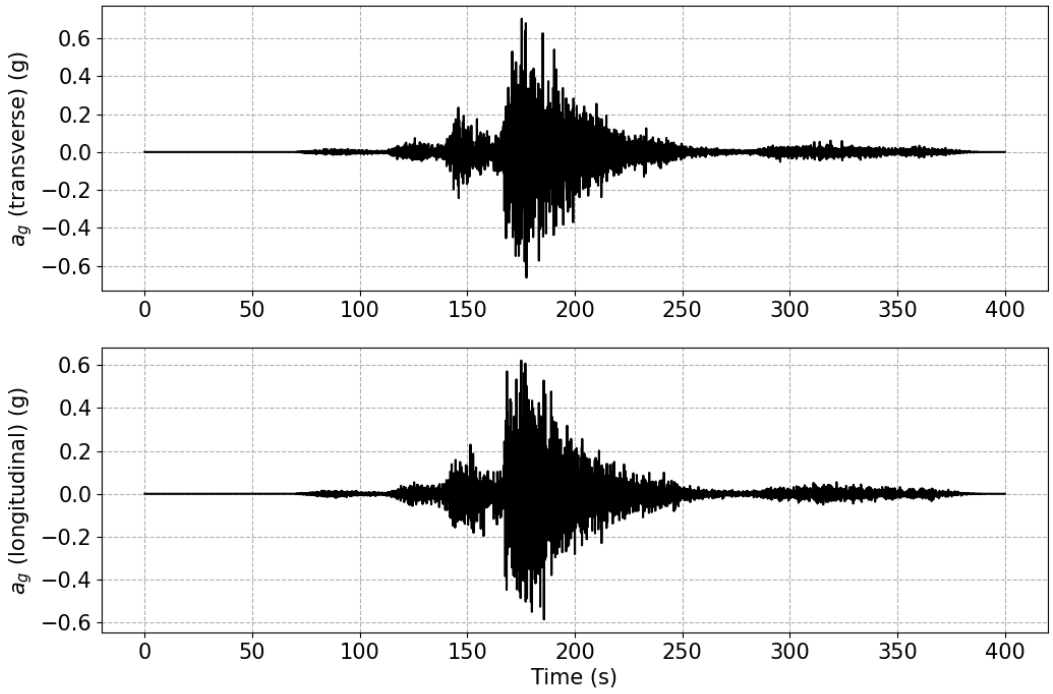

Figure 5.7: Baseline ground motion time history for realization csz002 for the Ocean Shores site

5.3.1 Dynamic Response of Bridge Columns

Figure 5.8 presents the dynamic response of the columns under the sample M9 ground motions. Although the ground motion time history in the x- and y-directions are very similar (with peak ground acceleration values close to 0.6 g), the maximum displacement in the transverse direction (3.18 inches) is almost two times of that in the longitudinal direction (1.65 inches). This results from the presence of the pounding elements in the longitudinal direction, providing large stiffness in the longitudinal direction compared to that in the transverse direction (Figure 5.5). Furthermore, from the almost identical displacements at bent 1, the center of mass of the bridge, and bent 2, the bridge deck behaved as close to a rigid body during the earthquake excitation.

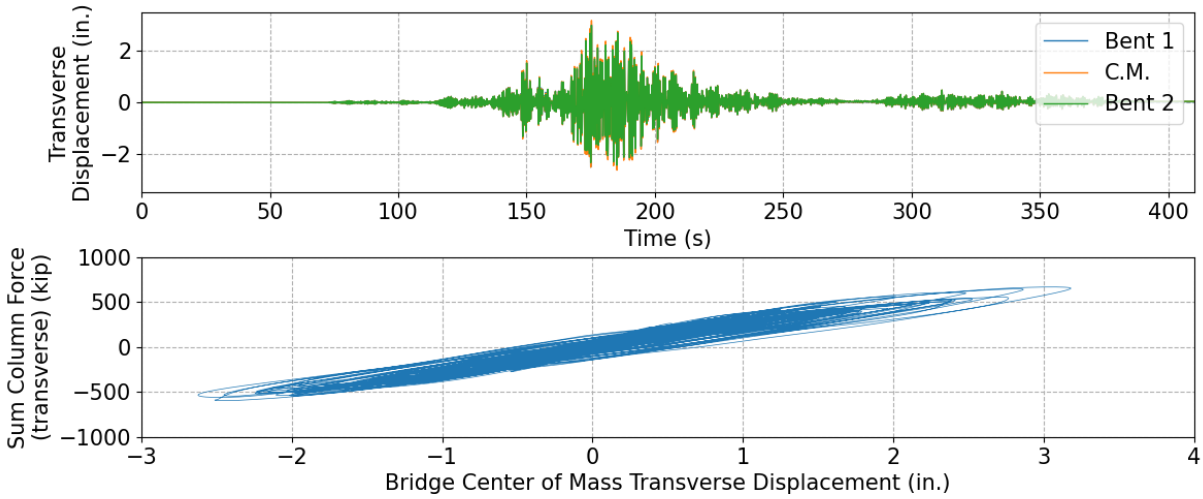

(a) Transverse direction

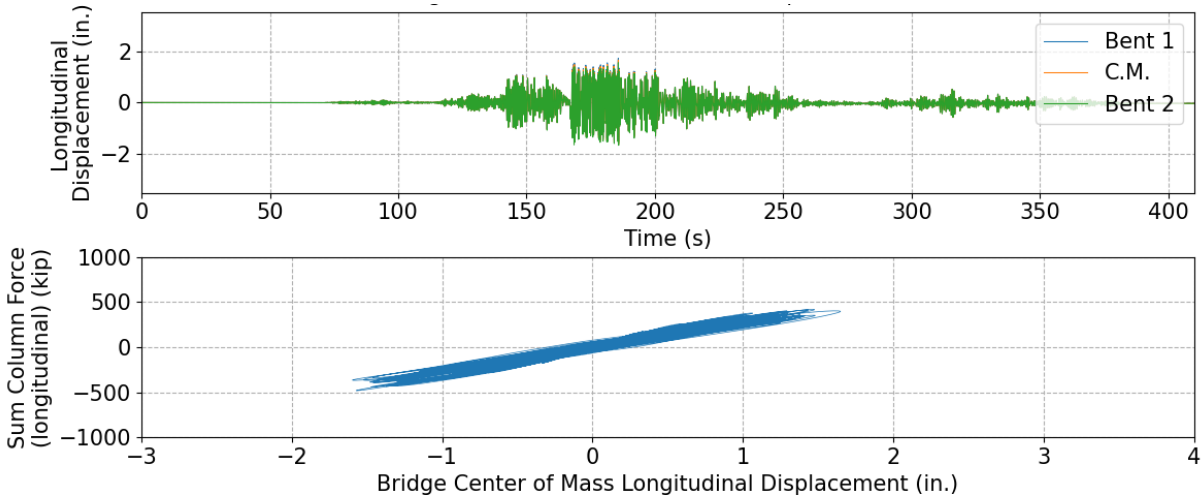

(b) Longitudinal direction

Figure 5.8: Dynamic response of bridge columns in the transverse and longitudinal directions

5.3.2 Dynamic Response of Abutment Springs

The responses of the various abutment springs are shown in Figures 5.9 and 5.10 for the left and right abutments, respectively. The bearing springs had elastic plastic material models and reached a maximum capacity of 17.79 kips. Shear key springs began to resist seismic forces when the shear key gap was closed at 0.5-inch deck displacement in the transverse direction. The piles/spread springs had a hysteretic bi-linear material model and had larger responses in the transverse direction. The pounding and backfill springs had large forces due to their high stiffness values, which resulted in smaller displacement response for the bridge in the longitudinal direction than in the transverse direction. Furthermore, the displacement responses are symmetric in the longitudinal direction, which is expected for the left and right abutments.

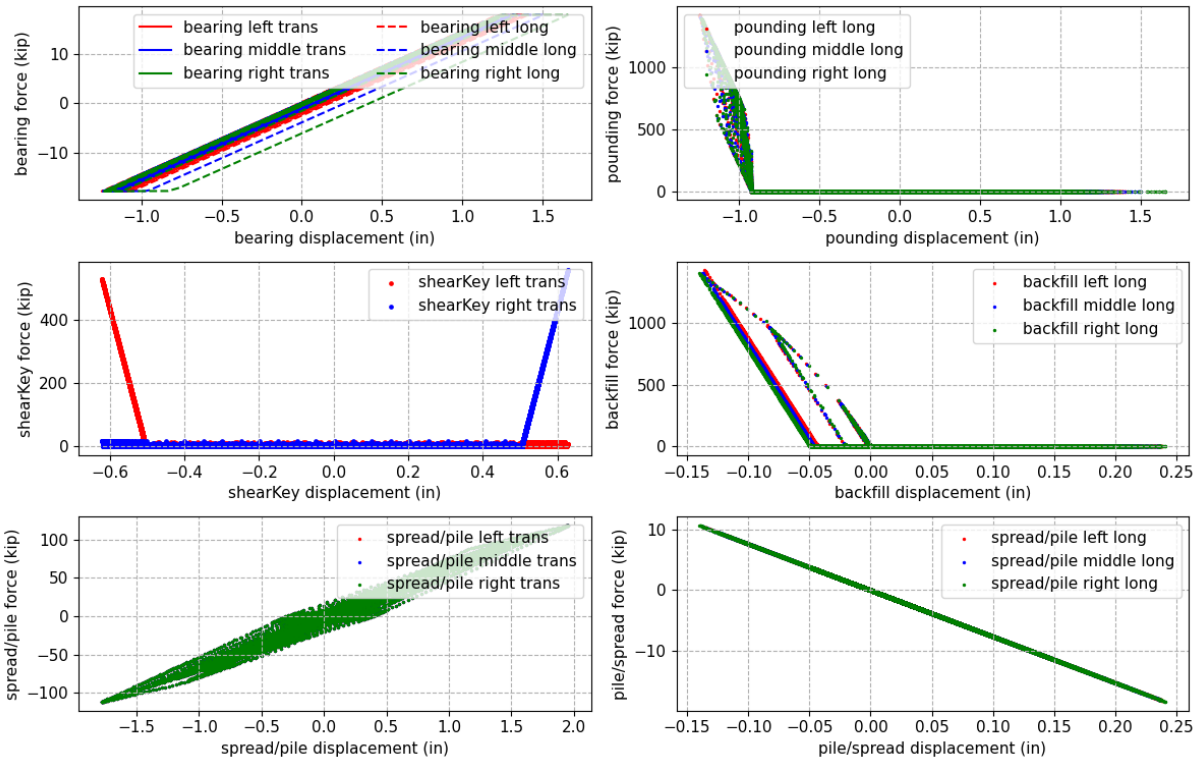

Figure 5.9: Dynamic response of abutment springs at the left abutment

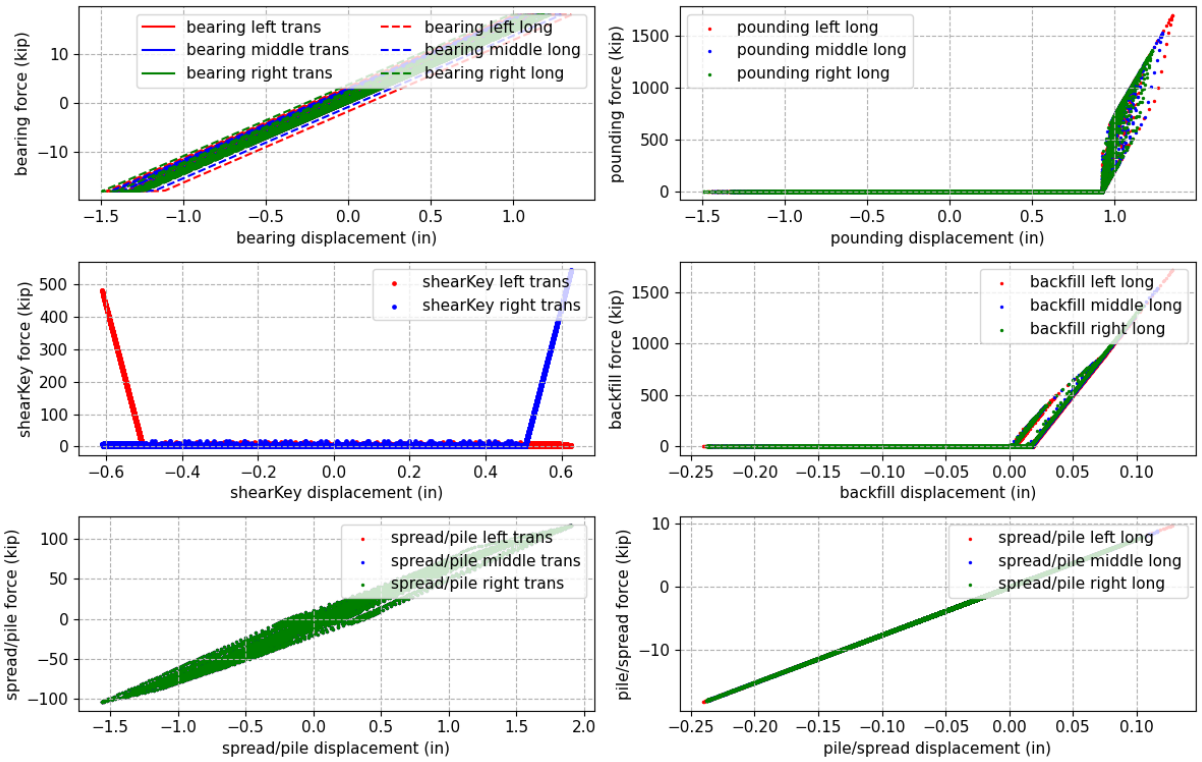

Figure 5.10: Dynamic response of abutment springs at the right abutment

5.4 Comparison with an Idealized SDOF Bridge Model

Kortum et al. (2022) developed an idealized SDOF model to study the impact of M9 ground motions on highway bridges without considering the existence of abutments (Section 2.4). The SDOF model used the stiffness and the lateral capacity of the columns along with other input parameters (i.e., the total bridge mass) to approximate the force-displacement response of the entire bridge. In this section, comparisons for dynamic response were made between the idealized SDOF model (Kortum et al. 2022) and the MDOF model developed in Chapter 5 before the parametric study in Chapter 6, 7, and 8. Furthermore, the MDOF model for the analysis in this

section corresponds to Case 1 in Table 5.1 as that is comparable to the SDOF model that neglected the abutment response.

Section 5.4.1 describes the methodology of the comparison and Section 5.4.2 presents the results of the dynamic analyses for the SDOF and MDOF models.

5.4.1 SDOF Model Properties

The input effective stiffness and lateral capacity for the SDOF model were derived from the pushover curve of the MDOF model following the recommendations of Elwood-Eberhard (2009). The resulting bi-linear force-displacement relationship was then used for the idealized SDOF model. Figure 5.11 shows the definition of the measured yield displacement and the effective stiffness that were used to construct the bi-linear force-displacement relationship for the SDOF.

The effective stiffness of the bridge was calculated by connecting the origin with the point of first yield of steel (most outer steel strain equal to 0.002). The lateral capacity of the bridge was the force where the extension of this curve intersected with the point where the concrete strain equaled 0.004. The line is then continued with a slope of 1.5%. Figure 5.12 shows the MDOF pushover curve along with the idealized bi-linear force-displacement relationship following the recommendations of Elwood-Eberhard (2009). The resulting idealized curve had an effective stiffness of 377.66 kip/in and a lateral capacity of 710 kips.

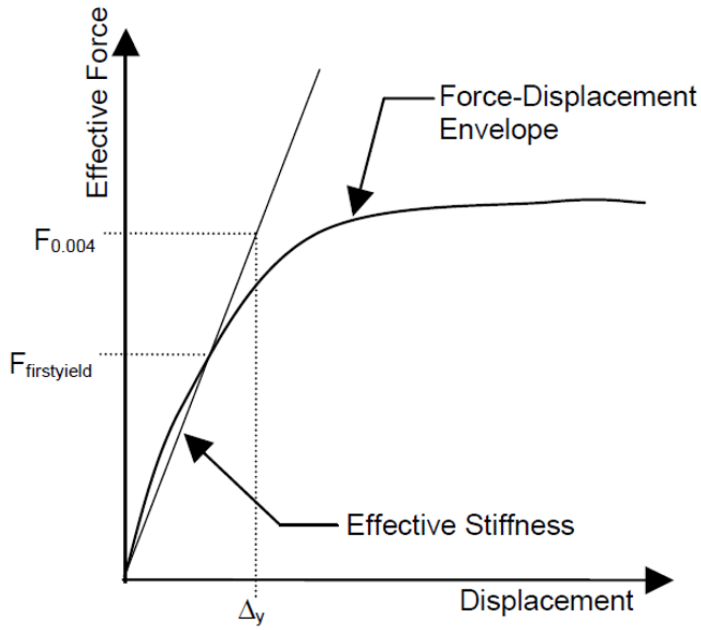

Figure 5.11: Definition of measured yield displacement and effective stiffness

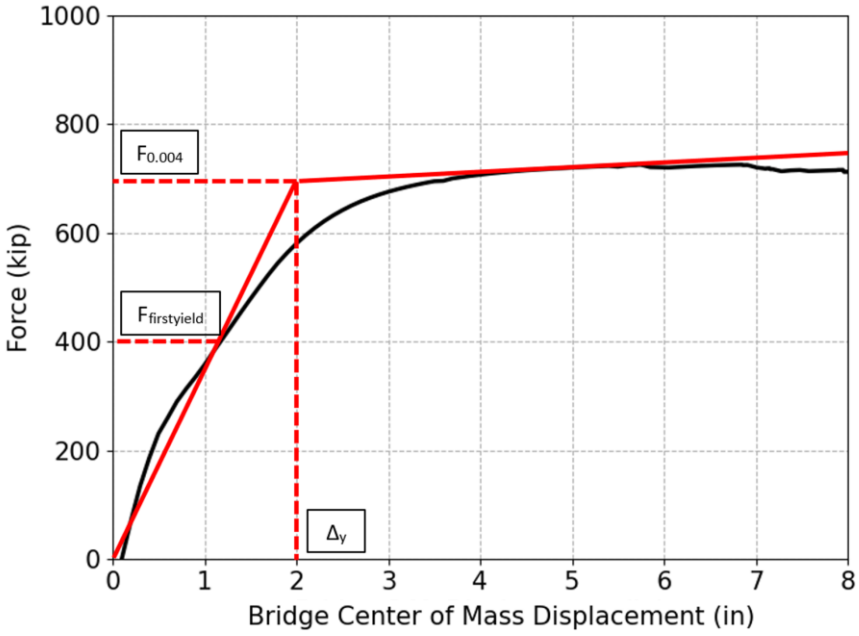

Figure 5.12: Pushover curve for the Case 1 MDOF model (black) and the idealized bi-linear curve (red)

5.4.2 Comparison of MDOF and SDOF Dynamic Response

The M9 ground motions used for comparing the dynamic response of the idealized SDOF model and the MDOF model are listed in Table 5.2. Ground motions from two cities (Ocean Shores and Seattle) were chosen. For each location the x-component of all 30 realizations were run, each using 10 randomly chosen soil profiles for site class C2. This results in a total of 600 analyses (300 for each city). The ground motions were applied in the transverse directions of both the MDOF and SDOF model.

Table 5.2: Selected ground motions for comparison of the dynamic response of the SDOF and MDOF bridge models

Cities	**Number of Realizations**	**Site Class**	**Soil profile category**	**Direction**	**Number of ground motions**
Ocean Shores	30	C2	Random 10	x	300
Seattle	30	C2	Random 10	x	300

Figures 5.13 and 5.14 compares the maximum displacement dynamic response for the SDOF and MDOF models for Ocean Shores and Seattle. The displacement responses for Ocean Shores are larger than that for Seattle. For both cities, the responses of the SDOF and the MDOF models were close to each other as illustrated by how close the track to the 1-to-1 line in the figures. This provides confidence in the dynamic results of the more complicated MDOF model.

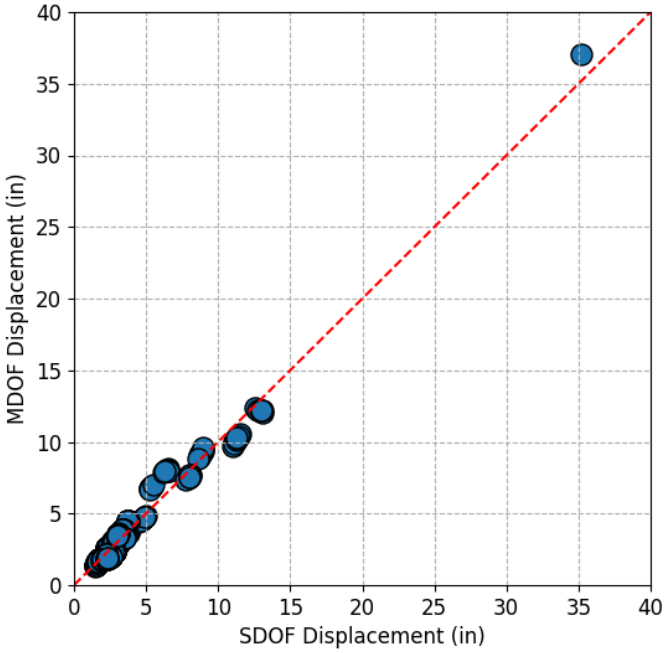

(a)

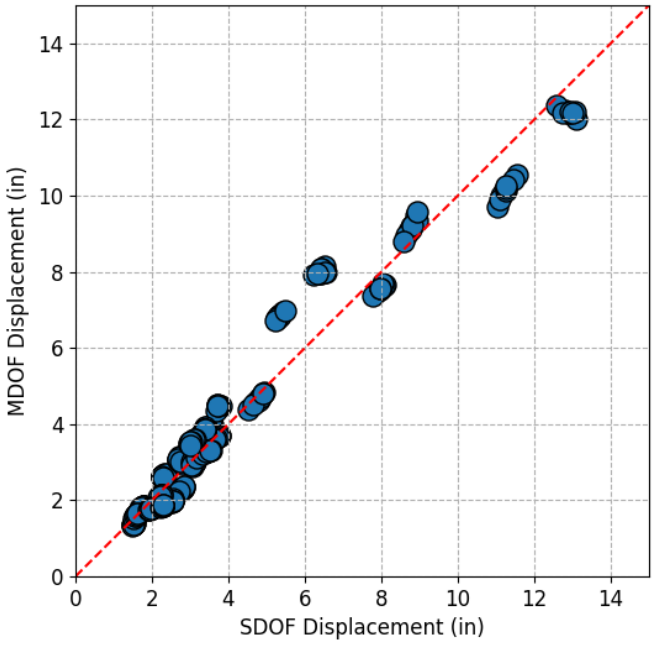

(b)

Figure 5.13: Comparison of dynamic response of SDOF and MDOF models for Ocean Shores. (a) figure showing all data, (b) figure showing the data between 0 and 15 inches of bridge displacement

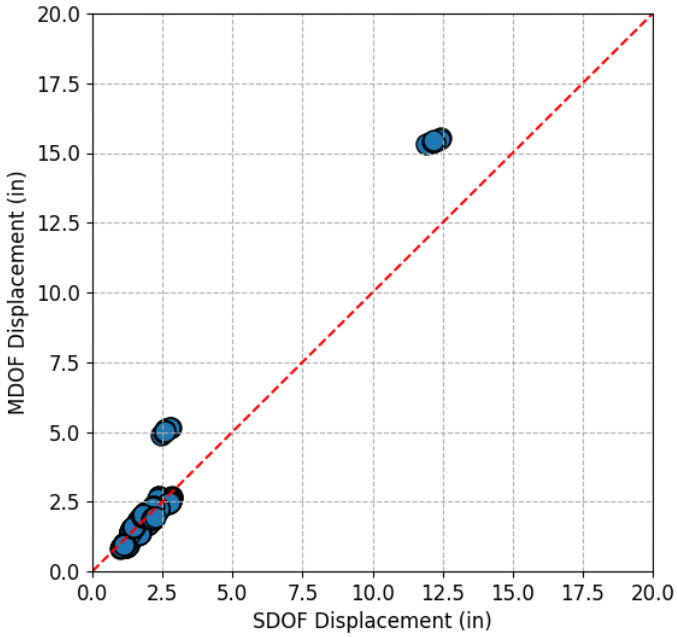

(a)

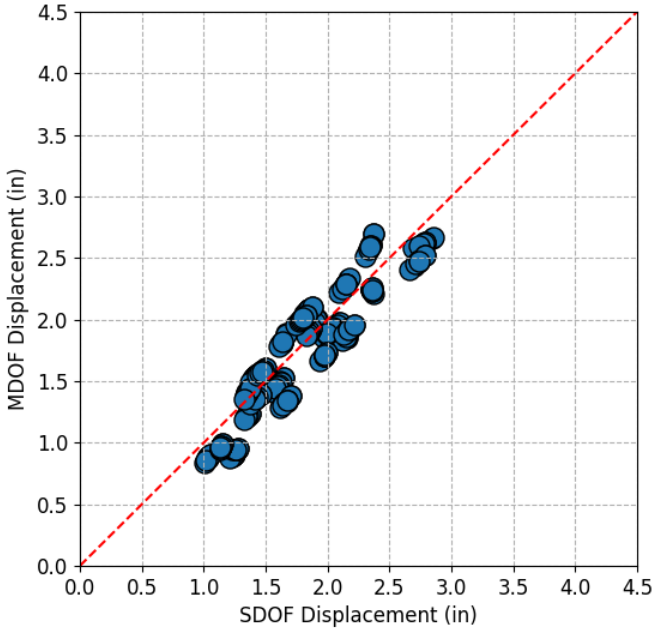

(b)

Figure 5.14: Comparison of dynamic response of SDOF and MDOF models for Seattle. (a) figure showing all data, (b) figure showing the data between 0 and 4.5 inches of bridge displacement

Chapter 6: Effects of Geographic Location and Site Class

This chapter describes a parametric study of the effects of geographic location, site class, and the 30 different earthquake rupture scenarios (Section 2.3) on the simulated performance of the reference bridge during an M9 CSZ earthquake. The development of the ground motions used in the parametric study are described in Chapter 2, the OpenSeesPy model of the reference bridge is discussed in Chapter 4, and the behavior of that model is examined in Chapter 5.

The ground motions used for the parametric study included all 30 realizations (Section 2.3) of the M9 ground motions (Frankel et al. 2018). For each simulation, the orientation of the horizontal components (North-South and East-West) were randomly assigned to the transverse and longitudinal directions of the bridge model. The parametric study was conducted using the Stampede2 supercomputer at the Texas Advanced Computing Center (TACC) at the University of Texas at Austin.

Sections 6.1 and 6.2 discuss the selection of geographic locations and site classes, respectively, for the parametric study. Section 6.3 discusses the effects of geographic location and site class on the deformation demands for the reference bridge, Section 6.4 compares the bent deformations with the mean deformation estimates at spalling and bar buckling, and Section 6.5 discusses the force demands. Lastly, in Section 6.6, the effect of different earthquake scenarios (30 realizations) on the reference bridge are presented.

6.1 Selection of Representative Locations

In their SDOF studies, de Zamacona (2019) and Kortum et al. (2022) selected 10 cities (Section 2.2) to represent a wide variety of source-to-site distances and basin depths. The MDOF model developed for this parametric study required considerably more computational effort per simulation, so to reduce the computational demands, this study considered only six of these 10 cities, while maintaining a variety of geographic locations and basin depths. Table 6.1. lists the six selected representative cities and their key characteristics. All six selected cities were included in the analyses of the reference bridge.

Table 6.1: Six selected representative cities

City Name	**Latitude**	**Longitude**	**Basin Depth $Z_{2.5}$ (km)**	**Site Classification**	**Analyses Performed**
Forks	47.9504	-124.386	0.76	Coastal, Outside of Basin	Reference Bridge Only (Ch. 6)
Ocean Shores	46.9737	-124.156	0.98	Coastal, Outside of Basin	All Bridge Cases (Ch. 6, 7 and 8)
Port Angeles	48.1181	-123.431	2.29	Inland, Shallow Basin	All Bridge Cases (Ch. 6, 7 and 8)
Olympia	47.0379	-122.901	1.96	Inland, Outside of Basin	Reference Bridge Only (Ch. 6)
Seattle	47.6062	-122.332	6.70	Inland, Deep Basin	All Bridge Cases (Ch. 6, 7 and 8)
Everett	47.979	-122.202	3.42	Inland, Deep Basin	Reference Bridge Only (Ch. 6)

6.2 Selection of Representative Soil Profiles

De Zamacona (2019) and Kortum et al. (2022) used 30 soil profiles (Section 2.4) to represent the variation in soil profile within each site class. These profiles are listed in Table 6.2. To reduce computational demands, 10 out of the 30 soil profiles were randomly selected (for each combination of city, site class and realization) for this study. The selection procedure resulted in 300 combinations (30 realizations and 10 randomly selected soil profiles) for each of the 4 site classes (Section 2.4). To evaluate the impacts of downselecting the profiles, the results for Ocean Shores were compared including all 30 soil profiles with the results using 10 randomly selected soil profiles. The differences were negligible. This suggests that the downsizing of the 30 soil profile set (300 combinations, rather than 900 combinations) did not significantly affect the results of the analyses. This downsizing was used in the parametric study in this chapter, as well as in the studies discussed in Chapters 7 and 8.

Table 6.2: Soil profile identifiers used for random selection (Adhi et al. 2017)

Site Class C2	**Site Class C4**	**Site Class D1**	**Site Class D3**
WA-DNR-08_87	7026	WA-DNR-08_210	DOGAMI-13_196
WA-DNR-08_90	WA-DNR-08_69	WA-DNR-08_24	WA-DNR-08_196
WA-DNR-08_41	KIMB-1	WA-DNR-08_68	DOGAMI-13_179
SFER	WA-DNR-08_91	DOGAMI-13_255	SCPT94-1
WA-DNR-08_57	WA-DNR-08_14	DOGAMI-13_74	DOGAMI-13_233
WA-DNR-08_164	PCFR	WA-DNR-08_39	FD86-4
WA-DNR-08_161	DOGAMI-13_132	WA-DNR-08_171	DOGAMI-13_131
ALKI	WA-DNR-08_20	7041	DOGAMI-13_223
GL2	WISH	DOGAMI-13_89	SCP95-24

Site Class C2	Site Class C4	Site Class D1	Site Class D3
WA-DNR-08_85	WA-DNR-08_73	LAWT	DOGAMI-13_123
BUCK	DOGAMI-13_79	WA-DNR-08_97	WA-DNR-08_225
HAO	DOGAMI-13_146	7043	DOGAMI-13_180
LTY	WA-DNR-08_12	WA-DNR-08_172	DOGAMI-13_141
DOGAMI-13_102	WA-DNR-08_45	WA-DNR-08_165	WA-DNR-08_190
WA-DNR-08_21	WA-DNR-08_217	ROSS	FD97-5
WA-DNR-08_77	LANE	DOGAMI-13_187	WA-DNR-08_143
WA-DNR-08_231	WA-DNR-08_28	WA-DNR-08_123	WA-DNR-08_5
WA-DNR-08_3	WA-DNR-08_75	DOGAMI-13_106	DOGAMI-13_20
WA-DNR-08_26	WA-DNR-08_187	DOGAMI-13_78	DOGAMI-13_38
BEVT	MRIN	WA-DNR-08_121	WA-DNR-08_232
WA-DNR-08_62	DOGAMI-13_76	WA-DNR-08_65	DOGAMI-13_181
WA-DNR-08_128	WA-DNR-08_175	WA-DNR-08_129	DOGAMI-13_98
WA-DNR-08_176	WA-DNR-08_219	WA-DNR-08_33	DOGAMI-13_31
WA-DNR-08_44	WA-DNR-08_81	WA-DNR-08_208	DOGAMI-13_28
WA-DNR-08_36	DOGAMI-13_114	7027-A	WA-DNR-08_46
WA-DNR-08_6	WA-DNR-08_83	DOGAMI-13_164	WA-DNR-08_199
LYNC	7034	DOGAMI-13_150	WA-DNR-08_115
WA-DNR-08_18	QKTN	2172	WA-DNR-08_234
ERW	WA-DNR-08_151	WA-DNR-08_169	DOGAMI-13_64
BH_DEEPBH	SEW	WA-DNR-08_48	KNEL

6.3 Effects of Geographic Location and Site Class on Deformation Demands

This section presents the results of the parametric study on the effects of geographic location and site class (Sections 6.1 and 6.2) on the computed deformation demands induced by the M9 earthquake motions on the reference bridge.

The computed maximum displacements at the ends of the bridge in the transverse and longitudinal directions are summarized in Figure 6.1. Specifically, the figure shows the 15th, 50th (median), and 85th percentiles of displacement at the end of the superstructure as a function of location (6 cities) and site class (baseline, C2, C4, D1, D3). These displacements were slightly higher than the displacements of the foundation, because the bridge model included a 0.5-in. gap between the end of the superstructure and shear key (transverse direction) and backwall (longitudinal direction). The cities are arranged in the same order that they are listed in Table 6.1 and can be characterized as follows: coastal outside of basin (Forks, Ocean Shores), inland shallow basin (Port Angeles), inland outside of basin (Olympia), inland deep basin (Seattle, Everett).

Following a similar format, Figure 6.2 summarizes the maximum drift ratios for the bents in the transverse and longitudinal directions. The drift ratios were calculated as the maximum displacement (of either bent) divided by the clear column height, which was equal to 21.3 ft (256 inches), so a bent drift ratio of 1.0% corresponds to a bent displacement of 2.6 inches. By comparison, the calculated effective yield displacement (Section 5.4.1) was 1.88 inches, which corresponds to a drift ratio of 0.73%. Note that the relative magnitudes of the values in Figures 6.1 and 6.2 are similar, because the superstructure was stiff compared to the columns.

Some key observations from Figures 6.1 and 6.2:

- In the longitudinal direction, the computed end displacements and bent drift ratios varied little among the various locations and site classes. The longitudinal displacements were consistently small, reflecting the displacement constraint provided by the foundation backfill soil and pounding element. Across all six cities, the median longitudinal end displacement never exceeded 2 inches, and the median longitudinal bent drift ratio never exceeded 0.7%, which is below the drift ratio at the effective yield. Even the 85th percentile values were small too, never exceeding values of 2.5 inches at ends and 1.0% for bents.
- In the transverse direction, the coastal locations (Forks and Ocean Shores) had the largest displacement responses. The highest responses in coastal cities were for site class D1, with the highest 85th percentile responses reaching values of almost 6 inches for the maximum end displacement and almost 2.5% for the maximum bent drift ratio.
- The responses tended to decrease as the distance from the coast increased. The median transverse displacements were 2 inches or less at the bridge ends and the median bent drifts were less than 0.8% for the two cities located far from the coast and on deep basins (Seattle and Everett). For these two locations, the responses consistently increased as the site became softer, reaching maximum value for site class D3, but the 85th percentile values never exceeded 2.5 inches at ends and 1% at bents.

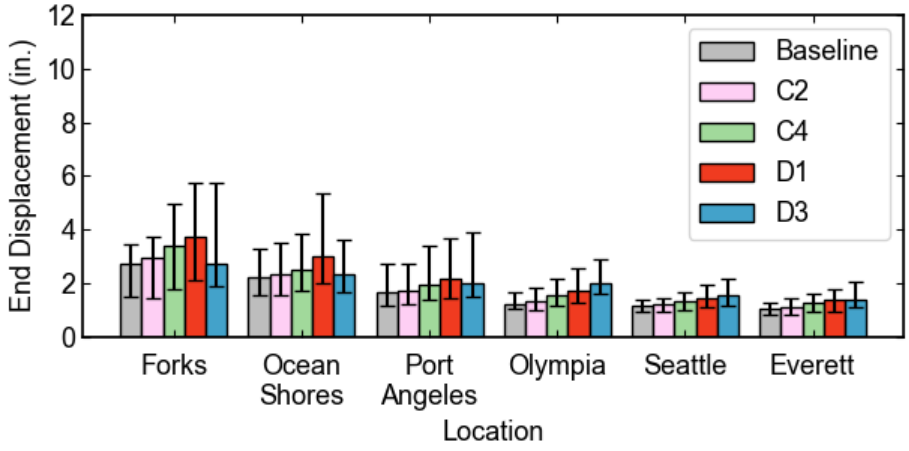

(a) Transverse direction

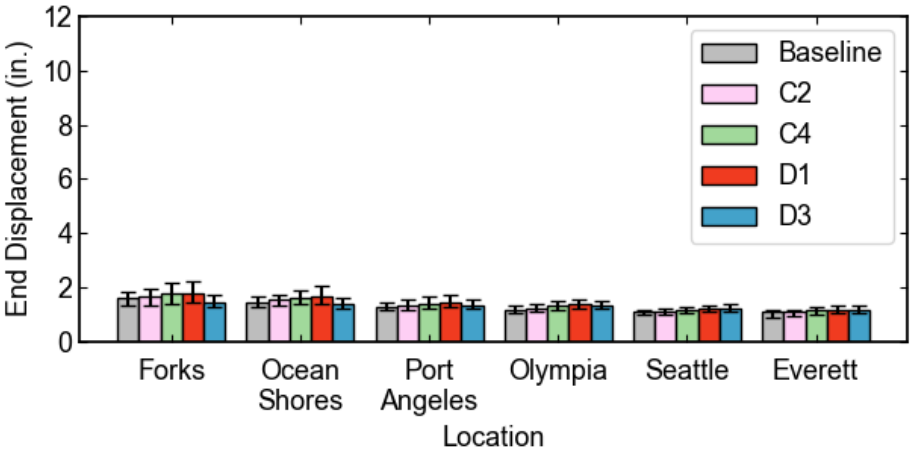

(b) Longitudinal direction

Figure 6.1: Maximum displacements at end of deck for median, 15th, and 85th percentiles

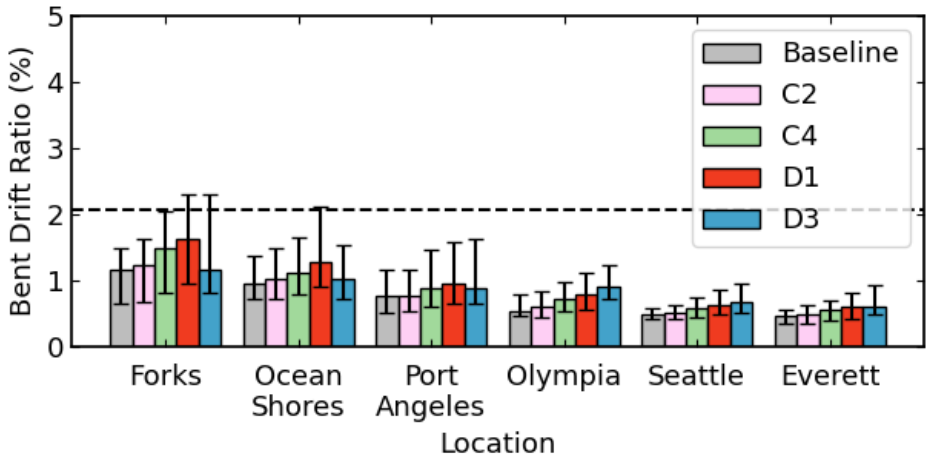

(a) Transverse direction

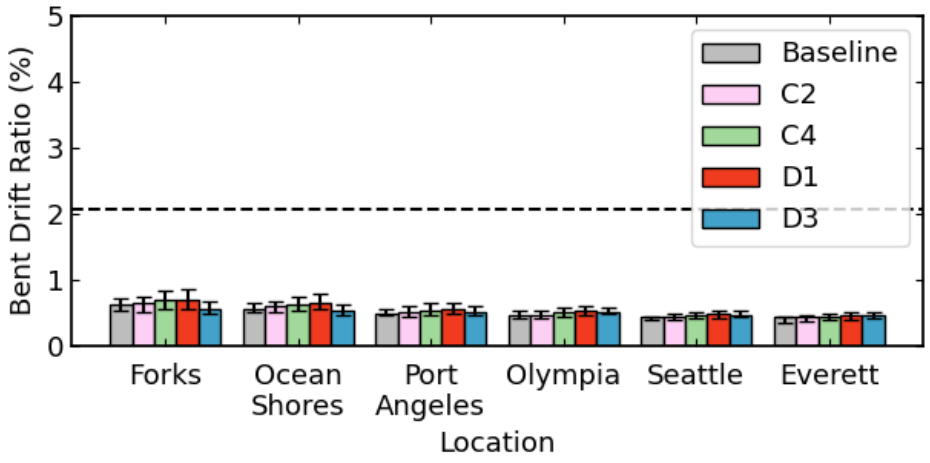

(b) Longitudinal direction

Figure 6.2: Maximum bent drift ratio for median, 15th, and 85th percentiles
(Dashed line represents the bent drift ratio corresponds to concrete spalling in Section 6.4)

6.4 Estimates of Bent Column Damage

The displacement demands in Figure 6.2 can be compared with the estimates of the deformations at the onset of column spalling and bar buckling. These two damage states are important, because spalling generally represents the first visible damage to a column that may require repairs, whereas bar buckling represents a more severe form of damage that may require long-term bridge closure and expensive repairs. The median drift ratios for both damage levels were computed following the recommendations of Berry and Eberhard (2007):

$$\frac{\Delta_{sp,calc}}{H_{col}}(\%) = 1.6\left(1 - \frac{P}{A_g f_c'}\right)\left(1 + \frac{L}{10D}\right) \qquad \text{(Equation. 6-1)}$$

where the axial-load ratio, $\frac{P}{A_g f_c'}$, was taken as 0.05, and the ratio of the distance to inflection point, normalized by the column depth was taken as $\frac{21.3\ (ft)}{2{\times}3\ (ft)} = 3.55$.

The resulting calculated mean drift ratio at spalling was 2.06%, which is shown as a horizontal, dashed line in Figure 6.2. In the longitudinal direction, the 85 percentile bent drift ratios were below the mean spalling value for all cities and soil classes. In the transverse direction, the median values never exceed 2.06%, but the 85% values do exceed this value for the two coastal cities (Forks, Ocean Shores).

Similarly, the mean drift ratio at the onset of bar buckling was calculated following the recommendations of Berry and Eberhard (2005), where the median drift ratio causing bar buckling is given by:

$$\frac{\Delta_{bb,calc}}{H_{col}}(\%) = 3.25\left(1 + k_{e,bb}\rho_{eff}\frac{d_b}{D}\right)\left(1 - \frac{P}{A_g f_c'}\right)\left(1 + \frac{L}{10D}\right) \qquad \text{(Equation. 6-2)}$$

$k_{e,bb}$ was taken as 150, ρ_{eff} was taken as 0.0 for old bridge, and the ratio of the longitudinal bar diameter to the column depth, $\frac{d_b}{D}$, was taken as 0.0313.

Based on Equation 6.2, the mean drift ratio at the onset of bar buckling was 4.18%. This drift ratio exceeds the 85th percentile values of bent deformation demands for all combinations of locations and site classes.

6.5 Effects of Geographic Location and Site Class on Maximum Forces

This section presents the results of the parametric study of the effects of geographic location and site class (Sections 6.1 and 6.2) on the computed column and shear-key force demands induced by the earthquake motions in the reference bridge.

The results in Figure 6.3 are given in terms of the maximum sum of column lateral forces normalized by the bridge weight (2066 kips). The lateral load at effective yield was 118 kips for each column, so the sum of the column resistances at effective yield of the six columns were approximately equal to 710 kips (Section 5.4.1), which corresponded to a base-shear strength ratio of 0.32. This value is shown as a horizontal dashed line in Figure 6.3.

In the longitudinal direction, the computed column horizontal forces varied little among the various locations and site classes. Due to the constraint provided by the foundation backfill soil and pounding element in longitudinal direction, the column forces were consistently small. Across all six cities, the median longitudinal sum of column forces never exceeded 22% of the bridge weight (64% of the effective yield force) and the 85th percentile values never reached 25% of the bridge weight (73% of the effective yield force).

The sum of column horizontal forces in the transverse direction had the highest values in coastal cities. In this direction, the median values of column resistance were near the yield values for all site classes. The values were largest in the coastal cities for site class D1.

In the transverse direction, as the location moves inland, the responses of the softest soil site class (D3) increased compared to the responses for other soil site classes within the same location. (Figure 6.3 and 6.4)

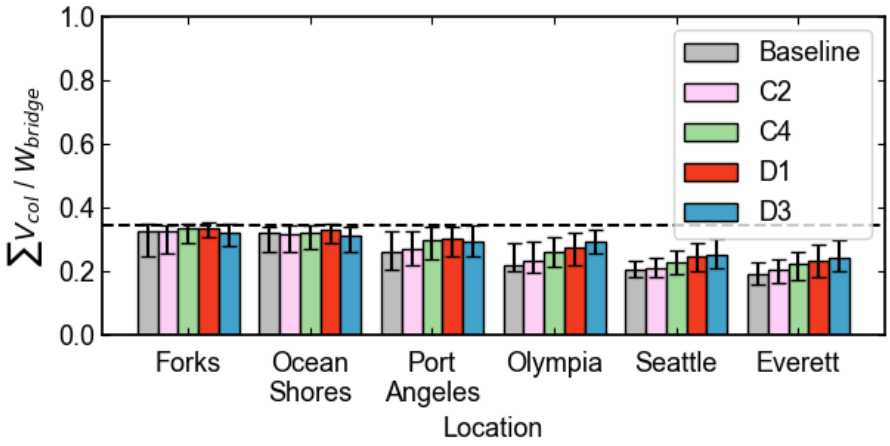

(a) Transverse direction

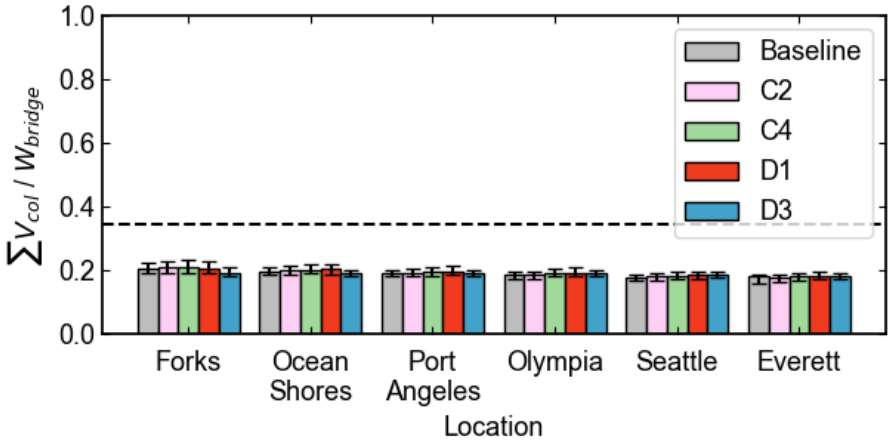

(b) Longitudinal direction

Figure 6.3: Sum of column maximum lateral forces normalized by bridge weight for median, 15th, and 85th percentiles.
(Dashed line represents the effective yield of bridge columns)

Figure 6.4 shows the maximum sum of the shear key transverse lateral forces normalized by bridge weight. The shear capacity of each modeled shear-key element was calculated as 2240 (kips) (Section 4.4.3), which corresponds to the resistance provided by five internal shear keys of the reference bridge. So, each shear-key element had a total capacity of 4480.5 (kips), which

corresponded to a lateral strength ratio of 2.17 (with respect to bridge weight), which is shown as a horizontal, dashed in Figure 6.4.

The shear keys forces were highest in coastal cities (for Site Class D1) and tended to decrease with increasing distance from the coast. As the location moves inland, the forces at each location tended to increase as the soil site class becomes softer. Most importantly, regardless of the location and site class, the force demands on the shear keys were far below the calculated capacity. The maximum 85% value for the shear-key force (Forks, site class D1) was only 33% of the nominal shear key capacity.

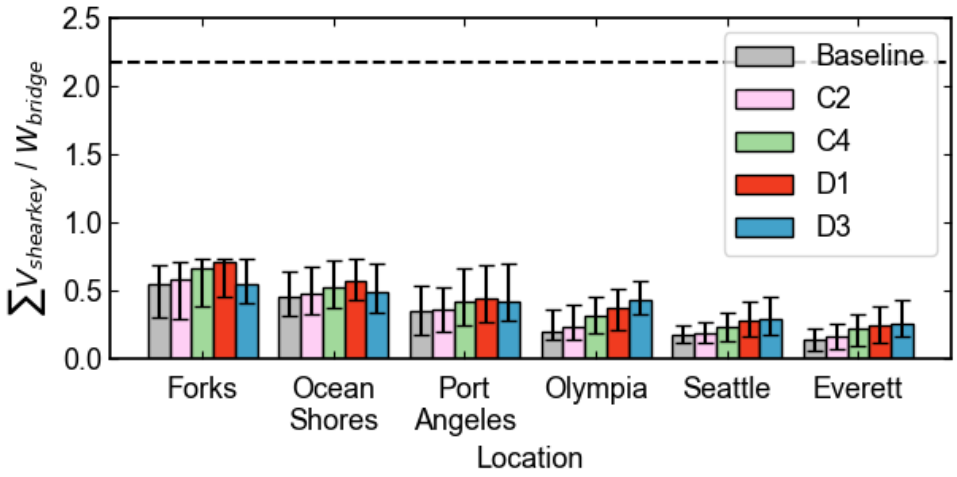

Figure 6.4: Sum of shear key maximum transverse force normalized by bridge weight for median, 15th, and 85th percentiles.
(Black dashed line represents the capacity of shear keys)

6.6 Effects of 30 Earthquake Scenarios on Reference Bridge

In the previous sections, each combination of location and site class included all 30 possible earthquake rupture scenarios and 10 soil profiles, resulting in 300 realization-profile combinations for each city and site class (Section 2.1). This section investigates the effect of the particular earthquake scenarios on the performance of the reference bridge. This information is reported for three cities: Ocean Shores, Port Angeles, and Seattle.

Figure 6.5 and Table 6.3 show the median, 15th and 85th percentiles of the maximum bent transverse drift ratio for Ocean Shores, for soil site classes C2 and D1 (the "N/A-" in Table 6.3 denotes the analysis failed to complete). Soil site classes C2 and D1 were selected since they are the most common soil type within Western Washington State (Section 2.4). The x-axis represents the 30 individual earthquake scenarios, with each bar representing the results of 10 analyses for that realization for 10 randomly selected soil profiles. Four rupture scenarios have the highest responses: csz004, csz009, csz012, csz020, csz025. Additionally, when the soil site class becomes softer, the responses of these scenarios are further amplified. The highest median bent drift ratio was around 2.5% and the 85th percentile values exceeded 5% for realizations csz004 and csz025.

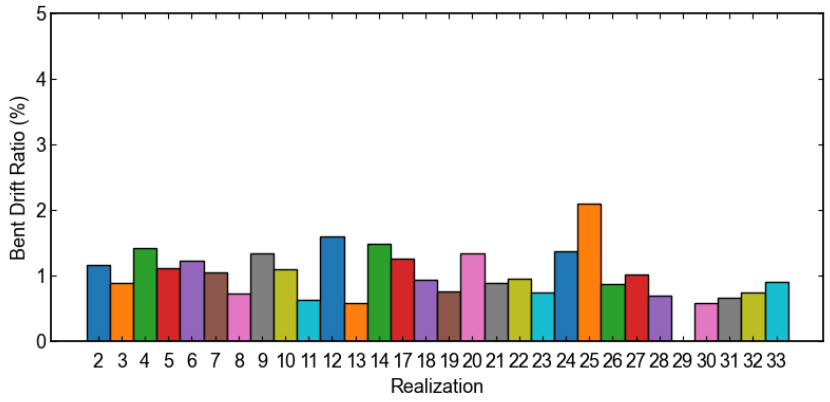

(a) Baseline

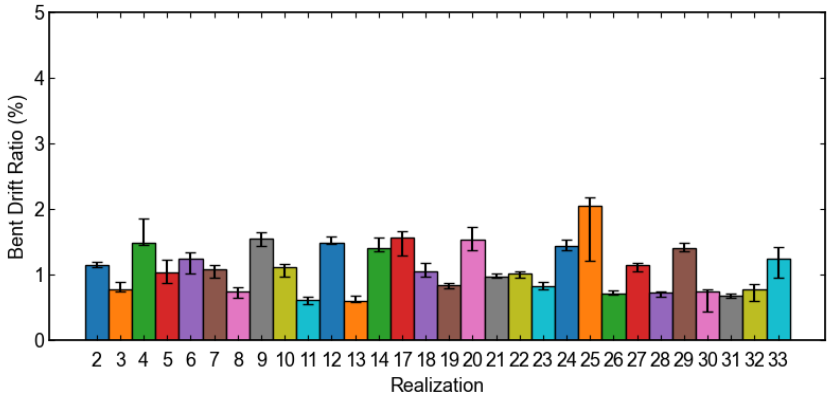

(b) Site class C2

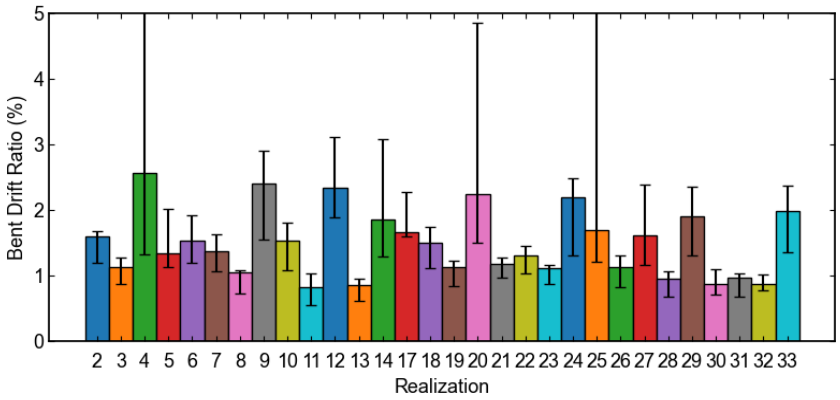

(c) Site class D1

Figure 6.5: Median, 15th and 85th percentiles of maximum bent drift ratio in the transverse direction for Ocean Shores

Table 6.3: Bent transverse drift ratios for Ocean Shores (%)

Realization	Baseline	C2			D1		
		15th Percentile	Median	85th Percentile	15th Percentile	Median	85th Percentile
csz002	1.163	1.127	1.155	1.181	1.227	1.592	1.667
csz003	0.894	0.750	0.772	0.883	0.901	1.140	1.251
csz004	1.423	1.461	1.481	1.722	1.467	2.566	5.946
csz005	1.123	0.872	1.044	1.194	1.175	1.336	1.797
csz006	1.234	1.025	1.244	1.334	1.250	1.539	1.885
csz007	1.049	0.969	1.083	1.135	1.180	1.371	1.610
csz008	0.737	0.650	0.753	0.794	0.765	1.060	1.083
csz009	1.343	1.474	1.545	1.605	1.612	2.411	2.776
csz010	1.106	0.988	1.117	1.154	1.151	1.531	1.774
csz011	0.634	0.555	0.623	0.659	0.638	0.820	1.000
csz012	1.608	1.471	1.491	1.550	2.102	2.344	2.875
csz013	0.583	0.582	0.595	0.669	0.654	0.859	0.945
csz014	1.492	1.361	1.403	1.540	1.410	1.863	2.912
csz017	1.263	1.308	1.575	1.594	1.597	1.666	2.062
csz018	0.944	0.977	1.046	1.163	1.202	1.497	1.698
csz019	0.770	0.799	0.841	0.867	0.892	1.131	1.217
csz020	1.344	1.384	1.540	1.637	1.547	2.248	4.494
csz021	0.899	0.958	0.973	1.011	1.016	1.186	1.272
csz022	0.951	0.958	1.019	1.036	1.060	1.310	1.451
csz023	0.754	0.794	0.822	0.879	0.918	1.121	1.158
csz024	1.380	1.391	1.443	1.529	1.344	2.196	2.378
csz025	2.098	1.246	2.055	2.150	1.229	1.697	7.891
csz026	0.876	0.703	0.710	0.745	0.861	1.139	1.270

Realization	Baseline	C2			D1		
		15th Percentile	Median	85th Percentile	15th Percentile	Median	85th Percentile
csz027	1.028	1.077	1.143	1.182	1.170	1.620	2.274
csz028	0.698	0.675	0.726	0.741	0.745	0.957	1.064
csz029	N/A-	1.358	1.410	1.472	1.371	1.909	2.329
csz030	0.588	0.470	0.741	0.765	0.725	0.876	1.085
csz031	0.667	0.648	0.684	0.700	0.730	0.968	1.031
csz032	0.749	0.655	0.777	0.835	0.790	0.868	0.966
csz033	0.910	0.965	1.247	1.419	1.414	1.993	2.320
Median	0.947	0.967	1.065	1.158	1.173	1.434	1.682
15% Value	0.651	0.649	0.718	0.743	0.738	0.917	1.048
85% Value	1.402	1.387	1.516	1.600	1.507	2.222	2.894

Figure 6.6 and Table 6.4 show the maximum bent drift ratio for Port Angeles for all 30 realizations (the "N/A-" in Table 6.4 denotes the analysis failed to complete). The responses in Port Angeles were smaller than those observed in Ocean Shores. The drift ratios again were amplified more for the softer soil site class. Three rupture scenarios induced significantly higher responses: csz003, csz019, csz030. Note that for csz019, the median response exceeded the largest value from Ocean Shores for the same site class, and the highest 85th percentile value exceeded 5%. The largest median value was recorded to be close to 3.5%, which was much larger than the highest median response from Ocean Shores.

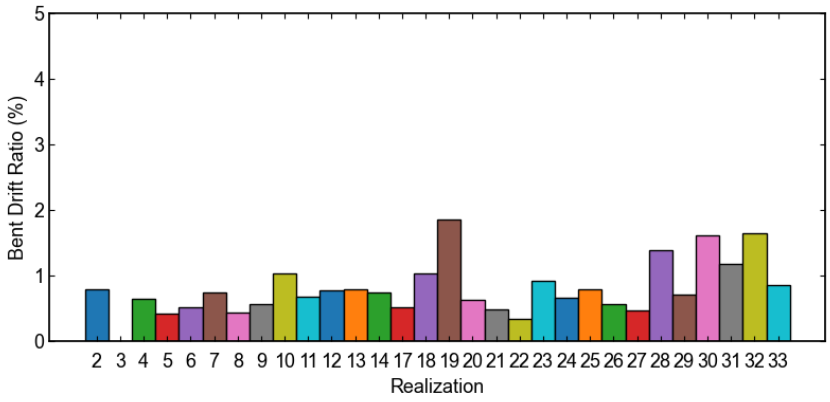

(a) Baseline

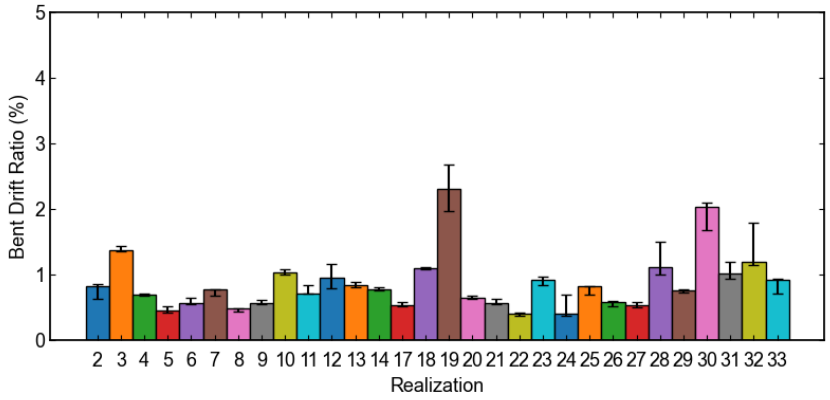

(b) Site class C2

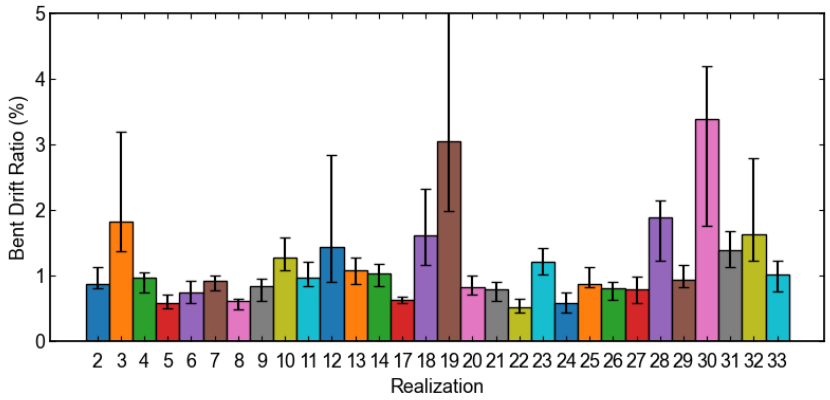

(c) Site class D1

Figure 6.6: Median, 15th and 85th percentiles of maximum bent drift ratio in transverse direction for Port Angeles

Table 6.4: Bent transverse drift ratios for Port Angeles (%)

Realization	Baseline	C2			D1		
		15th Percentile	Median	85th Percentile	15th Percentile	Median	85th Percentile
csz002	0.795	0.642	0.824	0.855	0.809	0.868	1.139
csz003	N/A-	1.358	1.371	1.445	1.379	1.832	3.192
csz004	0.644	0.684	0.703	0.708	0.750	0.967	1.051
csz005	0.421	0.432	0.453	0.517	0.504	0.583	0.720
csz006	0.525	0.552	0.567	0.653	0.588	0.744	0.923
csz007	0.749	0.687	0.778	0.785	0.774	0.923	1.002
csz008	0.440	0.443	0.484	0.494	0.488	0.625	0.656
csz009	0.565	0.552	0.570	0.613	0.617	0.851	0.949
csz010	1.036	1.011	1.037	1.078	1.090	1.286	1.589
csz011	0.687	0.709	0.715	0.844	0.837	0.971	1.208
csz012	0.775	0.790	0.953	1.160	0.904	1.446	2.840
csz013	0.793	0.817	0.846	0.893	0.877	1.083	1.286
csz014	0.752	0.762	0.780	0.816	0.840	1.036	1.174
csz017	0.515	0.526	0.532	0.583	0.587	0.640	0.687
csz018	1.034	1.085	1.100	1.111	1.168	1.609	2.325
csz019	1.858	1.978	2.309	2.685	1.994	3.052	14.134
csz020	0.638	0.639	0.656	0.674	0.707	0.827	1.001
csz021	0.495	0.547	0.573	0.630	0.610	0.795	0.901
csz022	0.350	0.369	0.401	0.421	0.436	0.528	0.649
csz023	0.920	0.841	0.931	0.966	1.015	1.206	1.431
csz024	0.672	0.381	0.411	0.696	0.444	0.581	0.744
csz025	0.802	0.693	0.824	0.834	0.830	0.883	1.129
csz026	0.568	0.515	0.582	0.595	0.629	0.809	0.913

Realization	Baseline	C2			D1		
		15th Percentile	Median	85th Percentile	15th Percentile	Median	85th Percentile
csz027	0.478	0.502	0.535	0.579	0.593	0.790	0.981
csz028	1.394	1.008	1.112	1.497	1.227	1.894	2.154
csz029	0.721	0.736	0.768	0.779	0.821	0.946	1.161
csz030	1.613	1.688	2.034	2.106	1.756	3.397	4.190
csz031	1.177	0.940	1.017	1.202	1.135	1.394	1.676
csz032	1.650	1.155	1.201	1.797	1.227	1.638	2.788
csz033	0.861	0.707	0.916	0.943	0.761	1.017	1.233
Median	0.735	0.700	0.779	0.825	0.815	0.957	1.150
15% Value	0.459	0.473	0.508	0.581	0.546	0.632	0.732
85% Value	1.285	1.048	1.106	1.350	1.197	1.623	2.557

Figure 6.7 and Table 6.5 show the maximum bent drift ratios for Seattle due to the 30 realizations. The responses significantly decreased compared to the responses recorded from Ocean Shores and Port Angeles. The responses from two rupture scenarios were the largest: csz010 and csz029. The highest median response was close to 1% while the highest 85th percentile value was around 1.2%. The softer site class was observed to magnify the overall responses across different rupture scenarios.

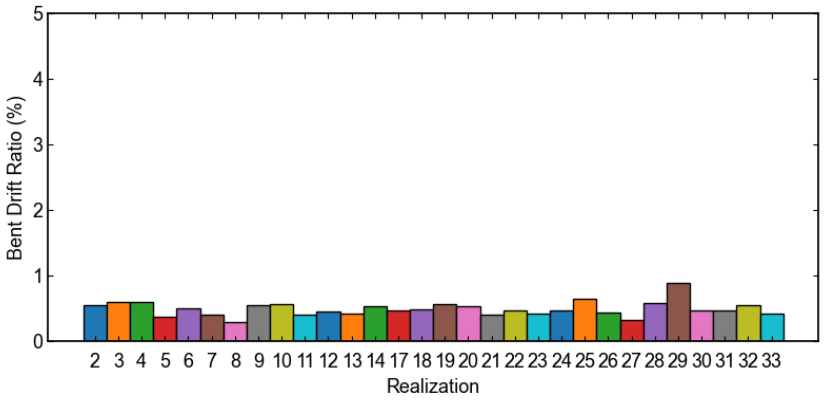

(a) Baseline

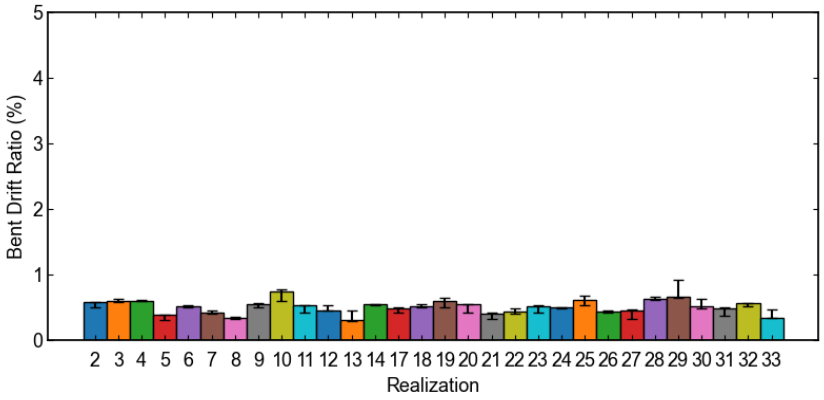

(b) Site class C2

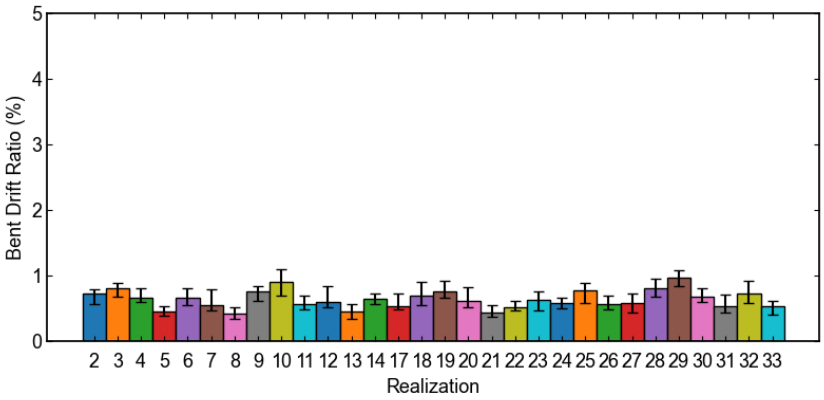

(c) Site class D1

Figure 6.7: Median, 15th and 85th percentiles of maximum bent drift ratio in transverse direction for Seattle

Table 6.5: Bent transverse drift ratios for Seattle (%)

Realization	Baseline	C2			D1		
		15th Percentile	Median	85th Percentile	15th Percentile	Median	85th Percentile
csz002	0.560	0.509	0.580	0.588	0.571	0.724	0.797
csz003	0.609	0.589	0.609	0.638	0.685	0.810	0.896
csz004	0.600	0.595	0.603	0.614	0.606	0.673	0.806
csz005	0.380	0.313	0.385	0.399	0.399	0.449	0.533
csz006	0.500	0.506	0.524	0.536	0.561	0.668	0.814
csz007	0.403	0.409	0.421	0.462	0.470	0.559	0.800
csz008	0.301	0.320	0.345	0.352	0.347	0.419	0.524
csz009	0.552	0.500	0.557	0.575	0.611	0.756	0.837
csz010	0.571	0.597	0.747	0.779	0.697	0.900	1.105
csz011	0.406	0.432	0.531	0.539	0.488	0.561	0.700
csz012	0.457	0.460	0.465	0.538	0.521	0.596	0.851
csz013	0.427	0.302	0.308	0.461	0.341	0.462	0.565
csz014	0.544	0.543	0.548	0.561	0.571	0.643	0.732
csz017	0.479	0.432	0.487	0.499	0.490	0.536	0.734
csz018	0.493	0.511	0.518	0.555	0.547	0.703	0.905
csz019	0.570	0.501	0.605	0.650	0.663	0.770	0.928
csz020	0.532	0.419	0.553	0.560	0.517	0.617	0.827
csz021	0.412	0.329	0.414	0.417	0.369	0.436	0.557
csz022	0.479	0.412	0.437	0.489	0.473	0.519	0.616
csz023	0.420	0.428	0.521	0.531	0.467	0.633	0.763
csz024	0.473	0.490	0.497	0.506	0.513	0.592	0.671
csz025	0.657	0.544	0.617	0.679	0.586	0.772	0.892
csz026	0.440	0.426	0.441	0.462	0.483	0.564	0.704

Realization	Baseline	C2			D1		
		15th Percentile	Median	85th Percentile	15th Percentile	Median	85th Percentile
csz027	0.330	0.332	0.457	0.478	0.443	0.589	0.734
csz028	0.582	0.621	0.638	0.660	0.683	0.814	0.951
csz029	0.889	0.650	0.662	0.921	0.836	0.968	1.091
csz030	0.470	0.489	0.529	0.641	0.603	0.676	0.812
csz031	0.473	0.382	0.484	0.501	0.448	0.529	0.715
csz032	0.552	0.513	0.561	0.571	0.579	0.733	0.920
csz033	0.417	0.340	0.347	0.465	0.402	0.545	0.622
Median	0.479	0.474	0.523	0.538	0.519	0.625	0.799
15% Value	0.405	0.330	0.399	0.462	0.400	0.490	0.590
85% Value	0.576	0.569	0.611	0.655	0.637	0.771	0.924

Chapter 7: Effects of Abutment Properties

This chapter describes the parametric study of the effects of variations in abutment properties on the performance of the reference bridge during an M9 earthquake. In the abutment parametric study, the performance of the bridges was investigated for three cities: Ocean Shores, Port Angeles, and Seattle. Ocean Shores is near the Coast (and earthquake source), Seattle is located inland on a deep sedimentary basin, and Port Angeles combines an intermediate source-to-site distance and a moderate basin depth. Due to the constraint provided by the abutment resistance in the longitudinal direction (sections 6.3 and 6.4), this chapter discusses only the results in the transverse direction. In the abutment parametric study, the column height remained constant at 21.3 ft, and the transverse reinforcement ratio remained constant at 0.5%, which was representative of older bridges.

Section 7.1 discusses how the properties of the abutments were varied in the parametric study. Section 7.2 discusses the effects of abutment configuration, foundation type, and soil type (sand versus clay). Section 7.3 discusses the effects of the contributions of the shear keys and bearing pads.

7.1. Variation of Abutment Properties

The abutment parametric study considered the following abutment characteristics, which were informed by the variations of abutment characteristics in the abutment database (Section 3.4):

- Abutment configurations: L, semi-integral, and integral abutment (Section 4.4.1).
- Abutment foundation types: spread footings, piles (Section 4.4.2)
- Shear keys: present or absent (Section 4.4.3)

- Bearings: present or absent (Section 4.4.4)
- Soil types: medium sand and medium clay (Section 4.4.2)

Table 7.1 shows the cases considered in the abutment parametric study, which include the reference bridge (Section 3.4) and six cases that are variations from the reference bridge. Cases 1 and 2 considered the effect of abutment configuration, Case 3 changed the abutment foundation type, and Case 4 assumed that the soil at the abutment was medium clay instead of medium sand. Cases 5 and 6 varied the contributions of the shear keys and bearing pads. Case 5 represents a bridge that does not have a shear key, whereas Case 6 represents a bridge with no transverse resistance at the abutments. This case indirectly represents the response of a bridge with a discontinuous superstructure that cannot transmit lateral forces to the abutments.

Table 7.1: Cases for abutment parametric study

Parameter	**Reference Bridge**	**Case 1**	**Case 2**	**Case 3**	**Case 4**	**Case 5**	**Case 6**
Shear Key Stiffness/Strength	Present	Present	N/A-	Present	Present	**Absent**	**Absent**
Bearing Stiffness/ Strength	Present	Present	N/A-	Present	Present	Present	**Absent**
Abutment Type	L	**Semi-integral**	**Integral**	L	L	L	L
Abutment Foundation Type	Piles	Piles	Piles	**Spread**	Piles	Piles	Piles
Soil Type	Medium sand	Medium sand	Medium sand	Medium sand	**Medium clay**	Medium sand	Medium sand

7.2 Effects of Variation in Abutment Configuration and Soil Type

The reference bridge has an L-type abutment, supported on piles with a medium-sand soil type. In this section, four other configurations at the abutment were considered: semi-integral abutment (Case 1 in Table 7.1), integral abutment (Case 2), abutment foundation of spread footing (Case 3), and abutments supported on medium clay (Case 4). Sections 7.2.1 and 7.2.2 discusses the effects of the abutment configurations and soil type on the deformation and force demands, respectively.

7.2.1 Effects on Deformation Demands

Figure 7.1 shows the median as well as the 15th and 85th percentiles of the maximum displacement at the end of the bridge deck. As was the case for the reference bridge, the median end displacements tended to be largest for Ocean Shores and smallest for Seattle for all abutment configurations.

For all fifteen combinations of cities (3) and site classes (5), the bridge with the integral abutment had the smallest median displacement responses, and for nearly all cases (13 of 15), it had the smallest 85% percentile displacement response. This trend was expected, because the displacement in the transverse direction is restrained by the integral abutments without there being a gap between the bridge deck and the shear keys.

The median transverse displacements for the bridges with L and semi-integral abutments were similar, which was expected, as they had the same constraint in the transverse direction.

For almost all (13 of 15) combinations of cities and site classes, bridges with spread footings had the largest median response. This is because of the lower lateral resistance of the spread footing (140 kips per footing, 0.07 of bridge weight) compared to piles.

The change from medium sand to medium clay increased the end displacements slightly, but this difference in soil type had less effect than the change between the foundation piles to the spread footings

Of all the combinations shown in Figure 7.1, the largest median end displacement (3.2 inches) was observed for semi-integral abutment in Ocean Shores with site class D1.

The 85th percentile values differed more from the median values for Port Angeles than for the other two cities. Of all the combinations, the maximum 85th percentile value was 13.5 in., for Port Angeles, site class D3 and an abutment supported on spread footings.

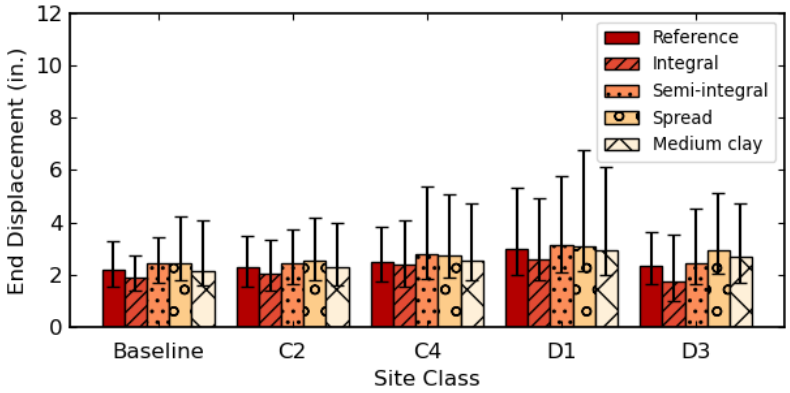

(a) Ocean Shores

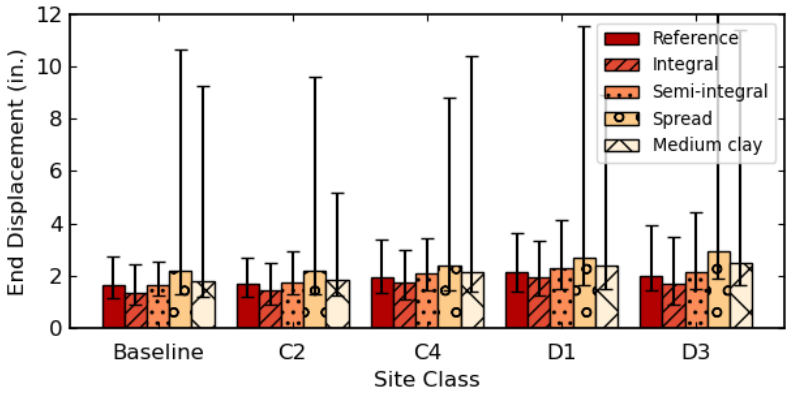

(b) Port Angeles

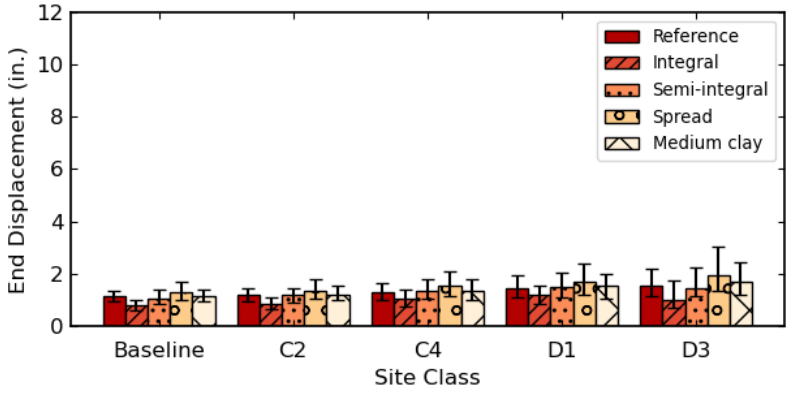

(c) Seattle

Figure 7.1: Maximum bent drift ratio for median, 15th, and 85th percentiles in Ocean Shores, Port Angeles, and Seattle

Figure 7.2 presents the same sets of plots for maximum bent drift ratio. Since the superstructure behaved nearly rigidly during the earthquake, the trends at the bents are similar to those observed for the end displacements of the deck (Figure 7.1). The maximum median bent drift ratio is again seen in the coastal city (Ocean Shores) and is approximately 1.3%, while the drift ratio was the lowest in the inland city on deep basin (Seattle). The highest response was observed for spread footing and medium clay cases at 85th percentile, with bent drift ratio greater than 5% (Port Angeles).

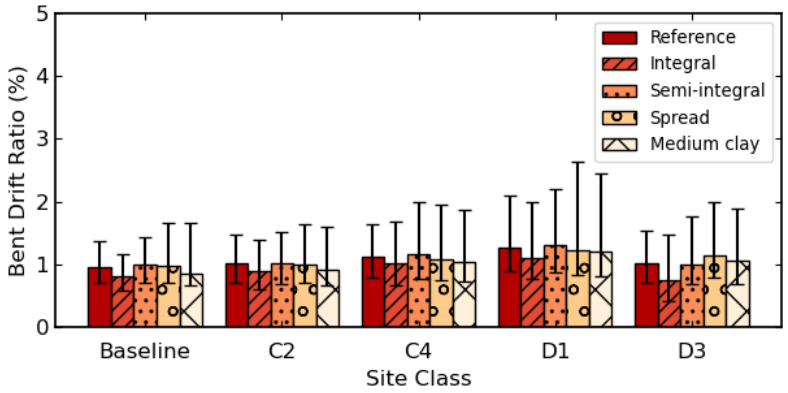

(a) Ocean Shores

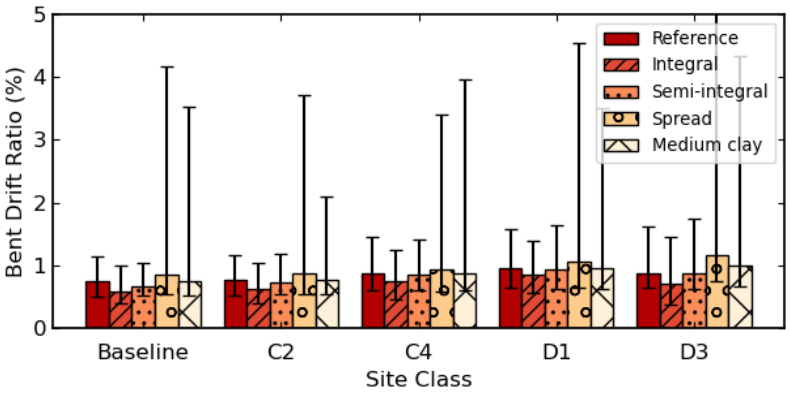

(b) Port Angeles

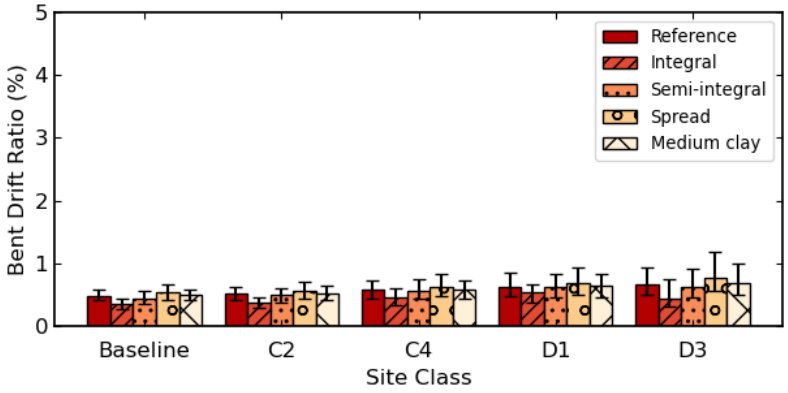

(c) Seattle

Figure 7.2: Maximum bent drift ratio for median, 15th, and 85th percentiles in Ocean Shores, Port Angeles, and Seattle

7.2.2 Effects on Force Demands

Figure 7.3 shows the median as well as the 15th and 85th percentiles of the maximum sum of column transverse forces normalized by bridge weight. As was the case for the deformation responses (Section 7.2.1), the maximum column forces were higher in cities closer to the coast and tended to decrease as the location moved inland. For all three cities, the column forces did not change significantly among the soil site classes. Additionally, although the differences were small, the bridge with the integral abutment tended to have the lowest median sum of column forces except for some site classes in Ocean Shores. This could be explained by the high restraint that the integral abutments provided for the deck, which resulted in lower movement for the columns and thus lower forces.

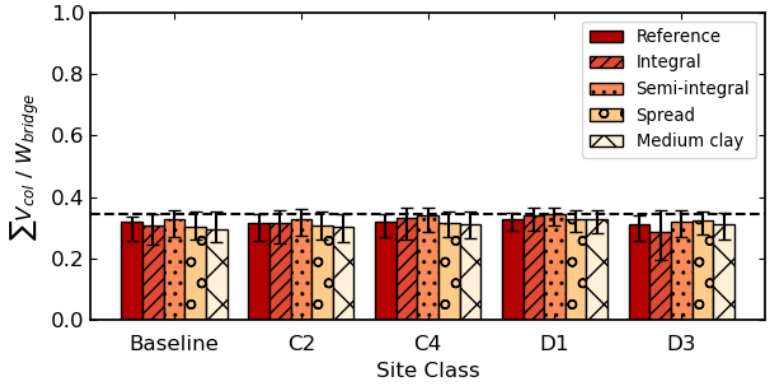

(a) Ocean Shores

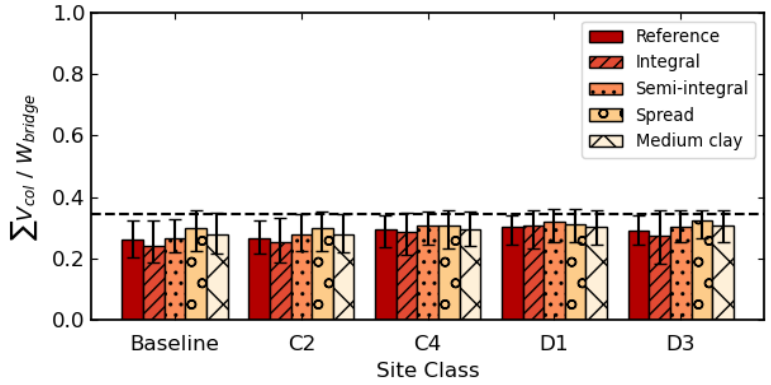

(b) Port Angeles

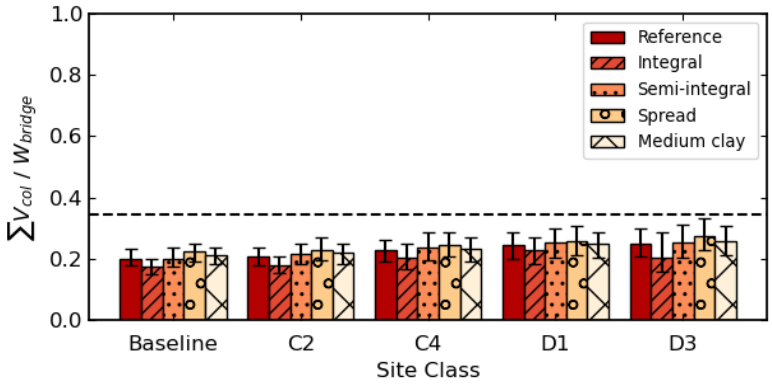

(c) Seattle

Figure 7.3: Sum of column maximum lateral forces normalized by bridge weight for median, 15th, and 85th percentiles in Ocean Shores, Port Angeles, and Seattle (Black dashed line represents the effective yield of bridge columns)

Figure 7.4 shows the maximum sum of the shear key forces normalized by bridge weight. Note that the integral abutment does not have a shear key. The maximum shear key forces tended to decrease as the location moved away from the coast. The highest median value was around 0.7 for site class D1 in Ocean Shores, and it also had the highest 85th percentile, with a value close to 1.5. Even for this case, the shear keys still did not reach their capacity (2.17 when normalized by the bridge weight). For the inland cities, the shear key forces tended to increase as the soil site class became softer, but again, the force demands were far below the capacities.

The responses of the reference bridge (L-abutment) and the case with semi-integral abutment are very similar in all the cases as they have the same force-resisting elements in the transverse direction. The change of abutment foundation type to spread footing significantly decreased the forces of shear keys. This is because of the lower lateral capacity (140 kips, 0.07 of the bridge weight) of the spread footing which directly limited the maximum lateral force that could be applied to the shear keys. Lastly, the variation of soil type also decreased the shear key force due to similar reasons, as the softer soil type (medium clay) had a lower first yield force (88 kips versus 42 kips per pile), which resulted in lower transverse strength at the abutment foundation piles.

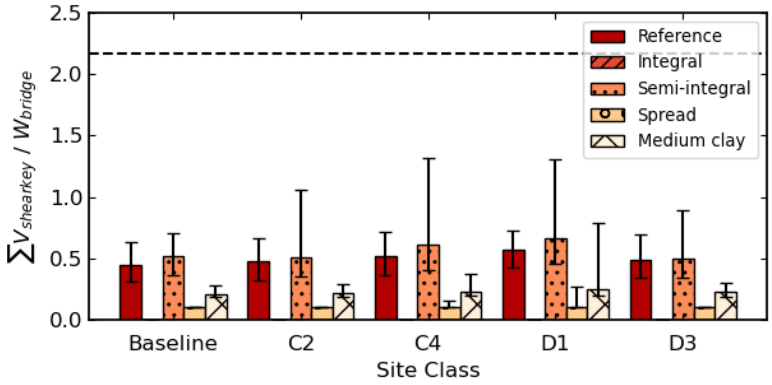

(a) Ocean Shores

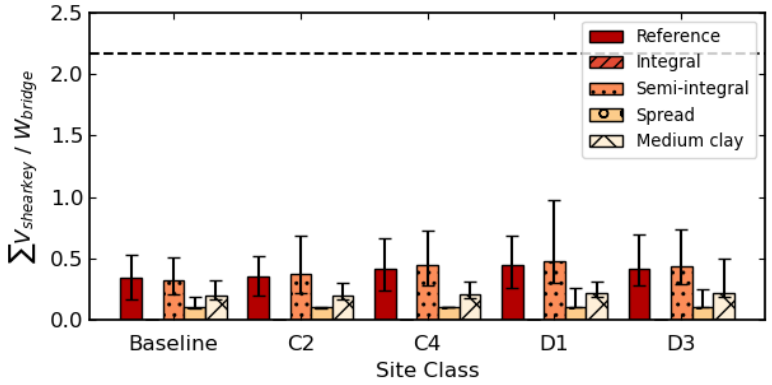

(b) Port Angeles

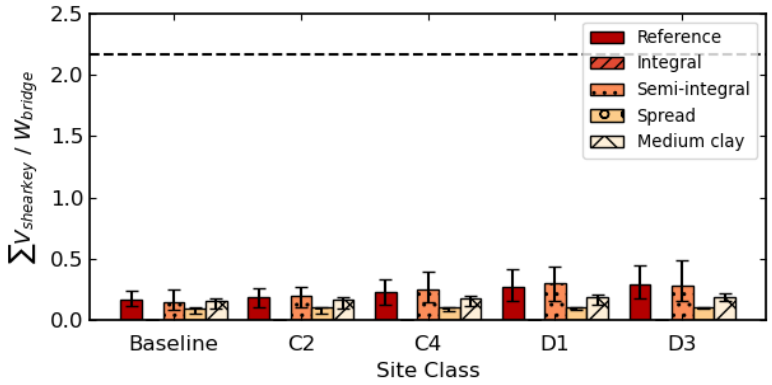

(c) Seattle

Figure 7.4: Sum of shear key maximum transverse force normalized by bridge weight for median, 15th, and 85th percentiles in Ocean Shores, Port Angeles, and Seattle (Black dashed line represents the capacity of shear keys)

7.3 Effects of Shear Keys and Bearings

The reference bridge has shear keys and bearing pads. In this section, two other situations are considered to represent circumstances in which there is no shear key, or the superstructure is not continuous, so it cannot transmit transverse forces to the abutment. The two cases are: the bridge without shear keys but with bearing pads (Case 5 in Table 7.1) and bridge without shear keys and without bearing pads (Case 6 in Table 7.1). The first case represents bridges without shear keys while the second one approximates situations in which bridges are not continuous.

Section 7.3.1 and 7.3.2 discusses the effects of different stiffnesses of shear key and bearing pads on deformation and force demands, respectively.

7.3.1 Effects on Deformation Demands

This section discusses the effect of abutment shear key and bearing stiffnesses on the deformation demands.

For all the cities and site classes (15 combinations), the displacements at the end of the deck (Figure 7.5) increased when the resistance provided by the shear key was removed (Case 5). The median displacement responses also tended to become higher as the soil site class became softer. The maximum median end displacement was observed to be around 4 inches and the highest 85th percentile was over 12 inches for the Port Angeles of site class D3.

The displacements further increased when the resistance of the bearing pads was removed (Case 6). This observation indicates that the bearing pads played an important role in transmitting forces from columns to the abutment structures. Note that the largest response happened in Port Angeles which is on the Olympic Peninsula (but not on the Pacific Coast), and located on a medium

depth sedimentary basin, with a median value of almost 8 inches and the 85th percentile over 12 inches. This could be explained by the basin amplification as the response became higher when the period of the structure increased.

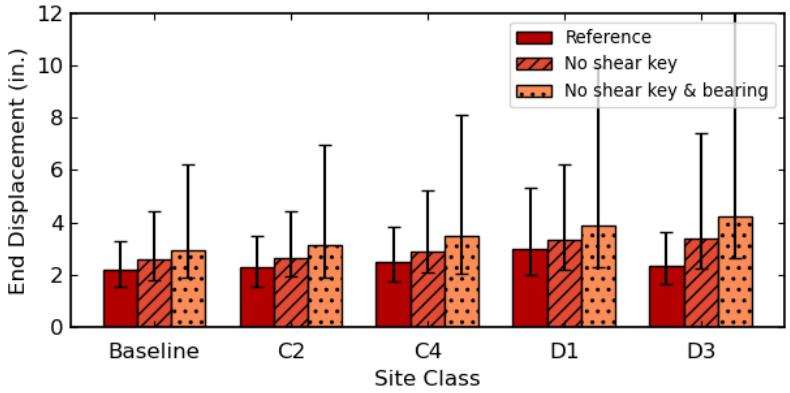

(a) Ocean Shores

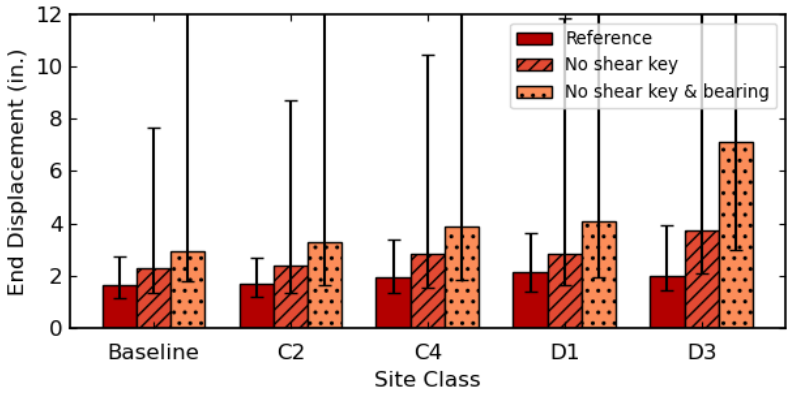

(b) Port Angeles

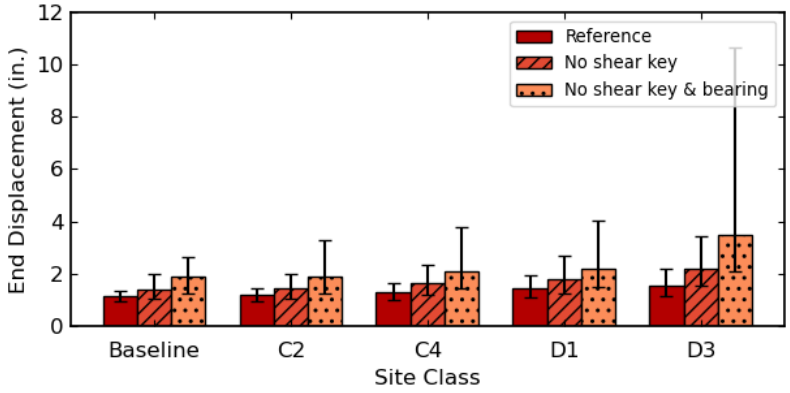

(c) Seattle

Figure 7.5: Maximum displacements at end of deck for median, 15th, and 85th percentiles in Ocean Shores, Port Angeles, and Seattle

Figure 7.6 shows the effects of shear keys and bearing pads on the maximum bent drift ratio. Again, the trends observed for bent drift ratio (Figure 7.5) were similar to the maximum end displacement due to the stiffness of the superstructure. The highest median bent drift ratio (2.8%) was observed in Port Angeles. The city also had the largest 85th percentile value (5.8%).

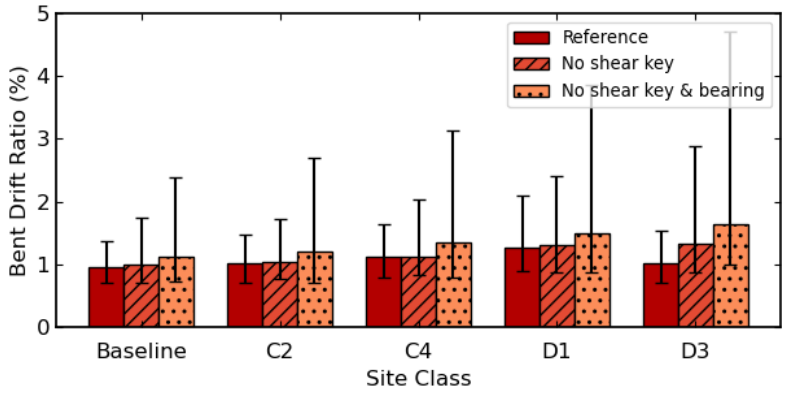

(a) Ocean Shores

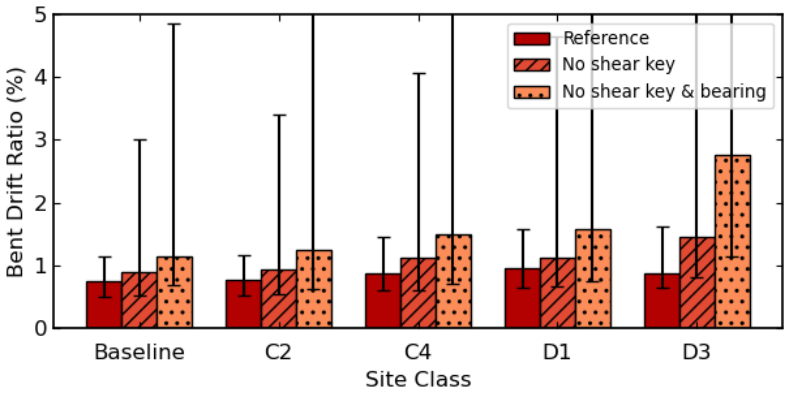

(b) Port Angeles

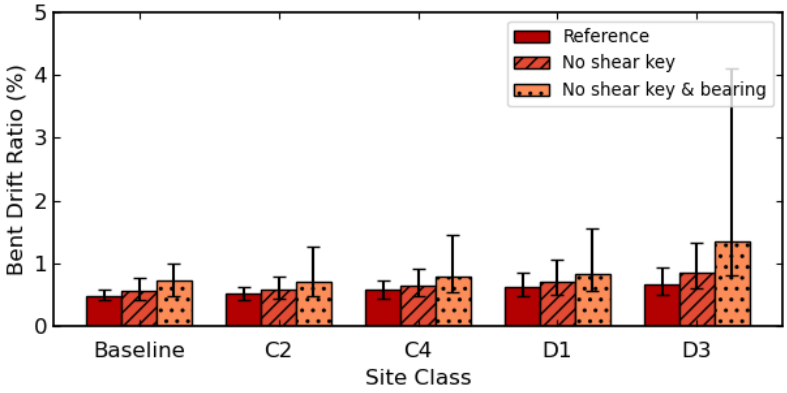

(c) Seattle

Figure 7.6: Maximum bent drift ratios for median, 15th, and 85th percentiles in Ocean Shores, Port Angeles, and Seattle

7.3.2 Effects on Force Demands

Figure 7.7. shows the effects of shear keys and bearings on maximum sum of column forces. For the two cases (cases 5 and 6), the forces tended to be higher in cities closer to the coast and also as the soil site classes became softer. The highest value was over 0.34 (dashed line), indicating the bridge columns had yielded. Note that the removal of shear keys caused an overall increase in the forces in the columns, and the removal of the bearing pads also had a similar influence on the column forces.

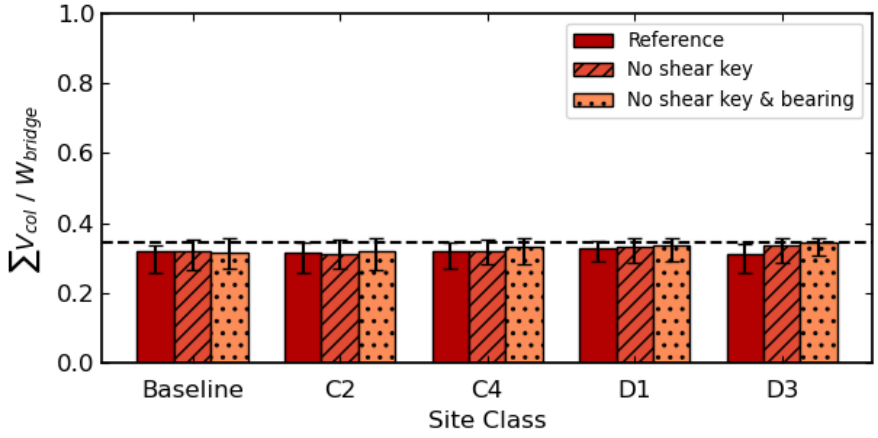

(a) Ocean Shores

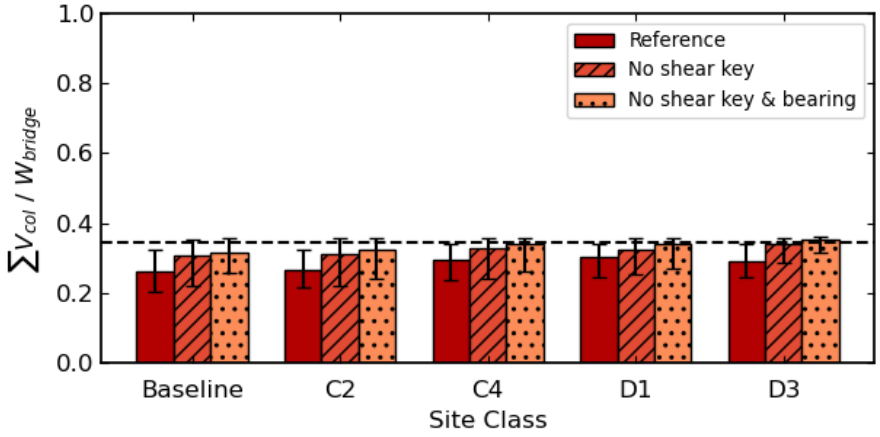

(b) Port Angeles

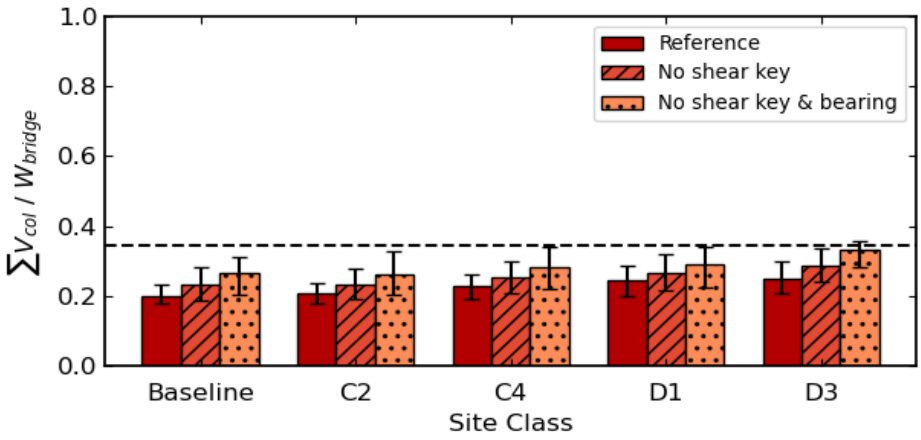

(c) Seattle

Figure 7.7: Sum of column maximum lateral forces normalized by bridge weight for median, 15th, and 85th percentiles in Ocean Shores, Port Angeles, and Seattle (Black dashed line represents the effective yield of bridge columns)

The maximum sum of shear key forces is not discussed in this section since these cases did not include shear keys in the analyses.

Chapter 8: Effects of Column Properties

This chapter discusses a parametric study of the effects of column properties on the performance of the reference bridge. Similar to the abutment parametric study (Chapter 7), the column properties parametric study focused on three cities: Ocean Shores, Port Angeles, and Seattle, and the results are shown only for the transverse direction. In this parametric study, the bridges all had an L-abutment type, pile abutment foundations founded on piles on medium sand, and bearing pads.

Section 8.1 introduces the cases considered for the variations of the column properties. Section 8.2 discusses the effects of column height, whereas Section 8.3 discusses the effects of column transverse reinforcement ratio, with 0.5% assumed for old bridges and 1.5% assumed for newer bridges.

8.1. Variation of Column Properties

The column parametric study varied the following column characteristics:

- effective height of the bridge columns: reference height (21.3 ft), one half the reference height, and double the reference height (Section 3.4). The effects of varying the column height were studied for bridges with and without shear keys.
- representative transverse reinforcement ratio of new and old bridges: 0.5% for older and 1.5% for newer bridges (Section 3.4).

Table 8.1 shows all the cases considered to evaluate the effects of the column characteristics. These cases included the reference bridge (Section 3.4) and four cases (7 through 10) that correspond to combinations of various column heights and whether or not the shear key

resistance was included in the model. The resistance of the shear keys was removed for cases 8 and 10 to evaluate the effects of column height when the abutment resistance was reduced. Lastly, Case 11 assumed that the bridge had newer columns with a higher transverse reinforcement ratio (1.5% versus 0.5%).

Table 8.1: Column parametric study cases

Parameter	**Reference Bridge**	**Case 7**	**Case 8**	**Case 9**	**Case 10**	**Case 11**
Effective Height (ft)	21.3	**21.3 x 2**	**21.3 x 2**	**21.3 x 1/2**	**21.3 x 1/2**	21.3
Transverse Reinforcement Ratio (%)	0.5 (old bridge)	0.5 (old bridge)	0.5 (old bridge)	0.5 (old bridge)	0.5 (old bridge)	**1.5 (new bridge)**
Shear Key Stiffness/Strength	Present	Present	**Absent**	Present	**Absent**	Present

8.2 Effects of Column Height

The reference bridge had a column height of 21.3 ft, a transverse reinforcement ratio of 0.5%, and shear keys. In this section, the effects of doubling or halving the column heights are investigated with four analysis cases: double column height of reference bridge (42.6 ft) with shear keys (Case 7 in Table 8.1), double column height of reference bridge without shear keys (Case 8 in Table 8.1), and half of column height of reference bridge (10.65 ft) with shear keys (Case 9 in Table 8.1), and half of column height of reference bridge without shear keys (case 10 in Table 8.1). Section 8.2.1 and 8.2.2 discuss the effects of column height on the deformation and force demands, respectively.

8.2.1 Effects on Deformation Demands

Figure 8.1 shows the effects of varying the column height on the displacement at the end of the bridge for the cities of Ocean Shores, Port Angeles and Seattle. As documented in chapters 6 and 7, the displacements of the end of the reference bridge were largest for Ocean Shores and smallest for Seattle, for all site classes. For the reference bridge, the displacements for softer site classes (D1 and D3) were consistently higher than those for the stiffer soil site classes (C2 and C4).

When the column height was doubled (with shear key, Case 7), the end displacements consistently increased, but the relative order of the end displacements was the same among the three cities. Note that the median displacement among all three cities and all four soil types never exceeded 5.0 inches.

When the column height was doubled and the shear key was removed (Case 8), the displacements increased greatly, particularly for the locations with a basin (Port Angeles, Seattle), where the median displacement increased by a factor of approximately five. The highest median and 85th percentile values exceeded 10 inches and 12 inches, respectively for Port Angeles. This large increase could be explained by the ground motion amplification of higher periods within the sedimentary basin.

When the column height was reduced to half, the end displacement significantly decreased, either with or without the existence of shear keys (cases 9 and 10). This was because the stiffness of columns increased greatly as the height of the columns decreased, which tended to reduce the resistance provided by the shear keys. Theoretically, the elastic flexural displacement (neglecting the effects of bond slip and shear deformations) would be inversely proportional to the cubic of the column height (Elwood and Eberhard, 2009). The highest median end displacement of the half column height cases never exceeded 2 inches.

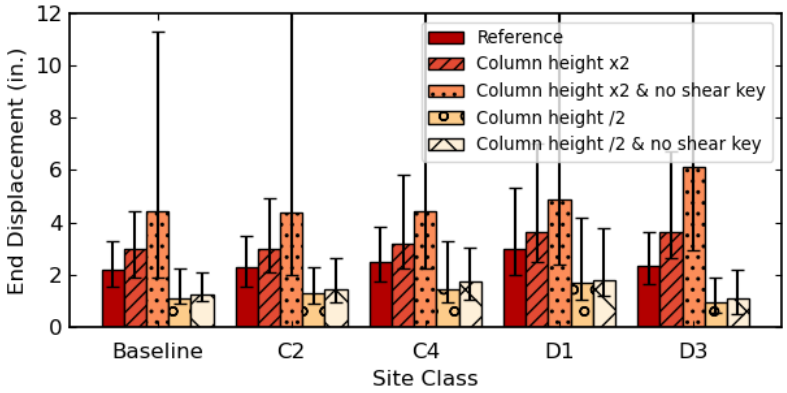

(a) Ocean Shores

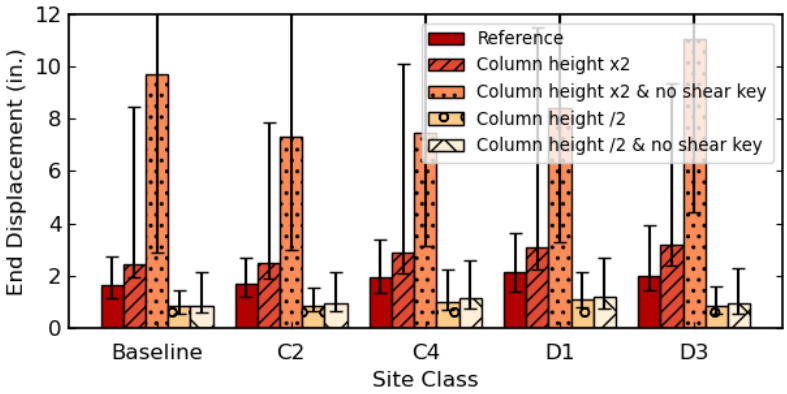

(b) Port Angeles

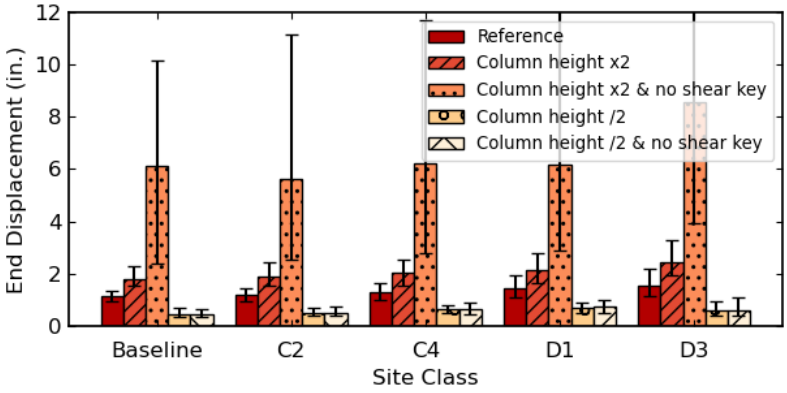

(c) Seattle

Figure 8.1: Maximum displacements at end of deck for median, 15th, and 85th percentiles in (a) Ocean Shores, (b) Port Angeles, and (c) Seattle

Figure 8.2 shows the maximum bent drift ratio for the same three cities. Note that the column height for the reference bridge and the other variation cases are different, thus the denominator for the calculations of the drift ratio were different. Nonetheless, the trends observed from Figure 8.1 for bridges with doubled and half column height were the same as the superstructure behaved like a rigid element.

For bridges that had doubled column height, those with shear keys had the lowest responses. This is because shear keys limited the displacement of the deck while the column height was doubled, resulting in lower drift ratio. However, when shear keys were removed with doubled column height, the bent drift ratio significantly increased as the resistance provided by shear keys no longer existed. This is especially the case for cities on top of sedimentary basins. The highest drift ratio was over 2% and the 85th percentile was close to 5%.

The lowest bent drift ratios were observed for those bridges that had half column height. The median values for these bridges never exceeded 0.5%.

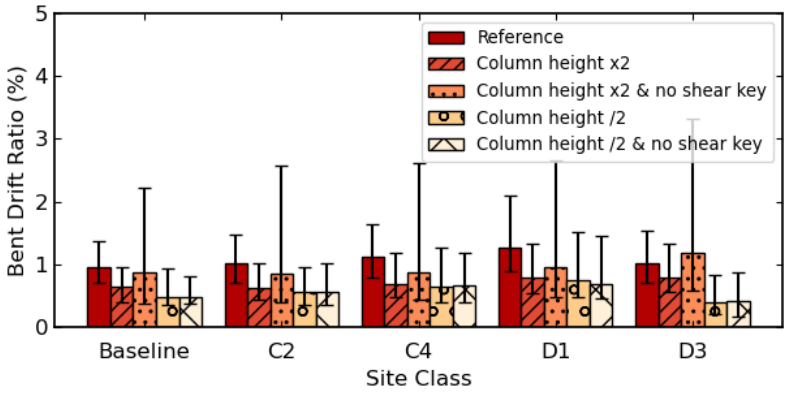

(a) Ocean Shores

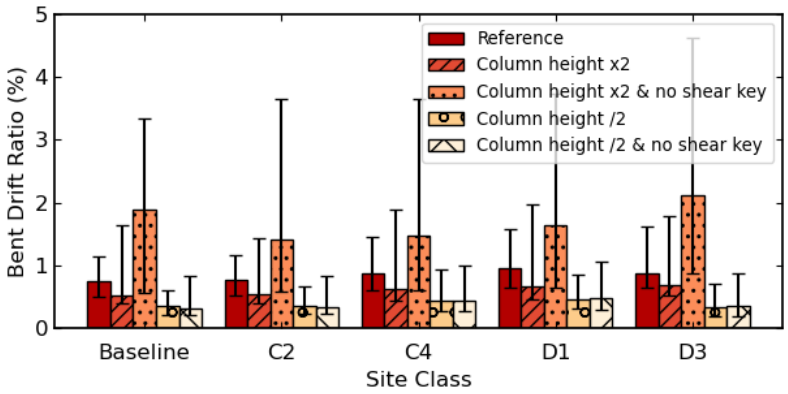

(b) Port Angeles

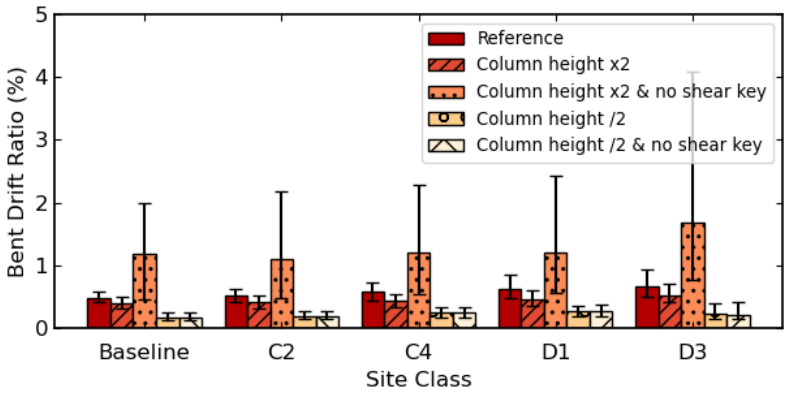

(c) Seattle

Figure 8.2: Maximum bent drift ratio for median, 15th, and 85th percentiles in Ocean Shores, Port Angeles, and Seattle

8.2.2 Effects on Force Demands

Figure 8.3 shows the maximum sum of column forces for three cities. When the column height was doubled, the sum of column forces significantly decreased, especially for the case where the shear keys were not removed. The column forces of bridges without shear keys were consistently greater than that for bridges with shear keys. This was because shear keys were taking lateral loads as the columns were having larger displacements.

When column height was reduced to half, the column forces significantly increased, with the median value around two times of the reference bridge. The maximum median value was recorded to be around 0.6 of the bridge weight and the 85th percentile value was around 0.7 of the bridge weight. For the two bridges with half column height, the presence of shear keys did not make a significant difference. Additionally, although the correlation between the column forces and the soil site classes was not obvious, D1 tended to have the largest responses.

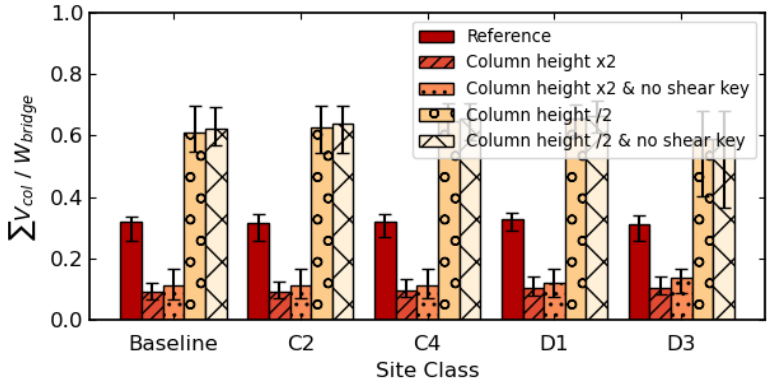

(a) Ocean Shores

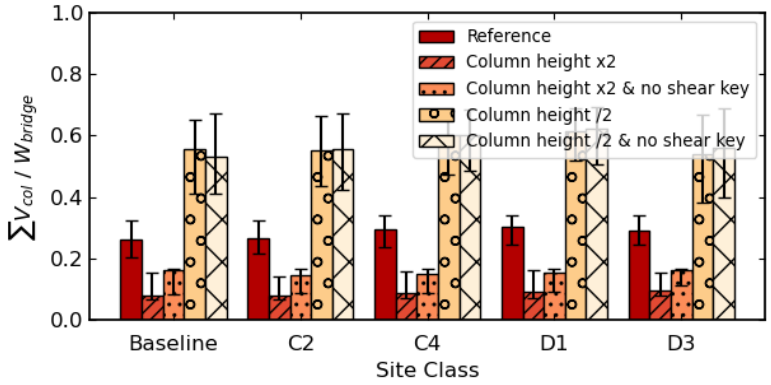

(b) Port Angeles

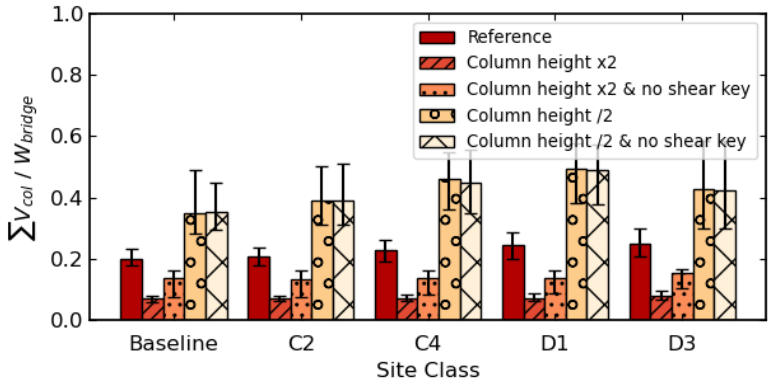

(c) Seattle

Figure 8.3: Sum of column maximum lateral forces normalized by bridge weight for median, 15th, and 85th percentiles in Ocean Shores, Port Angeles, and Seattle (Dashed line represents the effective yield of bridge columns)

Figure 8.4 shows the maximum sum of shear key forces normalized by bridge weight for the three cities. When the column height was doubled and with shear key, the shear key forces increased, which is consistent with the decrease in column forces in Figure 8.3. Except for the case with half of column height and shear key, the shear key force ratio tended to increase slightly as the soil condition became softer, with the highest value to be no more than 1.5, which was far from reaching their maximum capacity. The shear key force significantly decreased as the column height was reduced to half of its original value, which corresponds to the increase of the horizontal column forces in Figure 8.3. And as expected, the shear key forces were zero for the cases where the shear keys were removed.

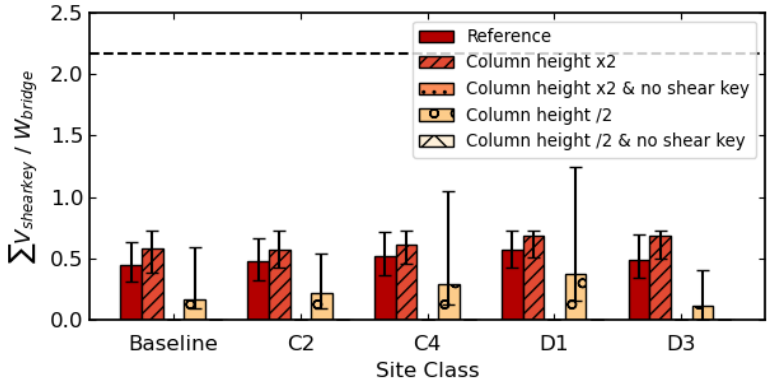

(a) Ocean Shores

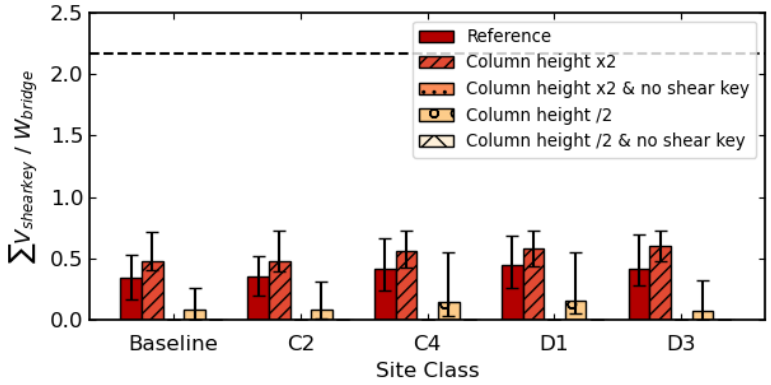

(b) Port Angeles

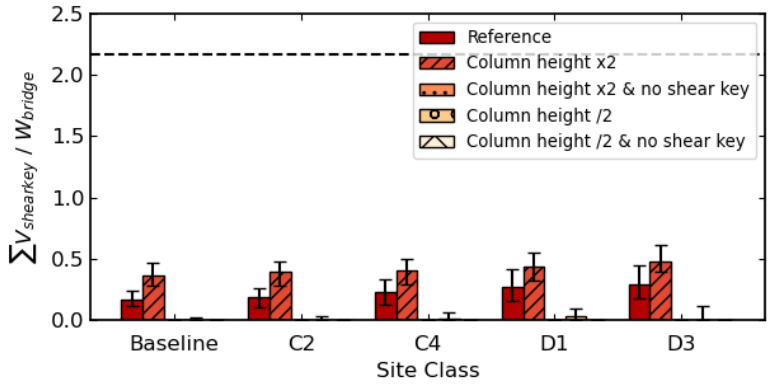

(c) Seattle

Figure 8.4: Sum of shear key maximum transverse force normalized by bridge weight for median, 15th, and 85th percentiles in Ocean Shores, Port Angeles, and Seattle (Dashed line represents the capacity of shear keys)

8.3 Effects of Column Transverse Reinforcement

This section discusses the response differences for old and new columns (corresponding to bridges designed before and after 1976). The transverse reinforcement ratio of the bridge columns represents the division of column ages, with 0.5% stands for old columns and 1.5% stands for new columns. Since the transverse reinforcement provides confinement to the concrete core, higher transverse reinforcement ratio value allows higher confined concrete strength (Figure 4.5). The difference can be especially seen when columns are subjected to large displacement, causing concrete to have higher strain.

From Figure 8.5 to Figure 8.8 show the responses of the reference bridge (old columns) and the bridge case with new columns. The deformation and force median responses for bridges with new and old columns had almost no difference, regardless of locations and soil conditions. This similarity was expected since the displacements of columns were largely restricted by the shear key at both ends of the abutments in the transverse direction, preventing the concrete from having large strain. In Figure 8.5, the highest median value for bent drift ratio was around 1.2% for site class D1 in Ocean Shores, indicating the columns did not have large displacements. And in Figure 8.7, the median values for column lateral forces did not reach the yield lateral force. For the shear key forces, as for the reference bridge, none of the cases reached the maximum capacity.

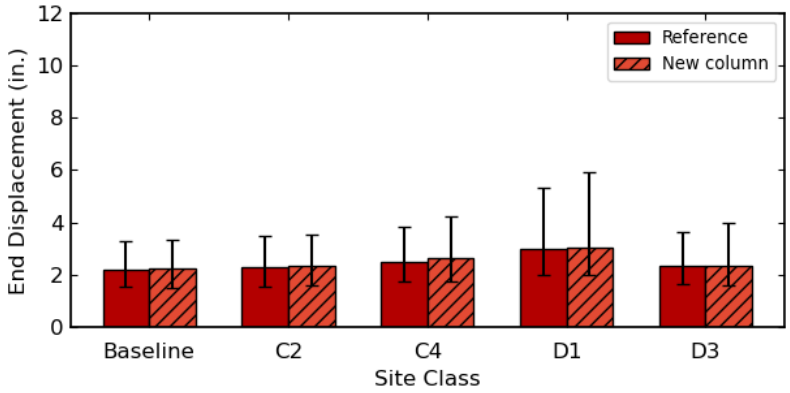

(a) Ocean Shores

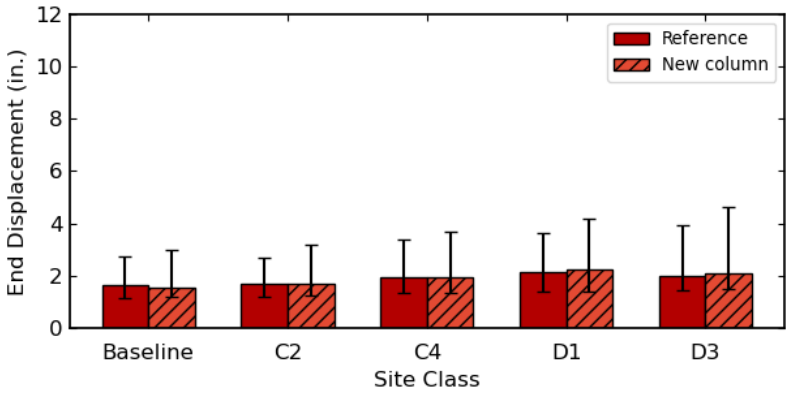

(b) Port Angeles

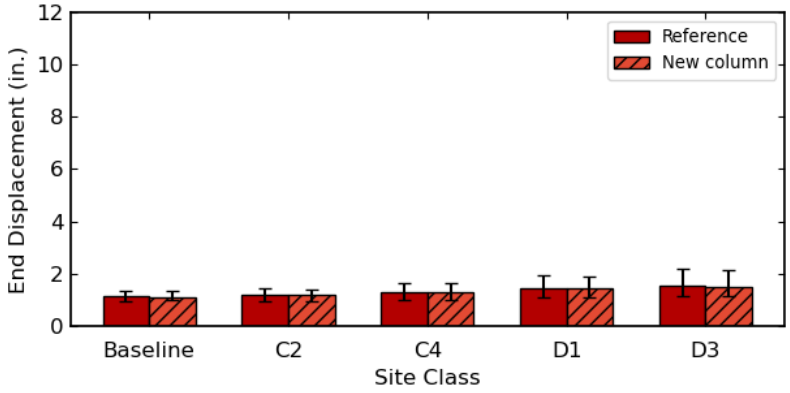

(c) Seattle

Figure 8.5: Maximum displacements at end of deck for median, 15th, and 85th percentiles in Ocean Shores, Port Angeles, Seattle

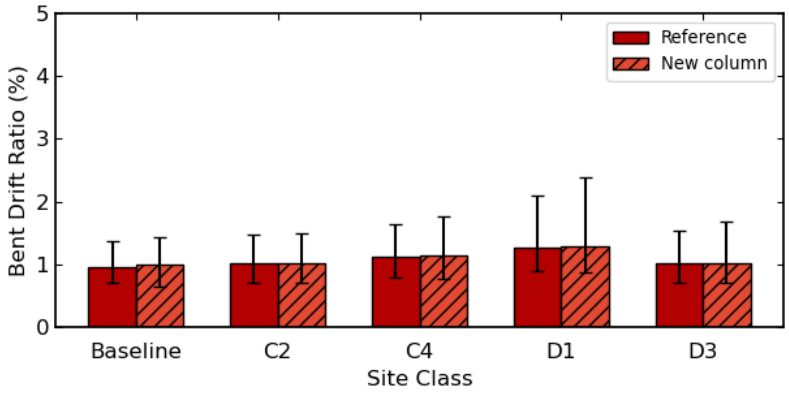

(a) Ocean Shores

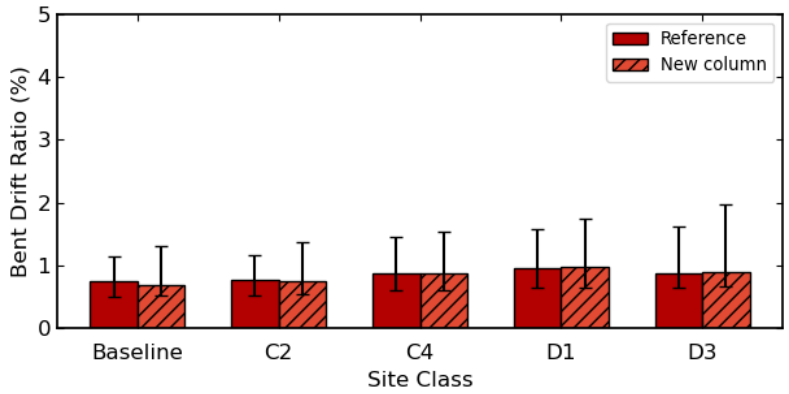

(b) Port Angeles

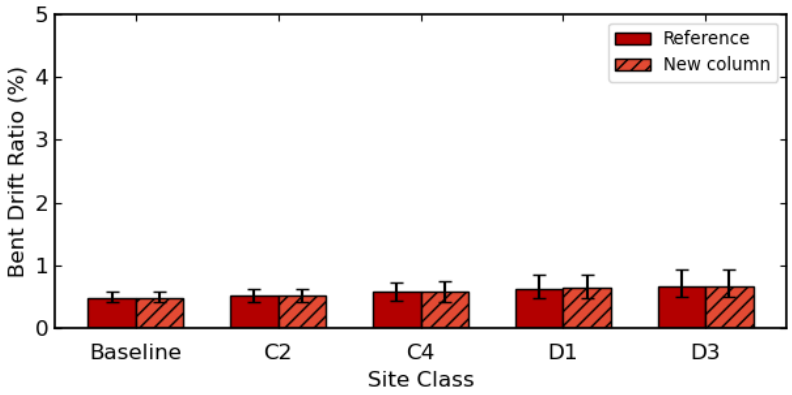

(c) Seattle

Figure 8.6: Maximum bent drift ratio for median, 15th, and 85th percentiles in Ocean Shores, Port Angeles, Seattle

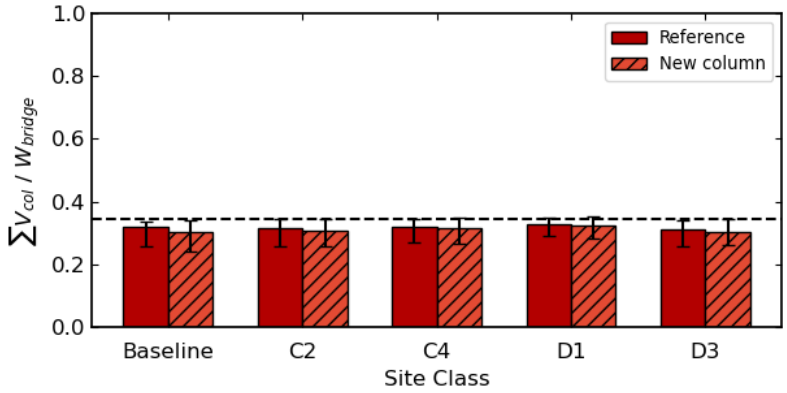

(a) Ocean Shores

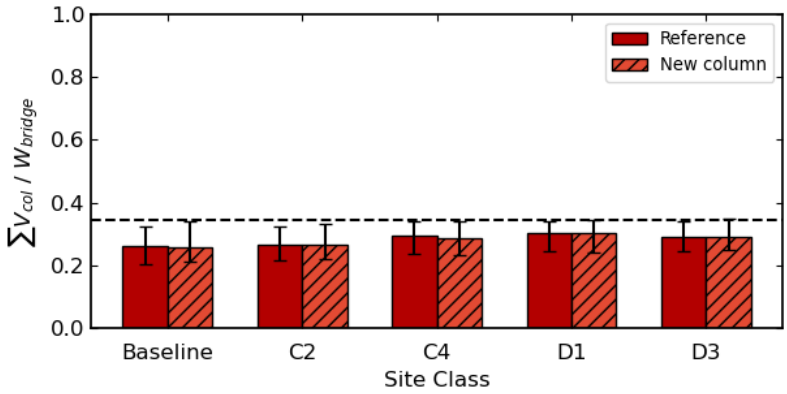

(b) Port Angeles

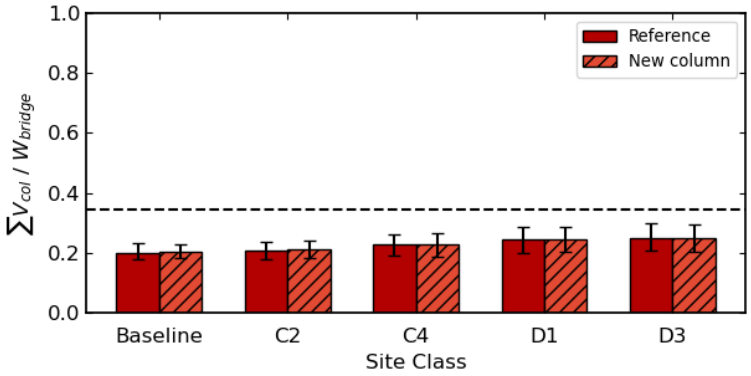

(c) Seattle

Figure 8.7: Sum of column maximum lateral forces normalized by bridge weight for median, 15th, and 85th percentiles in Ocean Shores, Port Angeles, Seattle (Dashed line represents the effective yield of bridge columns)

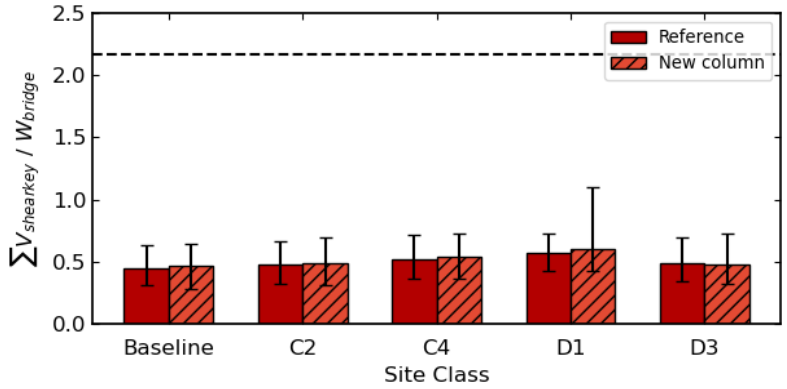

(a) Ocean Shores

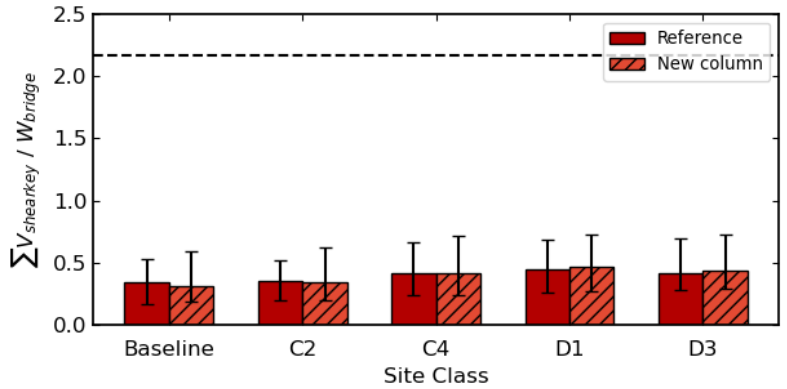

(b) Port Angeles

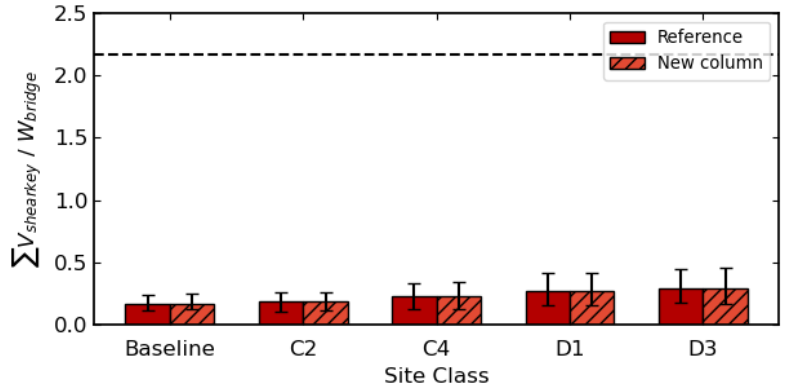

(c) Seattle

Figure 8.8: Sum of shear key maximum transverse force normalized by bridge weight for median, 15th, and 85th percentiles in Ocean Shores, Port Angeles, Seattle (Dashed line represents the capacity of shear keys)

Chapter 9: Conclusions

9.1 Research Motivation

The western portions of Northern California, Oregon and Washington could be subjected to M9 earthquakes generated by the Cascadia Subduction Zone (CSZ), which could cause tremendous damage to the many communities. These communities rely on efficient transportation infrastructure for pre-tsunami evacuations (for cities near coast), post-earthquake emergency supply and economic recovery. Consequently, the performance of bridges in a CSZ event is an essential feature of the resilience of these communities.

Coastal cities in Western Washington are close to the subduction zone, so motions are expected to be intense there. Seattle, along with many other cities in the Puget Sound region, are far from the subduction zone but underlain by deep sedimentary basins. Such basins have been shown to amplify long-period components of earthquake ground motions.

This study examined the effects of M9 earthquakes on typical bridges for a variety of site classes, source distances, basin presence, and key features of bridges, considering six representative cities in Western Washington State. This research builds directly upon the results of recent research of simulations of M9 earthquakes (Frankel et al. 2018), SDOF modeling of the effect of local site conditions (de Zamacona 2019, and Kortum et al. 2022), and detailed bridge database compiled by WSDOT and researchers from the University of Washington.

9.2 Research Approach

The baseline (Frankel et al. 2018) and soil-adjusted M9 ground motions (de Zamacona 2019) were used to conduct parametric studies to investigate the performance of bridges in Washington State. Six representative cities were selected to consider four geological conditions in Western Washington State: coastal outside of basin (Forks and Ocean Shores), inland shallow basin (Port Angeles), inland outside of basin (Olympia), and inland deep basin (Seattle and Everett).

- WSDOT engineers and University of Washington researchers compiled a database of 582 highway bridges along major highways in the Puget Sound region (Chapter 3). A study of this database made it possible to identify common properties of typical bridges.
- A detailed three-dimensional finite-element model was developed for a reference bridge that is representative of typical highway bridges in Washington State.
- The performance of the reference bridge model was evaluated with a series of pushover and cyclic analyses, and by comparing the dynamic response of the MDOF model with the results of SDOF analyses performed by Kortum et al. (2022).
- A series of parametric studies were performed to investigate the simulated performance of the reference bridge during an M9 earthquake. The first study (Chapter 6) investigated the effects of geographic location, site class, and the 30 different earthquake rupture scenarios for the six representative cities. The second parametric study (Chapter 7) evaluated the effects of the abutment characteristics for three representative cities, and the third study (Chapter 8) evaluated the effects of the column characteristics, both in the presence of shear keys and when there are no shear keys.

9.3 Properties of Typical Bridges

Most of the bridges along major highways in the Puget Sound region were built before the incorporation of ductile detailing. Of the 582 bridges documented in the database, 435 (74.7%) were built before 1976. A total of 74 bridges had a single span, whose failure mode tends to be span unseating, which early WSDOT retrofit efforts have targeted. Out of 508 bridges with multiple spans, 416 (71.6%) of the intermediate supports contained at least one reinforced concrete column, which is a common location of bridge damage and failure. As expected, the transverse reinforcement ratio for older reinforced concrete columns (pre-1976) tended to be much smaller than for newer columns, but interestingly, the longitudinal reinforcement ratio did not vary greatly based on the era of construction (Chapter 3).

A key question addressed in this study is the effectiveness of the abutments in restraining the expected deformations of the bridge. This restraint depends greatly on the continuity of the superstructure and on the presence of transverse shear keys at the abutments. The database study found that 76% of pre-1976 bridges had continuous superstructures, and this percentage increased to 97% for modern bridges (1976-present). A study of a subset of 94 bridges found that 90.3% (65/72 bridges) of the older bridges and 100% (19 bridges) of newer bridges had an internal or external shear key.

9.4 Earthquake Performance of Reference Bridge

The simulated deformation responses of the typical bridge in the longitudinal direction were consistently smaller than those in the transverse direction due to the high resistance provided

by the abutment and backfill soil. For all six locations and four site classes, the 85th percentile longitudinal deformations at the end of the deck were below 2.5 inches and the bent drift ratio was below 1.0%. The following conclusions, drawn from Chapter 6, are provided regarding the response of the bridge in the transverse direction.

In the transverse direction, the coastal locations (Forks and Ocean Shores) had the largest displacement responses. The highest responses in coastal cities were for site class D1, with the 85th percentile responses reaching values of almost 6 inches for the maximum end displacement and almost 2.5% for the maximum bent drift ratio. This drift ratio is slightly above the mean drift ratio at spalling (2.3%) for reinforced concrete columns, and it is less than half the mean drift ratio at bar buckling for older bridges (4.9%).

The responses tended to decrease as the distance from the coast increased. The median transverse displacements were 2 inches or less at the bridge ends and the median bent drifts were less than 0.8% for the two cities located far from the coast and on deep basins (Seattle and Everett).

The force demands on the internal transverse shear keys tended to be far below their nominal capacity. For example, the highest demand corresponded to the city of Forks and site class D1. In this location, the 85% value for the maximum shear-key force corresponded to only 33% of the nominal shear key capacity.

9.5 Effects of Variations in Properties of Typical Bridge

The type of abutment (e.g., L-type, semi-integral, and integral) did not significantly affect the transverse response of the bridge, with the median bent drift consistently between 0.5% and

1.5%. In particular, the L-type abutment and the semi-integral abutment produced similar displacement responses while the integral abutments tended to produce smaller responses.

The abutment foundation type, i.e., piles or spread footings, and the associated soil type, i.e., medium sand and medium clay did have a small impact on the bridge response. The spread footings allowed more transverse displacement relative to the pile but the magnitude of the increase was ground motion realization dependent. There was a slight increase in the median bent drift ratio, but it still never exceeded 1.5% and the end displacement was consistently smaller than 3.5 inches. However, the variability in the response increased significantly as the 85t percentile value for bent drift ratio was greater than 5% and the 85th percentile value for end displacement was greater than 12 inches for the bridge with spread footings and on medium clay.

A significant increase in transverse displacement response was found with removal of the shear keys and bearing pads, and when the column height was increased. When both the shear keys and bearing pads were removed, the median bent drift ratio was more than 3 times higher than the original value for the reference bridge, i.e., the end displacement of the deck was close to 8 inches, with the highest 85^{h} percentile end deck displacement greater than 12 inches (Figures 7.5 and 7.6). This condition, with the shear keys and bearings removed, indirectly approximates the response of bridges with discontinuous super structures and the results indicate that such bridges are likely to have severe damage. When the shear keys were removed *and* the column height was doubled, the median bent drift ratio further increased to nearly 5 times that obtained for reference bridge and the end deck displacements reaching close to 12 inches. This indicates that discontinuous bridges with tall columns should be prioritized for seismic evaluation and retrofit.

Decreasing the column height also influenced the response significantly when the shear keys and bearings were not present. When the column height was reduced to half the height for the reference bridge, the median sum of column forces was observed to increase to twice the value for the reference bridge, with the highest sum of column of shear forces reaching 70% (1446 kips) of the bridge weight. This indicates that shorter columns could have shear failure problems and should be prioritized for seismic evaluation and retrofit.

Shear keys provided large resistance for the bridges in the transverse direction. For the reference bridge in this study, the total maximum capacity of the shear keys was 2.17 times the bridge weight. Thus, none of the scenarios considered were close to reaching the maximum capacity of the shear keys.

For most scenarios that were considered in this research where shear keys were present, the 85th percentile values for the sum of the column forces were close to or just reaching the effective yield of the columns.

When the shear keys were included in the analysis, the change of the transverse reinforcement ratio (old and new columns) had minimal effect on the performance of the bridges. In the case where the bridge had old columns and without shear keys, the displacement became larger.

In sum, when the flexibility of the bridge was increased from the reference bridge, i.e., when the shear keys and bearing pads were removed, larger column heights were considered, when the abutment had a spread footing, or when the abutment foundation had a softer soil type, the deformation response of the bridge increased relative to the reference bridge. Furthermore, bridges with less flexibility were observed to have the largest deformation response in cities closer to the

coast (Ocean Shores) while those with higher flexibility had the largest response in the inland city on the sedimentary basin (Port Angeles), especially for ground motions generated with the softest soil site class (D3). This observation is consistent with expected effects of basin amplification. In cities in the deepest part of the ground motions, the motions were not found to be strong enough to cause yielding and softening of the bridge, thus their response was smaller than that for cities closer to the coast.

9.6 Recommendations for WSDOT

The results of the research presented provide WSDOT an opportunity to prioritize the seismic evaluation and retrofit of bridges for the CSZ hazard, which can potentially decrease the cost and increase the efficiency of identifying bridges with higher seismic risk. While the CSZ represents only one portion of the aggregate seismic hazard, it dominates along the Washington coast and the amplification of the ground shaking from the deep sedimentary basin that underlies much of the Puget Sound region has been of concern.

The abutments contribute greatly to the seismic performance of typical bridges by restraining the bridge motion, but this restraint depends on the presence of a continuous superstructure and shear keys. Bridges that lack these two features, particularly if they were built before 1976 should be a high priority for retrofit, particularly along the coast, where the damage is likely to be the greatest. In the Puget Sound region, bridge deformation response and corresponding column drift demands were found to be largest for bridges that have taller columns, no shear keys and no bearing pads.

The study also found that the largest bridge responses tended to happen in cities on shallower portions of the basins and closer to the fault plane (e.g., Port Angeles). In these regions the shaking is strong enough at short periods to cause some damage and period elongation of the bridge due to the proximity to the fault plane. The shollower basin depth then amplifies somewhat shorter period content of the ground motion, relative to deeper basin locations such as Seattle. That amplified content aligns with the elongated period of the bridge and results in larger response. Thus, bridge location in terms of both distance from the CSZ fault plane and basin depth may also be used to prioritize bridge evaluation and retrofit.

Notably, the recommendations for WSDOT are limited to bridges studied and the assumptions used in the modeling. Importantly, shear failure, shear-flexure interaction, and damage from soil liquefaction and lateral spreading were not considered and remain important priorities for bridge seismic retrofit. Additionally, ground motions from only the CSZ source were considered and the crustal faults in the region should be considered in a complete seismic evaluation.

9.7 Future Work

There is much additional research needed to fully assess the bridges in Washington State for the complete seismic hazard. This critical additional research includes:

- Soil liquefaction was not included in this report. It is likely that soil liquefaction can happen during severe earthquakes.

- The developed bridge model did not consider cases where the bridges are skewed or curved. The symmetricity can significantly influence the response of bridge structures during an earthquake event.
- Shear failure of the bridge columns was not considered in this study. The column parametric studies in Chapter 8 showed that the lateral force demands at columns significantly increased as the column heights were reduced to half of its original value. This result suggests a higher potential of shear failure for bridges that have shorter column heights.

Reference

AASHTO. 2017. LRFD Bridge Design Specifications. American Association of State Highway and Transportation Officials.

Ahdi, S.K, Stewart, J., Ancheta, T, Kwak, D., and Mitra, D. 2017. "Development of VS Profile Database and Proxy-based Models for VS30 Prediction in the Pacific Northwest Region of North America." Bulletin of the Seismological Society of America 107: 1781-1801.

Arthur Frankel, Erin Wirth, Nasser Marafi, John Vidale, and William Stephenson; Broadband Synthetic Seismograms for Magnitude 9 Earthquakes on the Cascadia Megathrust Based on 3D Simulations and Stochastic Synthetics, Part 1: Methodology and Overall Results. Bulletin of the Seismological Society of America 2018; 108 (5A): 2347–2369. doi: https://doi.org/10.1785/0120180034

Berry, M., 2006. "Experimental Calibration of OpenSees Components Using the PEER Column Database." Ph. D. thesis, Department of Civil and Environmental Engineering, University of Washington.

Berry, Michael, and Eberhard, Marc. 2005. "Practical Performance Model for Bar Buckling." Journal of Structural Engineering.

Berry, Michael, and Eberhard, Marc, 2007. "Performance Modeling Strategies for Modern Reinforced Concrete Bridge Columns," PEER-2007/07, Pacific Earthquake Engineering Research Center, University of California, Berkeley.

Berry, M., M. Parrish, and M. Eberhard, 2004. "PEER Structural Performance Database User's Manual." Pacific Earthquake Engineering Research Center, Berkely, CA.

Bournonville, M., Dahnke, J., and Darwin, D., 2004. "Statistical Analysis of the Mechanical Properties and Weight of Reinforcing Bars." Structural Engineering and Material Laboratory, University of Kansas.

De Zamacona Cervantes, Gloria, 2019. "Response of Idealized Structural Systems to Simulated M9 Cascadia Subduction Zone Earthquakes Considering Local Soil Conditions." Master's Thesis, University of Washington, Seattle.

Elwood, Kenneth, and Eberhard, Marc, 2009. "Effective Stiffness of Reinforced Concrete Columns," ACI Structural Journal/July-August 2009: 476-484.

Erin A. Wirth, Arthur D. Frankel, Nasser Marafi, John E. Vidale, and W. J. Stephenson; Broadband Synthetic Seismograms for Magnitude 9 Earthquakes on the Cascadia Megathrust Based on 3D Simulations and Stochastic Synthetics, Part 2: Rupture Parameters and Variability.

Bulletin of the Seismological Society of America 2018; 108 (5A): 2370–2388. doi: https://doi.org/10.1785/0120180029

Evans, L. T. and Duncan, J. M., 1982. “Simplified Analysis of Laterally Loaded Piles.” No. UCB/GT/82-04, University of California, Berkeley, CA.

FEMA (Federal Emergency Management Agency). 1995. NEHRP Recommended Seismic Provisions for Seismic Regulations for New Buildings (FEMA 222A and 223A).

Frankel, Arthur, Wirth, Erin, Marafi, Nasser. 2018. "The M9 Project Ground Motions", in The M9 Project Ground Motions. DesignSafe-CI. https://doi.org/10.17603/DS2WM3W.

Karthik Narayan, Ramanathan, 2012. “Next Generation Seismic Fragility Curves for California Bridges Incorporating The Evolution in Seismic Design Philosophy” Ph. D. thesis, Georgia Institute of Technology, Georgia.

Khaleghi, Bijan. 2019. Memo to All Design Section Staff. Washington State Department of Transportation Bridge and Structures Office.

Lehman, D. E. and J. P. Moehle, 2000. Seismic Performance of Well-Confined Concrete Bridge Columns. PEER 1998/01, Pacific Earthquake Engineering Research Center, Berkeley, CA.

Mander, J. B., Priestley, M. J. N., and Park, R., 1988. “Theoretical Stress-Strain Model for Confined Concrete” Journal of Structural Engineering, V. 114, No. 8: 1804-1826.

Megally, S. H., Silva, F. P., and Seible, F., 2002. “Seismic Response of Sacrificial Shear Keys in Bridge Abutments.” Report No. SSRP-2001/23, Department of Structural Engineering, University of California, San Diego, CA.

Lignos, D.G. and Krawinkler, H. 2012. “Sidesway collapse of deteriorating structural systems under seismic excitations,” Rep.No.TB 177, The John A. Blume Earthquake Engineering Research Center, Stanford University, Stanford, CA.

Marafi, N.A., Eberhard, M.O., Berman, J.W., Wirth, E.A., and Frankel, A.D., 2017. “Effects of Deep Basins on Structural Collapse During Large Subduction Zone Earthquakes.” Earthquake Spectra, 33(3), 963-997. https://doi.org/10.1193/071916EQS114M

Marafi, Nasser, Eberhard, Marc, and Berman, Jeffrey. 2019. “Impacts of Simulated M9 Cascadia Subduction Zone Motions on Idealized Systems”. Earthquake Spectra, Vol 35, Issue 3, 2019.

Marafi, Nasser, Eberhard, Marc, Berman, Jeffrey, Wirth, Erin, and Frankel, Arthur. 2017. “Effects of Deep Basins on Structural Collapse during Large Subduction Earthquakes.” Earthquake Spectra. 33(3), 963-997.

Marafi, Nasser, Makdisi, Andrew, Eberhard, Marc, and Berman, Jeffrey. 2020. “Performance of RC Core-Wall Buildings during Simulated M9 Cascadia Subduction Zone Earthquake Scenarios”. Journal of Structural Engineering, Volume 146, Issue 2.

Muthukumar, S. and DesRoches, R. (2006). A Hertz contact model with non-linear damping for pounding simulation. Earthquake Engineering and Structural Dynamics, 35, pp:811-828.

Nasser Abdulazim, Marafi, 2018. “Impacts of an M9 Cascadia Subduction Zone Earthquake on Structures Located in Deep Sedimentary Basins.” Ph. D. thesis, University of Washington, Seattle.

Pacific Northwest Seismic Network. “Cascadia Subduction Zone.” https://pnsn.org/outreach/earthquakesources/csz (May 31, 2021)

Palmer, S., Magsin, S., Bilderback, E., Poelstra, J., Folger, D., and Niggemann, R. 2007. “Liquefaction Susceptibility and Site Class Maps of Washington State, By County.” Washington Division of Geology and Earth Resources. Open File Report 2004-20. ftp://ww4.dnr.wa.gov/geology/pubs/ofr04-20/ (June 4, 2019).

Ranf, R. (2006). Performance Based Evaluation of Seismic Modeling Strategies for Bridges. Ph. D. thesis, University of Washington, Seattle.

Richard Tyler, Ranf, 2007. “Model Selection for Performance-Based Earthquake Engineering of Bridges.” Ph. D. thesis, University of Washington, Seattle.

Shamsabadi, A. and Yan, L. (2008). Closed-form force-displacement backbone curves for bridge abutment-backfill systems. Geotechnical Earthquake Engineering and Soil Dynamics IV. 2008. 1-10.

Sujith, Mangalathu, 2017. “Performance Based Grouping and Fragility Analysis of Box-Girder Bridges in California” Ph. D. thesis, Georgia Institute of Technology, Georgia.

United States Geological Survey (USGS), 2017, Illustration of Seismic Source Zones in the Pacific Northwest, https://geomaps.wr.usgs.gov/pacnw/pacnweq/pdf/subd_eqpg.pdf

University of Washington-Pacific Earthquake Engineering Research Structural Performance Database. https://nisee.berkeley.edu/spd/. Accessed June 2020.

Zachary, Kortum, 2021. “Impacts of Cascadia Subduction Zone M9 Earthquakes on Bridges in Washington State: SDOF Idealized Bridges.” Master’s Thesis, University of Washington, Seattle.

Zhu, M., McKenna, F., and Scott, M. H., 2018. “OpenSeesPy: Python Library for the OpenSees Finite Element Framework”. Volume 7, School of Civil and Construction Engineering, Oregon State University, OR.

Appendix

Appendix A: Selected Bridges for Abutment Database

Table A.1: Selected Bridges for Abutment Database

Bridge Number	Longitude	Latitude	Year
167/110	47.29569	-122.2578	1975
167/122E	47.37778	-122.2444	1967
167/123W	47.3812	-122.2446	1967
167/126E	47.39223	-122.2373	1967
167/128E	47.39825	-122.2284	1967
167/138HOV	47.46492	-122.218	2018
167/16	47.21353	-122.3419	1970
167/20W	47.20189	-122.294	1971
167/38	47.23572	-122.2521	2004
405/104P	47.79386	-122.2124	2007
405/105E	47.79786	-122.2205	1968
405/108W	47.81989	-122.2422	1968
405/10A	47.46489	-122.2482	1994
405/11	47.4637	-122.2459	1964
405/112W	47.83114	-122.2615	1982
405/13	47.46715	-122.2343	2009
405/15	47.46771	-122.2184	1989
405/17	47.47031	-122.2064	2010
405/23E-N	47.50228	-122.1963	1997
405/23W	47.50253	-122.1968	1966
405/30E	47.5675	-122.1799	1965
405/35E	47.57939	-122.1741	1969
405/35HOV	47.5799	-122.1744	1969
405/41E	47.60297	-122.1836	1971

Bridge Number	Longitude	Latitude	Year
405/45.4NE	47.63166	-122.1847	2011
405/45E	47.62978	-122.1883	1965
405/47S-W	47.6341	-122.1882	1966
405/50	47.66945	-122.1878	1970
405/52W	47.67889	-122.1847	1971
405/56W	47.70667	-122.1783	1970
405/59W	47.71822	-122.1876	1970
405/64	47.7425	-122.1875	1969
405/73	47.76855	-122.19	1968
5/439	47.23111	-122.4431	2007
5/445S-S	47.23316	-122.4319	1965
5/455	47.23942	-122.4048	1963
5/457	47.24172	-122.3857	1961
5/461	47.24389	-122.3361	1960
5/461A	47.24467	-122.3363	1962
5/464W	47.252	-122.3328	1960
5/504E	47.30033	-122.3028	1959
5/508E	47.35233	-122.2955	1960
5/509E	47.35764	-122.2963	1961
5/516W	47.43119	-122.2715	1963
5/519E	47.45072	-122.2653	1966
5/520HOV	47.45744	-122.2639	1996
5/521E	47.46147	-122.2636	1966
5/522HOV	47.46108	-122.2639	1996
5/522S-E	47.46247	-122.2653	1966

Bridge Number	Longitude	Latitude	Year
5/525.5H	47.48342	-122.2707	1996
5/526.1	47.48906	-122.2641	1966
5/526E	47.48692	-122.2662	1964
5/532W	47.53528	-122.2972	1967
5/533A	47.54842	-122.3177	1966
5/534N-W	47.55267	-122.3181	1967
5/534W	47.55327	-122.3176	1966
5/535E	47.56055	-122.3213	1966
5/536E-S	47.57108	-122.324	1967
5/537N	47.57322	-122.3159	1967
5/538S-E	47.57428	-122.3202	1967
5/538S-W	47.57408	-122.3203	1967
5/539.5	47.58611	-122.3222	1966
5/542E	47.59553	-122.3203	1965
5/542NCD	47.59553	-122.3197	1965
5/543SCD	47.59808	-122.3215	1965
5/545R	47.60414	-122.3274	1964
5/548	47.60872	-122.3314	1964
5/551	47.61417	-122.3306	1965
5/553	47.61845	-122.3293	1962
5/566N-E	47.63325	-122.3235	1963
5/574	47.66497	-122.3225	1962
5/583	47.68682	-122.3269	1964
5/588N-N	47.70841	-122.3294	1995
5/588SCD	47.70842	-122.3304	1964

Bridge Number	Longitude	Latitude	Year
5/593W	47.74096	-122.329	1964
5/599SCD	47.77739	-122.3183	1995
5/601N-E	47.78272	-122.3162	1995
5/607E	47.80633	-122.3062	1963
5/631E	47.9663	-122.1987	1967
5/638W	47.98083	-122.1885	1967
5/646	48.00753	-122.1748	1967
5/647W	48.02314	-122.1758	1968
5/649E	48.04014	-122.179	1968
5/650E	48.0433	-122.1805	1969
5/654A	48.07558	-122.1794	1996
512/10S	47.15894	-122.4158	1966
512/12	47.15903	-122.4057	1965
512/13	47.15867	-122.4026	1965
90/47E-N	47.57989	-122.1753	1969
90/50N	47.58055	-122.1686	1940
90/66N	47.54053	-122.036	1971
90/67E-E	47.53136	-122.0256	2003
90/89S	47.46481	-121.7165	1971
90/99	47.42705	-121.4158	1969

Appendix B: Design Plan for Bridge 405/23E-N

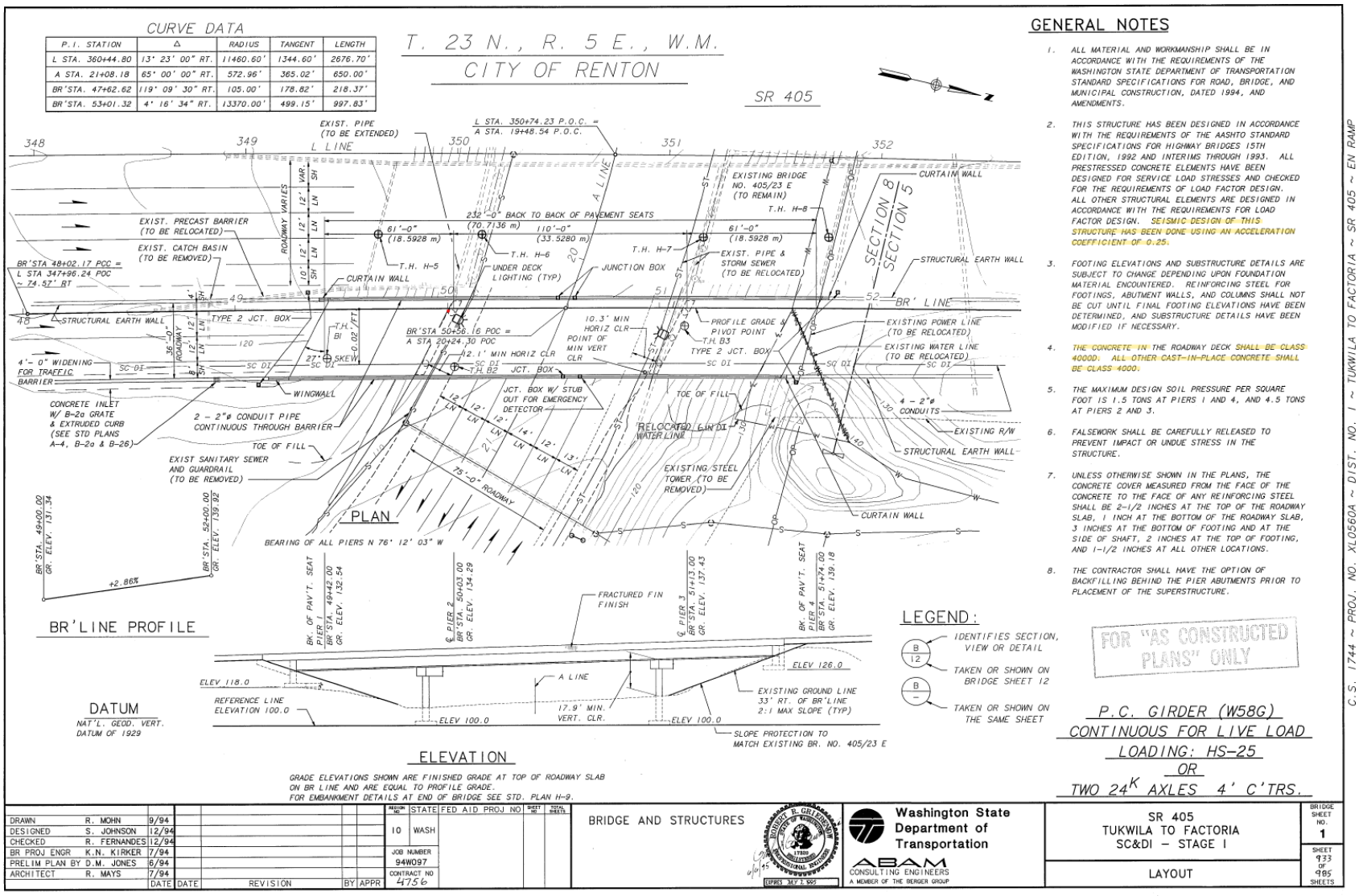
CURVE DATA
P.I. STATION | Δ | RADIUS | TANGENT | LENGTH
L STA. 360+44.80 | 13° 23' 00" RT. | 11460.60' | 1344.60' | 2676.70'
A STA. 21+08.18 | 65° 00' 00" RT. | 572.96' | 365.02' | 650.00'
BR'STA. 47+62.62 | 119° 09' 30" RT. | 105.00' | 178.82' | 218.37'
BR'STA. 53+01.32 | 4° 16' 34" RT. | 13370.00' | 499.15' | 997.83'
T. 23 N., R. 5 E., W.M.
CITY OF RENTON
SR 405
GENERAL NOTES
1. ALL MATERIAL AND WORKMANSHIP SHALL BE IN ACCORDANCE WITH THE REQUIREMENTS OF THE WASHINGTON STATE DEPARTMENT OF TRANSPORTATION STANDARD SPECIFICATIONS FOR ROAD, BRIDGE, AND MUNICIPAL CONSTRUCTION, DATED 1994, AND AMENDMENTS.
2. THIS STRUCTURE HAS BEEN DESIGNED IN ACCORDANCE WITH THE REQUIREMENTS OF THE AASHTO STANDARD SPECIFICATIONS FOR HIGHWAY BRIDGES 15TH EDITION, 1992 AND INTERIMS THROUGH 1993. ALL PRESTRESSED CONCRETE ELEMENTS HAVE BEEN DESIGNED FOR SERVICE LOAD STRESSES AND CHECKED FOR THE REQUIREMENTS OF LOAD FACTOR DESIGN. ALL OTHER STRUCTURAL ELEMENTS ARE DESIGNED IN ACCORDANCE WITH THE REQUIREMENTS FOR LOAD FACTOR DESIGN. SEISMIC DESIGN OF THIS STRUCTURE HAS BEEN DONE USING AN ACCELERATION COEFFICIENT OF 0.25.
3. FOOTING ELEVATIONS AND SUBSTRUCTURE DETAILS ARE SUBJECT TO CHANGE DEPENDING UPON FOUNDATION MATERIAL ENCOUNTERED. REINFORCING STEEL FOR FOOTINGS, ABUTMENT WALLS, AND COLUMNS SHALL NOT BE CUT UNTIL FINAL FOOTING ELEVATIONS HAVE BEEN DETERMINED, AND SUBSTRUCTURE DETAILS HAVE BEEN MODIFIED IF NECESSARY.
4. THE CONCRETE IN THE ROADWAY DECK SHALL BE CLASS 4000D. ALL OTHER CAST-IN-PLACE CONCRETE SHALL BE CLASS 4000.
5. THE MAXIMUM DESIGN SOIL PRESSURE PER SQUARE FOOT IS 1.5 TONS AT PIERS 1 AND 4, AND 4.5 TONS AT PIERS 2 AND 3.
6. FALSEWORK SHALL BE CAREFULLY RELEASED TO PREVENT IMPACT OR UNDUE STRESS IN THE STRUCTURE.
7. UNLESS OTHERWISE SHOWN IN THE PLANS, THE CONCRETE COVER MEASURED FROM THE FACE OF THE CONCRETE TO THE FACE OF ANY REINFORCING STEEL SHALL BE 2-1/2 INCHES AT THE TOP OF THE ROADWAY SLAB, 1 INCH AT THE BOTTOM OF THE ROADWAY SLAB, 3 INCHES AT THE BOTTOM OF FOOTING AND AT THE SIDE OF SHAFT, 2 INCHES AT THE TOP OF FOOTING, AND 1-1/2 INCHES AT ALL OTHER LOCATIONS.
8. THE CONTRACTOR SHALL HAVE THE OPTION OF BACKFILLING BEHIND THE PIER ABUTMENTS PRIOR TO PLACEMENT OF THE SUPERSTRUCTURE.
PLAN
BR'LINE PROFILE
ELEVATION
DATUM
NAT'L. GEOD. VERT. DATUM OF 1929
LEGEND:
IDENTIFIES SECTION, VIEW OR DETAIL
TAKEN OR SHOWN ON BRIDGE SHEET 12
TAKEN OR SHOWN ON THE SAME SHEET
FOR "AS CONSTRUCTED PLANS" ONLY
P.C. GIRDER (W58G)
CONTINUOUS FOR LIVE LOAD
LOADING: HS-25
OR
TWO 24K AXLES 4' C'TRS.
DRAWN R. MOHN 9/94
DESIGNED S. JOHNSON 12/94
CHECKED R. FERNANDES 12/94
BR PROJ ENGR K.N. KIRKER 7/94
PRELIM PLAN BY D.M. JONES 6/94
ARCHITECT R. MAYS 7/94
DATE REVISION BY APPR
REGION NO. 10 | STATE WASH | FED AID PROJ NO | SHEET NO | TOTAL SHEETS
JOB NUMBER 94W097
CONTRACT NO 4756
BRIDGE AND STRUCTURES
Washington State Department of Transportation
ABAM CONSULTING ENGINEERS
A MEMBER OF THE BERGER GROUP
SR 405
TUKWILA TO FACTORIA
SC&DI - STAGE 1
LAYOUT
BRIDGE SHEET NO. 1
SHEET 933 OF 985 SHEETS
SR 405 JOB NO. 7062 SHEET 1 OF 22
C.S. 1744 ~ PROJ. NO. XL0560A ~ DIST. NO. 1 ~ TUKWILA TO FACTORIA ~ SR 405 ~ EN RAMP

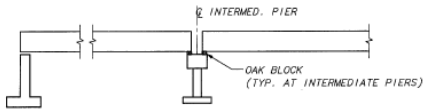

STAGE 1 – SET GIRDERS IN PLACE

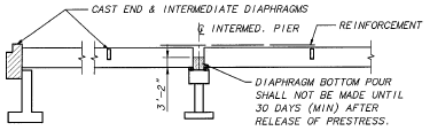

STAGE 2 – POUR DIAPHRAGMS AND PLACE REINFORCEMENT

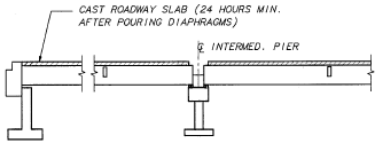

STAGE 3 – POUR ROADWAY SLAB

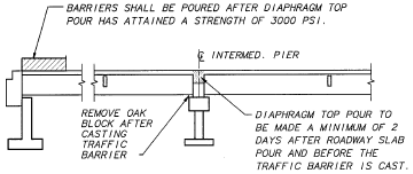

STAGE 4 – POUR DIAPHRAGMS AT INTERMEDIATE PIERS AND BARRIERS

CONSTRUCTION SEQUENCE – SUPERSTRUCTURE

EXISTING ELEVATION A LINE			
STATION	ELEVATION LT SHOULDER	ELEVATION CENTER LINE	ELEVATION RT SHOULDER
19+00.00	–	–	102.32
19+20.00	–	105.35	103.06
19+40.00	107.59	106.06	103.79
19+60.00	108.26	106.74	104.50
19+80.00	108.95	107.44	105.28
20+00.00	109.68	108.16	105.14
20+20.00	110.45	109.16	107.03
20+40.00	111.15	109.81	107.88
20+60.00	111.88	110.58	108.73
20+80.00	112.69	111.42	109.58
21+00.00	113.64	112.28	110.47
21+20.00	114.36	113.11	111.42
21+40.00	115.16	113.92	112.39

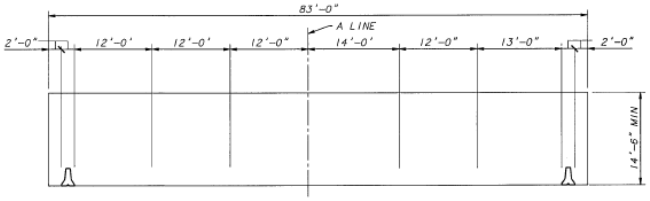

CONSTRUCTION OPENING DIAGRAM

NORMAL TO A LINE

FOR "AS CONSTRUCTED PLANS" ONLY

SR 405 JOB NO. 106Z SHEET 2 OF 22

DRAWN	R. MOHN	9/94					REGION NO	STATE	FED. AID PROJ. NO.	SHEET NO.	TOTAL SHEETS
DESIGNED	E. DORNSEIF	12/94					10	WASH			
CHECKED	R. FERNANDES	12/94					JOB NUMBER 94W097				
BR. PROJ. ENGR.							CONTRACT NO 4756				
PRELIM. PLAN BY											
ARCHITECT											
		DATE	DATE	REVISION	BY	APPR					

BRIDGE AND STRUCTURES

JAMES S. GUARDE — 14886 — REGISTERED PROFESSIONAL ENGINEER — EXPIRES: JUNE 4, 2003

Washington State Department of Transportation

ABAM CONSULTING ENGINEERS — A MEMBER OF THE BERGER GROUP

SR 405
TUKWILA TO FACTORIA
SC&DI - STAGE 1

CONSTRUCTION SEQUENCE AND PROFILE GEOMETRY

BRIDGE SHEET NO. 2

SHEET 934 OF 995 SHEETS

SR 405/ 4/7

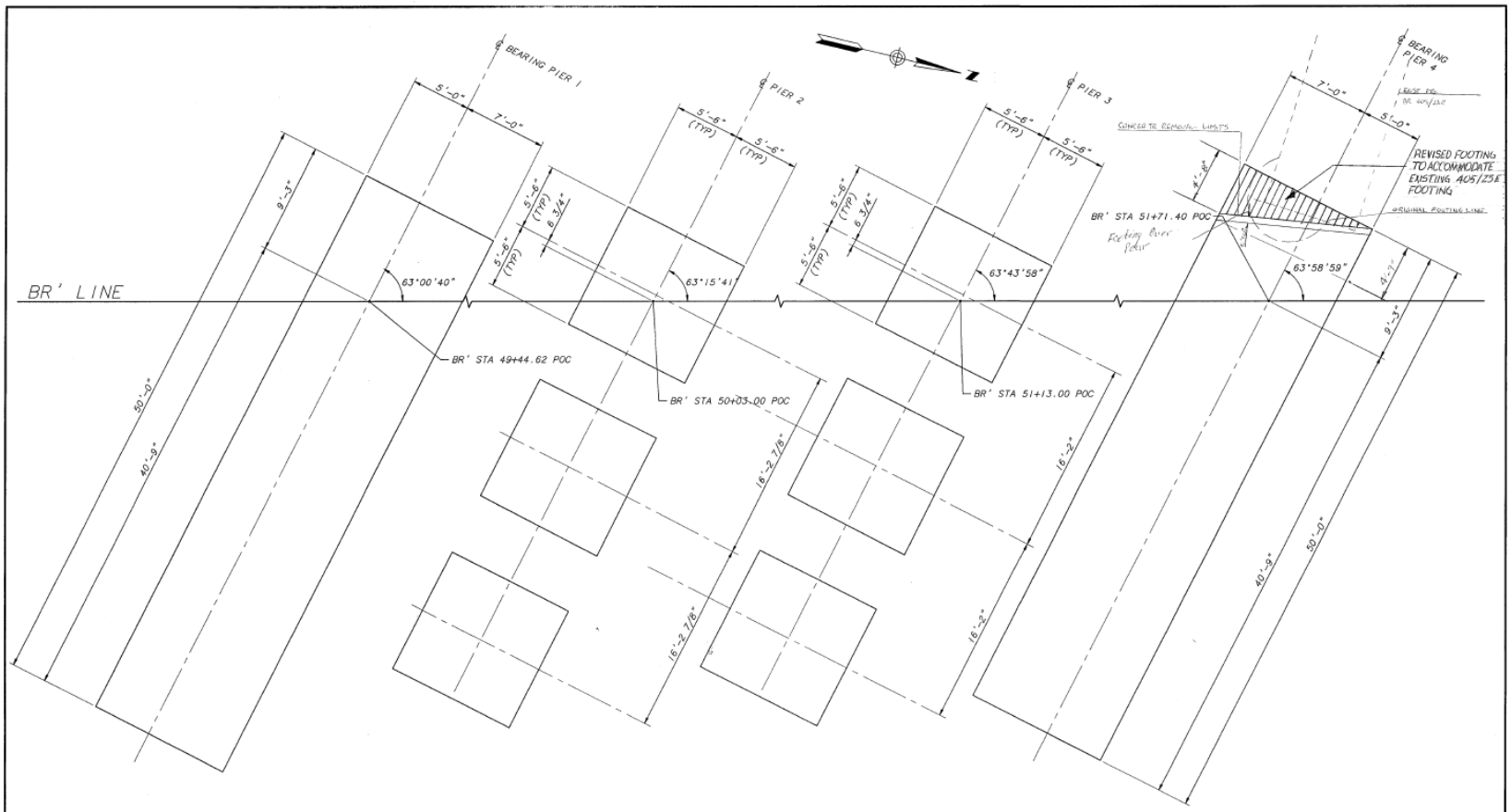

FOOTING LAYOUT

BEARING OF ALL PIERS = ~~N 76°12'08" W~~ N 76°44'09" W

FOR "AS CONSTRUCTED PLANS" ONLY

DRAWN	B. HUYNH	9/94			REVISION NO	STATE	FED AID PROJ NO	SHEET NO	TOTAL SHEETS	BRIDGE AND STRUCTURES	Washington State Department of Transportation
DESIGNED	E. DORNSEIF	12/94			10	WASH					ABAM CONSULTING ENGINEERS A MEMBER OF THE BERGER GROUP
CHECKED	R. FERNANDES	12/94			JOB NUMBER	94W097					SR 405 TUKWILA TO FACTORIA SC&DI - STAGE 1
BR PROJ ENGR					CONTRACT NO	4756					FOOTING LAYOUT
PRELIM PLAN BY											BRIDGE SHEET NO. 3
ARCHITECT											SHEET 925 OF 985 SHEETS
		DATE	DATE	REVISION	BY	APPR					

SR 405 JOB NO. 7067 SHEET 3 OF 32

SR405/417

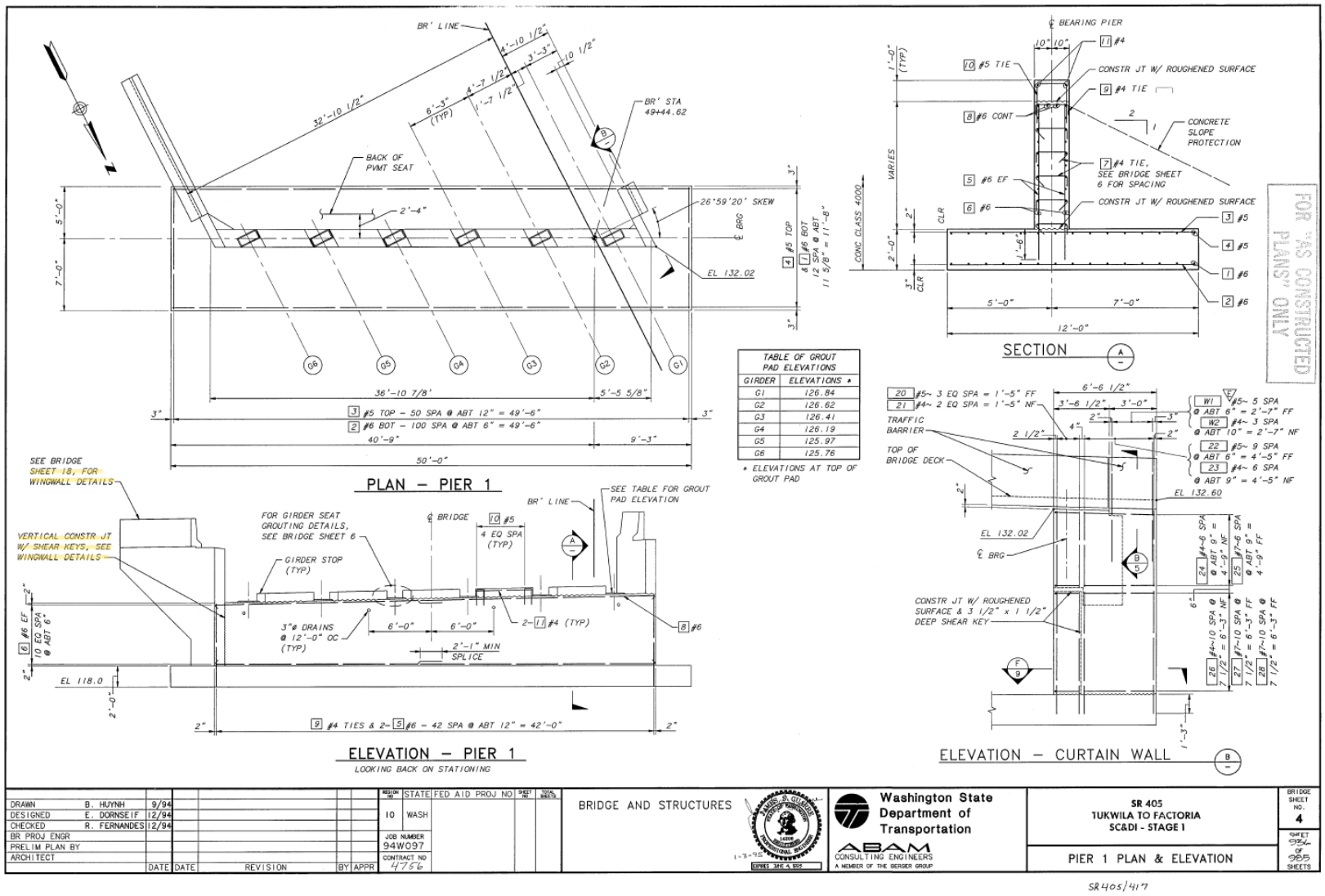

DRAWN	B. HUYNH	9/94				REGION NO	STATE	FED AID PROJ NO	SHEET NO	TOTAL SHEETS
DESIGNED	E. DORNSEIF	12/94				10	WASH			
CHECKED	R. FERNANDES	12/94				JOB NUMBER 94W097				
BR PROJ ENGR						CONTRACT NO 4175				
PRELIM PLAN BY										
ARCHITECT										
	DATE	DATE	REVISION	BY	APPR					

BRIDGE AND STRUCTURES

Washington State Department of Transportation

ABAM CONSULTING ENGINEERS
A MEMBER OF THE BERGER GROUP

SR 405
TUKWILA TO FACTORIA
SC&DI - STAGE 1

PIER 1 PLAN & ELEVATION

BRIDGE SHEET NO. 4

SHEET 95 OF 955 SHEETS

SR 405 JOB NO. 7062 SHEET 4 OF 18

SR405/417

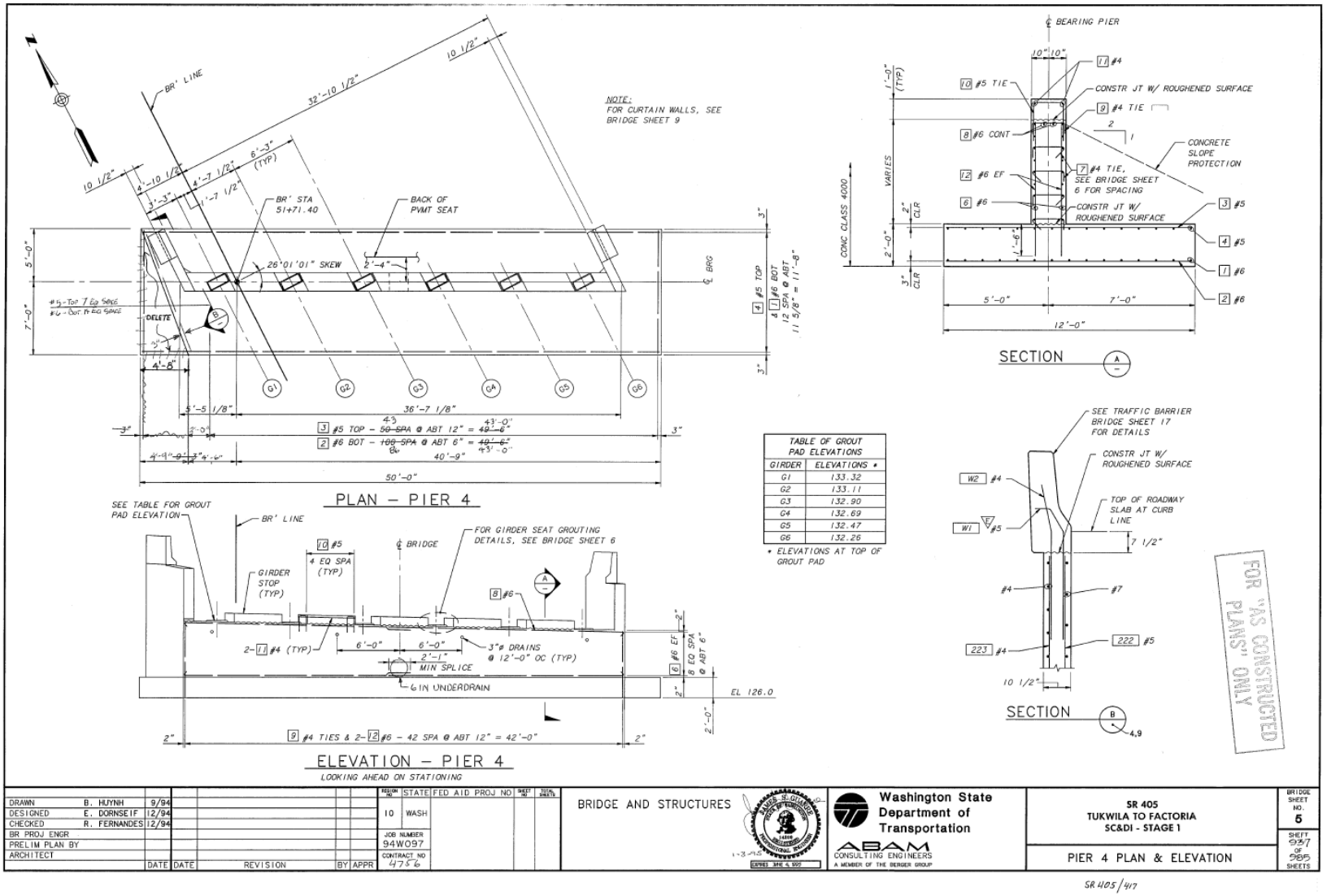

TABLE OF GROUT PAD ELEVATIONS	
GIRDER	ELEVATIONS *
G1	133.32
G2	133.11
G3	132.90
G4	132.69
G5	132.47
G6	132.26

* ELEVATIONS AT TOP OF GROUT PAD

DRAWN	B. HUYNH	9/94
DESIGNED	E. DORNSEIF	12/94
CHECKED	R. FERNANDES	12/94
BR PROJ ENGR		
PRELIM PLAN BY		
ARCHITECT		

DATE	DATE	REVISION	BY	APPR

REGION NO	STATE	FED AID PROJ NO	SHEET NO	TOTAL SHEETS
10	WASH			

JOB NUMBER 94W097
CONTRACT NO 4756

BRIDGE AND STRUCTURES

Washington State Department of Transportation

ABAM CONSULTING ENGINEERS
A MEMBER OF THE BERGER GROUP

SR 405
TUKWILA TO FACTORIA
SC&DI - STAGE 1

PIER 4 PLAN & ELEVATION

BRIDGE SHEET NO. 5
SHEET 937 OF 985 SHEETS

SR 405 JOB NO. 7067 SHEET 5 OF 12

SR 405/417

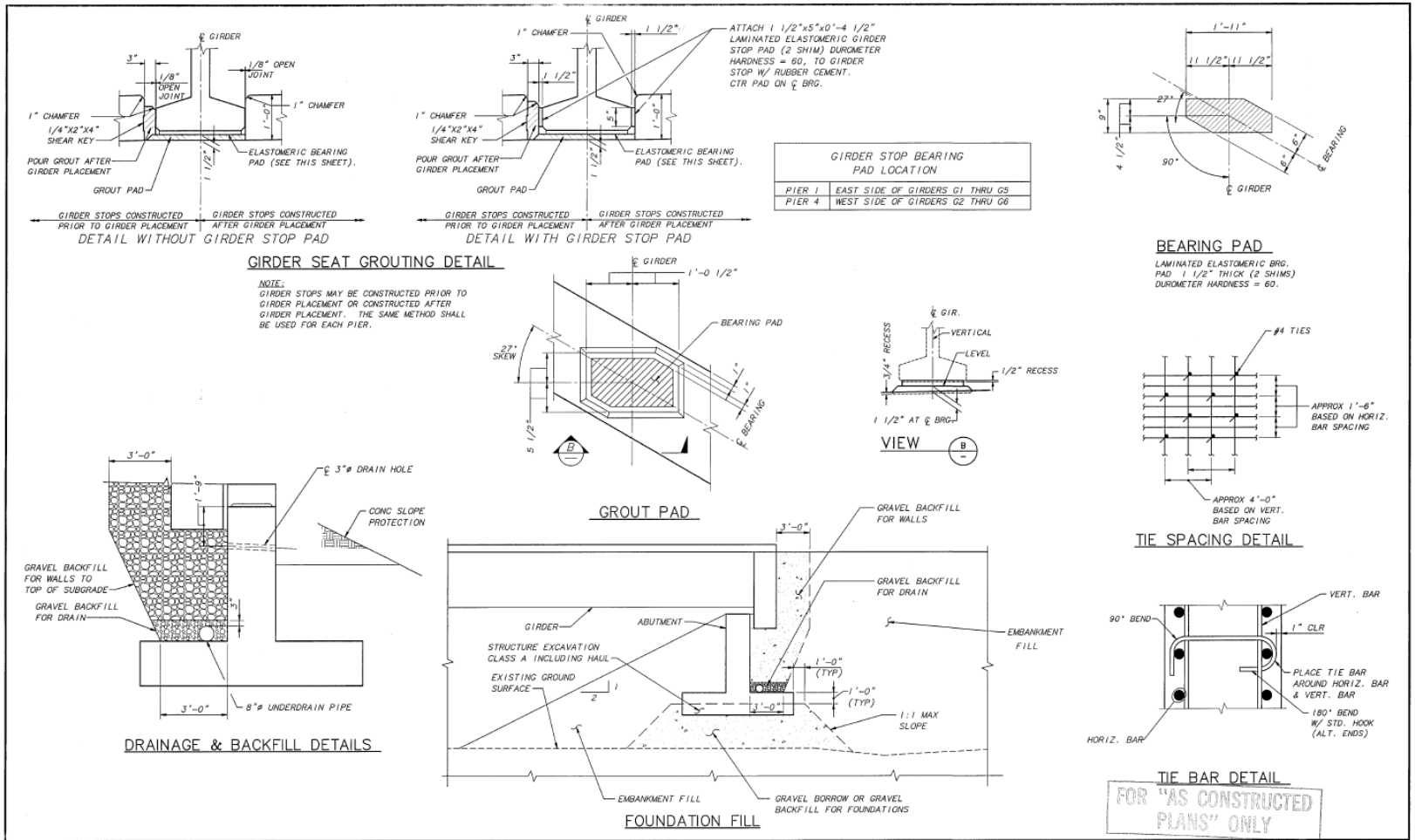

SR 405 JOB NO. 7062 SHEET 6 OF 22

DRAWN	R. MOHN	9/94					REGION NO	STATE	FED. AID PROJ. NO.	SHEET NO.	TOTAL SHEETS
DESIGNED	E. DORNSEIF	12/94					10	WASH			
CHECKED	R. FERNANDES	12/94					JOB NUMBER 94W097				
BR PROJ ENGR							CONTRACT NO 4756				
PRELIM PLAN BY											
ARCHITECT											
		DATE	DATE	REVISION	BY	APPR					

BRIDGE AND STRUCTURES

Washington State Department of Transportation

ABAM CONSULTING ENGINEERS
A MEMBER OF THE BERGER GROUP

SR 405
TUKWILA TO FACTORIA
SC&DI - STAGE 1

ABUTMENT DETAILS

BRIDGE SHEET NO. 6

SHEET 955 OF 955 SHEETS

SR 405/417

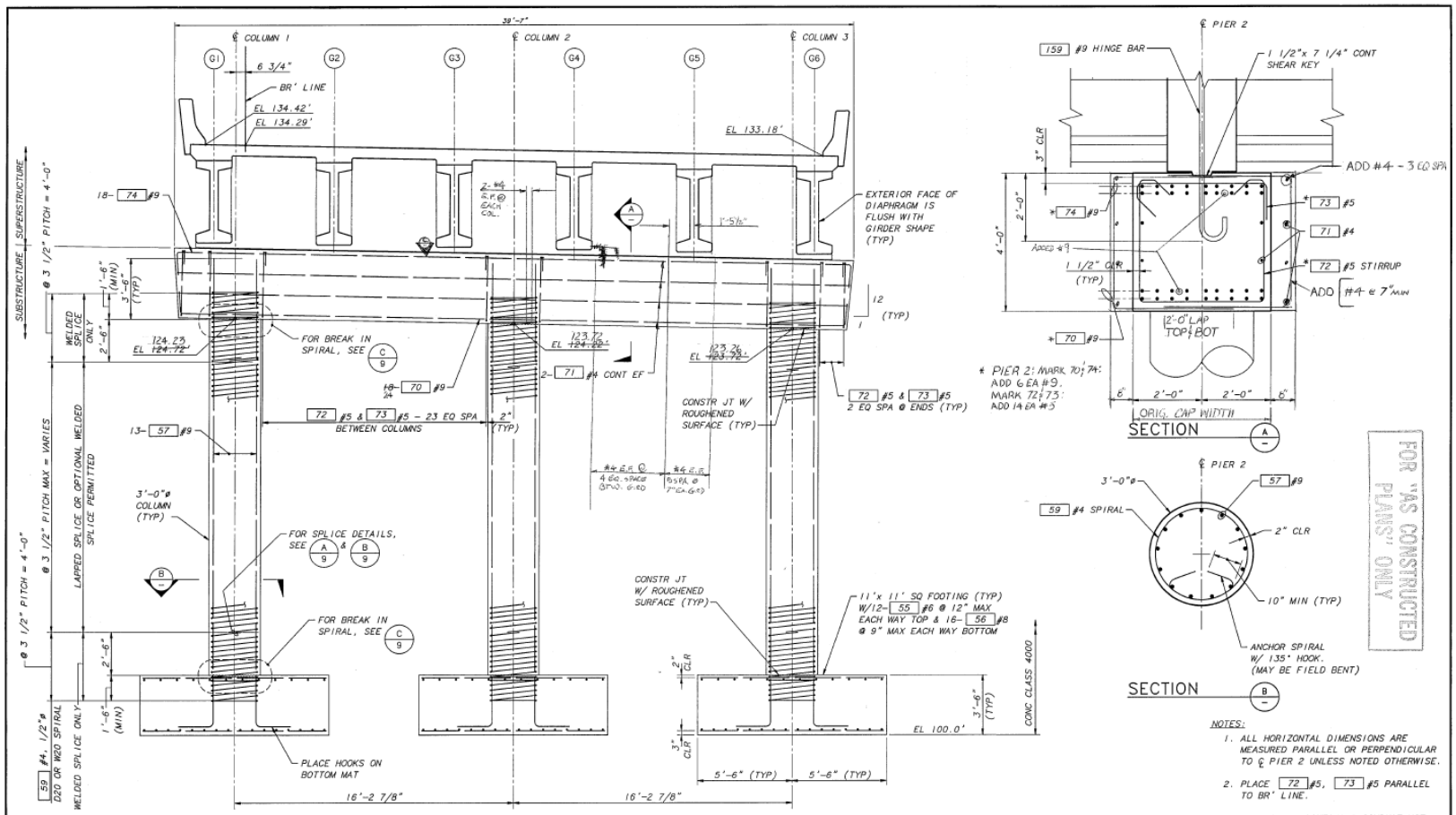

DRAWN	R. MOHN	10/94								
DESIGNED	E. DORNSEIF	12/94								
CHECKED	R. FERNANDES	12/94								
BR PROJ ENGR										
PRELIM PLAN BY										
ARCHITECT										
	DATE	DATE	REVISION	BY	APPR	REGION NO	STATE	FED AID PROJ NO	SHEET NO	TOTAL SHEETS
						10	WASH			

JOB NUMBER 94W097
CONTRACT NO 4756

BRIDGE AND STRUCTURES

Washington State Department of Transportation

ABAM CONSULTING ENGINEERS
A MEMBER OF THE BERGER GROUP

SR 405
TUKWILA TO FACTORIA
SC&DI - STAGE 1

PIER 2 ELEVATION & DETAILS

BRIDGE SHEET NO. 7

SHEET 959 OF 985 SHEETS

SR 405 JOB NO. 7067 SHEET 7 OF 22

SR 405/417

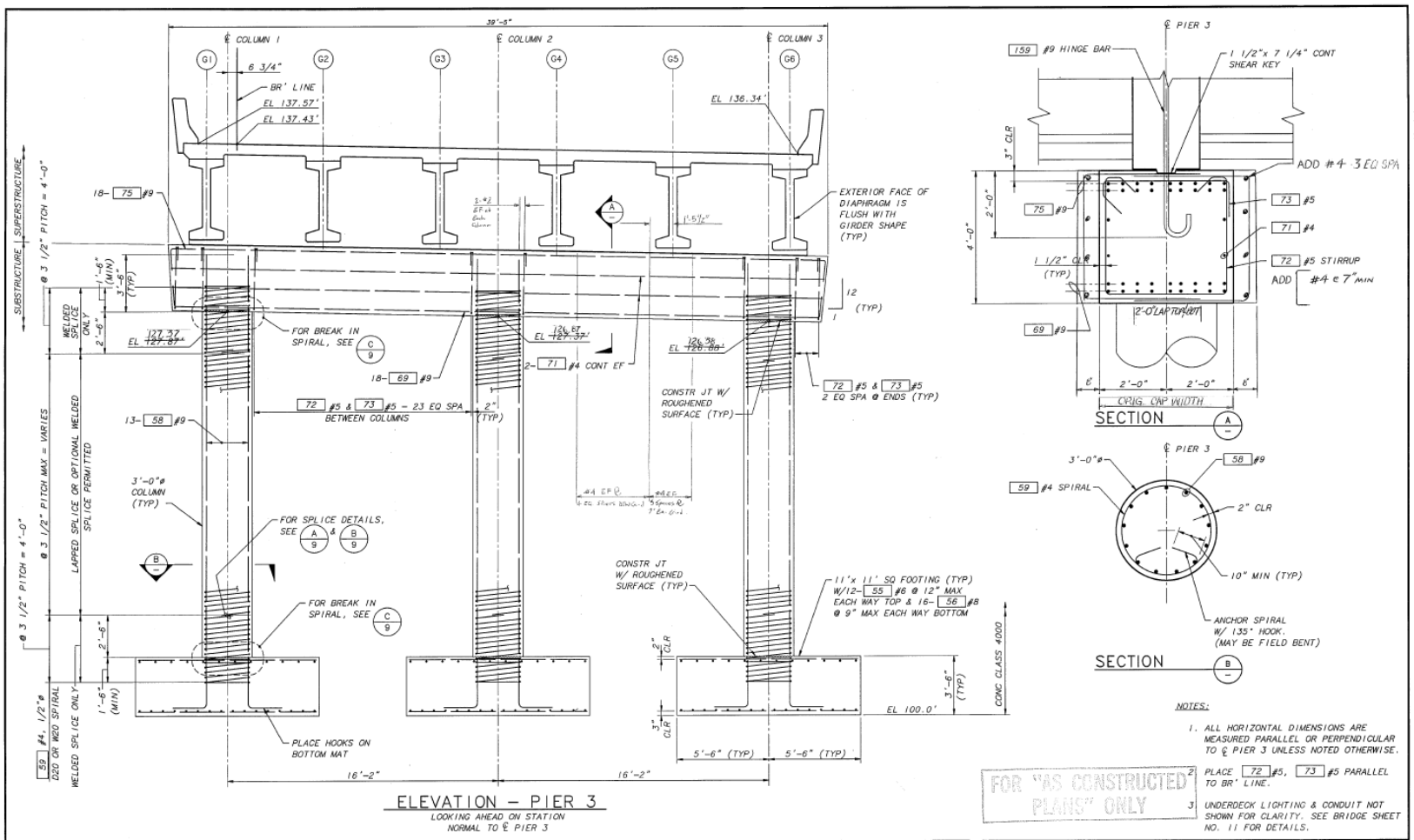

NOTES:

1. ALL HORIZONTAL DIMENSIONS ARE MEASURED PARALLEL OR PERPENDICULAR TO ℄ PIER 3 UNLESS NOTED OTHERWISE.
2. PLACE 72 #5, 73 #5 PARALLEL TO BR' LINE.
3. UNDERDECK LIGHTING & CONDUIT NOT SHOWN FOR CLARITY. SEE BRIDGE SHEET NO. 11 FOR DETAILS.

FOR "AS CONSTRUCTED" PLANS" ONLY

DRAWN	R. MOHN	10/94						
DESIGNED	E. DORNSEIF	12/94						
CHECKED	R. FERNANDES	12/94						
BR PROJ ENGR								
PRELIM PLAN BY								
ARCHITECT								
		DATE	DATE	REVISION	BY	APPR		

REGION NO	STATE	FED AID PROJ NO	SHEET NO	TOTAL SHEETS
10	WASH			

JOB NUMBER 94W097
CONTRACT NO 4776

BRIDGE AND STRUCTURES

Washington State Department of Transportation

ABAM CONSULTING ENGINEERS
A MEMBER OF THE BERGER GROUP

SR 405
TUKWILA TO FACTORIA
SC&DI - STAGE 1

PIER 3 ELEVATION & DETAILS

BRIDGE SHEET NO. 8

SHEET 940 OF 985 SHEETS

SR 405 JOB NO. 7067 SHEET 8 OF 12

SR 405/417

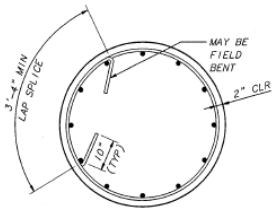

HOOKS SHALL BE PLACED TO AVOID VERTICAL REINF
NOTE: FOR WELDED SPLICE ALTERNATE SEE (B)

DETAIL – LAP SPLICE (A)

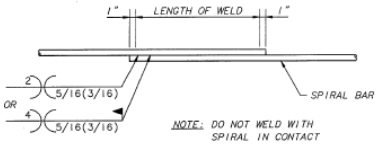

NOTE: DO NOT WELD WITH SPIRAL IN CONTACT WITH VERTICAL REINFORCING. ISOLATE VERTICAL REINFORCING FROM HEAT AND SPLATTER.

DETAIL
WELDED SPLICE ALTERNATE (B)

NOTES:

1. COLUMN SPIRAL BARS SHALL BE #4 DEFORMED BAR, 1/2" DIAMETER PLAIN STEEL BAR, OR W20 COLD DRAWN WIRE.
2. LAP SPLICES SHALL BE PERMITTED ONLY WITHIN THE CENTER HALF OF COLUMN HEIGHT. WELD SPLICE SHALL BE PERMITTED ENTIRE LENGTH OF COLUMN.

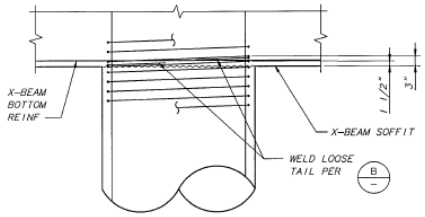

NOTES:

1. PROVIDE BREAK IN SPIRAL TO ALLOW PLACEMENT OF CROSSBEAM BOTTOM REINF OR FOOTING TOP REINF.
2. CROSSBEAM DETAILS SHOWN, FOOTING DETAILS SIMILAR.

DETAIL – SPIRAL BREAK (C)

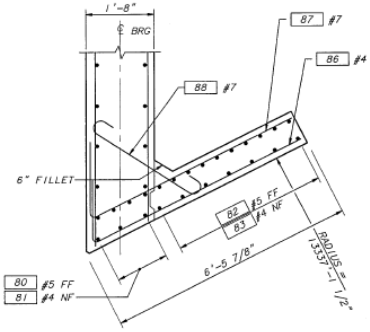

SECTION – EAST CURTAIN WALL @ PIER 4 (D)

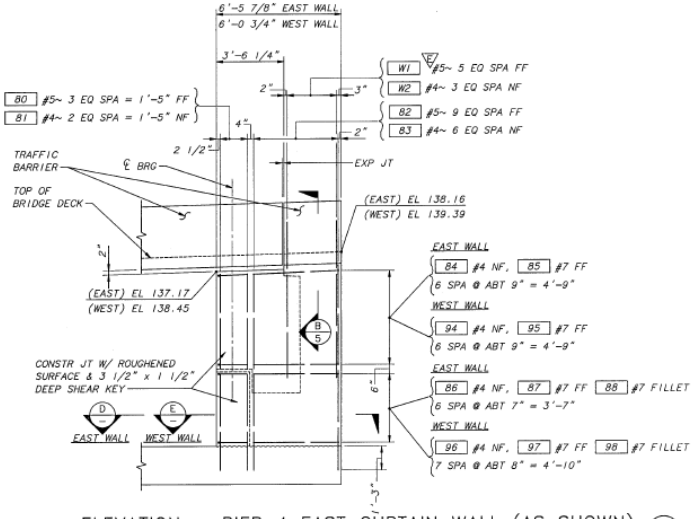

ELEVATION – PIER 4 EAST CURTAIN WALL (AS SHOWN)
PIER 4 WEST CURTAIN WALL (OPP HAND) (C)

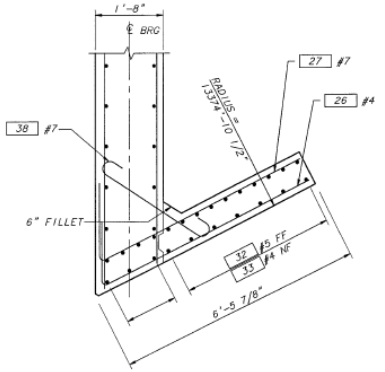

SECTION – WEST CURTAIN WALL @ PIER 1 (F 4)

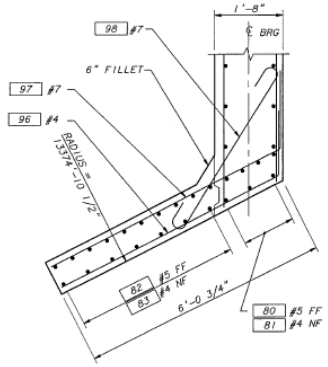

SECTION – WEST CURTAIN WALL @ PIER 4 (E)

FOR "AS CONSTRUCTED PLANS" ONLY

DRAWN	R. MOHN	9/94				REGION NO	STATE	FED AID PROJ NO	SHEET NO.	TOTAL SHEETS
DESIGNED	E. DORNSEIF	12/94				10	WASH			
CHECKED	R. FERNANDES	12/94				JOB NUMBER 94WC097				
BR PROJ ENGR						CONTRACT NO 4756				
PRELIM PLAN BY										
ARCHITECT										
	DATE	DATE	REVISION	BY	APPR					

BRIDGE AND STRUCTURES

Washington State Department of Transportation

ABAM CONSULTING ENGINEERS
A MEMBER OF THE BERGER GROUP

SR 405
TUKWILA TO FACTORIA
SC&DI - STAGE 1

MISCELLANEOUS PIER DETAILS

BRIDGE SHEET NO. 9

SHEET 94.1 OF 9905 SHEETS

SR 405 JOB NO. 706Z SHEET 9 OF 12

SK 405/417

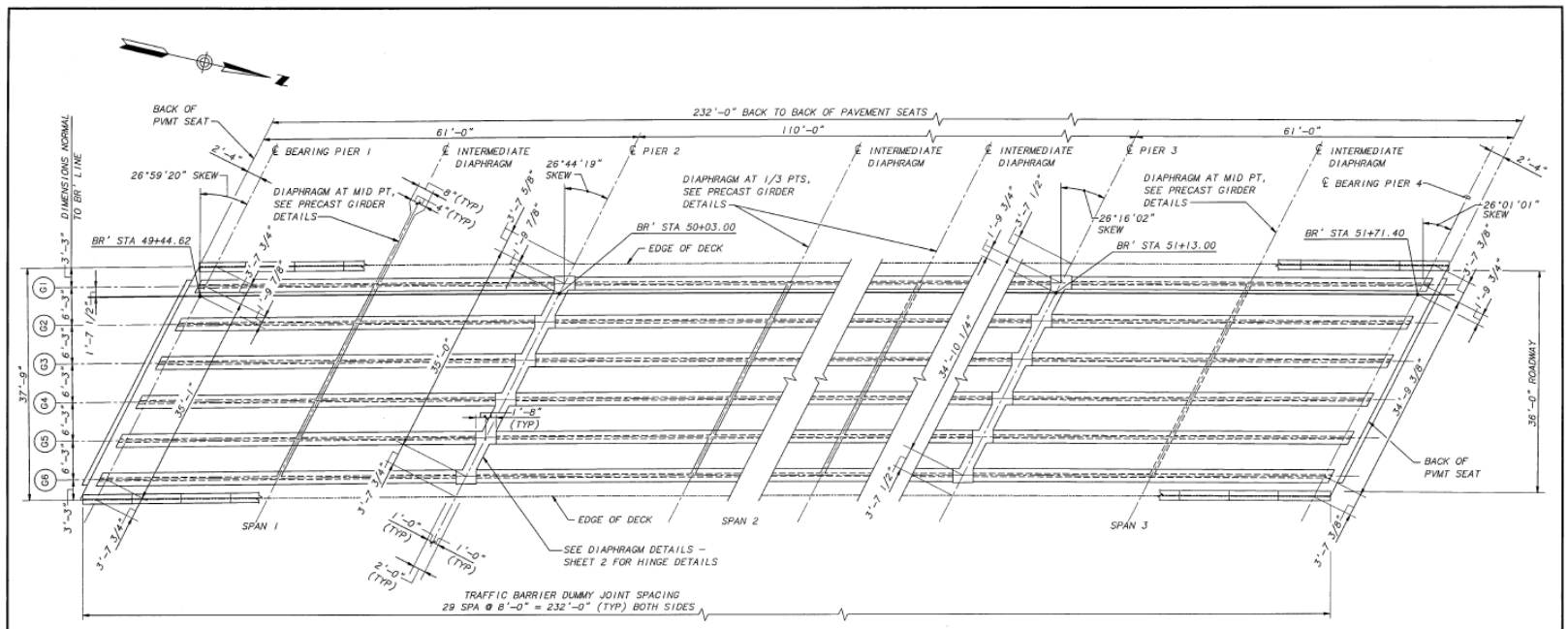

FRAMING PLAN

BEARING OF ALL PIERS AND DIAPHRAGMS = ~~N 76°12'03" W~~ N 76°44'03" W

FOR "AS CONSTRUCTED PLANS" ONLY

DRAWN	R. MOHN	9/94				REGION NO	STATE	FED. AID PROJ. NO	SHEET NO	TOTAL SHEETS	BRIDGE AND STRUCTURES
DESIGNED	E. DORNSEIF	12/94				10	WASH				
CHECKED	R. FERNANDES	12/94				JOB NUMBER 94W097					
BR PROJ ENGR						CONTRACT NO 4756					
PRELIM PLAN BY											
ARCHITECT											
	DATE	DATE	REVISION	BY	APPR						

Washington State Department of Transportation

ABAM CONSULTING ENGINEERS
A MEMBER OF THE BERGER GROUP

SR 405
TUKWILA TO FACTORIA
SC&DI - STAGE 1

FRAMING PLAN

BRIDGE SHEET NO. 10

SHEET 942 OF 985 SHEETS

SR 405 JOB NO. 7062 SHEET 10 OF 22

SR 405/417

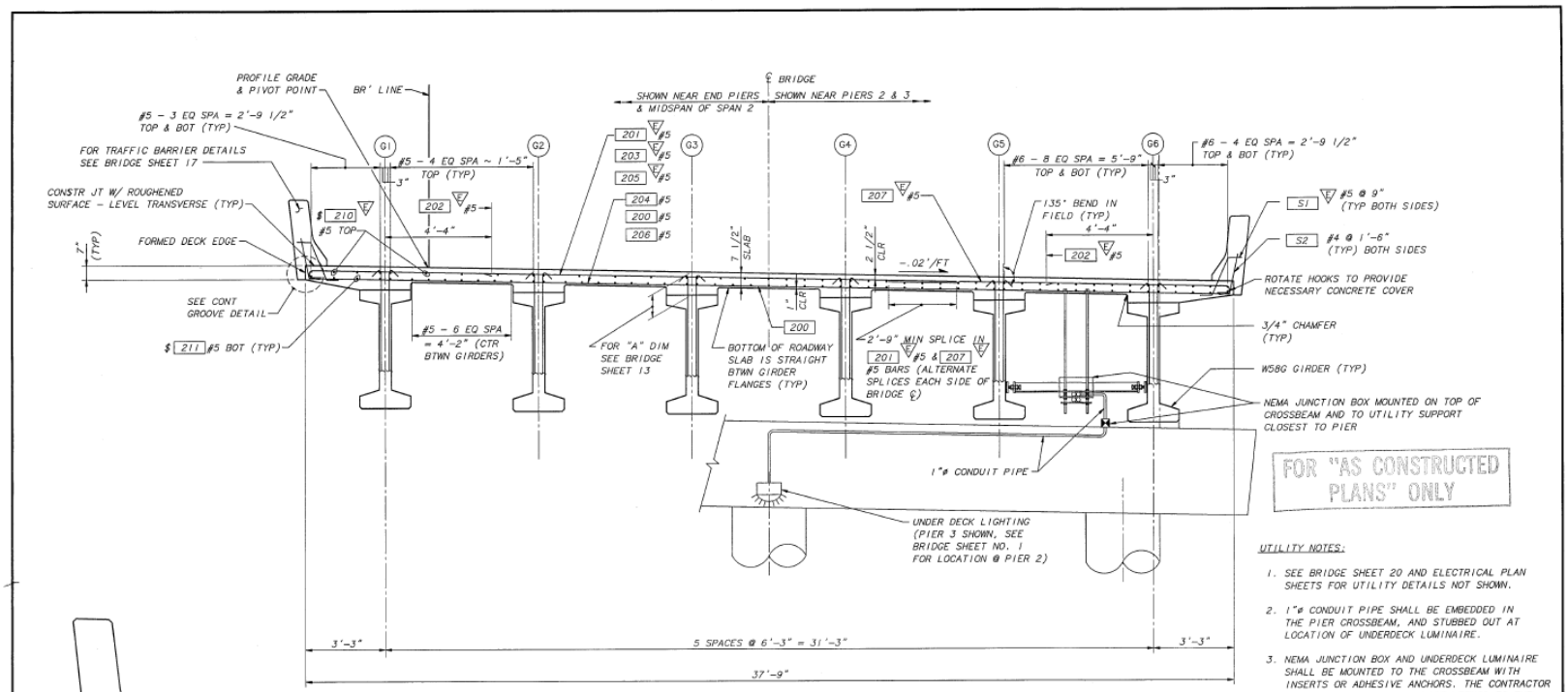

BRIDGE CROSS SECTION

SHOWN LOOKING AHEAD ON STATIONING

E DENOTES EPOXY COATED BARS

$ - LENGTH OF BARS TO BE DETERMINED BY CONTRACTOR

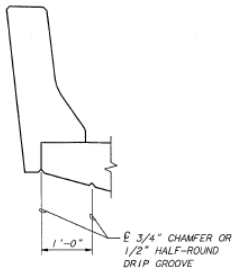

DETAIL - CONTINUOUS GROOVE

UTILITY NOTES:

1. SEE BRIDGE SHEET 20 AND ELECTRICAL PLAN SHEETS FOR UTILITY DETAILS NOT SHOWN.
2. 1"ø CONDUIT PIPE SHALL BE EMBEDDED IN THE PIER CROSSBEAM, AND STUBBED OUT AT LOCATION OF UNDERDECK LUMINAIRE.
3. NEMA JUNCTION BOX AND UNDERDECK LUMINAIRE SHALL BE MOUNTED TO THE CROSSBEAM WITH INSERTS OR ADHESIVE ANCHORS. THE CONTRACTOR SHALL SUBMIT THE ANCHORAGE METHOD TO THE ENGINEER FOR APPROVAL.
4. THE CONTRACTOR SHALL SUBMIT DETAILS FOR ATTACHMENT OF THE NEMA JUNCTION BOX AT THE UTILITY SUPPORT TO THE ENGINEER FOR APPROVAL.
5. ALL CONDUIT AND ALL STEEL IN UTILITY SUPPORTS, INCLUDING FASTENINGS AND ANCHORAGES, SHALL BE GALVANIZED UNLESS OTHERWISE SPECIFIED.
6. DRILLING THROUGH REINFORCING STEEL WILL NOT BE PERMITTED. IF STEEL IS HIT WHEN DRILLING FOR ADHESIVE ANCHORS, THE ANCHORAGE LOCATION SHALL BE MOVED AND THE ABANDONED HOLE FILLED WITH GROUT.

DRAWN	R. MOHN	9/94					REGION NO	STATE	FED AID PROJ NO	SHEET NO	TOTAL SHEETS
DESIGNED	E. DORNSEIF	12/94					10	WASH			
CHECKED	R. FERNANDES	12/94					JOB NUMBER 94W097				
BR PROJ ENGR							CONTRACT NO 4756				
PRELIM PLAN BY											
ARCHITECT											
		DATE	DATE	REVISION		BY APPR					

BRIDGE AND STRUCTURES

JAMES E. GUARINO — STATE OF WASHINGTON — 14009 — REGISTERED PROFESSIONAL ENGINEER — 2-8-95 — EXPIRES JUNE 4, 1995

Washington State Department of Transportation

ABAM CONSULTING ENGINEERS — A MEMBER OF THE BERGER GROUP

SR 405
TUKWILA TO FACTORIA
SC&DI - STAGE I

BRIDGE CROSS SECTION

BRIDGE SHEET NO. 11

SHEET 943 OF 985 SHEETS

SR 405/417

SR 405 JOB NO. 206Z SHEET 11 OF 22

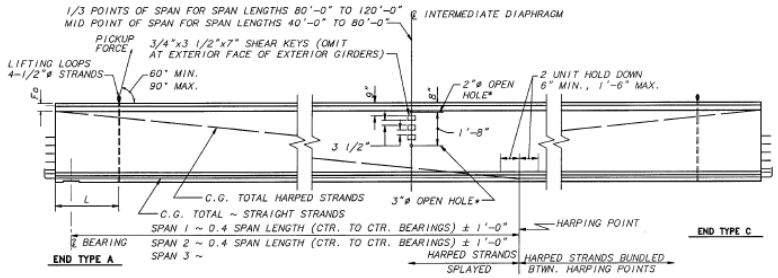

GIRDER ELEVATION

*OMIT HOLES AND PLACE INSERTS ON THE INTERIOR FACE OF EXTERIOR GIRDERS. PLACE HOLES AND INSERTS PARALLEL TO SKEW. INSERTS SHALL BE 1" RICHMOND ROCKET, BURKE HI-TENSILE, LANCASTER MALLEABLE OR APPROVED EQUAL.

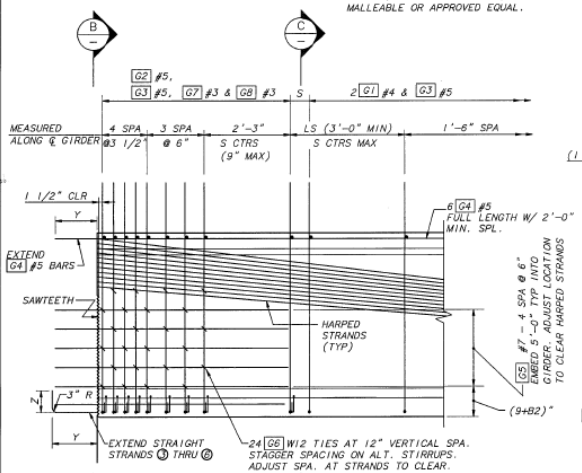

TYPICAL END ELEVATION

END TYPE C SHOWN ~ OTHER ENDS SIMILAR

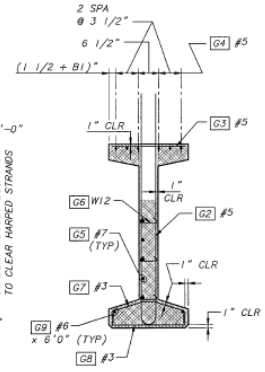

SECTION B

SAWTEETH SHOWN BY SHADED AREA.

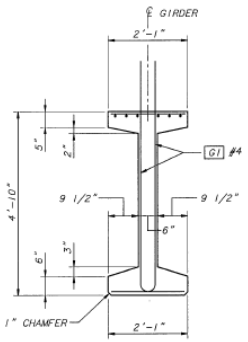

SECTION C

NOTES

ALL DETAILS ON THIS SHEET ARE FOR PRETENSIONED DESIGN ONLY.

PLAN LENGTH SHALL BE INCREASED AS NECESSARY TO COMPENSATE FOR SHORTENING DUE TO PRESTRESS AND SHRINKAGE.

EXTRA CAUTION MUST BE EXERCISED IN HANDLING AND PLACING ALL GIRDERS.

ALL GIRDERS OVER 105' LONG SHALL BE BRACED LATERALLY TO PREVENT TIPPING OR BUCKLING.

THE TOP SURFACE OF THE GIRDER FLANGE SHALL BE ROUGHENED IN ACCORDANCE WITH SECTION 6-02.3(25)H OF THE STANDARD SPECIFICATIONS.

IF THE LIFTING LOOPS EXTEND WITHIN 3" OF THE TOP OF THE ROADWAY SLAB THEY SHALL BE CUT OFF PRIOR TO POURING THE ROADWAY SLAB. ALL LIFTING STRANDS SHALL BE OF THE SAME MATERIAL AND STRENGTH AS THE PRESTRESSING STRANDS. WRAP THE LIFTING LOOPS SO THAT EACH STRAND WILL CARRY ITS SHARE OF THE TOTAL LOAD. EXTEND LIFTING LOOPS ENDING WITH A 9" LONG 90° HOOK TO WITHIN 3" CLEAR OF THE BOTTOM OF THE GIRDER.

CUT ALL STRANDS FLUSH WITH THE GIRDER ENDS AND PAINT WITH AN APPROVED EPOXY RESIN EXCEPT FOR EXTENDED STRANDS AS SHOWN.

FORMS FOR BEARING PAD RECESSES SHALL BE CONSTRUCTED AND FASTENED IN SUCH A MANNER AS NOT TO CAUSE DAMAGE TO THE GIRDER DURING THE STRAND RELEASE OPERATION.

ALL STRANDS ARE 1/2"ø LOW RELAXATION STRANDS (AASHTO M203 GRADE 270).

EXTENDED STRANDS AND BARS ARE PARALLEL TO GIRDER.

FOR SAWTOOTH DETAILS, SEE W58G GIRDER DETAILS II.

ENDS AHEAD ON STATION
G5 BARS LEFT OF ℄
B1 = 0"
B2 = 0"
ENDS BACK ON STATION
G5 BARS RIGHT OF ℄
B1 = 1 1/2"
B2 = 3"

END TYPE	BEARING RECESS	Y	Z	SAWTEETH
A	YES	9"	1'-6"	YES
C	NO	1'-10"	9"	YES

BENDING DIAGRAM

ALL DIMENSIONS ARE OUT TO OUT

MARK	LOCATION	SIZE	
G1	GIRDER STIRRUPS	4	
G2	GIRDER END STIRRUPS	5	
G3	GIRDER TOP FLANGE	5	STR
G4	GIRDER LONGIT FULL LENGTH	5	STR
G5	GIRDER END LONGIT	7	STR
G6	GIRDER END TIES	WI2	†
G7	GIRDER END TIES	3	
G8	GIRDER END TIES	3	
G9	GIRDER LONGIT	6	STR

** = VARIES FOR SKEWED SPANS

NOTE: FOR DIMENSION A, SEE "GIRDER SCHEDULE"

† #3 OR #4 MAY BE SUBSTITUTED FOR WI2, FIELD BENDING IS OPTIONAL

FOR "AS CONSTRUCTED PLANS" ONLY

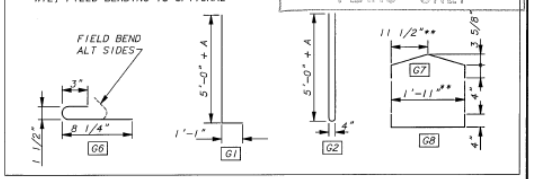

DRAWN	R. MOHN	9/94					REGION NO	STATE	FED AID PROJ NO	SHEET NO	TOTAL SHEETS
DESIGNED	E. DORNSEIF	12/94					10	WASH			
CHECKED	R. FERNANDES	12/94					JOB NUMBER				
BR PROJ ENGR							94W097				
PRELIM PLAN BY							CONTRACT NO				
ARCHITECT							4756				
		DATE	DATE	REVISION		BY	APPR				

BRIDGE AND STRUCTURES

Washington State Department of Transportation

ABAM CONSULTING ENGINEERS
A MEMBER OF THE BERGER GROUP

SR 405
TUKWILA TO FACTORIA
SC&DI - STAGE 1

W58G GIRDER DETAILS – SHEET 1

BRIDGE SHEET NO. 12

SHEET 944 OF 965 SHEETS

SR 405 JOB NO. 206Z SHEET 13 OF 22

SR 405/417

GIRDER SCHEDULE

DIMENSION A AT ℄ BEARINGS = 11.00"
BASED ON GIRDER DEFLECTION = D AT TIME OF SLAB POUR (120 DAYS)

SPAN	GIRDER	END 1 TYPE	END 2 TYPE	L	θ1	θ2	N1	N2	P1	P2	PLAN LENGTH (ALONG GIRDER GRADE)	MIN CONC COMPR STRENGTH		S (IN)	LS (FT)	HARPED		STRAIGHT		LOCATION OF C.G. STRANDS (IN)				*C (IN)	D (IN)	Ld (IN)	X (IN)
												28 DAYS F'C KSI	RELEASE F'CI KSI			NO. OF STRANDS	JACKING FORCE (KIPS)	NO. OF STRANDS	JACKING FORCE (KIPS)	E	F℄	Fb	Fo				
1	ALL	A	C	4.25'	117°	90°	1'-3"	1 1/2"	1'4 7/8"	0'-1 1/2"	58'-2"	6.0	4.5	9	3'-0"	4	124	10	310	1.88	0	3.0	7.0	0.15	0.51	0	0
2	ALL	C	C	4.25'	90°	90°	1 1/2"	1 1/2"	0'-1 1/2"	0'-1 1/2"	106' - 9"	7.0	6.0	9	3'-0"	14	434	26	806	3.57	3.42	3.0	3.0	1.72	3.58	0	0
3	ALL	C	A	4.25'	90°	117°	1 1/2"	1'-3"	0'-1 1/2"	1'-4 7/8"	58'- 2"	6.0	4.5	9	3'-0"	4	124	10	310	1.88	0	3.0	7.0	0.15	0.51	0	0

* SEE BRIDGE SHEET 16 FOR SCREED SETTING DIAGRAM

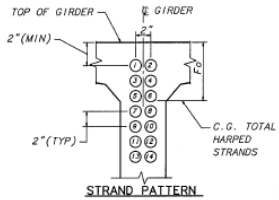

STRAND PATTERN AT GIRDER END

HARPED STRAND LOCATION SEQUENCE SHALL BE AS SHOWN ①, ② ETC.

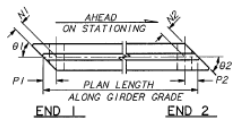

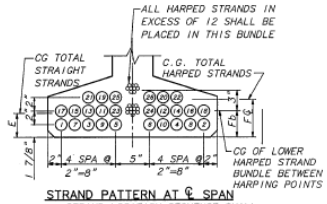

STRAND PATTERN AT ℄ SPAN

STRAND LOCATION SEQUENCE SHALL BE AS SHOWN ①, ② ETC.

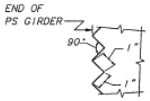

SAWTOOTH DETAILS

SAWTEETH ARE FULL WIDTH – USE SAWTOOTH KEYS FROM BOTTOM OF BOTTOM FLANGE TO BOTTOM OF LOWEST HARPED STRAND AS WELL AS TOP FLANGE ADJACENT TO HARPED STRANDS AS SHOWN IN SECTION B.

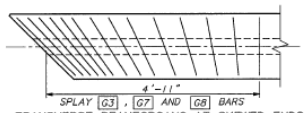

TRANSVERSE REINFORCING AT SKEWED ENDS

ONLY TRANSVERSE REINF. SHOWN.

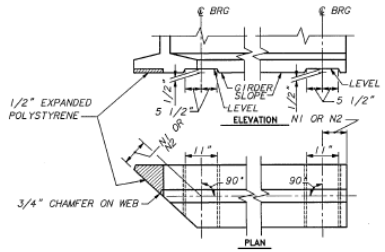

BEARING RECESS DETAIL

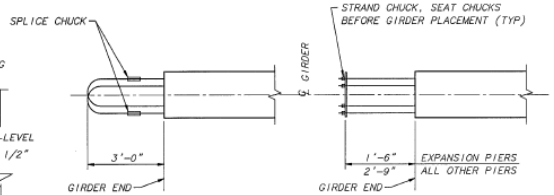

ALTERNATE 1

ALTERNATE 2

STRAND EXTENSION DETAIL

NOTE TO DESIGNERS:
STRAND EXTENSION DETAIL TO BE USED FOR CONTINUOUS SPANS AT MOMENT-RESISTING DIAPHRAGM. THIS DETAIL NOT APPLICABLE TO CONTINUOUS SPANS UTILIZING HINGE DIAPHRAGMS.

FOR "AS CONSTRUCTED PLANS" ONLY

DRAWN	R. MOHN	9/94					
DESIGNED	E. DORNSEIF	12/94					
CHECKED	R. FERNANDES	12/94					
BR PROJ ENGR							
PRELIM PLAN BY							
ARCHITECT							
		DATE	DATE	REVISION	BY	APPR	

REGION NO	STATE	FED AID PROJ NO	SHEET NO	TOTAL SHEETS
10	WASH			

JOB NUMBER
94W097

CONTRACT NO
4756

BRIDGE AND STRUCTURES

1-3-95
EXPIRES JUNE 4, 1995

Washington State Department of Transportation

ABAM
CONSULTING ENGINEERS
A MEMBER OF THE BERGER GROUP

SR 405
TUKWILA TO FACTORIA
SC&DI - STAGE 1

W58G GIRDER DETAILS – SHEET 2

BRIDGE SHEET NO. 13

SHEET 945 OF 985 SHEETS

SR 405 JOB NO. 7067 SHEET 13 OF 22

SR 405/417

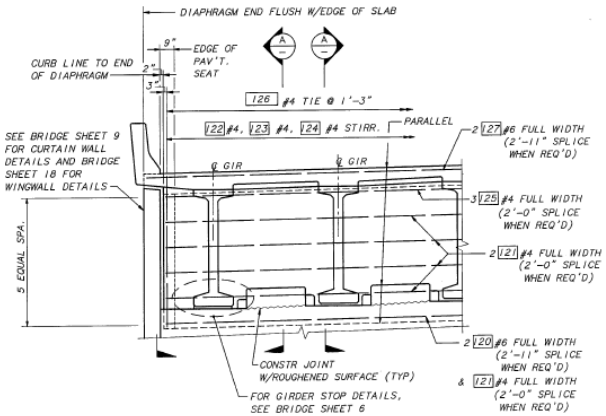

TYPICAL END DIAPHRAGM AT END PIERS

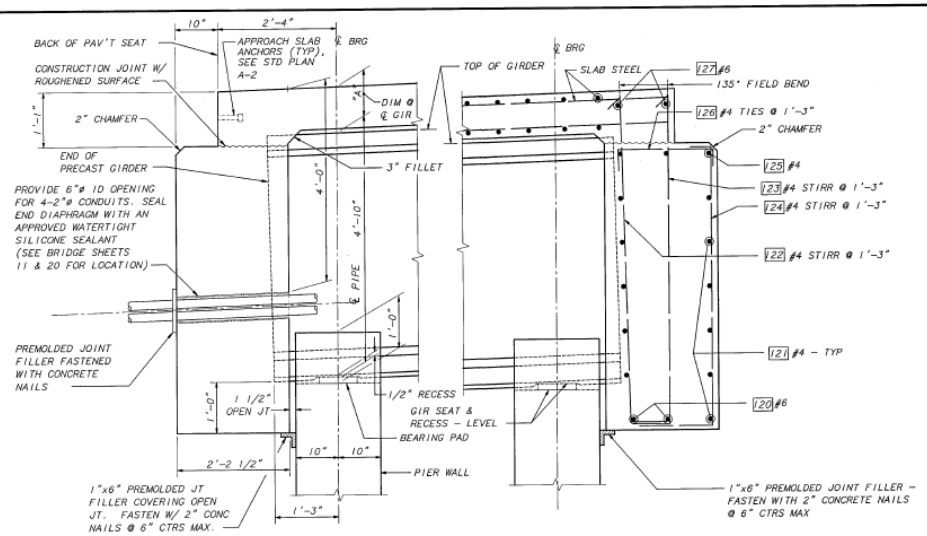

SECTION A

SECTIONS THRU END DIAPHRAGMS AT END PIERS
SEE "GIRDER DETAILS" SHEET FOR DIMENSION "A"
ALL LONGITUDINAL DIMENSIONS ARE NORMAL TO SKEW

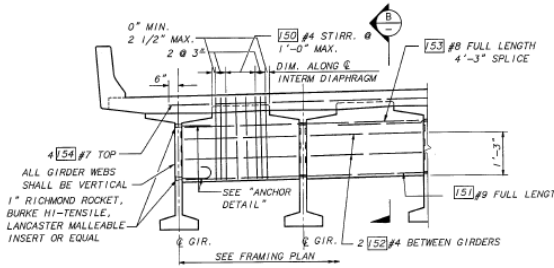

TYPICAL INTERMEDIATE DIAPHRAGM

NOTE:
GIRDERS SHALL BE HELD RIGIDLY IN PLACE WHEN DIAPHRAGMS ARE POURED. REINFORCING BARS SHALL BE THREADED THROUGH HOLES IN GIRDERS PRIOR TO PLACING OF EXTERIOR GIRDERS. SEE PLANS FOR 'TRAFFIC BARRIER' DIMENSIONS & LOCATIONS. SEE 'GIRDER DETAILS' SHEET FOR DIMENSION "A".

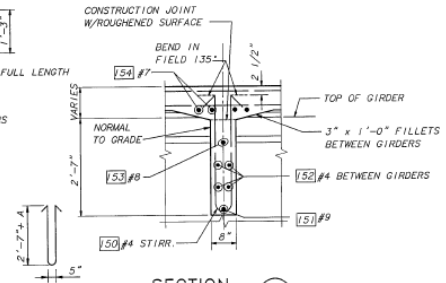

SECTION B

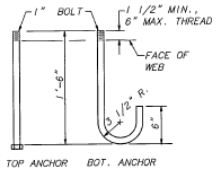

ANCHOR DETAILS
ASTM A-307

FOR "AS CONSTRUCTED PLANS" ONLY

DRAWN	R. MOHN	9/94				REGION NO.	STATE	FED. AID PROJ. NO.	SHEET NO. / TOTAL SHEETS
DESIGNED	E. DORNSEIF	12/94				10	WASH		
CHECKED	R. FERNANDES	12/94				JOB NUMBER	94W097		
BR PROJ ENGR						CONTRACT NO.	4756		
PRELIM PLAN BY									
ARCHITECT									
	DATE	DATE	REVISION	BY	APPR				

BRIDGE AND STRUCTURES

Washington State Department of Transportation

ABAM CONSULTING ENGINEERS
A MEMBER OF THE BERGER GROUP

SR 405
TUKWILA TO FACTORIA
SC&DI - STAGE 1

DIAPHRAGM DETAILS – SHEET 1

BRIDGE SHEET NO. 14

SHEET 946 OF 985 SHEETS

SR 405 JOB NO. 7062 SHEET 14 OF 22

SR 405/917

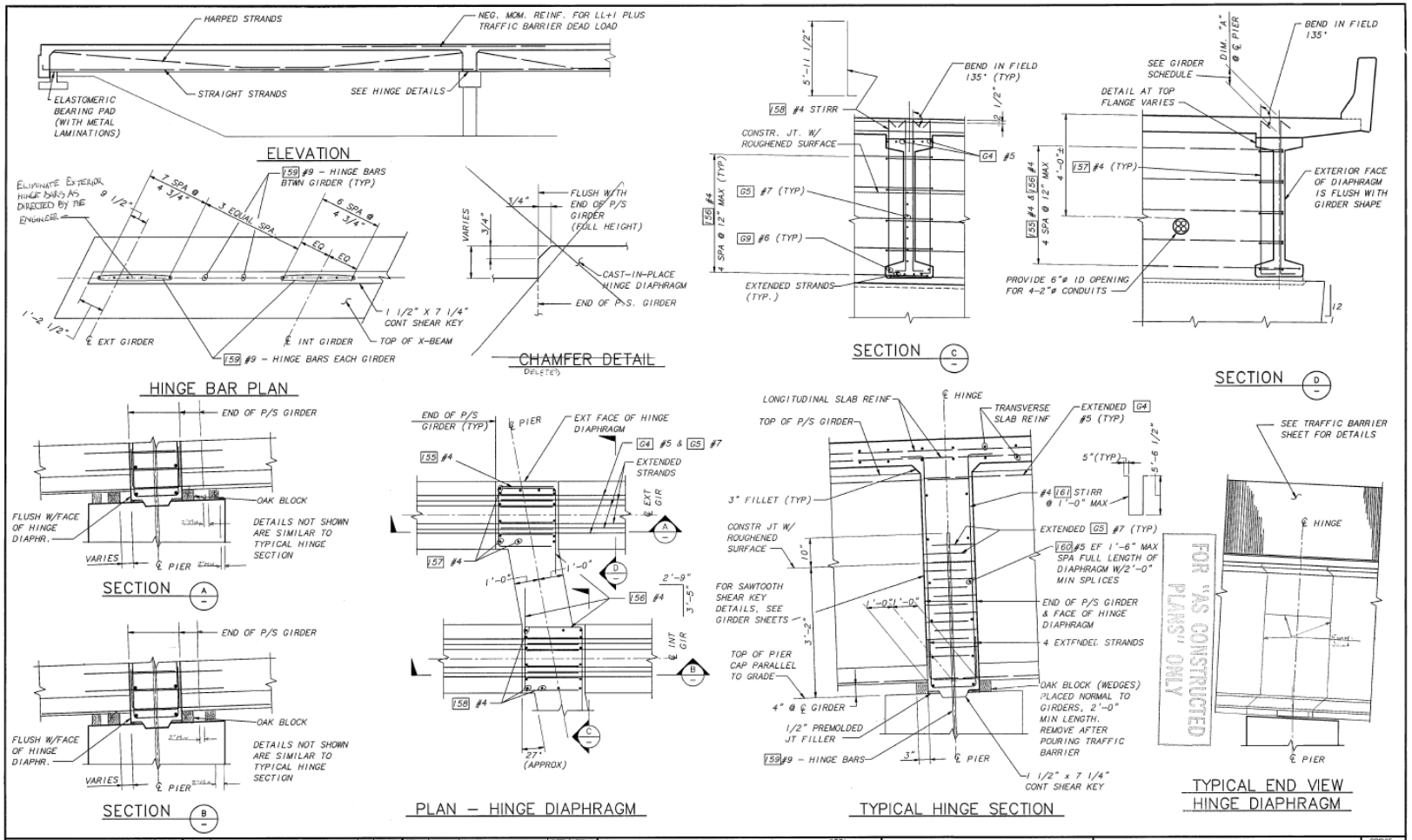

SR 405 JOB NO. 106Z SHEET 15 OF 22

DRAWN	R. MOHN	9/94						WORK NO	STATE	FED AID PROJ NO	SHEET NO	TOTAL SHEETS
DESIGNED	E. DORNSEIF	12/94						10	WASH			
CHECKED	R. FERNANDES	12/94						JOB NUMBER	94W097			
BR PROJ ENGR								CONTRACT NO	4756			
PRELIM PLAN BY												
ARCHITECT												
		DATE	DATE	REVISION		BY	APPR					

BRIDGE AND STRUCTURES

1-3-95 EXPIRES JUNE 4, 1995

Washington State Department of Transportation

ABAM CONSULTING ENGINEERS
A MEMBER OF THE BERGER GROUP

SR 405
TUKWILA TO FACTORIA
SC&DI - STAGE 1

DIAPHRAGM DETAILS - SHEET 2

BRIDGE SHEET NO. 15

SHEET 947 OF 985 SHEETS

SR 405/417

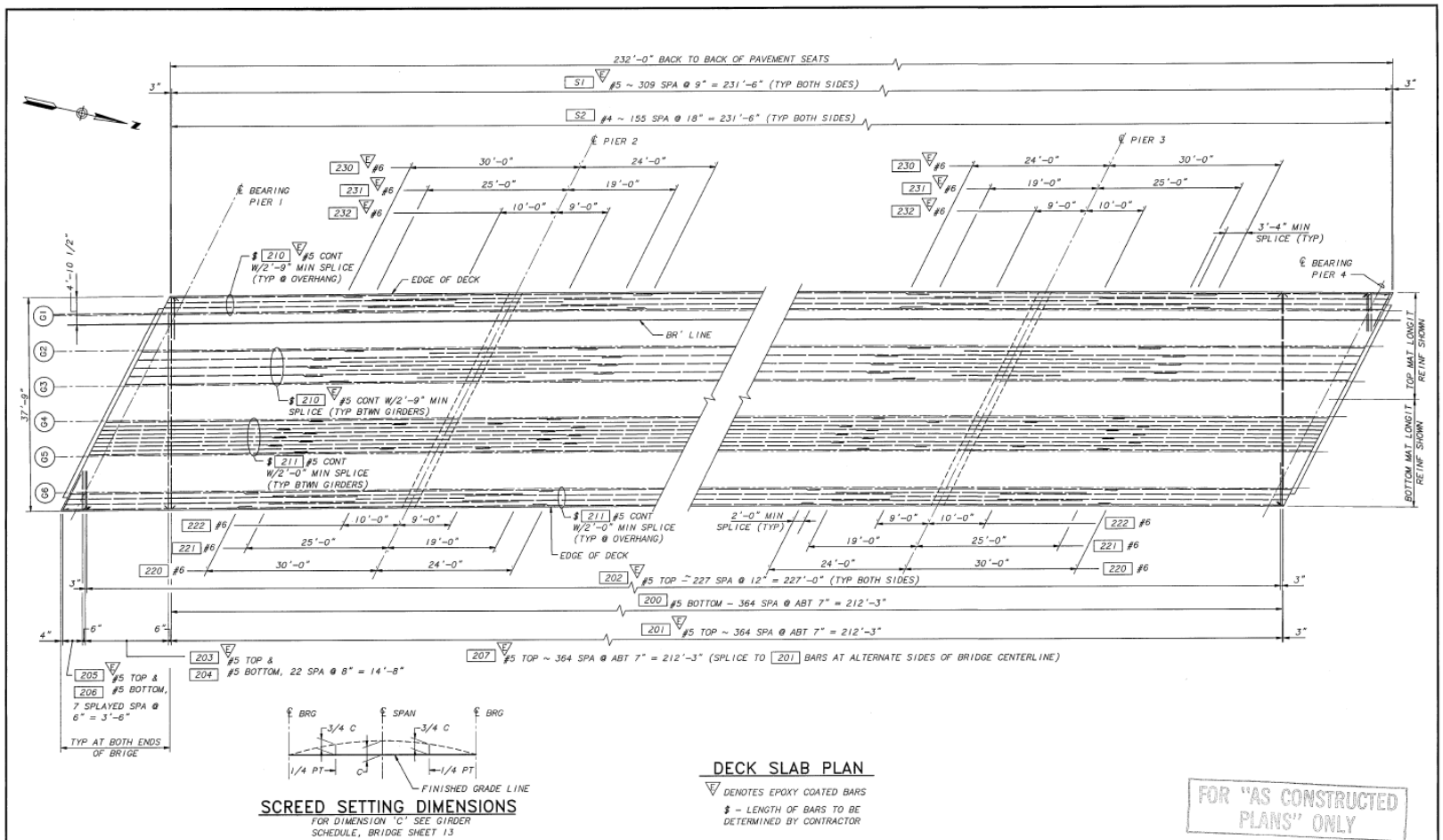

SCREED SETTING DIMENSIONS

FOR DIMENSION 'C' SEE GIRDER SCHEDULE, BRIDGE SHEET 13

DECK SLAB PLAN

▽ DENOTES EPOXY COATED BARS

$ = LENGTH OF BARS TO BE DETERMINED BY CONTRACTOR

FOR "AS CONSTRUCTED PLANS" ONLY

SR 405 JOB NO. 7067 SHEET 16 OF 22

DRAWN	R. MOHN	9/94				REGION NO.	STATE	FED AID PROJ NO	SHEET NO	TOTAL SHEETS
DESIGNED	E. DORNSEIF	12/94				10	WASH			
CHECKED	R. FERNANDES	12/94				JOB NUMBER				
BR PROJ ENGR						94W097				
PRELIM PLAN BY						CONTRACT NO				
ARCHITECT						4756				
	DATE	DATE	REVISION	BY	APPR					

BRIDGE AND STRUCTURES

JAMES R. GRUNDER — REGISTERED PROFESSIONAL ENGINEER — 14906 — STATE OF WASHINGTON — 1-3-95 — EXPIRES JUNE 4, 1995

Washington State Department of Transportation

ABAM CONSULTING ENGINEERS — A MEMBER OF THE BERGER GROUP

SR 405
TUKWILA TO FACTORIA
SC&DI - STAGE 1

DECK SLAB PLAN

BRIDGE SHEET NO. 16

SHEET 948 OF 3845 SHEETS

SR 405/417

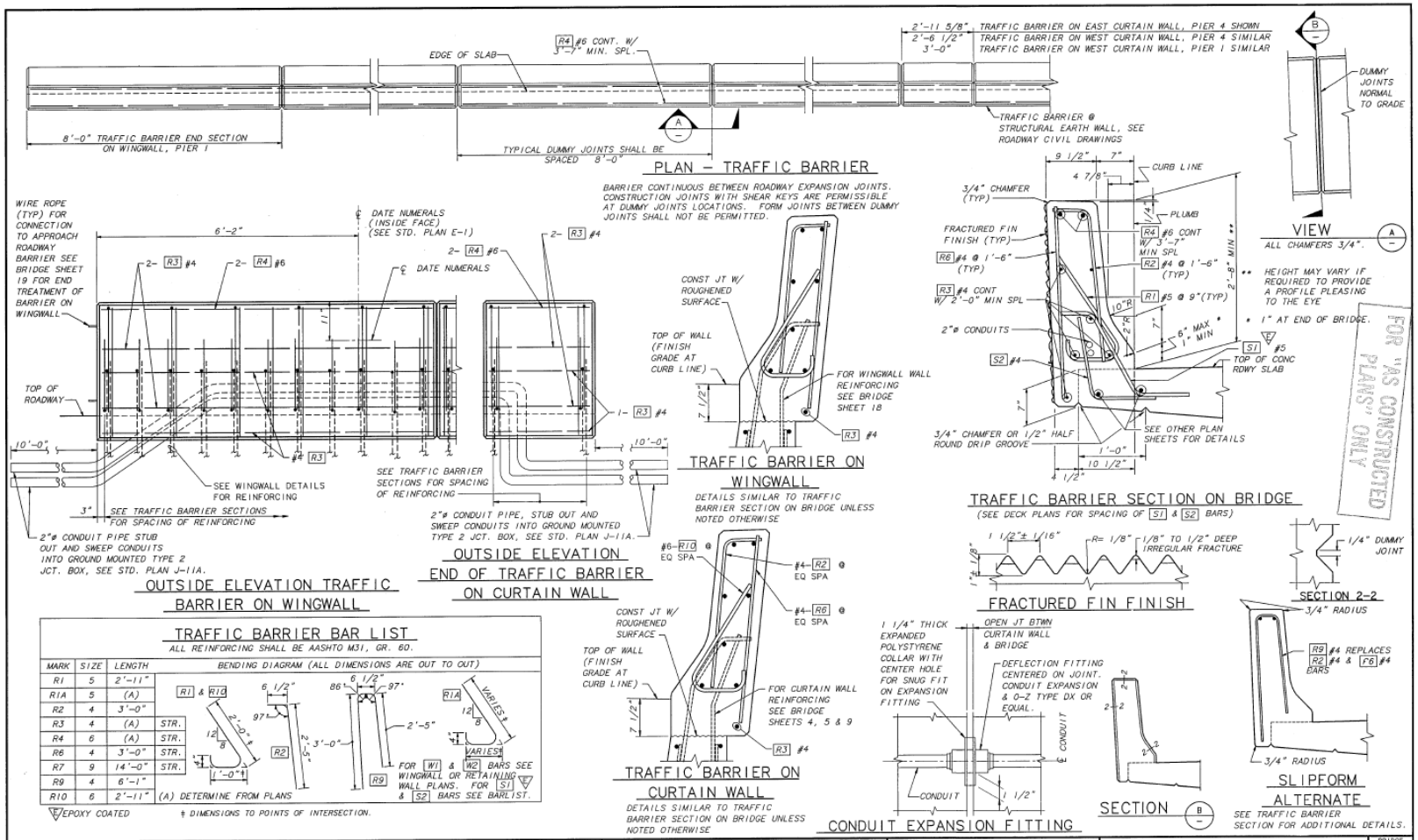

MARK	SIZE	LENGTH	
R1	5	2'-11"	
R1A	5	(A)	
R2	4	3'-0"	
R3	4	(A)	STR.
R4	6	(A)	STR.
R6	4	3'-0"	STR.
R7	9	14'-0"	STR.
R9	4	6'-1"	
R10	6	2'-11"	(A) DETERMINE FROM PLANS

DRAWN	R. MOHN	9/94
DESIGNED	E. DORNSEIF	12/94
CHECKED	R. FERNANDES	12/94
BR PROJ ENGR		
PRELIM PLAN BY		
ARCHITECT		

DATE	REVISION	BY	APPR

REGION NO	STATE	FED AID PROJ NO	SHEET NO	TOTAL SHEETS
10	WASH			

JOB NUMBER 94W097
CONTRACT NO 4756

BRIDGE AND STRUCTURES

Washington State Department of Transportation

ABAM CONSULTING ENGINEERS
A MEMBER OF THE BERGER GROUP

SR 405
TUKWILA TO FACTORIA
SC&DI – STAGE 1

TRAFFIC BARRIER

BRIDGE SHEET NO. 17

SHEET 945 OF 985 SHEETS

SR 405 JOB NO. 7067 SHEET 17 OF 22

SR 405/417

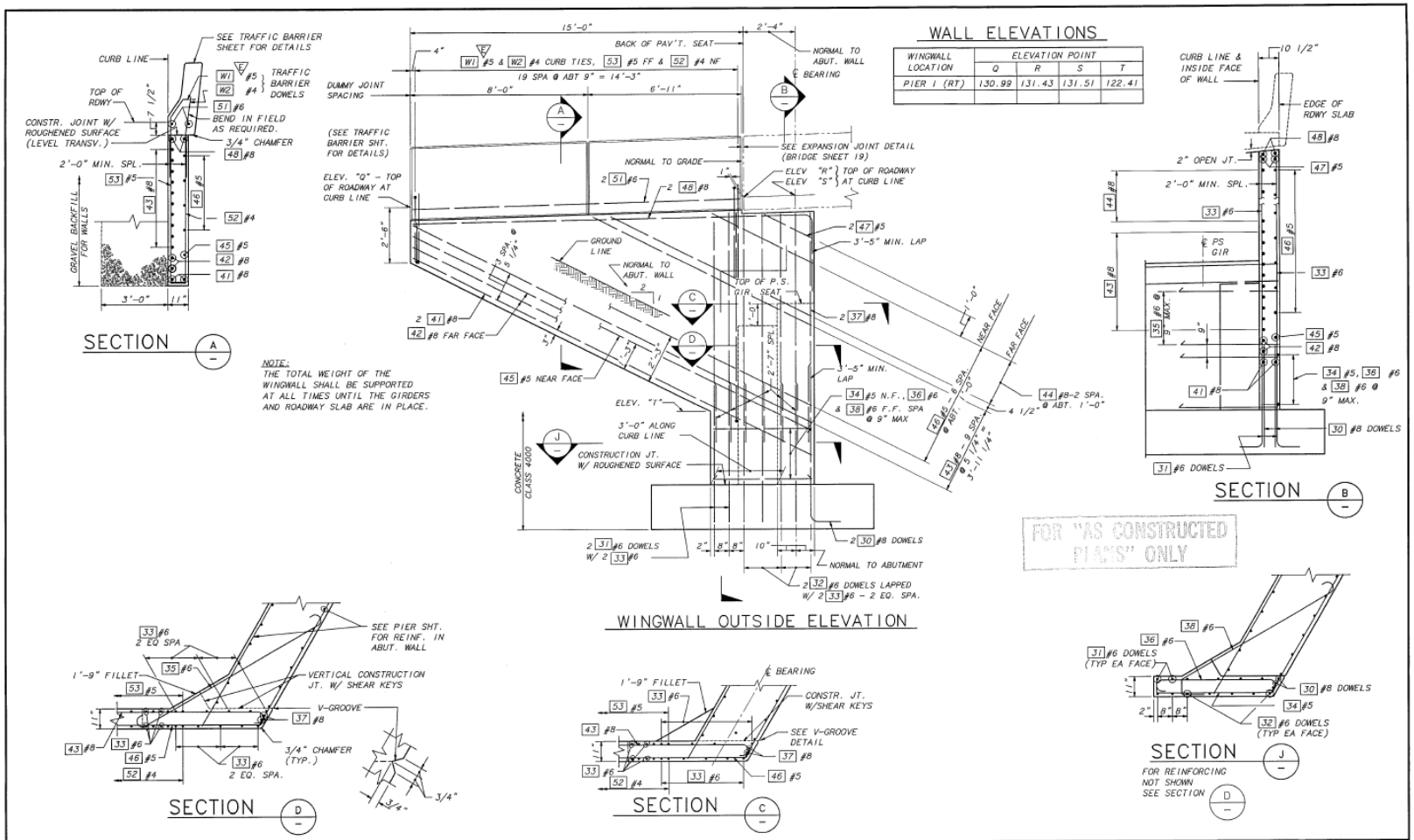

WINGWALL LOCATION	ELEVATION POINT			
	Q	R	S	T
PIER 1 (RT)	130.99	131.43	131.51	122.41

DRAWN	R. MOHN	12/94
DESIGNED	B. GARRETT	12/94
CHECKED	R. FERNANDES	12/94
BR PROJ ENGR		
PRELIM PLAN BY		
ARCHITECT		

DATE	DATE	REVISION	BY	APPR

REGION NO.	STATE	FED AID PROJ NO	SHEET NO.	TOTAL SHEETS
10	WASH			

JOB NUMBER 94W097
CONTRACT NO 4756

BRIDGE AND STRUCTURES

Washington State Department of Transportation

ABAM CONSULTING ENGINEERS
A MEMBER OF THE BERGER GROUP

SR 405
TUKWILA TO FACTORIA
SC&DI - STAGE 1

WINGWALL

BRIDGE SHEET NO. 18

SHEET 950 OF 985 SHEETS

SR 405 JOB NO. 7062 SHEET 18 OF 22

SR 405/417

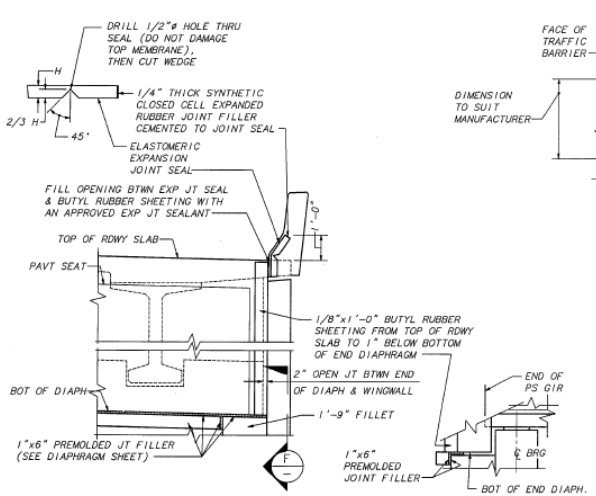

SECTION E

SECTION F

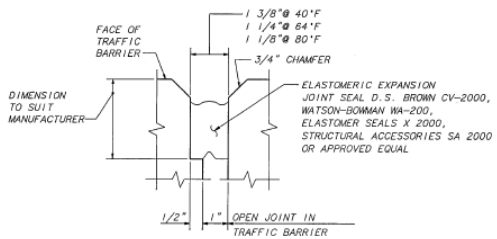

SECTION G

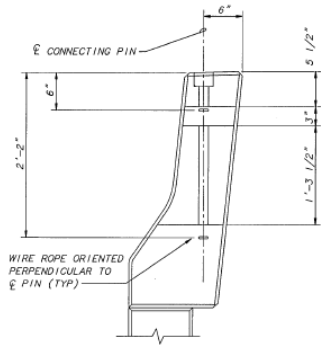

END VIEW

BARRIER ON WINGWALL

SEE STANDARD PLAN C-8 FOR ADDITIONAL END CONFIGURATION DETAILS AND WIRE ROPE DETAILS

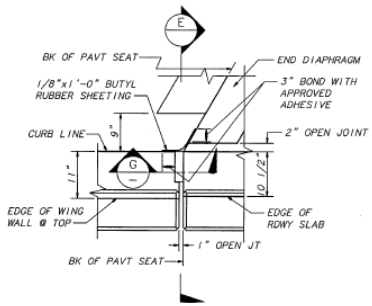

EXPANSION JOINT DETAIL

FOR "AS CONSTRUCTED PLANS" ONLY

DRAWN	R. MOHN	12/94				REGION NO	STATE	FED AID PROJ NO	SHEET NO	TOTAL SHEETS	BRIDGE AND STRUCTURES
DESIGNED	B. GARRETT	12/94				10	WASH				
CHECKED	R. FERNANDES	12/94				JOB NUMBER 94W097					
BR PROJ ENGR						CONTRACT NO 4756					
PRELIM PLAN BY											
ARCHITECT											
		DATE	DATE	REVISION	BY	APPR					

Washington State Department of Transportation

ABAM CONSULTING ENGINEERS
A MEMBER OF THE BERGER GROUP

SR 405
TUKWILA TO FACTORIA
SC&DI - STAGE 1

WINGWALL DETAILS

BRIDGE SHEET NO. 19

SHEET 951 OF 9595 SHEETS

SR 405 JOB NO. Z067 SHEET 19 OF 22

SR 405/417

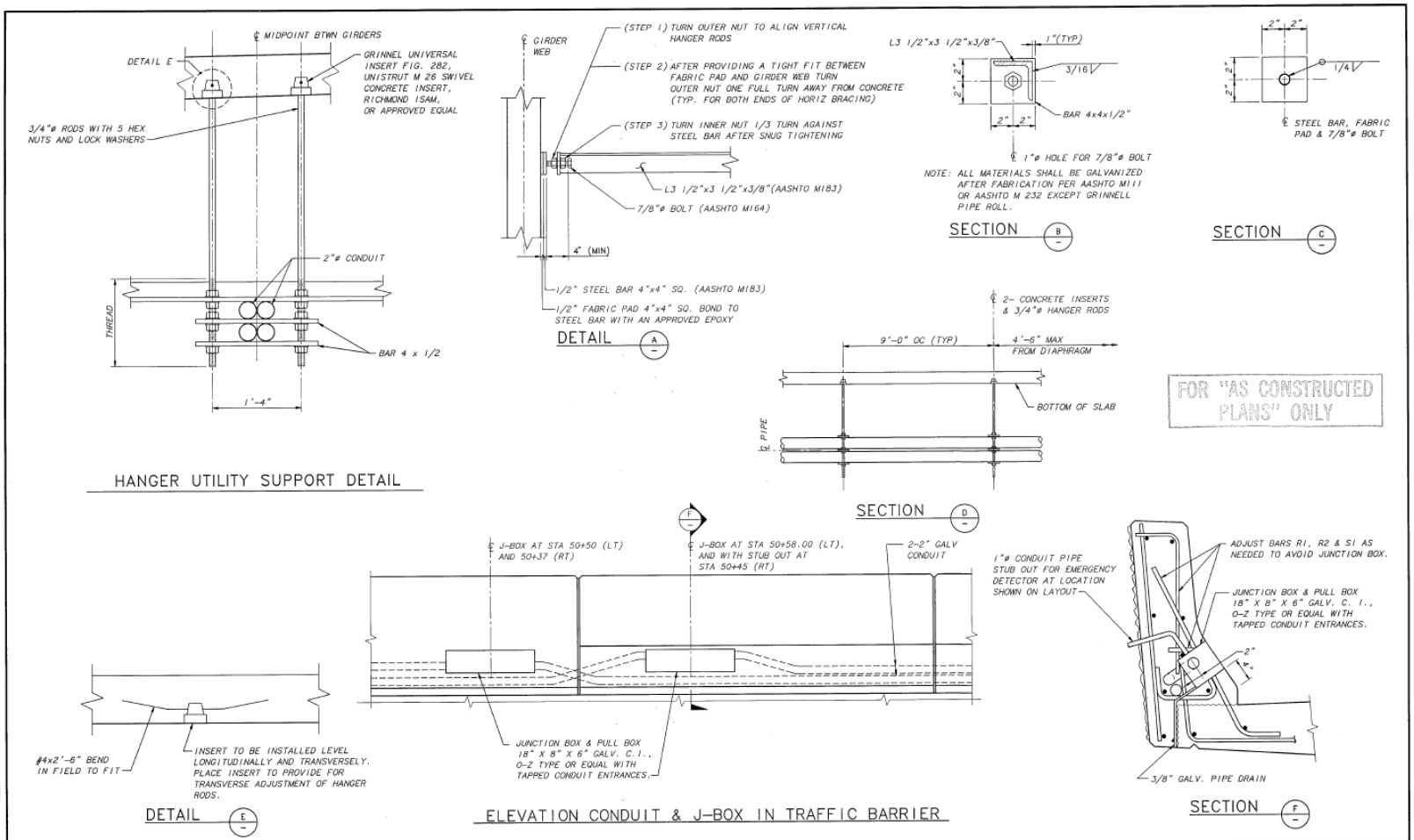

SR 405 JOB NO. 7062 SHEET 20 OF 22

DRAWN	R. MOHN	12/94
DESIGNED	S. JOHNSON	12/94
CHECKED	R. FERNANDES	12/94
BR PROJ ENGR		
PRELIM PLAN BY		
ARCHITECT		

DATE	REVISION	BY	APPR

REGION NO	STATE	FED AID PROJ NO	SHEET NO	TOTAL SHEETS
10	WASH			

JOB NUMBER 94W097
CONTRACT NO 4756

BRIDGE AND STRUCTURES

Washington State Department of Transportation

ABAM CONSULTING ENGINEERS
A MEMBER OF THE BERGER GROUP

SR 405
TUKWILA TO FACTORIA
SC&DI – STAGE I

UTILITY SUPPORT DETAILS

BRIDGE SHEET NO. 20

SHEET 952 OF 985 SHEETS

SR 405/417

S=BAR IS INCLUDED IN SUBSTRUCTURE QUANTITIES
LUMP SUM QUANTITY
T OR S=TIE OR STIRRUP RADIUS
E=EARTHQUAKE TAIL W/ TIE OR STIRRUP RADIUS
E=BAR IS EPOXY COATED
V=BAR DIMENSIONS VARY BETWEEN DIMENSIONS SHOWN ON THIS LINE AND THE FOLLOWING LINE

MARK NO.	LOCATION	SIZE	NO. REQ'D	BEND TYPE	LUMP SUM	SUBSTRUCT	EPOXY COATED	VARIES	DIMENSIONS U FT	U IN.	W FT	W IN.	X FT	X IN.	Y FT	Y IN.	Z FT	Z IN.	θ_1 DEG	θ_2 DEG	LENGTH (EACH) FT	LENGTH (EACH) IN.	TOTAL WEIGHT LBS
	SUBSTRUCTURE																						
	PIER 1																						
1	FOOTING BOTTOM	6	13	50		S			49	6.0											49	6	967
2	FOOTING BOTTOM	6	101	50		S			11	6.0											11	6	1745
3	FOOTING TOP	5	51	50		S			11	6.0											11	6	612
4	FOOTING TOP	5	13	50		S			49	6.0											49	6	671
5	ABUTMENT VERTICAL	6	86	50		S	V		8	4.0											8	4	
									7	1.0											7	1	996
6	ABUTMENT HORIZONTAL	6	44	51		S			23	1.0											23	9	1571
7	ABUTMENT TIES	4	60	58	T	S			1	6.0											2	2	87
8	ABUTMENT TOP HORIZONTAL	6	4	51		S			23	1.0											23	9	143
9	ABUTMENT TOP TIES	4	43	56	T	S			1	6.0											2	1	60
10	GIRDER STOP	5	25	61	T	S			1	5.0	2	0.0	2	0.0							5	3	136
11	GIRDER STOP HORIZONTAL	4	10	50		S			3	5.0											3	5	23
	PIER 1 CURTAIN WALL																						
20	VERT FF	5	4	50		S			13	0.0											13	0	54
21	VERT NF	4	3	50		S			13	0.0											13	0	26
22	VERT FF	5	10	50		S			13	0.0											13	0	136
23	VERT NF	4	7	50		S			13	0.0											13	0	61
24	HORIZ TOP NF	4	7	80		S			6	0.0			0	10.0			0	1.5	62	6	10		32
25	HORIZ TOP FF	7	7	80		S			5	9.0			1	6.0			0	3.0	62	7	3		104
26	HORIZ TOP NF	4	11	80		S			6	0.0			0	10.0			0	1.5	62	6	10		50
27	HORIZ TOP FF	7	11	80		S			5	9.0			1	6.0			0	3.0	62	7	3		163
28	HORIZ AT FILLET	7	11	52		S			3	0.0											4	7	104
W1	TRAFFIC BARRIER DOWEL	5	6	91		S	E														4	1	26
W2	TRAFFIC BARRIER DOWEL	4	4	92		S															4	3	11
	PIER 1 WINGWALL																						
30	DOWEL	8	2	54		S			6	0.0											7	2	38
31	DOWEL	6	4	54		S			6	0.0											6	10	41
32	DOWEL	6	10	54		S			6	0.0											6	10	103
33	VERTICAL	6	14	50		S			8	10.0											8	10	186
34	STUB HORIZONTAL	5	6	80		S			4	2.0	0	8.0	0	9.0	0	2.5	0	2.5	90	117	5	5	34
35	FILLET HORIZONTAL	6	3	52		S			7	0.0											8	5	38
36	STUB HORIZONTAL	6	6	52		S			4	4.0											5	9	51
37	VERTICAL	8	2	50		S			9	9.0											9	9	52
38	FILLET HORIZONTAL	6	6	79		S			0	9.0	1	0.0	5	9.0	0	3.0	0	3.0	90	120	7	11	71
41	BOTTOM OUTSIDE FACE	8	2	51		S			19	5.0											20	4	109
42	SLOPE INSIDE FACE	8	2	51		S			19	5.0											20	4	109
43	SLOPE INSIDE FACE	8	10	51		S	V		19	5.0											20	4	
									9	9.0											10	8	414
44	SLOPE INSIDE FACE	8	3	51		S	V		8	9.0											9	8	
									4	2.0											5	1	59
45	SLOPE OUTSIDE FACE	5	1	51		S			19	5.0											20	0	21
46	SLOPE OUTSIDE FACE	5	7	51		S	V		17	11.0											18	6	
									4	2.0											4	9	85
47	TOP CORNER	5	2	51		S	V		1	4.0											1	11	
									1	2.0											1	9	4
48	TOP HORIZONTAL	8	2	61		S	V		17	11.0	3	9.0									21	6	
									17	9.0	3	9.0									21	4	114
51	CURB TOP HORIZONTAL	6	2	50		S			14	8.0											14	8	44
52	VERTICAL	4	20	54		S	V		1	6.0											2	1	
									8	5.0											9	0	74

S=BAR IS INCLUDED IN SUBSTRUCTURE QUANTITIES
LUMP SUM QUANTITY
T OR S=TIE OR STIRRUP RADIUS
E=EARTHQUAKE TAIL W/ TIE OR STIRRUP RADIUS
E=BAR IS EPOXY COATED
V=BAR DIMENSIONS VARY BETWEEN DIMENSIONS SHOWN ON THIS LINE AND THE FOLLOWING LINE

MARK NO.	LOCATION	SIZE	NO. REQ'D	BEND TYPE	LUMP SUM	SUBSTRUCT	EPOXY COATED	VARIES	DIMENSIONS U FT	U IN.	W FT	W IN.	X FT	X IN.	Y FT	Y IN.	Z FT	Z IN.	θ_1 DEG	θ_2 DEG	LENGTH (EACH) FT	LENGTH (EACH) IN.	TOTAL WEIGHT LBS
53	VERTICAL	5	20	54		S	V		1	6.0											2	3	
									8	5.0											9	2	118
W1	TRAFFIC BARRIER DOWEL	5	20	91		S	E														4	1	87
W2	TRAFFIC BARRIER DOWEL	4	20	92		S															4	3	55
	PIER 2																						
55	FOOTING	6	72	50		S			10	6.0											10	6	1136
56	FOOTING	8	96	50		S			10	6.0											10	6	2691
57	COLUMN VERTICAL	9	39	68		S			1	8.0	27	3.0									28	6	3777
58	COLUMN SPIRAL	4	3	67		S			2	8.0	81	0.0	0	3.5							678	6	1360
70	CROSS BEAM HORIZONTAL BOTTOM	9	24	50		S			38	10.0											38	10	7130
71	CROSS BEAM HORIZONTAL	4	4	50		S			34	1.0											34	1	273
72	CROSS BEAM STIRRUP	5	68	72	S	S			3	9.0	3	7.0	3	7.0							11	8	703
73	CROSS BEAM TOP TIE	5	68	58	T	S			3	9.0											4	7	277
74	CROSS BEAM HORIZONTAL	9	24	50		S			39	2.0											39	2	7191
	PIER 3																						
55	FOOTING	6	72	50		S			10	6.0											10	6	1136
56	FOOTING	8	96	50		S			10	6.0											10	6	2691
58	COLUMN VERTICAL	9	39	68		S			1	8.0	30	4.0									31	7	4186
59	COLUMN SPIRAL	4	3	67		S			2	8.0	92	0.0			5	8.0					770	9	1545
69	CROSS BEAM HORIZONTAL BOTTOM	9	18	50		S			38	8.0											38	8	7099
71	CROSS BEAM HORIZONTAL	4	4	50		S			34	1.0											34	1	273
72	CROSS BEAM STIRRUP	5	54	72	S	S			3	9.0	3	7.0	3	7.0							11	8	703
73	CROSS BEAM TOP TIE	5	54	58	T	S			3	9.0											4	7	277
74	CROSS BEAM HORIZONTAL	9	18	50		S			39	0.0											39	0	7160
	PIER 4																						
1	FOOTING BOTTOM	6	13	50		S			49	6.0											49	6	967
2	FOOTING BOTTOM	6	101	50		S			11	6.0											11	6	1745
3	FOOTING TOP	5	51	50		S			11	6.0											11	6	612
4	FOOTING TOP	5	13	50		S			49	6.0											49	6	671
6	ABUTMENT HORIZONTAL	6	44	51		S			23	1.0											23	9	1571
7	ABUTMENT TIES	4	48	58	T	S			1	6.0											2	2	69
8	ABUTMENT TOP HORIZONTAL	6	4	51		S			23	1.0											23	9	143
9	ABUTMENT TOP TIES	4	43	56	T	S			1	6.0											2	1	60
10	GIRDER STOP	5	25	61	T	S			1	5.0	2	0.0	2	0.0							5	3	136
11	GIRDER STOP HORIZONTAL	4	10	50		S			3	5.0											3	5	23
12	ABUTMENT VERTICAL	6	86	50		S	V		7	0.0											7	0	
									5	7.0											5	7	813
	PIER 4 CURTAIN WALL EAST																						
80	VERT FF	5	4	50		S			10	6.0											10	6	44
81	VERT NF	4	3	50		S			10	6.0											10	6	21
82	VERT FF	5	10	50		S			10	6.0											10	6	110
83	VERT NF	4	7	50		S			10	6.0											10	6	49
84	HORIZ TOP NF	4	7	80		S			5	11.0			0	10.0			0	1.5	64	6	9		32
85	HORIZ TOP FF	7	7	80		S			5	8.0			1	6.0			0	3.0	64	7	2		103
86	HORIZ TOP NF	4	7	80		S			5	11.0			0	10.0			0	1.5	64	6	9		32
87	HORIZ TOP FF	7	7	80		S			5	8.0			1	6.0			0	3.0	64	7	2		103
88	HORIZ AT FILLET	7	7	52		S			3	0.0											4	7	66
W1	TRAFFIC BARRIER DOWEL	5	6	91		S	E														4	1	26
W2	TRAFFIC BARRIER DOWEL	4	4	92		S															4	3	11

BENDING DIAGRAMS

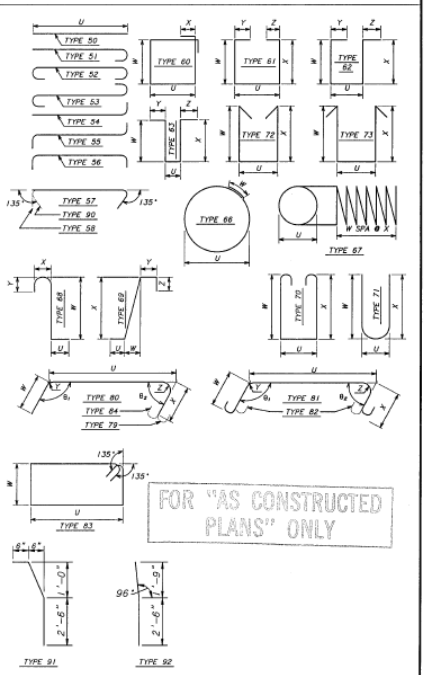

NOTES:

1. ALL REINFORCING BARS ON THIS SHEET SHALL BE AASHTO M31 GRADE 60 UNLESS SHOWN OTHERWISE.
2. REINFORCING FOR TRAFFIC BARRIER IS NOT SHOWN IN THIS BAR LIST EXCEPT FOR BARS S1, S2, W1, AND W2. SEE TRAFFIC BARRIER, SHEET 17.
3. BEND FOR TRANSVERSE BARS DUE TO ROADWAY CROWN CONDITIONS HAVE NOT BEEN SHOWN. THESE BARS SHALL BE BENT AS REQUIRED TO CONFORM TO THE CONFIGURATION OF THE STRUCTURE.
4. # NUMBER AND LENGTH OF BARS TO BE DETERMINED BY THE CONTRACTOR FROM THE PLANS.
5. LENGTHS OF SPIRAL SHOWN IN BARLIST DOES NOT INCLUDE LENGTH OF SPLICES
6. DIMENSIONS FOR BENT REINFORCING BARS (INCLUDING LENGTH) ARE POINTS OF INTERSECTION (OUT TO OUT).

FOR "AS CONSTRUCTED PLANS" ONLY

SR 405 JOB NO. 7067 SHEET 21 OF 22

DRAWN	R. MOHN	10/94
DESIGNED	E. DORNSEIF	12/94
CHECKED	R. FERNANDES	12/94
BR PROJ ENGR		
PRELIM PLAN BY		
ARCHITECT		

DATE	DATE	REVISION	BY	APPR

REGION NO	STATE	FED AID PROJ NO	SHEET NO	TOTAL SHEETS
10	WASH			
JOB NUMBER 94W097				
CONTRACT NO 4756				

BRIDGE AND STRUCTURES

JAMES SLIGHTAM — 13000 — REGISTERED PROFESSIONAL ENGINEER — STATE OF WASHINGTON — 1-3-95 — SIGNED THIS 4, 505

Washington State Department of Transportation

ABAM CONSULTING ENGINEERS
A MEMBER OF THE BERGER GROUP

SR 405
TUKWILA TO FACTORIA
SC&DI - STAGE 1

BAR LIST – SHEET 1

BRIDGE SHEET NO. 21

SHEET 955 OF 985 SHEETS

SR 405/417

S=BAR IS INCLUDED IN SUBSTRUCTURE QUANTITIES — LUMP SUM QUANTITY — T OR S=TIE OR STIRRUP RADIUS — E=EARTHQUAKE TAIL W/ TIE OR STIRRUP RADIUS — E=BAR IS EPOXY COATED — V=BAR DIMENSIONS VARY BETWEEN DIMENSIONS SHOWN ON THIS LINE AND THE FOLLOWING LINE

MARK NO.	LOCATION	SIZE	NO. REQ'D	BEND TYPE	BEND RADIUS	LUMP SUM	SUBSTRUCT	EPOXY COATED	VARIES	DIMENSIONS U FT	U IN.	W FT	W IN.	X FT	X IN.	Y FT	Y IN.	Z FT	Z IN.	θ1 DEG	θ2 DEG	LENGTH (EACH) FT	LENGTH (EACH) IN.	TOTAL WEIGHT LBS
	PIER 4 CURTAIN WALL WEST																							
80	VERT FF	5	4	50			S			11	9.0											11	9	49
81	VERT NF	4	3	50			S			11	9.0											11	9	24
82	VERT FF	5	10	50			S			11	9.0											11	9	123
83	VERT NF	4	7	50			S			11	9.0											11	9	55
94	HORIZ TOP NF	4	7	80			S			5	8.0	0	8.0			0	1.5			64		6	2	29
95	HORIZ TOP FF	7	7	80			S			5	11.0	1	2.0			0	3.0			64		6	9	98
96	HORIZ TOP NF	4	8	80			S			5	8.0	0	8.0			0	1.5			64		6	2	33
97	HORIZ TOP FF	7	8	80			S			5	11.0	1	2.0			0	3.0			64		6	9	110
98	HORIZ AT FILLET	7	8	52			S			4	6.0											6	1	100
W1	TRAFFIC BARRIER DOWEL	5	6	91			S	E														4	1	26
W2	TRAFFIC BARRIER DOWEL	4	4	32			S															4	3	11
	SUPERSTRUCTURE																							
	END DIAPHRAGM – PIER 1																							
120	BOTTOM HORIZONTAL	6	2	50						40	11.0											40	11	123
121	HORIZONTAL	4	22	50						21	6.0											21	6	316
122	STIRRUP	4	32	54	S					7	0.0											7	4	156
123	STIRRUP	4	32	54	S					7	0.0											7	4	156
124	STIRRUP	4	32	61	S					5	4.0	1	9.0	0	8.0							7	7	162
125	TOP HORIZONTAL	4	6	50						21	6.0											21	6	86
126	TOP TIES	4	31	56	T					1	7.0											2	2	45
127	TOP HORIZONTAL	6	2	50						40	11.0											40	11	123
	END DIAPHRAGM – PIER 4																							
120	BOTTOM HORIZONTAL	6	2	50						39	5.0											39	5	118
121	HORIZONTAL	4	11	50						38	1.0											38	1	280
122	STIRRUP	4	32	54	S					7	0.0											7	4	156
123	STIRRUP	4	32	54	S					7	0.0											7	4	156
124	STIRRUP	4	32	61	S					5	4.0	1	9.0	0	8.0							7	7	162
125	TOP HORIZONTAL	4	3	50						39	5.0											39	5	79
126	TOP TIES	4	31	56	T					1	8.0											2	3	47
127	TOP HORIZONTAL	6	2	50						39	5.0											39	5	118
	INTERMEDIATE DIAPHRAGMS																							
150	STIRRUP	4	180	71	S					0	5.0	4	8.5	4	8.5							9	7	1153
151	BOTTOM HORIZONTAL	9	4	50						34	1.0											34	1	464
152	HORIZONTAL BETWEEN GIRDERS	4	180	50						6	2.0											6	2	741
153	HORIZONTAL FULL LENGTH	8	4	50						34	1.0											34	1	364
154	TOP HORIZONTAL	7	16	50						35	11.0											35	11	1175
	INTERMEDIATE HINGE DIAPHRAGM																							
155	HORIZONTAL TIE	4	20	61	S					1	0.5	2	9.0	2	9.0							6	5	85
156	HORIZONTAL TIE	4	100	61	T					2	9.0	3	5.0									6	1	406
157	STIRRUP	4	60	54	S					5	5.0											5	9	229
158	STIRRUP	4	120	54	S					5	11.5											6	3	501
159	HINGE BAR	9	64	51						6												7	3	1575
160	HORIZONTAL	5	20	50						36	9.0											36	9	767
161	STIRRUP	4	50	63	S					1	9.0	5	6.5	5	6.5	0	5.0	0	5.0			13	4	445

S=BAR IS INCLUDED IN SUBSTRUCTURE QUANTITIES — LUMP SUM QUANTITY — T OR S=TIE OR STIRRUP RADIUS — E=EARTHQUAKE TAIL W/ TIE OR STIRRUP RADIUS — E=BAR IS EPOXY COATED — V=BAR DIMENSIONS VARY BETWEEN DIMENSIONS SHOWN ON THIS LINE AND THE FOLLOWING LINE

MARK NO.	LOCATION	SIZE	NO. REQ'D	BEND TYPE	BEND RADIUS	LUMP SUM	SUBSTRUCT	EPOXY COATED	VARIES	DIMENSIONS U FT	U IN.	W FT	W IN.	X FT	X IN.	Y FT	Y IN.	Z FT	Z IN.	θ1 DEG	θ2 DEG	LENGTH (EACH) FT	LENGTH (EACH) IN.	TOTAL WEIGHT LBS
	ROADWAY SLAB																							
200	TRANSVERSE BOTTOM	5	365	50				E		37	6.0											37	6	14276
201	TRANSVERSE TOP	5	365	51				E		26	5.0											27	0	10275
202	CANTILEVER	5	456	51				E		7	4.0											7	11	3760
203	TRANSVERSE TOP END	5	48	51				E	V	34	3.0											34	10	
										7	9.0											8	4	1035
204	TRANSVERSE BOTTOM END	5	48	50					V	34	3.0											34	3	
										7	7.0											7	7	1004
205	TRANSVERSE TOP SPLAYED	5	16	51				E	V	5	1.0											5	8	
										7	7.0											8	2	115
206	TRANSVERSE BOTTOM SPLAYED	5	16	50					V	5	1.0											5	1	
										7	7.0											7	7	106
207	TRANSVERSE TOP	5	365	51				E		13	11.0											14	6	5516
210	LONGITUDINAL TOP	5	$	50	L			E		$	$											$	$	5321
211	LONGITUDINAL BOTTOM	5	$	50	L					$	$											$	$	8887
220	PIER LONGITUDINAL BOTTOM	6	38	50						54	0.0											54	0	3082
221	PIER LONGITUDINAL BOTTOM	6	48	50						44	0.0											44	0	3172
222	PIER LONGITUDINAL BOTTOM	6	24	50						19	0.0											19	0	685
230	PIER LONGITUDINAL TOP	6	38	50				E		54	0.0											54	0	3082
231	PIER LONGITUDINAL TOP	6	48	50				E		44	0.0											44	0	3172
232	PIER LONGITUDINAL TOP	6	24	50				E		19	0.0											19	0	685
S1	TRAFFIC BARRIER TIE	5	620	69				E		0	6.0	0	9.0	1	6.0	0	6.0					2	7	1690
S2	TRAFFIC BARRIER TIE	4	312	69						1	6.0	0	2.0	1	6.0							2	11	610

BENDING DIAGRAMS

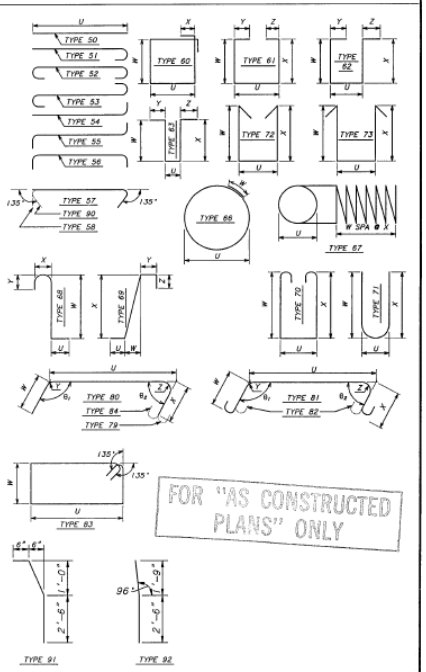

FOR "AS CONSTRUCTED PLANS" ONLY

NOTES:

1. ALL REINFORCING BARS ON THIS SHEET SHALL BE AASHTO M31 GRADE 60 UNLESS SHOWN OTHERWISE.
2. REINFORCING FOR TRAFFIC BARRIER IS NOT SHOWN IN THIS BAR LIST EXCEPT FOR BARS S1, S2, W1, AND W2. SEE TRAFFIC BARRIER, SHEET 17.
3. BEND FOR TRANSVERSE BARS DUE TO ROADWAY CROWN CONDITIONS HAVE NOT BEEN SHOWN. THESE BARS SHALL BE BENT AS REQUIRED TO CONFORM TO THE CONFIGURATION OF THE STRUCTURE.
4. # NUMBER AND LENGTH OF BARS TO BE DETERMINED BY THE CONTRACTOR FROM THE PLANS.
5. LENGTHS OF SPIRAL SHOWN IN BARLIST DOES NOT INCLUDE LENGTH OF SPLICES
6. DIMENSIONS FOR BENT REINFORCING BARS (INCLUDING LENGTH) ARE POINTS OF INTERSECTION (OUT TO OUT).

SR 405 JOB NO. Z067 SHEET 22 OF 22

DRAWN	R. MOHN	10/94
DESIGNED	E. DORNSEIF	12/94
CHECKED	R. FERNANDES	12/94
BR PROJ ENGR		
PRELIM PLAN BY		
ARCHITECT		

DATE	DATE	REVISION	BY	APPR

REGION NO.	STATE	FED AID PROJ NO	SHEET NO	TOTAL SHEETS
10	WASH			

JOB NUMBER 94W097
CONTRACT NO 4756

BRIDGE AND STRUCTURES

1-3-95 EXPIRES JUNE 4, 1995

Washington State Department of Transportation

ABAM CONSULTING ENGINEERS
A MEMBER OF THE BERGER GROUP

SR 405
TUKWILA TO FACTORIA
SC&DI - STAGE 1

BAR LIST – SHEET 2

BRIDGE SHEET NO. 22

SHEET 254 OF 3695 SHEETS

SR 405/417